EIGHTH INTERNATIONAL COLLOQUIUM ON ULTRAVIOLET AND X-RAY SPECTROSCOPY OF ASTROPHYSICAL AND LABORATORY PLASMAS

(IAU Colloquium 86)

CONF-8408124--

DE85 010677

Meeting Sponsors

The International Astronomical Union

The Naval Research Laboratory

National Aeronautics and Space Administration

U.S. Department of Energy

27-29 AUGUST 1984

CHAIRPERSON OF THE COLLOQUIUM

G.A. Doschek

All sessions of papers were held at

the Capitol Holiday Inn, Washington, D.C.

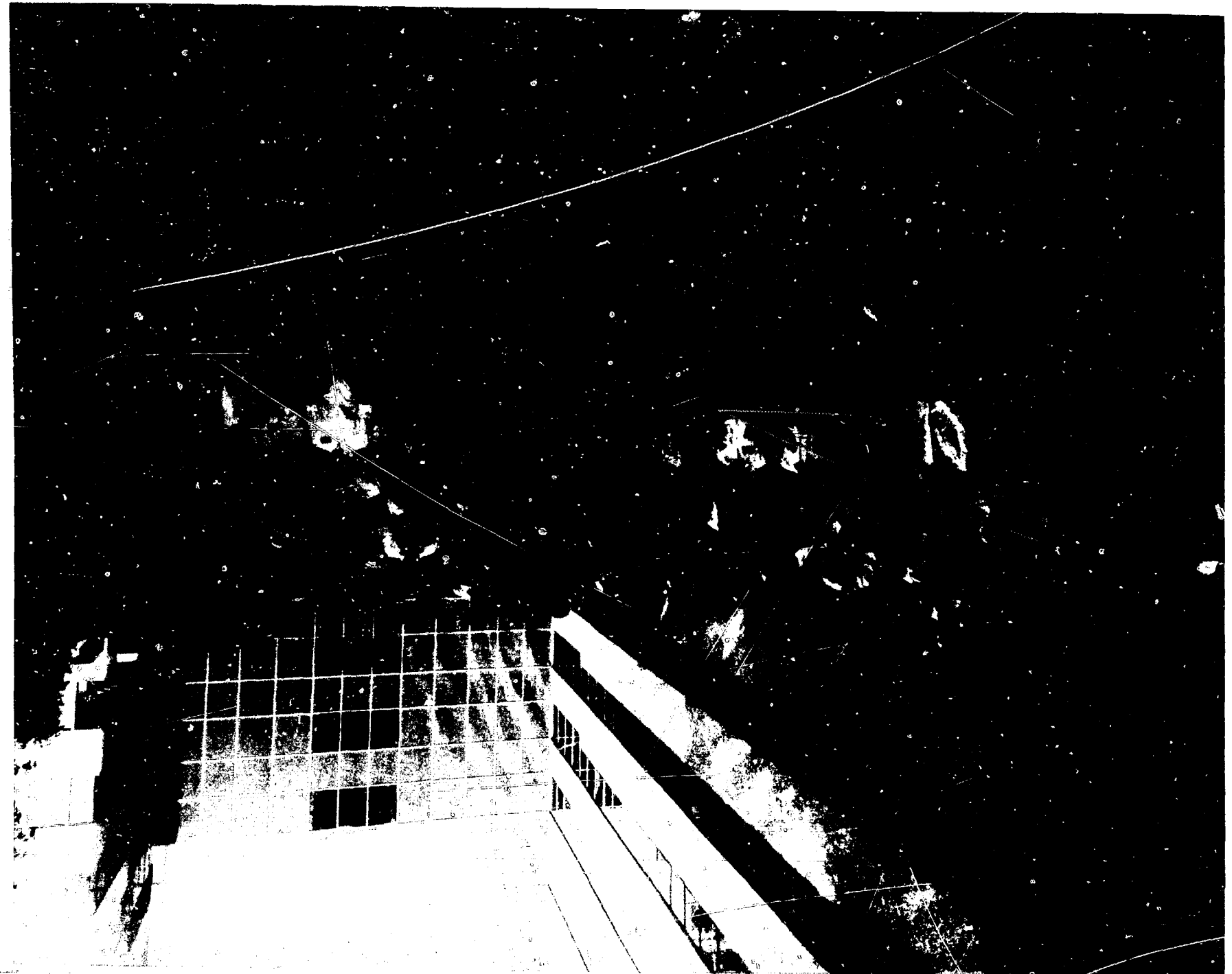

EIGHTH INTERNATIONAL COLLOQUIUM ON

ULTRAVIOLET AND X-RAY SPECTROSCOPY OF

ASTROPHYSICAL AND LABORATORY PLASMAS

(IAU Colloquium 86)

EIGHTH INTERNATIONAL COLLOQUIUM ON

ULTRAVIOLET AND X-RAY SPECTROSCOPY OF

ASTROPHYSICAL AND LABORATORY PLASMAS

(IAU Colloquium 86)

Local Organizing Committee

M. Blaha (University of Maryland)

R. Bleach (Naval Research Laboratory)

J.D. Bohlin (National Aeronautics and Space Administration)

P.B. Boyce (American Astronomical Society)

G.A. Doschek (Naval Research Laboratory)

R. Elton (Naval Research Laboratory)

H. Gursky (Naval Research Laboratory)

R.W. Kreplin (Naval Research Laboratory)

W.R. Ott (National Bureau of Standards)

A. Temkin (NASA/Goddard Space Flight Center)

FORWARD AND ACKNOWLEDGEMENTS

This volume represents the Proceedings of the Eighth International Colloquium on Ultraviolet and X-ray Spectroscopy of Astrophysical and Laboratory Plasmas, held 27-29 August 1984 at the Capitol Holiday Inn, Washington, D.C. The aim of this series of colloquia has been to bring together workers in the fields of astrophysical spectroscopy, laboratory spectroscopy, and atomic physics, in order to interchange ideas and results on problems which are really common to the different disciplines. In the past such an interchange has been extremely fruitful, and I hope that this meeting has been similarly successful.

The Proceedings are made possible by the enthusiastic support of the participants, most of whom agreed to submit Extended Abstracts of their papers for publication. These abstracts are not meant to be alternatives to publications in refereed journals, but rather are meant to comprise a working document that hopefully will be useful to the participants. In order to be complete, Short Abstracts have been retyped and included for those papers for which Extended Abstracts were not received. Two Extended Abstracts were received from authors who, although intending to participate, were finally unable to attend. These papers appear at the end of the volume.

This colloquium was sponsored by the International Astronomical Union, the Naval Research Laboratory, the National Aeronautical and Space Administration, and the Department of Energy. It was hosted by the Naval Research Laboratory. I would like to thank these organizations for their generous support and encouragement. Much of the work in organizing the meeting was carried out by Mr. Gary Cogdell and Mrs. Charlotte Pascoe of Dynamic Systems, Incorporated, who did an outstanding job in attending to a myriad of arrangements and solving the many problems accompanying them. I would like to thank Gary and Charlotte for their efforts. Similarly, I would like to thank Bob Kreplin at the Naval Research Laboratory for his methodical and time consuming help with the meeting, help which was essential for the successful organization of the Colloquium. I would also like to thank the members of the International and Local Organizing Committee for their support and insights, and the Session Chairpersons for keeping the meeting on schedule. I would like to thank Dr. David H. DeVorkin, of the Smithsonian Institution National Air and Space Museum, for an excellent after-dinner banquet talk that was enjoyed by all those present. Finally, I would like to express my warmest appreciation to my secretarial staff, Mrs. Marlene Wedding, Mrs. Dorothy Waters, and Mrs. Judith Hardison, for the very large amount of excellent secretarial work that was necessary to make this meeting possible.

George A. Doschek
Chairman, [illegible]nizing Committees
Decembe[illegible]4

CHAIRPERSONS

Session 1. Solar Astrophysics

Dr. R.W.P. McWhirter
Rutherford Appleton Laboratory (UK)

Session 2. Low Density Laboratory Plasmas

Prof. W.R.S. Garton
Imperial College (UK)

Session 3. Non-Solar Astrophysics

Dr. H. Gursky
Naval Research Laboratory (USA)

Session 4. Theoretical Spectroscopy

Dr. A. Temkin
NASA/Goddard Space Flight Center (USA)

Session 5. Experimental Atomic Physics

Dr. J.L. Schwob
The Hebrew University of Jerusalem (ISRAEL)

Session 6. Poster Papers - No Chairperson

Session 7. High Density Laboratory Plasmas

Dr. W.H. Parkinson
Harvard-Smithsonian Center for Astrophysics (USA)

TABLE OF CONTENTS

SESSION 7. HIGH DENSITY LABORATORY PLASMAS

PAPERS NOT PRESENTED AT THE MEETING

SESSION 1. SOLAR ASTROPHYSICS

THE SOFT X-RAY AND EUV SPECTRA OF SOLAR FLARES.

K.Nishi and K.Tanaka
Tokyo Astronomical Observatory, University of Tokyo
Mitaka Tokyo Japan

HINOTORI

The Japanese solar maximum satellite HINOTORI was launched on 21 February 1981, and so far 720 Solar flares were detected including many large flares; the largest observed was a X12 class flare occurred on June 6, 1982. Unfortunately, the data recorder malfunctioned in June, 1982, since then the real time basis observation has been possible to continue. The general introductory explanation and some important results were already published in some proceedings(1,2,3), therefore we would like to focus on presenting some new results of the Soft X-ray spectra obtained by the spectrometers rather than on talking a review.

The Soft X-ray crystal spectrometers (SOX) measure spectral features around 1.85A emitted from highly ionized iron ions with two different spectral ranges and resolutions; low (SOX-1;1.72-1.99A; 2.5mA) high (SOX-2; 1.83-1.89A; 0.15mA), with temporal resultion of 8-10 seconds. They were newly designed Bragg type spectrometers for the spin stabilized satellite. The wavelength scan is made automatically by the spin without moving any parts of the spectrometers. (Tanaka et al., 1978) The idea to use the attitude of space vehicle is our traditional method applied for the Solar observation from rockets (Nishi, 1973,1975). Another instrument for Flare Monitor (FLM) was used to measure Soft X-ray spectrum in the energy range of 1.5-30 kev. The detector is a gas-sealed scintillation proportional counter, and the energy resulution is 10.5% at 5.9 kev nearly twice superior to ordinary proportional counters. An example of spectra obtained by the crystal spectrometers is shown in the figure 1. The high resolution spectra (lower) cover lines from FeXXV to FeXXIII, and low resolution spectra (upper) show lines from FeXIX to FeXXVI, $K\alpha$ and $K\beta$. The FeXXVI lines are resolved into four peaks: 1.778A($L\alpha_1$), 1.784A($L\alpha_2$), 1.789A and 1.792A. The latter two peaks are from the satellite lines(FeXXV) associated with FeXXVI. Their relative intensities are various from flare to flare. An example of time behaviors of various lines and plasma parameters such as electron temperature(Te), ionization temperature(Tz), dI(total iron lines intensity)/dt, and Hard X-ray seen in one of the published papers (Tanaka et al.,1982). There are many types of variations, but some common characteristics can be summarized as follows. At the initial phase of the flare the lines are broad(200km/s) and have blue shift component (400km/s), and the blue-shifted components show limb weakening. The line width of unshifted components monotonically decreases from the start to the end of flare, which suggests that large non-thermal broadening (turbulent motion) occurred in the flaring plasma at the beginning of flare. For the analysis of velocity shift a method of line

profile fitting to synthesized spectra by using the atomic parameters from Dubau et al. (1981) and Bely-Dubau et al. (1982a, b) is used. In rare cases lines with red shift component are also found and is shown in the figure 2. In the very initial phase of the biggest flare observed by HINOTORI a double-peaked w line profile was detected in low resolution spectra of two consecutive scans made with 10sec. interval, and the separation corresponds to 300km/s. (Fig.3) If the blue shift is interpreted as rising motion of heated plasma from denser atmosphere which is heated by electron beam or heat conduction, and if the rising plasmas are confined in the lower portion of the coronal loops, then the increse of total electron number of stationary hot plasma is explained by supply of input electron number from the blue-shifted plasma. An analysis is now under progress comparing with the filtergrams of $H\alpha$ and D_3 emission and the X-ray image by K.Tanaka and others.

The electron temperatures (Te) for FeXXV are derived from the well-known method of using the line intensity ratio of dielectronic satellite (j) to resonance (w) shown by Gabriel et al.(1972); Doschek et al.(1980) or the spectal line profile fitting method, and their values are quite consistent with each other. Te for FeXXVI plasma are derived from the synthesized spectra calculated from the atomic data by Dubau et al, (1981) with the crystal resolution, and we can safely assumed that the fitting accuracy is within ± 2 million K at most. In the figure 4 we see that Te from the FeXXVI and FeXXV spectra are different significantly. One of the most important characteristic of our instruments is that we can obtain FeXXVI spectra, and the more intensive FeXXVI spectra were observed the more clear the difference appeared. The time behavior of FeXXVI line in some flares is quite similar to the Hard X-ray intensity but different from FeXXV and lower ionization stage lines; it reachs its maximum about 1 minute before FeXXV lines reach the peak. According to the characteristics and time behaivors of hot thermal component derived from FeXXVI lines as shown above, flares could be classified into two categories; Type A and B. (Tanaka et al. 1983 for Type C see Tsuneta et al. 1984) In Type A flare, the lowest energy of hard X-ray shows no spiky compoments and its time behavior is quite similar to FeXXVI lines. The FeXXVI spectra show the existence of hot thermal component with Te $30\text{-}40 \times 10^6$K, and the obtained emission measure Ne^2V is 10^{49} $-10^{50}/cm^3$. These flares are very compact and short-lived in the low corona from the X-ray telescope (SXT), then electron density can be derived as $10^{11-12}/cm^3$, since it is safely assumed that emitting regions of FeXXVI and hard X-ray are overlapped. Type B flares show quite different characteristics at the beginning. While hard X-ray time profiles consist of spikes to the lowest channel, FeXXVI lines behave differently except for later phases. Most valuable characteristics could be the similarity of time profile of dI/dt(I:total iron line emission) to that of the hard X-ray bursts. This fact suggests that production of thermal component (Te$\sim$20

$\times 10^6$K) is closely associated with the occurrence of hard X-ray spike bursts. Continum observations by FLM show also this characteristics (Watanabe et al. 1983). The difference between Type A and Type B may originate from the difference of relative importance of two components, i.e. in Type A flares contribution of hot thermal component dominates spike component, while in Type B flares, hot thermal component contributes somewhat only in the decay phase.

For the ionization balance between FeXXIV and FeXXV Te and Tz are derived from j/w and q/w (q; inner shell excitation line) respectively, and the observed data are almost consistent with the Shull and Van Steenberg (1982) computations. (F.Moriyama, 1984) But observed FeXXVI/FeXXV values derived from the values of $I\alpha/w$ and z/w are quite different from the theoretical curves (Fig. 5:a,b). On the other hand at the Maximum phase of type A flares the ratios show nearly equilibrium if Te derived from FeXXVI line profile fitting is referred (Fig. 5,c). From the time profile of Te(XXVI) and Te(XXV) we see that Te(XXVI)$>$ Te(XXV) at the maximum phase (Fig. 5,d) but Te(XXVI)$\gtrsim$ Te(XXV) at the later phase (Fig. 6). Does the discrepancy depend on the physical situation of the flare plasmas or on the theoretical calculations of atomic parameters? The differential emission measure calculations are also not able to solve the problem. (Akita, 1984) The exceptionally intense iron Kα emissions associate with hard X-ray burst were observed by the spectrometer. High resolution continuum spectra from 1.5 to 12.5kev and hard X-ray spectra from 18 to 400kev of the flares were obtained by the gas scintillation counter and the scintillation counter. They show remarkable power-law photon distribution extending from below 10kev to above 100 kev in the early phase of the flares. The intense Kα emission is attributed to fluorescence of photospheric neutral iron by the power-law X-ray flux that extends down to the K-shell ionization threshold at 7.1 kev. On the other hand, the gradually increasing K_α emission after the decay of the hard X-ray burst can be explained by fluorescence due to the X-ray flux of thermal origin. (Tanaka et al. 1984)

As SOX has two independent crystals with different phase angles, it provides a new technique for measuring linear polarization of iron emission line (Akita et al. 1983). The upper limit of averaged polarization degree was determined as about 4%.

From the FLM data we can derive Te and EM (Emission measure) by adopting a proper modeling. From time behavior Te v.s. EM in a flare we see that EM increases as Te increases like heating due to adiatic compression. However, EM reaches maximum after Te maximum, and then EM remains though Te decreases. If the dominant process of this phase is radiative cooling, electron density is estimated to be $5 \times 10^{11}/cm^3$ (Watanabe et al. 1982).

TENMA

The second X-ray astronomy satellite, nicknamed TENMA (a Japanese for Pegasus) was put into orbit sucessfully on

20 February 1983. TENMA carries four scientific instruments; GSPC (gas scintillation proportional counter), XFC (X-ray Focusing Concentrator), TSM (Transient Source Monitor), and GBD/RBM(Gamma-ray Burst Detector/Radiation Belt Monitor). The main instrument is GSPC consisting of ten modular units, two of which are equipped with modulation collimators. It is the same type dector as FIM on HINOTORI, and provides a powerful capability for the spectroscopic study of various categories of cosmic X-ray sources in 1-60 kev. Its large effective area, about 640cm^2 for eight GSPCs, ensures a sensitivity down to 1/2000 the Crab Nebula flux, making the observations of various extragalatic sources possible. Its capability is illustrated by the X-ray spectrum of a supernova Cas A compared with one of the solar flares (Fig. 7). Since the launch, TENMA has been yielding many significant results (Y.Tanaka 1983), but we would like to show two of them obtained by GSPC.

The spectra from X-ray pulsars (mostly composed of a massive star and a magnetized neutron star) often exhibit a K-emission line at about 6.4 kev as well as iron K absorption edge around 7.1 kev (Fig. 8), indicating that there is a relatively cold matter around the X-ray emitting neutron star. Another example is the discovery of an X-ray absorption line at about 4.1 kev in X-ray burst spectra from 4U 1636-53. (Fig. 9) This may be interpreated as the iron absorption line, redshifted due to a high gravity of the neutron star surface. These results lead to direct measurements of the mass and size of the neutron star.

Rocket observation of the EUV images of a flare and active regions.

Heliograms of a flare and active regions were obtained in EUV emission lines such as CIII 970A, NeVIII 770A, HI Ly$_\beta$, and hydrogen Lyman continua with a spatial resolution of 10 seconds of arc and pointing accuracy of about 0.5 seconds of arc by a Japanese sounding rocket S520-5CN. The instrument was composed of a 10cm Cassegrain telescope (F/15), a 50cm stigmatic spectrograph, and a two dimensional microchannel plate. The second mirror of the telescope was used for the fine pointing and raster scan. The entrance slit of the spectrograph and the group of slits to separate emission lines and hydrogen continua were set on the Rowland circle, and the microchannel plate was set on the spatial (vertical) foci. The rocket was launched on Sept. 6 1982, at 02h00m00s UT from the Kagoshima Space Center, reaching maximum hight of 237 km at 246s. after firing. Very fortunately an 1B flare was occuring 01h52m-02h22m UT (Max. 01h53m) at N14 and E12. From the obtained data some physical parameters such as Te, Tb, and thickness of emitting layer for quite region, active region, and flare were derived (Hirayama et al. 1984).

REFERENCES

(1) Proceedings of HINOTORI symposium on Solar Flares; (Tokyo, 27-29 January, 1982) published by ISAS, May(1982)

(2) Proceedings of US-Japan Seminor on Recent Advance in Understanding of Solar Flares, Solar Phys., 86, Nos. 1,2(1983)
(3) Proceedings of the Japan-France Seminor on Active Phenomena in the Outer Atmosphere of the Sun and Stars, (Paris, 3-7 Octover 1983) publiched by CNRS, (1984)
Akita, K., Tanaka, K., and Watanabe, T. 1983, Solar Phys., 86, 101.
Akita, K., 1984, private communication.
Bely-Dubau, F., Dubau, J., Faucher, P., and Gabriel, A. H. 1982a, M. N. R. A. S., 198, 239.
Bely-Dubau, F. et al. 1982b, M. N. R. A. S., 201, 1155.
Doschek, G.A., Feldmann, U., Kreplin, R.W., and Cohen, L., 1980 Astrophys. J., 239, 725
Dubau, J. et al. 1981, M. N. R. A. S., 195, 705.
Gabriel, A.H. 1972, M. N. R. A. S., 160, 99.
Hirayama, T., et al., 1984; submitted to Solar Phys.
Moriyama, F., 1984; private communication.
Nishi, K., 1973, Solar Phys., 33, 23.
Nishi, K., 1975, Solar Phys., 42, 37.
Shull, J.M., and Van Steenberg, M., 1982, Astrophys. J., Sup. Ser., 48, 95.
Tanaka, K. and Nishi, K., 1978, Jap. J. Applied Phys. 17, Suppl. 17-2, 461.
Tanaka, K., Watanabe, T., Nishi, K. and Akita, K., 1982, Astrophys. J. Letters, 254, L59.
Tanaka, K., Nitta, N., Akita, K., and Watanabe, T., 1983, Solar Phys., 86, 91.
Tanaka et al., 1984, Astrophys. J. July 15 issue.
Tanaka, Y., 1983, ISAS Research Note No. 240.
Tsuneta, S., Takakura, T., Nitta, N., Ohki, K., Tanaka, K., Makishima. K., Murakami, T., Oda, M., Ogawara, Y., Kondo, I., 1984, Astrophys. J., 280, 887.
Watanabe, T., Tanaka, K., and Matsuoka, M., 1982, p.14; HINITORI Symp. on Solar Flares; published by ISAS.
Watanabe, T., Tanaka, K., Akita, K., and Nitta, N., 1983, Solar Phys., 86, 107.

FIGURE CAPTIONS

Fig.1 An example of Soft X-ray spectra; upper is low resolution and lower is high resolution.
Fig.2 An example of red shift component. The spectra are fitted to theoretically synthesized spectra (dash line).
Fig.3 An example of double-peaked w line profiles; June 6 1982 flare, two successive data of 16h30m31s-41s and 16h30m41s-50s show double peak at 1.85Å.
Fig.4 The existence of two temperature plasmas. upper; when Te (26.9×10^6K) determined by the Fe(XXV) profile fitting is adopted, the observed FeXXVI line profile do not fit to the calculated profile (dashed). lower; when Te (40×10^6K) determined by the Fe(XXVI) line profile fitting is adopted, the observed FeXXV profile

do not fit the calculated one.

Fig.5 (a)H/He derived from Lα/w v.s. Te determined by the FeXXV line profile fitting.
(b)H/He derived from z/w v.s. Te determined by the FeXXV line profile fitting.
(c)H/He derived from Lα/w v.s. Te determined by the FeXXI line profile fitting.
(d)Te(FeXXVI) v.s. Te(FeXXV) at the maximum phase.
(from Tanaka, K., and Akita, k., 1984 in preparation.)

Fig.6 Time profile of plasma parameters. (from Tanaka, K., Ohki, K., and Zirin, H., 1984, to be submitted to Astrophys. J.).

Fig.7 Comparison of Soft X-ray spectra of a solar flare observed by FLM on HINOTORI(left) and a typical young supernova remnant Cas A observed with GSPC on TENMA (right). K-emmission lines from various elements, including silicon, sulpher, argon, calcium, and iron are clearly resolved. (from SPACE RESEARCH IN JAPAN 1984, National report submitted to the 25 Plenary Meeting of the ICSU Committee on Space Research)

Fig.8 X-ray spectra of X-ray pulsars some times show strongly absorbed features. This is an example observed from Vela X-1 by the TENMA GSPC. An intense iron fluoresence line emission at about 6.4kev is seen, as well as a deep absorption edge by cold iron at about 7.1 kev. (from SPACE RESEARCH IN JAPAN 1984)

Fig.9 An X-ray absorption line was discovered with the TENMA GSPC in X-ray burst spectra from 4U 1636-53. This line, at about 4.1kev, is tentatively identified with the iron K-line, orginally at 6.4kev, redshifted due to an immense gravity on the neutron star surface. (from SPACE RESEARCH IN JAPAN 1984)

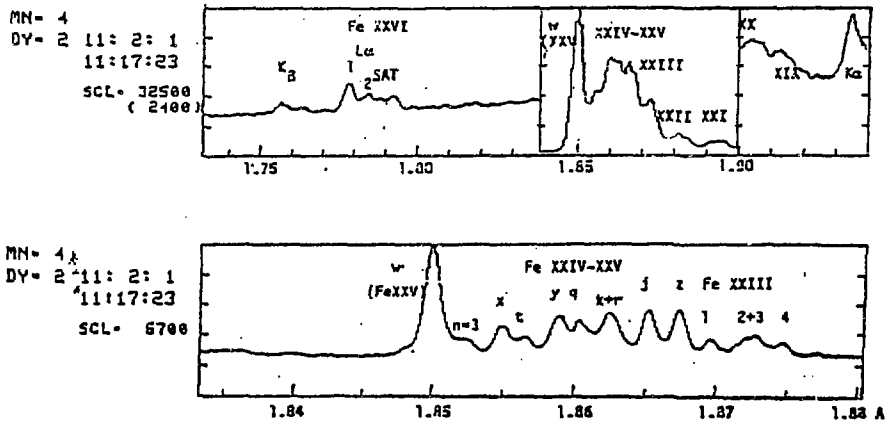

Fig.1

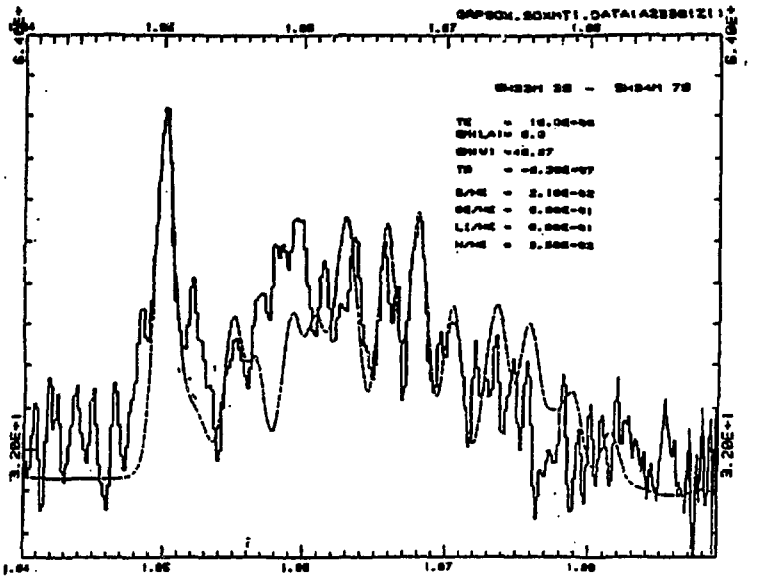

Fig.2

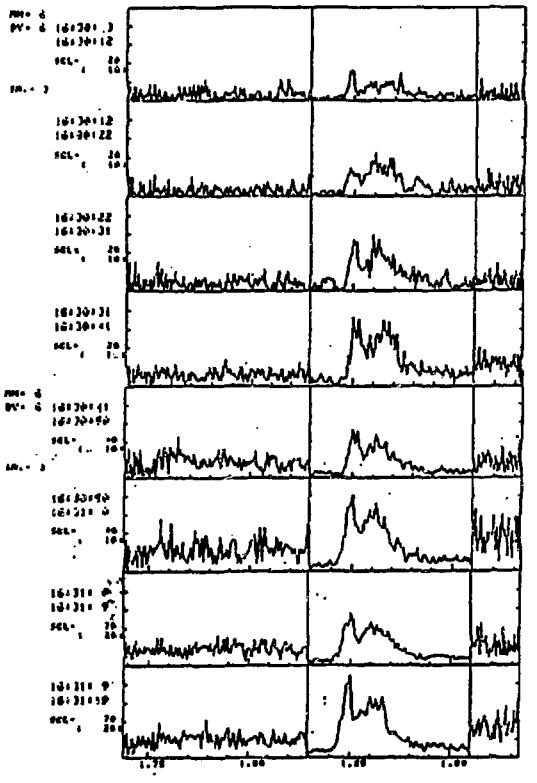

Fig.3

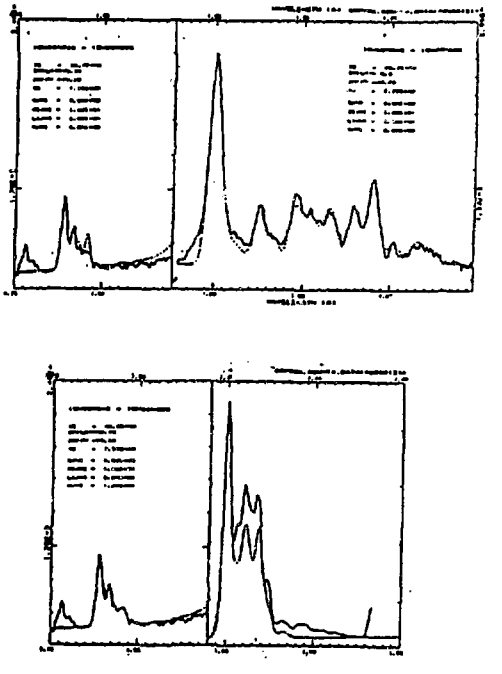

Fig.4

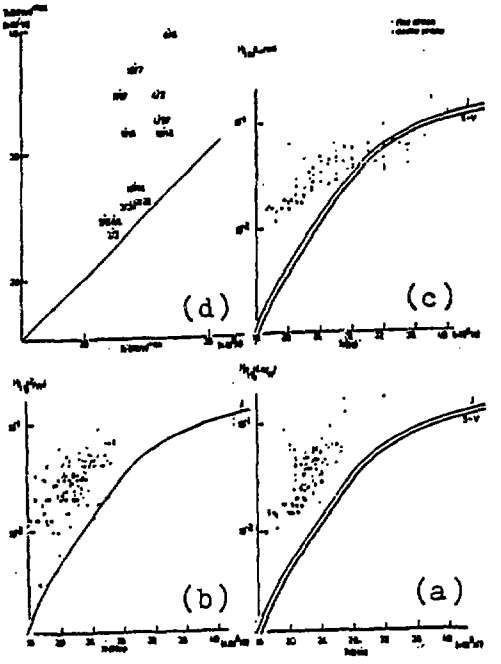

Fig.5

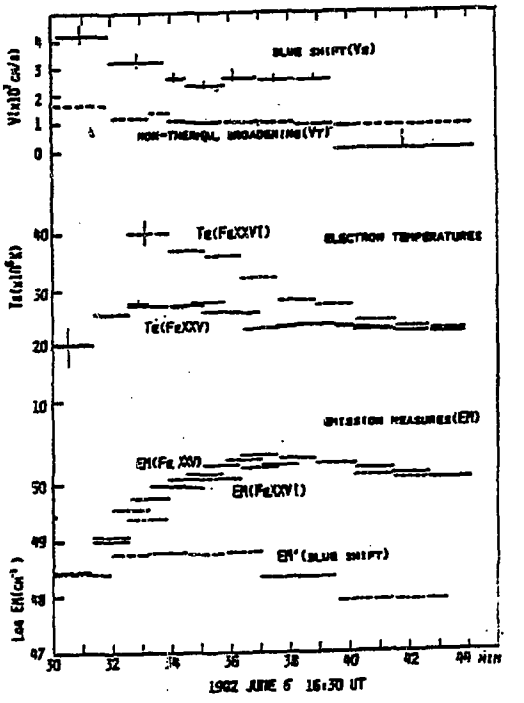

Fig.6

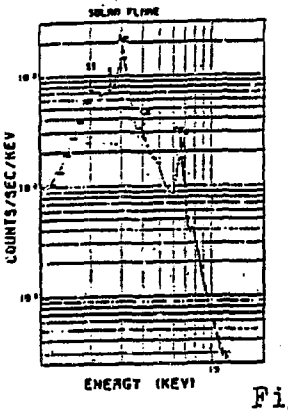

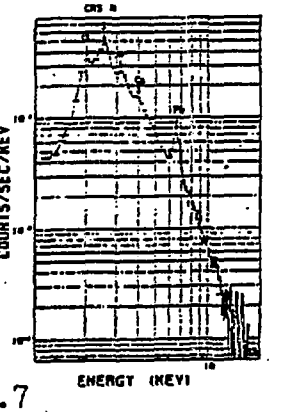

Fig.7

Fig.8

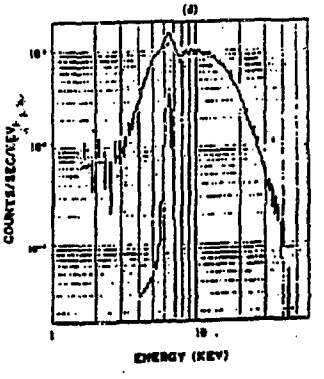

Fig.9

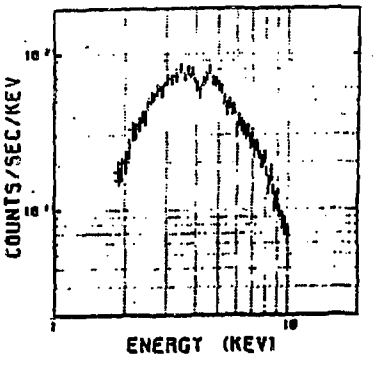

SOFT X-RAY SPECTROSCOPY FROM THE X-RAY POLYCHROMATOR ON THE NEWLY REPAIRED SOLAR MAXIMUM MISSION

K.T. Strong and R.A. Stern
Lockheed Palo Alto Research Laboratory,
Palo Alto, Ca 94304

J.R. Lemen
Mullard Space Science Laboratory,
University College, London, GB.

K.J.H. Phillips
Rutherford Appleton Laboratory,
Didcot, Oxfordshire, GB.

INTRODUCTION

The X-Ray Polychromator (XRP) resumed operations on 24 April 1984 following the successful in-orbit repair of the Solar Maximum Mission Satellite. Since that time the two instruments that comprise the XRP, the Flat Crystal Spectrometer (FCS) and the Bent Crystal Spectrometer (BCS), have been used to obtain new spectroscopic data from active regions and flares. The FCS, in particular, has accumulated far more observations of soft X-ray line profiles than were obtained during SMM-1 in 1980. For this short presentation, we have chosen two topics to illustrate the type of data that we have obtained since the repair.

OBSERVATIONS OF THE FE XVII LINE RATIOS

During the period of high activity in April and May 1984, the FCS was used to scan repeatedly Fe XVII lines in the 15-17A wavelength range. These neon-like lines are formed over a wide range of temperature and are consequently produced by both active regions and flares. During the decay of a GOES class M3 flare on 2 May 1984, there was a secondary energy release that resulted in the soft X-ray flux remaining essentially constant throughout the Fe XVII scans. We have derived the relative intensities for five Fe XVII lines observed during the flare decay. The resulting line photon flux ratios from the sum of ten scans, with respect to the line at 15.013A, are listed in the table below.

The theoretical values of these line ratios from calculations by Loulergue and Nussbaumer (1975) are shown in the table for comparison. While the uncertainties in the observed values are large in this current data set, there appears to be a systematic difference in the 17.051/15.013 ratio from their calculated value. We hope to better determine these ratios with future observations.

FE XVII LINE RATIOS

WAVELENGTH (A)	TRANSITION	MEAN OBSERVED FLUX RATIO	THEORETICAL (L & N)
15.013	$2p^6\ {}^1S_0 - 2p^5\ 3d\ {}^1P_1$	1	1
15.261	$2p^6\ {}^1S_0 - 2p^5\ 3d\ {}^3D_1$	0.35 (0.05)	0.31
16.775	$2p^6\ {}^1S_0 - 2p^5\ 3s\ {}^1P_1$	0.70 (0.07)	0.60
17.051	$2p^6\ {}^1S_0 - 2p^5\ 3s\ {}^3P_1$	0.90 (0.07)	1.12
17.096	$2p^6\ {}^1S_0 - 2p^5\ 3s\ {}^3P_2$	0.85 (0.07)	0.83

MASS MOTIONS IN AN ACTIVE REGION

Acton et al. (1981) gave the first evidence for significant mass motions in a quiescent active region. This result was based on a single observation of a limb active region and could not be confirmed by later FCS observations due to technical difficulties. With the renewal of operations we made observations of soft X-ray line profiles in an active region to further investigate this phenomenon. The figure below represents a sum of six 2x1 arcmin rasters over NOAA Active Region 4474 during a quiescent period, with Mg XI resonance line profiles taken at each of the 15 arcsec pixels. There were no significant variations from one raster to the next. The summed profiles are uniformly normalized to a peak rate of 100 counts s^{-1}.

We have fitted a Voigtian to each of these line profiles using a non-linear least squares technique to derive the wavelength and width of the lines. We find that the line profiles vary from the nominal width of the crystal rocking curve plus a thermal width equivalent to about 1-2 x 10^6K, consistent with the active region temperatures derived from the line ratios, to a thermal width of about 14.5 x 10^6K for the broadest lines. Such a high temperature thermal plasma would result in a substantial flux in the FCS higher temperature channels, which was not seen in these data. We conclude that the excess width is due to plasma turbulence thus confirming Acton's earlier result. If this line broadening were due solely to turbulence, the velocity would be 95 (+/- 30) km s^{-1}. We also investigated the possiblility of vertical plasma motions, but within the uncertainty of these data (+/- 20 km s^{-1}) none was detected.

FCS Spectroscopic Scan in a Raster
Mg XI Profile
Data taken on 28 April 1984

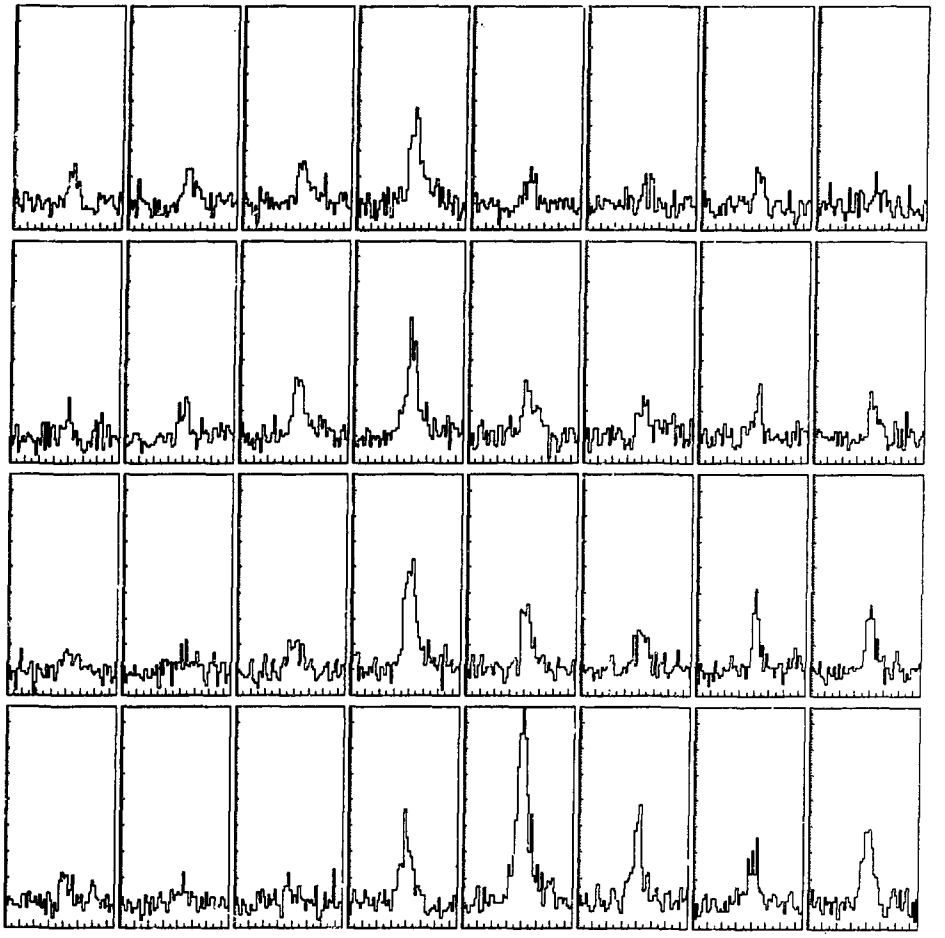

Wavelength Range 9.15 - 9.18 A

ACKNOWLEDGEMENTS

KTS and RAS are supported by NASA contract NAS5-23758 and the Lockheed Independent Research Programme. KJHP and JRL are funded by the UK Science & Engineering Research Council. We would like to thank Dr. J.R. Saba and M.X. Levay for their help in preparing this presentation.

REFERENCES

L.W. Acton et al. 1981, Astrophys. J. (Lett.), 244, L137.
M. Loulergue and H. Nussbaumer 1975, Astron. & Astrophys., 45, 125.

MEASUREMENT OF THE INCREASE IN ALTITUTE OF THE SOFT X-RAY EMISSION REGIONS OF SOLAR FLARES

J.F. Seely and U. Feldman
E.O. Hulburt Center for Space Research
Naval Research Laboratory
Washington, DC 20375-5000

The upward motion of the hot thermal regions of several large (M type) solar flares have been determined from the soft X-ray spectral data recorded by the scanning spectrometer (SOLFLEX) on the P78-1 spacecraft. The change in position of the emission is measured with a spatial resolution of 2000 km and a temporal resolution of 58 sec. For the limb flares that are studied, the centroid of the Ca XIX emission region moves to a higher altitude with a speed of 20 to 40 km/sec for a period of 20 to 30 minutes following onset of the flare and reaches an altitude of 30,000 to 40,000 km. The speed of ascent decreases with time, and in several flares that are studied, there is an indication that the centroids of the Ca XIX emission oscillate in altitude with amplitudes of 5,000 to 10,000 km and with periods of 5 to 8 minutes.

DERIVATION OF THE IONIZATION BALANCE FOR IRON XIV/XXV AND XXIII/XXIV USING SOLAR X-RAY DATA

E. Antonucci, M.A. Dodero
Istituto di Fisica, University of Torino, Italy
A.H. Gabriel
Rutherford Laboratory, Chilton, U.K.
K. Tanaka
Tokyo Astronomical Observatory, University of Tokyo, Japan

The relative concentrations of different ionization stages of iron are measured using the spectral emission of plasmas formed during solar flares. This is an extension of a study on the ionization balance of heavy elements, initiated with the analysis of calcium solar spectra (Antonucci et al., 1984). The data consist of a large set of iron spectra in the wavelength range from 1.84 to 1.88 Å, detected during the recent maximum of activity with the X-ray Polychromator Bent Crystal Spectrometer (BCS) on the NASA Solar Maximum Mission satellite and on the Soft X-ray Crystal Spectrometer (SOX) on the Hinotori satellite.

At the low densities typical of the solar corona, in the steady state the ionization balance of an element is a function of the plasma electron temperature. Hence, it can be measured for plasmas of known temperature and in slowly varying physical conditions, and in most cases, solar flare plasmas can be considered to be in such conditions.

The flares have been chosen to cover a wide range of temperatures. The iron spectra at flare onset have not been included in the analysis. A set of 273 spectra detected with the BCS and 54 spectra detected with the SOX spectrometer have been studied. The flare emission has been accumulated for periods varying from 60 to 120 seconds.

One example of iron spectrum, used in the analysis is shown in Figure 1; it has been obtained with the SOX spectrometer. At the longer wavelength side of the Fe XXV resonance line, well-resolved satellite lines are observed. The use of dielectronic satellite spectra to derive a number of plasma parameters is discussed in Gabriel (1972). The ratio of j to w, the resonance line, depends only on the electron temperature T_e, while the ratio of q to w depends predominantly on the Li-like to He-like ion concentration, N (Li)/N (He), and the ratio l to w depends almost entirely on the Be-like to He-like ion concentration, N (Be)/N (He). The notation of Gabriel (1972) is used for lines. The electron temperature and ion concentrations are determined by computing the synthetic spectrum which best fits the data. The method of analysis is described in Antonucci et al. (1982) and the atomic theory used to compute the intensity of the emission for the He-like and Li-like ions is by Bely-Dubau et al. (1982) and for the Be-like ions is by Dubau (private communication).

The results of the fitting procedure are displayed in Figure 2 and 3, where the N (Li)/N (He) against Te and the N (Be)/N (Li) against T_e curves are plotted. The dots denote BCS data points and the crosses SOX data points. In the same figures, the theoretical ionization balance curves from Doyle and Raymond (1981), Shull and Van Steenberg (1982), Jordan (1969), Jacobs et al. (1977) and Urnov et al. (1981) are shown. The experimental results differ from the theoretical predictions by an amount which is larger than random errors.

The experimental curves are a measure of ionization balance, provided the flare plasma is in steady state and isothermal conditions. The steady state is ensured since the flare analysed have rise and decay times of minutes. Moreover,

the data points obtained in different flare phases define the same ionization balance curves.

In the case of non-isothermal plasmas the derived electron temperature and ion concentrations are average values. The effect of the weighting involved in the averaging on the definition of these quantities can be tested by constructing different model flare plasmas, with different non-isothermal distributions. The procedure is explained in more detail in Antonucci et al. (1984). A range of plasma temperature distributions from isothermal to almost flat distributions is considered. In this way it is possible to determine the uncertainty in the derivation of the Fe XXIII, Fe XXIV and Fe XXV ion abundances, due to temperature distributions substantially deviating from isothermal conditions. In Figure 4, the ion abundances experimentally measured (E) are compared with the theoretical curves (S-V) computed by Shull and Van Steenberg (1982).

The experimental continuous curves are derived for isothermal conditions, while the dashed ones are derived by considering the observed line ratios as produced by a non-isothermal plasma with temperature distributions of exponential form. The discrepancy between the experimental and theoretical values, in Figure 4, is considerably larger than the uncertainty in the derivation of the experimental values, due to possible deviations of the plasma from isothermal conditions. The discussion of the experimental ionization balance for iron will be presented in more extended form in a paper in preparation.

REFERENCES

Antonucci, E., Gabriel, A.H., Acton, L.W., Culhane, J.L., Doyle, J.G., Leibacher, J.W., Machado, M.E., Orwig, L.E., and Rapley, C.G., 1982, Solar Phys., 78, 107.

Antonucci, E., Gabriel, A.H., Doyle, J.G., Dubau, J., Faucher, P., Jordan, C., and Veck, N., 1984, Astron. Astrophys., 133, 239.

Bely-Dubau, F., Dubau, J., Faucher, P. and Gabriel, A.H., 1982, Monthly Notices Roy. Astron. Soc., 198, 239.

Doyle, J.G., and Raymond, J.C., 1981, Monthly Notices Roy. Astron. Soc., 196, 907.

Gabriel, A.H., 1972, Monthly Notices Roy. Astron. Soc., 160, 99.

Jacobs, V.L., Davis, J., Kepple, P.C. and Blaha, M., 1977, Astrophys. J., 211, 605.

Jordan, C., 1969, Monthly Notices Roy. Astron. Soc., 142, 501.

Shull, J.M. and Van Steenberg, M., 1982, Astrophys. J. Suppl., 49, 351.

Urnov, A. et al., 1981, Lebdev Inst. preprint.

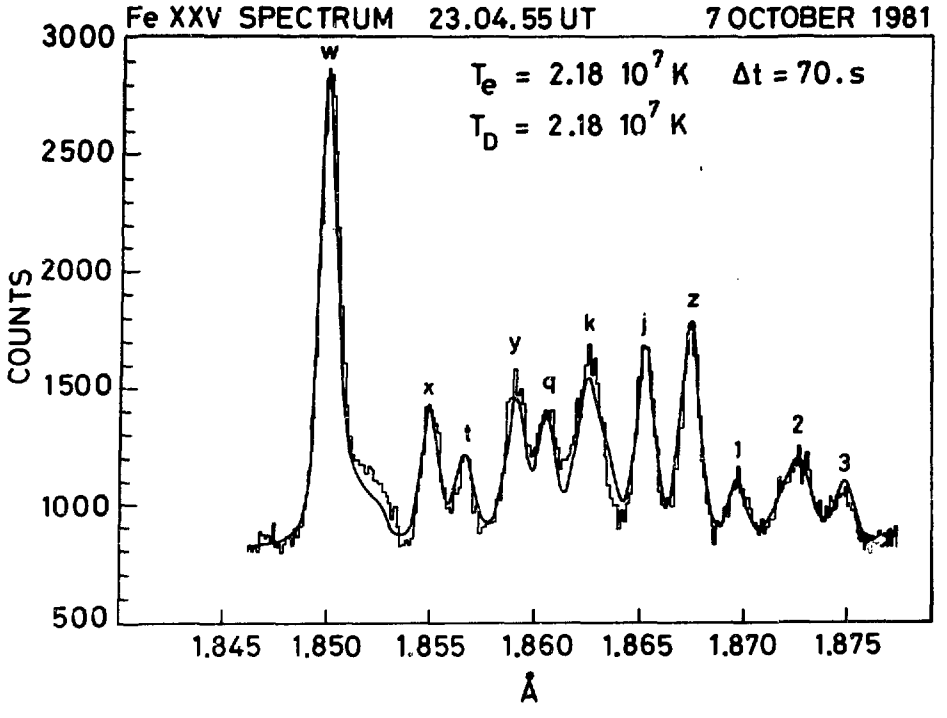

Figure 1. Fe XXV flare spectrum obtained with the SOX spectrometer

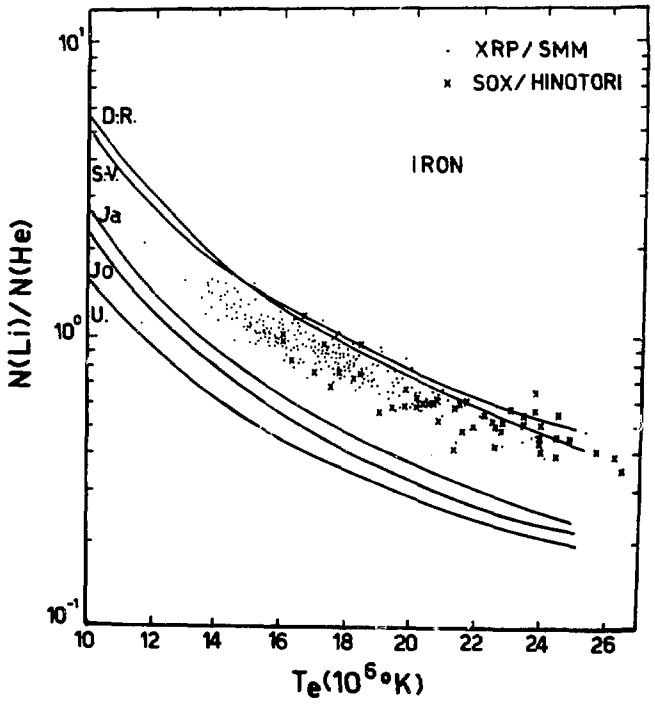

Figure 2. Ionization balance versus temperature for flare spectra

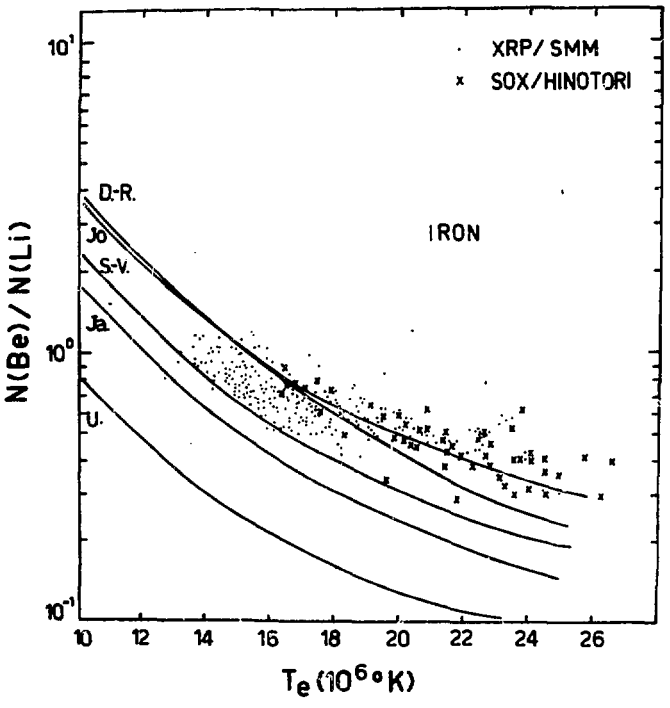

Figure 3. Ionization balance versus temperature for flare spectra

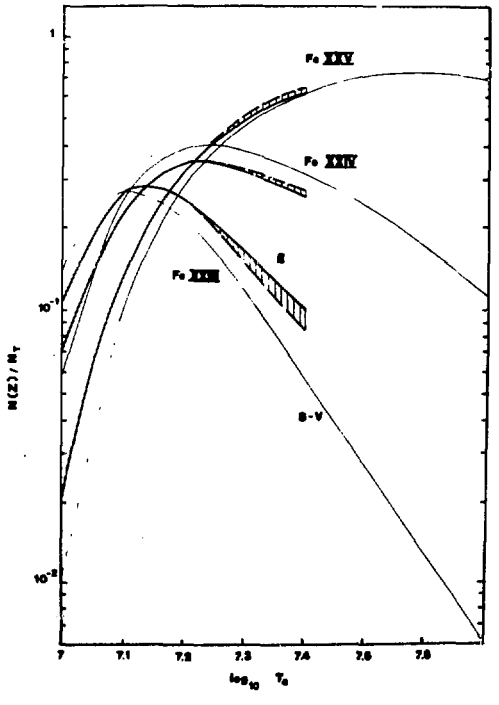

Figure 4. Fe XXIII, Fe XXIV and Fe XXV ion abundances versus temperature.

OBSERVATIONAL EVIDENCE FOR CORONAL MAGNETIC RECONNECTION DURING THE TWO-RIBBON FLARE OF 21 MAY 1980

R.A. Kopp
Los Alamos National Laboratory
Los Alamos, NM 87545

G. Poletto
Osservatorio Astrofisico di Arcetri
50125 Firenze

The 21 May event was a large two-ribbon flare which occurred in active region 2456 at S13W15. The flare was extensively documented by coordinated Hα, X-ray, and magnetograph observations. In particular, spatially resolved images in hard X-rays were obtained by the Hard X-ray Imaging Spectrometer (HXIS) aboard SMM. Hence this flare comprises an ideal example for studying the spatial relationship between the X-ray and Hα-ribbon morphologies. Although evidence has been reported for magnetic flux emergence at the beginning of this flare (Harvey, 1983), it appears that a potential field (rising source-surface) model may adequately represent the major large-scale features of the magnetic configuration believed to result from fieldline reconnection in the corona during the decay phase (Kopp and Pneuman, 1976).

The enhanced ohmic heating associated with magnetic merging suggests trying to observe the signature of the reconnection process directly in the form of localized thermal X-ray emission from the region around the neutral point. As reconnection proceeds and the neutral point rises into the corona, we would expect the X-ray source region to move to sequentially greater heights above the flare site and the emission to shift toward lower energies. For a flare located at some distance from the center of the solar disk, then, the centroid of X-ray emission should appear to drift toward the limb as the event progresses. Moreover, the X-ray source drift rate should roughly mimic that of the Hα ribbons - i.e., it should be rapid at first, whereas later in the event, as the ribbons become nearly stationary in position, this motion should be greatly reduced. These trends should be readily observable for the flare of 21 May, 1980.

To this end we measured the flare ribbon separation over the time interval from 21:00 to 23:00 U.T. from full-disk Hα filtergrams provided by NOAA's World Data Center. The resulting profile of ribbon separation versus time displays a steep initial rise, starting from a separation of ~25,000 km at 21:05 U.T. and growing to ~38,000 km at 21:30 U.T. Subsequently the ribbon motion slows down considerably, and a maximum separation of ~45,000 km is reached by 23:00 U.T.

In the same time interval an analysis of HXIS images of the flare region reveals that the location of maximum X-ray emission shifts gradually southwards with time, while showing up in progressively lower energy channels. We assume that, in the highest energy channel of HXIS for which measurable emission is present at any instant, the position of the brightest pixel corresponds to the tops of newly reconnected field lines. Then one can take into account projection effects and easily derive the true height of these loops, provided that they lie vertically above the chromospheric magnetic neutral line. The position of strongest HXIS emission is shown as a function of time in Figure 1, in

terms of either projected distance from the $H_{\parallel} = 0$ line (left scale) or height above the solar surface (right scale). A more detailed description of the HXIS observations of this flare has been given by Švestka and Poletto (1984).

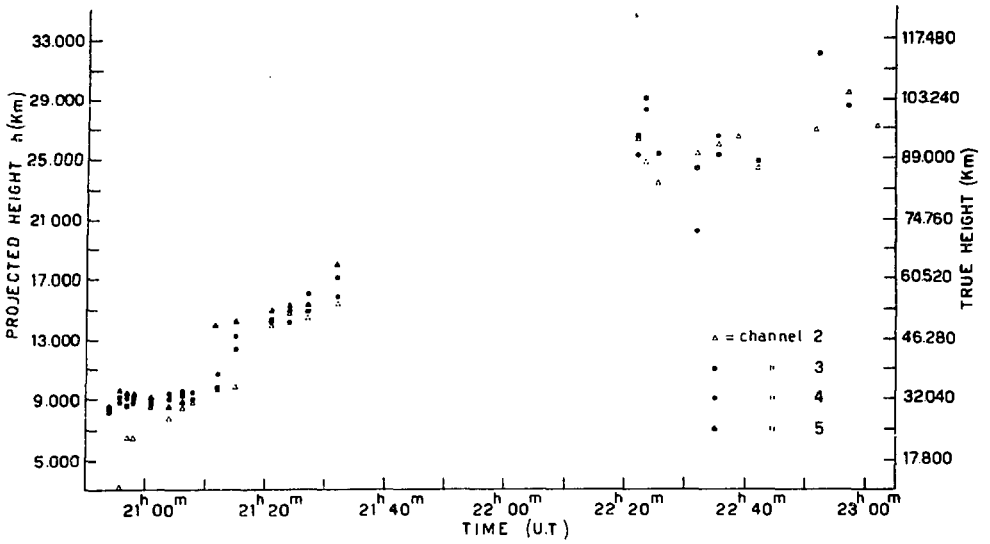

Figure 1. Position of the brightest X-ray emitting region as a function of time. Left scale: the projected distance of the region from the magnetic neutral line ($H_{\parallel} = 0$) in the chromosphere. Right scale: true height derived under the hypothesis of vertical loops.

In view of the qualitative agreement between the observed and expected behaviors of the hard X-ray emitting region, we have attempted to test these ideas more rigorously by using a specific magnetic field model for the reconnection geometry to predict the height of the neutral point as a function of Hα ribbon separation. Using the observed ribbon-separation time history mentioned above, this prediction can then immediately be compared with the true heights of the X-ray source region shown in Figure 1.

The magnetic model used for this purpose has been described at length elsewhere (Kopp and Poletto, 1984). It consists of an axisymmetric potential field model between the solar surface ($r = r_o$) and an equipotential spherical source surface ($r = r_1 > r_o$), joined smoothly to a nonpotential radial field beyond r_1. For simplicity the normal component of the surface magnetic field in the active region is approximated by one "lobe" of a single high-degree Legendre polynomial, chosen to represent approximately the location and latitudinal width of the region. The neutral point lies on the source surface directly above the chromospheric $H_{\parallel} = 0$ line, and the reconnection process is modeled by allowing r_1 to increase with time in a prescribed manner. Within the framework of this simple model, the leading edges of the expanding flare ribbons are defined by the intersection with the solar surface of the two magnetic separatrices passing through the neutral point.

For the 21 May, 1980 flare, the physical size and disk position of the active region are well represented by the 21-st lobe of a P_{48}-field.

The solid curve in Figure 2 shows the resulting theoretical prediction of ribbon separation as a function of height of the neutral point. The open circles, by comparison, give the observed separation of the leading edges of the Hα ribbons versus the true height of X-ray emission. This comparison clearly reveals that, although the empirical relation exhibits the same overall trend as the predicted one, the X-ray emission for a given ribbon separation appears to originate from a greater height than that where the reconnection is occurring. There are at least two possible explanations as to why this behavior differs from the results of previous studies (e.g., Kopp and Poletto, 1984).

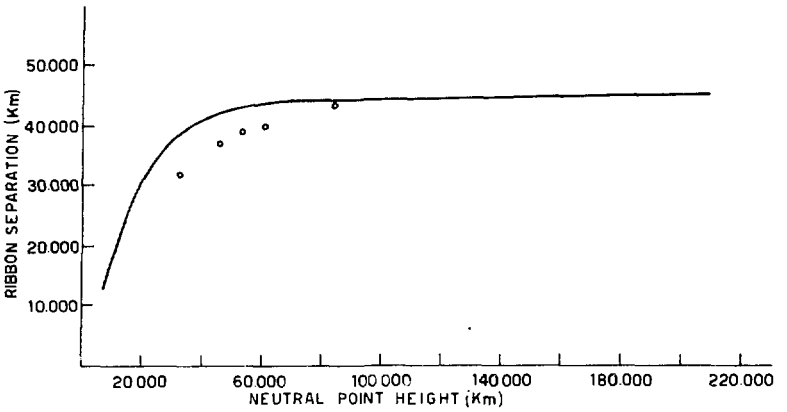

Figure 2. Solid curve: predicted relationship between ribbon separation and neutral point height. Open circles: HXIS loop heights versus ribbon separation.

First, note that spatially resolved X-ray observations of two-ribbon flares prior to the SMM generally tended to emphasize the softer spectral regions, with relatively low sensitivity in hard X-rays. But, as we indicated at the outset, the position of the reconnection region at any time should correspond to the zone from which the very hardest thermal X-rays are being emitted, with softer X-rays coming from lower heights. Therefore, unless the hard X-ray emission from a particular flare is unusually intense, such data could have easily caused one to underestimate the height where reconnection is occurring. In this case the apparent conformity found earlier between observations and model predictions would be fortuitous. To improve the agreement in the present example, one could perhaps modify the model slightly by considering that the actual fieldline geometry near the neutral point may have a more slender cusp shape than that which characterizes the source-surface model. This would raise the reconnection region to coincide spatially with the hard X-ray source region, while leaving unchanged the remaining properties of the model.

Alternatively, we consider the possibility that the reconnected loops do not lie in a vertical plane; such has already been suggested by Švestka et al. (1982). If the loops were inclined away from disk center, then the true heights from which the HXIS emission originates would be lower than we have estimated here, and the observed hot loop heights might still coincide with the predicted neutral point heights. However,

this situation could only be described adequately by a three-dimensional model.

On the basis of correlative observations of a single flare, one cannot decide between these two possibilities. It could also be the case that each of these explanations applies at different times during a given flare, depending upon the magnetic field configuration at the sun's surface; additional examples of two-ribbon flares with complete X-ray and magnetograph coverage are needed to draw a definite conclusion.

REFERENCES

Harvey, J.W. 1983, Adv. Space Res., 2, 31.

Kopp, R.A. and Pneuman, G.W. 1976, Solar Phys., 50, 85.

Kopp, R.A. and Poletto, G. 1984, Solar Phys., in press.

Švestka, Z., Stewart, R.T., Hoyng, P., Van Tend, W., Acton, L.W., Gabriel, A.H., Rapley, C.G., Boelee, A., Bruner, E.C., de Jager, C., Lafleur, H., Nelson, G., Simnett, G.M., Van Beek, H.F., and Wagner, W.J. 1982, Solar Phys., 75, 305.

Švestka, Z. and Poletto, G. 1984, Adv. in Space Res., in press.

VARIATION OF THE OBSERVED CORONAL CALCIUM ABUNDANCE FOR VARIOUS X-RAY FLARE PLASMAS

J. Sylwester
Space Research Center
Polish Academy Of Sciences

J.R. Lemen
Mullard Space Science Laboratory

R. Mewe
Laboratory for Space Research, Utrecht

We present the first observational evidence for the variation of the coronal calcium abundance in the high-temperature solar flare plasmas. The analyzed data consists of the X-ray flare spectra observed by the Solar Maximum Mission satellite with the Bent Crystal Spectrometer. From BCS spectra we derived the ratio of the line to continuum flux I_L/I_C for the resonance line of Ca XIX λ = 3.1781Å and the continuum at the same wavelength as a function of the temperature. The studies of 13 flares showed similar temperature dependence during the decay phases, but the agreement of the I_L/I_C ratio from flare to flare could only be achieved by adjusting an overall normalization factor. As the continuum flux depends weakly on the heavy elemental abundance, this variation of the I_L/I_C ratio can be attributed to the variation in the calcium abundance. For the flares considered, the variation between the extreme cases represented the factor of 2.5. We stress the consequences of the observed abundance variation for the analysis and interpretation of XUV and X-ray spectra.

HRTS ULTRAVIOLET SOLAR SPECTROSCOPY

K.P. Dere
E.O. Hulburt Center for Space Research
Naval Research Laboratory
Washington, D.C. 20375-5000, USA

The NRL High Resolution Telescope and Spectrograph (HRTS) consists of a telescope, stigmatic UV spectrograph, UV broadband spectroheliograph and Hα film and video cameras. An image of the Sun is focussed onto the slit jaws of the spectrograph by a 30 cm Cassegrain telescope with a spatial resolution of 1". The stigmatic UV spectrograph employs a tandem-Wadsworth mount and photographically records spectra along the 1000" (1 solar radius) slit with a resolution of 50 mÅ in the 1170-1710 Å wavelength region. Images of the slit jaws in a tunable 100 Å bandpass are produced on film by the UV spectroheliograph which uses a reversed tandem-Wadsworth mount. The slit jaws are also viewed through an Hα filter by video and film cameras. To date, the HRTS instrument has flown on four rocket flights and is being prepared for flight on Spacelab-2.

The data are returned as simultaneous stigmatic spectra of the complete 1170-1710 Å spectrum for each individual feature imaged on the slit. Visual inspections of the spectra turned up a number of phenomena which showed distinctive Doppler shifts. The first of these were termed "coronal jets" (Brueckner and Bartoe, 1983). They consist of plasma at temperatures from 2 x 10^4 K to 2 x 10^5 K which are accelerated at 5 km s^{-2} up to velocities of 400 km s^{-1}, roughly the coronal sound speed. In one case, four of these jets developed sequentially at the same location during a four minute rocket flight. Their extent along the slit is typically 7000 km. Erupting magnetic loops or bubbles would be consistent with the observed spectra. Brueckner and Bartoe suggested that there is enough mass, momentum and energy in these jets to cause the solar wind. Another possibility is that these are the small scale end of a range of eruptive phenomena, including coronal transients that are as a whole responsible for the production of the solar wind.

Another category of events with distinctive Doppler signatures is the so-called "explosive event." These have Doppler shifts (red, blue or both) on the order of 100 km s^{-1} and spatial scales which are often near the instrumental resolution. This category encompasses a wide range, not all of which are obviously related. However, in general, these features are distributed isotropically over the solar disk and there is no apparent correlation between their Doppler signature and solar latitude. Whether they are observed above the limb or on the disk, they appear to be more or less similar. From this it can be concluded that, in general, the flow velocities are isotropic as might result from an explosion. A wide range of timescales, from 20s to greater than 200s, is evident. There does appear to be a distinct subclass which are called "turbulent events," which are distinguished by the symmetry of their Doppler shifts that may be the result of enhanced turbulent velocities in the emitting plasma.

The two sunspots observed on the disk during separate flights both show high-speed downflows of chromospheric and transition zone material. In both cases, the sunspot contained a light bridge, but the nature of the flow pattern were considerably different. In the first case, small regions (1000 km across) were found scattered throughout the spot. The downflow velocities were on the order of 100-150 km s^{-1}. In the second case, a continuum of downflow velocities from 0 km s^{-1} up to a maximum of about 175 km s^{-1} were found throughout the area of the spot, with maximum velocity and intensity attained over the light bridge.

In the supergranular cell centers, the lines of the strong C I multiplets near 1561 Å and 1657 Å show small scale (2000 km FWHM) structures that are the site of 10-20 km s^{-1} flows which we refer to as chromospheric jets (Dere, Bartoe and Brueckner 1983). Both red and blue shifts are seen although the blue shifts are brighter and more numerous. Their average lifetime is on the order of 40s. There is considerable opacity in the C I lines so that the velocities deduced from the line profiles may be exaggerated by radiative transfer effects. The chromospheric jets are best seen in the C I lines but also appear in most chromospheric lines. In Si I, the deduced Doppler shifts are on the order of 3-5 km s^{-1}. Since these events occur in the cell center, the C IV intensity is on average quite low. Nevertheless, there is no indication from C IV emission that these chromospheric jets ever reach transition zone temperature (3×10^4 K or greater). What is surprising is that events such as these are found only in the cell centers. Spicules, when seen at the limb, show a 25 km s^{-1} outward velocity and it is generally assumed that spicules are found on the disk in the supergranular cell boundaries. We find no evidence of 25 km s^{-1} spicular flows in any of our chromspheric lines in the boundaries.

More typical profiles of optically thin chromospheric and transition zone lines are Gaussian with subsonic Doppler shifts. The wavelength scale on which these Doppler shifts are measured is derived from measurements of the numerous narrow Si I lines in this wavelength region. The Si I lines themselves show small flow velocities with a standard deviation of 2 km s^{-1}. The measurement of the Doppler shift of any individual line profile has an accuracy of about 2 km s^{-1}. Ions such as C IV and Fe II have multiple lines in the spectrum so that the errors in their measured Doppler shifts can be reduced through averaging. Chromospheric lines of Fe II show RMS Doppler shifts of ± 2.4 km s^{-1} about a near zero average Doppler shift. Again, there are no spicular (25 km s^{-1}) velocities derived from the Fe II profiles. The C IV disk velocity distribution is characterized by an average red shift (downflow) of 5 km s^{-1} with a standard deviation of 6 km s^{-1}. Clearly, there are very few blue shifts found and most that are tend to be associated with the explosive events. Syphon flows, therefore, cannot play any significant role in describing transition zone flow patterns. Pneumann and Kopp (1977) suggested that this downward enthalpy flux should be a significant source of the energy that is lost in the transition zone through radiation. If so, one might expect to find a correlation between

local downflow velocity and intensity. However, the data shows no such correlation. It has also been suggested that the turbulent velocities derived from transition zone line profiles are the result of propagating acoustic (Boland et al., 1973) or Alfven waves which could be an alternate source of transition zone heating. The HRTS data shows a relatively high correlation between C IV line intensity and line width for the near-Gaussian profiles, in support of these ideas (Dere, Bartoe and Brueckner, 1984).

From the data obtained on the third rocket flight, time series of profiles covering a duration of 200s at 20s intervals have been constructed. Aside from the chromospheric jets, chromospheric lines show small temporal variations and smooth variations along the slit. On the other hand, the time series of C IV spectra is made up of distinct individual elements with a FWHM size of 3" that evolve throughtout the rocket flight. Three such elements have been studied in some detail. Two show only small fluctuations (10% RMS) in intensity with small accelerations in downflow velocity of 2-5 km s^{-1} in 200s. A third shows a strong rise in red shift from 15 km s^{-1} to 22 km s^{-1} in 40s and a gradual decay to a red shift of 15 km s^{-1} in 100s, all accompanied by only 10% variations in the intensity of the emitting element.

During the third HRTS rocket flight, the slit was rastered across a 10" wide region of the quiet sun. The information in line profiles such as intensity, velocity and line width can then be assembled into images of these same quantities of a 10" x 800" area of the Sun. These images show definite patterns or structures outlined by the intensity and velocity fields. Consequently, the C IV elements revealed by the time series are segments of these larger structures which are most likely organized by the magnetic field configuration. Images of the chromospheric line intensities coincide with dark Hα mottles while the C IV emission is produced at the tips of the mottles, roughly 2000 km above the chromospheric emission. Downflow patterns in Fe II often resemble similar downflow patterns in C IV, although there may be a spatial displacement of several thousands of km between the two.

REFERENCES

Boland, B.C., Engstrom, S.F.T., Jones, B.B. and Wilson, R. 1973, Astr. Astrophys., 22, 161.

Brueckner, G.E. and Bartoe, J.-D.F. 1983, Astrophys. J., 272, 329.

Dere, K.P., Bartoe, J.-D.F. and Brueckner, G.E. 1983, Astrophys. J. (Letters), 267, L65.

Dere, K.P., Bartoe, J.-D.F. and Brueckner, G.E. 1984, Astrophys. J., 281, 870.

Pneuman, G.W. and Kopp, R.A. 1977, Astr. Astrophys., 55, 305.

INTERPRETATION OF ELECTRIC FIELDS IN CORONAL MAGNETIC LOOPS

P. Foukal
Atmospheric and Environmental Research, Inc., Cambridge, MA 02139
D. Landman
Institute for Astronomy, University of Hawaii, Honolulu, HI 96822

1. INTRODUCTION

Stark effect detected in high Balmer lines emitted from flares, prominences, and quiet chromosphere is generally interpreted as pressure broadening in a plasma of relatively high density. But a recent study of post-flare loops indicates that the densities of order 10^{12} cm^{-3} required to explain the observed Balmer line broadening are an order of magnitude higher than values derived using other plasma diagnostics such as Thomson scattering and Balmer line emission measures (Foukal, Miller, and Gilliam 1983). The disagreement might be explained as the difference expected between the true local density (measured by the Stark effect) in the obviously inhomogeneous loop plasma, and the straight mean or root mean square densities measured by Thomson scattering and line emission measures. More interestingly, the disagreement might imply a macroscopic electric field generated by, e.g., plasma waves in coronal magnetic loops.

The purpose of this study is to distinguish between these two interpretations using the density sensitivity of certain MgI, NaI, and SrII line intensity ratios recently calculated by Landman (1983, 1984). The lines of interest are formed at roughly the same temperatures as the Balmer lines and turn out to be quite bright in post flare loops. Since these line ratios respond to the local density in the loop condensations, comparison of the densities obtained simultaneously and co-spatially from them and from Stark effect should yield fairly direct information on possible macroscopic electric fields.

2. INSTRUMENTATION AND OBSERVING PROCEDURES

The spectra of post-flare loops analyzed here were obtained at the 40 cm coronograph and Universal spectrograph at the SPO Big Dome. Most of the spectra cover the wavelength region between approximately 3600 Å and 4500 Å in a single 10-30 sec exposure, at a dispersion of 1.6 Å/mm in third order at 3950 Å. This wavelength range includes the density sensitive line ratio MgI($\lambda\lambda$3833,3838)/SrII(λ4078) on one frame, together with the Balmer lines of interest down to the series limit. In order to measure the two other useful line ratios calculated by Landman; MgI($\lambda\lambda$5173,5184/SrII(λ4078) and NaI($\lambda\lambda$5890,5896)/SrII(λ4078) the intensities of the MgI b and NaI D lines must be measured from a separate spectrum obtained several minutes later. Since pointing errors and loop evolution can lead to significant changes over this time scale, the values of density obtained from these two ratios carry less weight.

3. DATA AND REDUCTION PROCEDURE

The spectra were traced on a microdensitometer and the background (sky-scattered Fraunhofer spectrum) was subtracted. The lines were then fitted with least-squares Gaussian profiles to derive FWHM values $\Delta\lambda_{1/2}$ for the Balmer lines, and peak intensities for the relevant lines of MgI, NaI, and SrII. Fig. 1 shows the spectral regions around the MgI($\lambda\lambda$3833,3838) lines and around the SrII(λ4078) line, for one of the spectra taken of a bright loop on 19 Dec. 1982. These lines were well calibrated in all our loop spectra. The calibration data required to compare I(λ4078) to the MgI b and NaI D line intensities were only available for the one loop of 11 Aug. 1972, so only for that loop were we able to derive densities from all three of the ratios calculated by Landman.

4. RESULTS

a) Stark effect

Fig. 2 shows plots of the observed Balmer line halfwidths $\Delta\lambda_{1/2}$ against the upper principal quantum number n, for two of the five loops. The solid curves are quadratic fits to the data. These two loops, for which four and five spectra each are averaged, show a clear broadening beyond H 12-14, which suggests Stark effect. The dashed curves represent the values of $\Delta\lambda_{1/2}$ taken from tabulated Stark effect calculations of Kurochka (1969). These tables give total halfwidths for different values of Gaussian broadening due to thermal, microturbulent motions and instrumental function. The plotted curves provide the best fit to the minimum observed halfwidth near n = 10 and to the halfwidth increase between n ~ 10 and n ~ 20. The densities required to produce the observed broadening are in the range 1-2 x 10^{12} cm^{-3}.

Similar plots for the three other loops, for which only one spectrum each was reduced, show some evidence of a broadening of comparable slope, but at a considerably lower significance level. Only for the two loops discussed above do we have sufficient data to show that the trend of halfwidth with Balmer number is significant.

b) Line Ratios

Fig. 3 shows calculated curves of the most observationally reliable line intensity ratio I($\lambda\lambda$3833,3838)/I(λ4078) against density for T_e = 5 x 10^3 K and 8 x 10^3 K, showing the range of the ratio observed in these loops and the corresponding densities. In the two loops for which several Balmer line spectra are available, the densities obtained from this intensity ratio are 1-2 x 10^{12} and > 10^{13} cm^{-3}. The densities found in the other three loops (at an equal level of significance) are much lower, between 1-3 x 10^{11} cm^{-3}.

The line-ratio densities obtained from the two ratios carrying lower weight show a large scatter, not in very good agreement with the I($\lambda\lambda$3833,38)/I(λ4078) ratio densities presented above. This large internal variation is probably caused by the pointing and loop evolution errors mentioned previously.

5. CONCLUSIONS

The main conclusions of this study so far are:

i) The Stark effect and line intensity ratio diagnostics agree to within a factor 2 when the data of highest statistical weight are compared. They both indicate high densities of $n_e \gtrsim 10^{12}$ cm^{-3} in the cool condensations within post-flare loops. This is encouraging agreement for two plasma diagnostic techniques with quite different sources of error.

ii) These data of highest weight indicate that electric fields in post flare loops can be understood as pressure broadening expected in a dense plasma. Large scale d.c. or plasma-wave electric fields as large as 10^2 volts cm^{-1} may also be present, but they would be difficult to detect by this technique alone.

iii) The I(λλ5173,5184)/I(λ4078) and I(λλ5890,5896)/I(λ4078) ratios seem to yield lower values for the loop condensations than does the I(λλ3833,3838)/ I(λ4078) ratios. This disagreement is most likely due to pointing changes and evolution of the loop condensations, since the former two ratios were not accessible on one exposure. But a larger sample of loop spectra on which at least one of the other two line ratios can be measured simultaneously would be desirable to verify the high densities recorded in the ratio I(λλ3833,3838/I(λ4078).

iv) The three loops for which the Balmer line broadening has lower weight show a Stark effect that would still require $n_e \sim 0.5\text{-}2 \times 10^{12}$ cm^{-3}, but the line ratio density yields a value of only $1\text{-}3 \times 10^{11}$ cm^{-3} for these loops. One might conclude that all post-flare loops contain macroscopic E fields of order 10^2 v cm^{-1}, and only in the most dense loops does the pressure broadening produce microscopic electric fields of the same order. A larger sample of loops needs to be studied to check this possibility.

ACKNOWLEDGEMENTS

We thank L. Gilliam at SPO for obtaining the excellent spectra analysed here, and C. Hoyt at AER for invaluable assistance in carrying out the microdensitometry and in the reduction. This work was supported at AER under NSF grant AST 8217384, and at the Institute for Astronomy under NASA grant NGL-12-001-011, and NSF grant AST 81-16311.

References

Foukal, P., P. Miller, and L. Gilliam, Sol. Phys., 83, 83, 1983.

Kurochka, L., Soviet Astr. (A.J.), 13, 64, 1969.

Landman, D., Ap. J., 269, 728, 1983.

Landman, D., Ap. J., 279, 438, 1984.

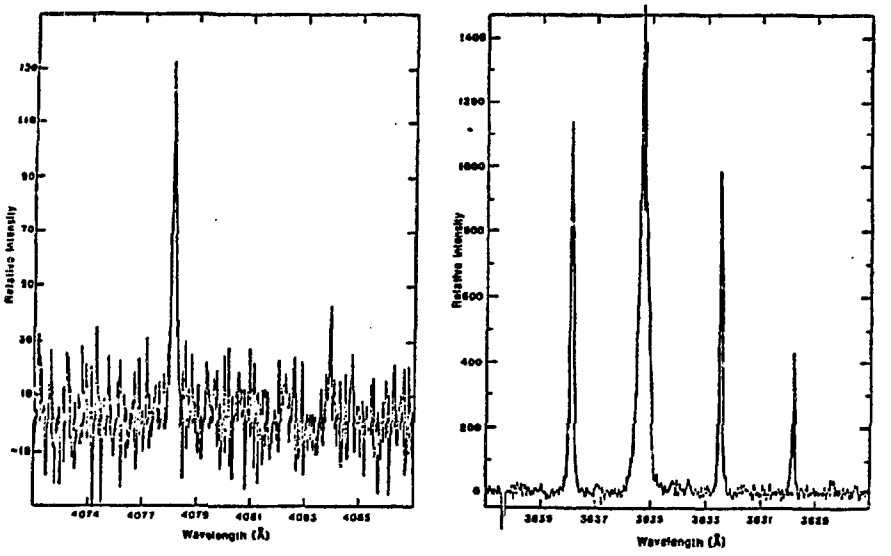

Figure 1. The spectral regions around the SRII(λ4078) line (left) and MgI(λλ3833,3838) lines (right) in the spectrum of the loop observed on 19 Dec. 1982.

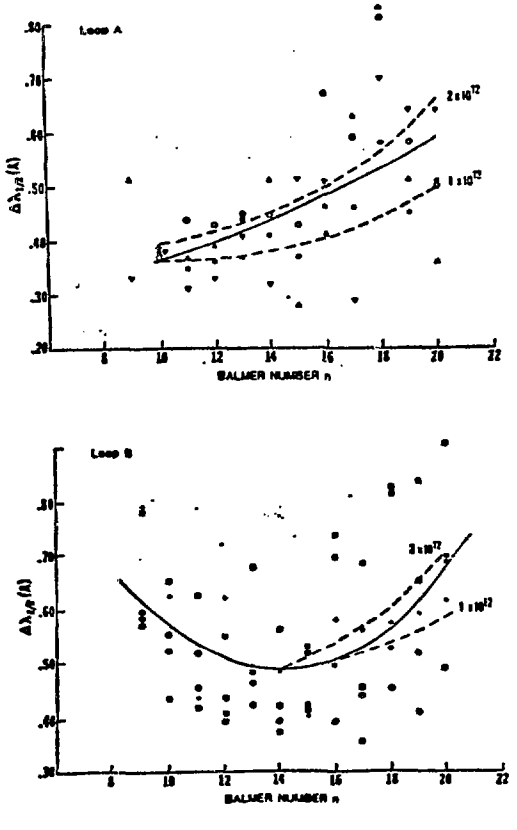

◄ Figure 2. Plots of the FWHM $\Delta\lambda_{1/2}$ of Balmer lines against upper principal quantum number n, for the two loops of highest statistical weight. See text for explanation of the dashed lines.

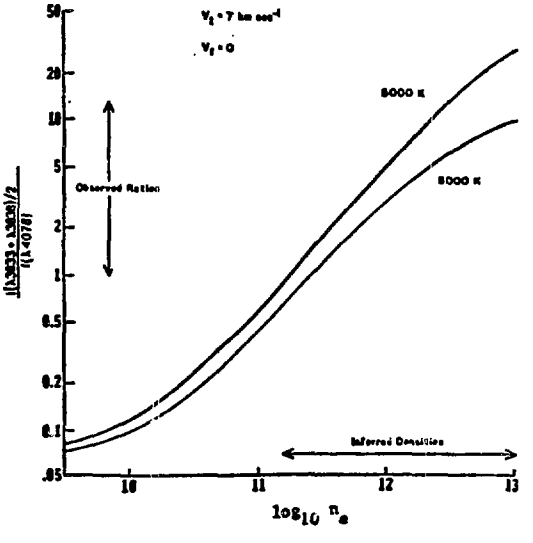

Figure 3. Plot of the MgI intensity ratio against electron density.

THE SOLAR WIND GENERATION EXPERIMENT FOR SPARTAN MISSION 201

J.L. Kohl, H. Weiser, G.L. Withbroe
Harvard-Smithsonian Center for Astrophysics
Cambridge, MA 02138

and

R.H. Munro
High Altitude Observatory
Boulder, CO 80307

The Solar Wind Generation Experiment consists of a UV Coronal Spectrometer (UVCS) provided by the Harvard-Smithsonian Center for Astrophysics and a White Light Coronagraph (WLC) of the High Altitude Observatory. The instruments are similar to those flown together on three sounding rocket flights [1,2,3] but they have enhanced capabilities to take advantage of Spartan's 27 hour observing period. The two instruments comprise a payload for Spartan 2, which is a self-contained instrument carrier that provides on-board data storage, power, thermal control, sun pointing and an observing program sequencer. Spartan is launched and deployed by the Shuttle and spends about 27 orbits in a detached mode before it is recovered and returned to the ground for data tape retrieval and post-flight instrument calibration.

A major scientific objective of the Spartan Mission 201, which is planned for mid-1986, is to discover the coronal source region of the "slow speed" solar wind. A new spectroscopic diagnostic technique which utilizes observations of the C VI lines at λ1032 and λ1037 and the polarization and brightness of visible light [4,5] will be used to measure slow speed ($\geq$ 30 km s^{-1}) outflows in helmet streamers, the boundaries of coronal holes, the quiet corona, and active region streamers. The instruments will also determine electron densities and proton kinetic temperatures in such regions [6]. Another major objective is to obtain a more complete description and understanding of the physical processes operating in broad polar coronal holes which are believed to be a source of high speed polar wind streams. The high outflow velocities in such regions will be determined from Doppler dimming of H I Lyman-α [6] and from the observed ratio of O VI λ1032/λ1037 [5]. The UVCS will also be used to assess the feasibility of determining coronal electron temperatures from measurements of the spectral line profile of electron scattered H I Lyman-α [6].

Spartan Mission 201 is intended to make a significant step toward achieving an understanding of the nature of the unknown sources of non-radiative energy flux that enters the corona from lower atmospheric layers and interacts with the coronal plasma to produce its high temperature and its acceleration to supersonic flow as the solar wind. The basic nature of the non-radiative energy flux and its mode of interaction with the coronal plasma, neither of which is understood, should be reflected in the measured temperature, density, and velocity structures of the corona.

An instrument similar to WLC has been described by MacQueen et al. [7]. The WLC for Spartan 2 is equipped with a CCD detection system which facilitates simultaneous polarization and brightness measurements of the electron-scattered white light radiation from a 270° segment of the corona between 1.5 and 6 $R_\odot$. The spatial resolution is 25" x 25". The wavelength band measured is 4400-5400 Å.

The occulting system for the UVCS has been described by Kohl, Kirkham and Reeves [8]. The instrument for Spartan 2 has a dual telescope-spectrometer system and two detection systems. One of the two separate optical systems is optimized for measurements of H I Lyman-α and the other for O VI λ1032 and λ1037. A discrete anode microchannel array detector simultaneously observes 42 spectral elements across the H I Lyman-α line profile and also detects the electron scattered H I Lyman-α profile with 2 Å resolution elements between λ1175 and λ1260 Å. The O VI lines are each detected with channel electron multipliers (CEM) with CsI photocathode coatings. The CEM's are protected from contamination by a vacuum valve that is opened during observations to provide an open path for the EUV radiation.

The spectral resolution is 0.3 Å for observations of the resonantly scattered component of Lyman-α, 2 Å for the electron scattered component and 2.5 Å for observation of O VI λ1032/λ1037 Å. The spatial resolution elements are 0.53' x 5' for the resonant Lyman-α profile, 4' x 5' for the electron scattered Lyman-α profile and 2.6' x 5' for the O VI λ1032/λ1037 Å intensities. The instantaneous field-of-view is illustrated in Figure 1. At any instant, both the resonantly scattered Lyman-α profile and O VI intensities are observed at one spatial height (represented by the X in Fig. 1) and the electron scattered Lyman-α profile is measured at a point (represented by the O in Fig. 1) which is displaced by 9.5' in the solar tangential direction. Using internal telescope mirror rotations, these elements can be scanned along a given radial direction between spatial heights of 1.5 $R_\odot$ and 3.5 $R_\odot$. The instrument field-of-view can be rotated through 360° about sun-center using the Spartan 2/Attitude Control System (Spartan 2/ACS). Offset pointing by Spartan 2/ACS will permit the instrument to view the solar disk (represented by the triangle in Fig. 1). For this observation, which is used to normalize the coronal intensities to a composite of disk intensities, a shutter mask mechanism places 14 μm pinholes in front of the entrance slits.

This work has been supported by NASA under Grants NAGW-291 and NSG 5-613 to the Smithsonian Institution and No. S-79634B to the High Altitude Observatory.

References

1. J.L. Kohl, H. Weiser, G.L. Withbroe, R.W. Noyes, W.H. Parkinson, E.M. Reeves, R.M. MacQueen and R.H. Munro, Astrophys. J. 241, L117 (1980).

2. R.H. Munro, J.L. Kohl, H. Weiser and G.L. Withbroe, Bull. Amer. Astron. Soc. 13, 912 (1982).

3. J.L. Kohl, H. Weiser, G.L. Withbroe and R. H. Munro, Bull. Amer. Astron. Soc. 14, 976 (1982).

4. J.L. Kohl and G.L. Withbroe, Astrophys. J. 256, 263 (1982).

5. G. Noci and J.L. Kohl, in preparation (1984).

6. G.L. Withbroe, J.L. Kohl, H. Weiser and R.H. Munro, Space Sci. Rev. 33, 17 (1982).

7. R.M. MacQueen, J.T. Gosling, E. Hildner, R.H. Munro, A.J. Poland and C.L. Ross, Proc. S.P.I.E. 44, 207 (1974).

8. J.L. Kohl, E.M. Reeves, and B. Kirkham, in New Instrumentation for Space Astronomy, eds. K. van der Hucht and G.S. Vaiana (Oxford and New York: Pergamon Press, 1978).

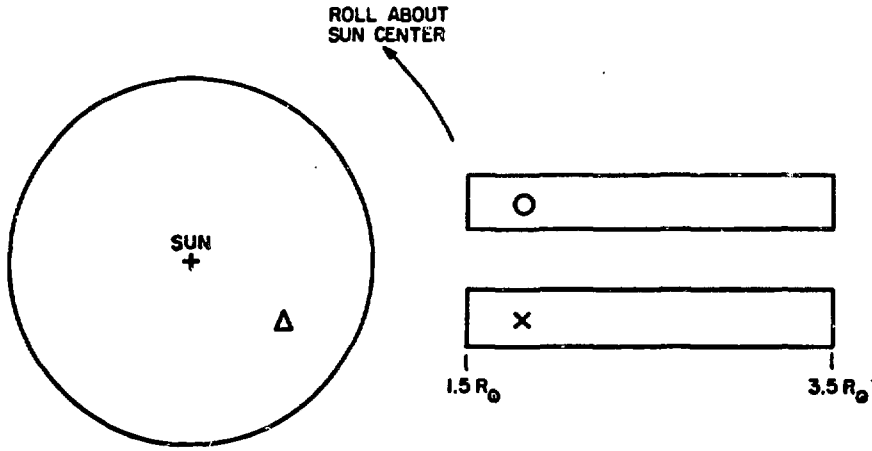

Fig. 1. Instantaneous Field-of-View of UVCS/Spartan 2.

HRTS EVIDENCE FOR ROTATION OF TRANSITION REGION TEMPERATURE SPICULES

J.W. Cook, G.E. Brueckner, J.-D.F. Bartoe, and D.G. Socker
E.O. Hulburt Center for Space Research
Naval Research Laboratory, Washington, DC 20375

INTRODUCTION

The HRTS (High Resolution Telescope and Spectrograph) instrument is a high spectral (0.05 Å) and spatial (<1 arc sec) resolution spectrograph with a slit length of 900 arc sec on the solar disk (see Bartoe and Brueckner 1975, 1978). HRTS contains in addition a double grating, zero dispersion broadband spectroheliograph which images the spectrograph slit jaw plate (see Cook et al. 1983). The central wavelength is tunable by changing the grating geometry. Hα images are also photographed from the slit jaw plate image. HRTS has been flown four times as a rocket payload, and will fly in April 1985 as one of the solar experiments aboard Spacelab 2. The four rocket flights of the HRTS program have each been customized for a particular scientific objective. For the fourth flight, because the original hardware was utilized as the basis of the Spacelab HRTS, the opportunity was used to design and build a new rocket HRTS instrument specialized for observations at the solar limb. In this configuration the photographic speed was increased, a new curved slit was fabricated, and the spectroheliograph was modified for limb observations. The scientific observing program was a study of structure and short term temporal evolution at the limb, with a comparison of quiet and coronal hole areas.

INSTRUMENT AND OBSERVATIONS

In order to increase speed the slit was opened wider, giving 0.1 Å spectral resolution instead of 0.05 Å, and a faster mechanically ruled grating was used instead of the original holographic second grating. Because ruled gratings cannot be produced uniformly to the large size of the original grating, two ruled gratings were used covering 1200-1310 Å and 1340-1560 Å, with a region of overlap.

The most original feature was a new curved slit for use at the limb. The slit radius of curvature was greater than the solar radius: if the slit were placed tangent to the limb and displaced 5 arc sec inside the limb at the center, the two ends would rise to 15 arc sec above the limb. Thus a sample of all heights from -5 to +15 arc sec above he limb could be obtained on slit spectra.

The spectroheliograph was tuned in wavelength to obtain images in C IV (1550 Å) of fine structure above the limb (on the disk the continuum is the main flux source; see Cook et al. 1983). A new coating was used on the bottom slit jaw to give a less reflectant surface for the area reflecting the bright disk, in order to cut stray light above the limb. This coating ended, on the disk side of the slit jaw plate, below the curved slit, tending to obscure the exact location of the solar limb. On Hα images this shows only as a line across the image at the coating edge, allowing the limb location to be identified.

The new HRTS instrument was flown on 7 March 1983 at White Sands, and obtained 145 slit spectra, 157 spectroheliograms, and 32 Hα images. The curved slit was placed at the solar limb with its center at the

western edge of the south polar coronal hole, giving both coronal hole and quiet region coverage (this position was obtained with help from J.W. Harvey at Kitt Peak). Because command control to the instrument was lost most of the time due to malfunction of a ground transmitting station, the slit pointing was not capable of fine adjustment, and the telescope focus could not be critically adjusted in flight. As a result the pointing was slightly off and drifted generally outward above the limb, and the spatial resolution of the data was approximately 3 arc sec instead of the potential sub arc sec resolution. For one brief period when commanding was possible a focus adjustment was attempted, and several of the spectroheliograms and a slit spectra have improved resolution, which should have been achieved for all the data.

RESULTS

In the slit spectra (see Figure 1) both the coronal hole and the quiet region show chromospheric and transition region line emission, but in the coronal hole hotter coronal lines are weak or essentially absent. While an expected result, the illustration with these data is striking. Si VIII 1446 Å (10^6 K) is noticeably weaker in the coronal hole, and Fe XII 1242 Å and 1349 Å (1.6×10^6 K) are suppressed. In both regions there is little apparent fine structure in the coronal lines, while C IV and Lα show fine structure at the instrumental resolution both on and above the disk.

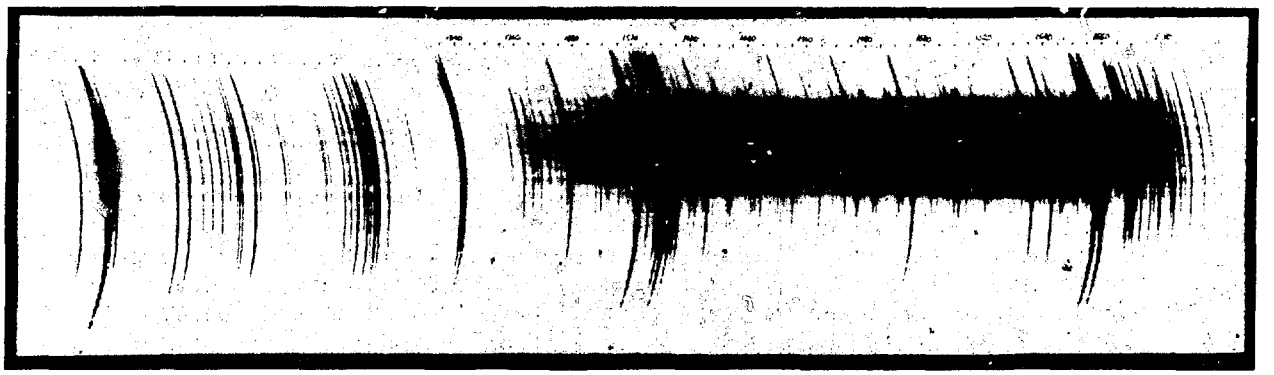

Figure 1. HRTS slit spectrum. The grating overlap can be seen around 1330 Å. Quiet region to top, coronal hole to bottom.

The C IV spectroheliograms show general spiked emission at the limb. These C IV spicules appear to fall somewhere between Hα spicules and macrospicules in their properties but more closely resemble macrospicules in size and height. A major difference from macrospicules is that the C IV spicules are <u>not</u> confined to the coronal hole side of the limb.

POSSIBLE ROTATION OF C IV SPICULES

The most interesting result from the rocket flight is the observation in slit spectra at C IV 1550 Å (and Lα) of features tilted with respect to the constant wavelength curve of the slit, at locations where the slit is passing over the tops of several of the spicular structures seen in the spectroheliograms (see Figure 2). Observations of such

tilts in spectra of Hα spicules have long been known, but their interpretation is apparently still somewhat contentious (see discussion in Bray and Loughhead 1974). Although other interpretations are possible, the axial rotation of a cylindrical body would give the observed tilted features (see Figure 3). Hα observations interpreted in this manner give rotational velocities of <30 km s^{-1} at the edges of a 1 arc sec diameter spicule.

Figure 2. C IV lines 1548 Å (bottom) and 1550 Å (top) from slit spectrum are shown between two spectroheliograph (SH) images. Examples of small tilted features are seen at extreme left, where the slit is crossing the tops of several spicules seen in the lower SH image, a 0.9 s exposure. Top SH image, a 0.1 s exposure, shows some of the spectrograph slit which is overexposed in the bottom SH image.

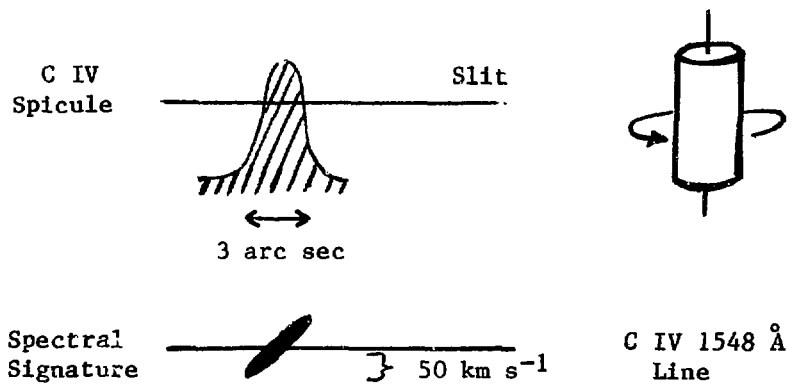

Figure 3. Rotational interpretation of tilted spectral feature.

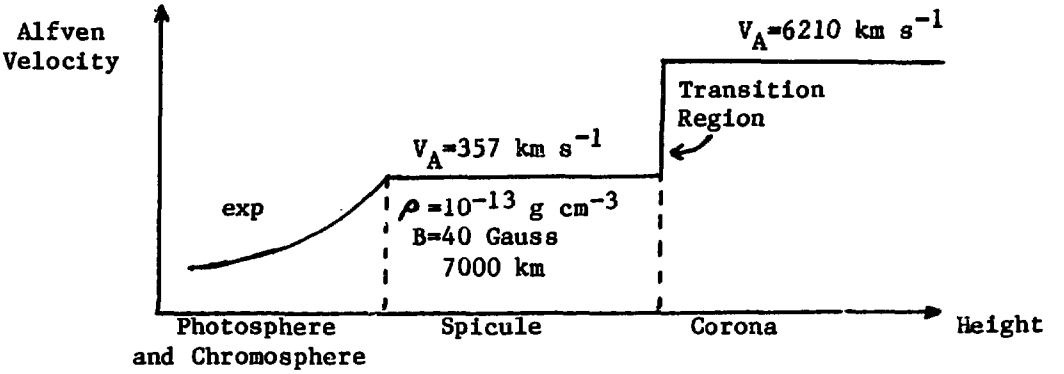

Figure 4. Model of Sterling and Hollweg (1984) for Hα spicule.

The attraction of the rotational interpretation is its possible explanation in terms of a propagating torsional wave. If the observed C IV features are interpreted as Doppler shift signatures of rotation, the HRTS observations show tilted features with a velocity at the outer edge of 50 km s^{-1}, where at least some examples do not appreciably slow or reverse tilt over the duration of the rocket observations (3 minutes). One recent model by Sterling and Hollweg (1984) for the heating of a (lower temperature Hα) spicule involves an Alfven wave in a resonant cavity. They approximate the increase of the Alfven speed $V_A=B/(4\pi\rho)^{1/2}$ (where B is the magnetic field strength and ρ the density) in the upper photosphere and chromosphere by an exponential function, assume a constant Alfven speed in the Hα spicule, and treat the transition region as a step function to a corona with much higher constant Alfven speed (see Figure 4). Alfven waves of certain frequencies are preferentially transmitted through the spicule, which acts as a resonant cavity. Sterling and Hollweg find an average rotational velocity of 20-30 km s^{-1} for Hα spicules, but at a fundamental period of around 80 s. They give the frequency of the fundamental as $4L/V_A$, where L is the spicule length and V_A the Alfven speed within the spicule. For the transition region the Alfven speed should be larger, and the spicule length perhaps somewhat greater. But the HRTS observational result on period is not as negative as first appears, because of the difficulty due to the drifting slit in following an individual spicule. The model needs to be extended to investigate what happens at transition region temperatures.

REFERENCES

Bartoe, J.-D.F., and Brueckner, G.E. 1975, J. Opt. Soc. Am., 65, 13.
Bartoe, J.-D.F., and Brueckner, G.E. 1978, in New Instrumentation for Space Astronomy, ed. K. Van der Hucht and G.S. Vaiana (Oxford: Pergamon), p. 81.
Bray, R.J., and Loughhead, R.E. 1974, The Solar Chromosphere (London: Chapman and Hall), pp. 58-60.
Cook, J.W., Brueckner, G.E., and Bartoe, J.-D.F. 1983, Ap. J. (Letters), 270, L89.
Sterling, A.C., and Hollweg, J.V. 1984, Alfvenic Resonances on Solar Spicules, Ap. J., in press.

SESSION 2. LOW DENSITY LABORATORY PLASMAS

THE RELEVANCY OF MAGNETICALLY CONFINED PLASMAS - TOKAMAK AND MIRROR - FOR ATOMIC SPECTROSCOPY AND ASTROPHYSICAL PLASMA DIAGNOSTICS.

M. Finkenthal
'Racah' Institute of Physics
The Hebrew University
Jerusalem, Israel

This talk presented the magnetic confinement experiments from a different angle, i.e. as laboratory sources which allow the study of various problems in such fields as atomic physics and astrophysics.

Tokamak and magnetic mirror plasmas have properties which make them particularly suitable for basic atomic physics experiments; they are stable over long intervals of time and have wide ranges of electrom densities and temperatures. Also, models on which electron density and temperature diagnostics are based in astrophysical research can be checked since these quantities are accurately measured by independent non-spectroscopic methods.

In a tokamak, the plasma is confined in a torus by a magnetic configuration obtained from the superposition of an external toroidal field and the poloidal field created by the plasma current (the current is induced in the plasma which acts as a secondary of a transformer, H. Furth, 1981). Once the current reached its maximum value, a steady state phase of the discharge is established, while for hundreds of milliseconds to several seconds the major plasma parameters at given radial positions in the plasma are practically constant. The radial profiles (across the minor radius of the torus, which varies in present day experiments from ten to a hundred cm.) of the electron density and temperature are peaked on the axis and their overall shape is fairly represented by a gaussian. The range of the central electron densities in tokamak experiments is from several times 10^{12} to 10^{14} cm^{-3} and peak electron temperatures of 1 to 2 keV are obtained in ohmically heated discharges. When additional heating (such as neutral beam injection or electron/ion cyclotron resonance heating) has been used, central ion temperatures as high as 8 keV and electron temperatures of the order of 4-5 keV have been attained (Eubank et al. 1979).The major plasma parameters are measured by various methods: microwave interferometry, electron cyclotron emission, Thomson scattering, energetic neutral particle spectra analysis, probes, etc. (Furth H, 1981). Most of these diagnostics when carefully built and calibrated can provide measurements with errors of the order of 10-20% (which represents a great improvement over the rather rough estimates in the complex and short lived high density plasmas, laser, spark, exploding wires, etc).

The tandem mirror machine is an open ended device, in which the plasma is confined in a central cell by magnetic and thermal barriers set up in the two end plugs. The densities here are 10^{11}-10^{12} cm^{-3} and the electron temperatures(without auxilliary heating) vary from several tens to 200 eV (Simonen et al. 1983).

The results presented here have been obtained from the PLT tokamak at Princeton Plasma Physics Laboratory and TMX U tandem mirror at Lawrence Livermore Laboratory.

(1) SPECTROSCOPY OF HIGHLY IONIZED ATOMS

The spectrum of a high Z element, having a complete n=3 shell, will be very complex when 3-3 transitions are emitted simultaneously by many ions having very close ionization potentials. For example, Mo XVI, IP 100eV) to $MoXXIV_5$ (IP 500eV) will emit thousands of lines originating from $3p^6 3d^k - 3p^5 3d^{k+1}$ transition in the 60-90 Å range. It is therefore very difficult to assign the lines to given ions unless some method is found to separate between various ionization states. In laser or spark produced plasmas, by varying the power deposition on the target or the energy content of the discharge one can separate a few states of ionization. But the difficulty still exists, since even three or four ions, such as for instance MoXVII to MoXX will emitt an enormous number of lines. It is practically impossible to follow the time histories of these lines simultaneously in the short lived plasmas (tens to hundreds of nanoseconds). On the contrary, in the tokamak spectra the identification and classification of the strong lines is possible because various ionization states recorded simultaneously are separated according to their time and space evolution. This simultaneous recording of the time resolved - wide spectral range was made possible by the use of image intensifier detectors mounted on high resolution grazing incidence spectrometers (Schwob at al. 1983, Hodge at al. 1984). In addition to the identification of the lines according to their individual time histories (Stratton et al. 1983) these instruments can scan radially the tokamak plasma, thus relating the emission to a given electron temperature. Zirconium, molybdenum and silver have been injected in the PLT tokamak by a laser blow off technique (Marmar et al.1975) and strong lines originating from 3-3 transitions belonging to ions isoelectronic to KI, ArI, CII and SiI have been identified. The identifications, based on both extrapolations/interpolations along the isoelectronic sequences and ab initio relativistic energy level computations, are presented and discussed in two papers (Finkenthal et al. 1984a, Schwob et al. 1984).

(2) ATOMIC PHYSICS

(a) COMPARISON OF DIFFERENT COLLISION STRENGTH COMPUTATIONS WITH EXPERIMENTAL DATA.

Two sets of computations of line intensity ratios in the case of the SiIII ion, lead to very different results insofar as their electron density dependence is concerned (Nicolas et al.1979, Dufton et al. 1984).

The levels considered and the assumptions concerning level populating mechanisms were similar in the two works. The computed transition probabilities were also very close. The difference between the two, was in the way the electron impact collision strength have been computed: the first work used the distorted wave technique while in the second, the R-matrix technique was used and the effect of the resonances has been included.

The comparison between the two, in the case of our particular line ratio and the experimental result obtained from the TMX U silicon spectrum is presented in figure 1.

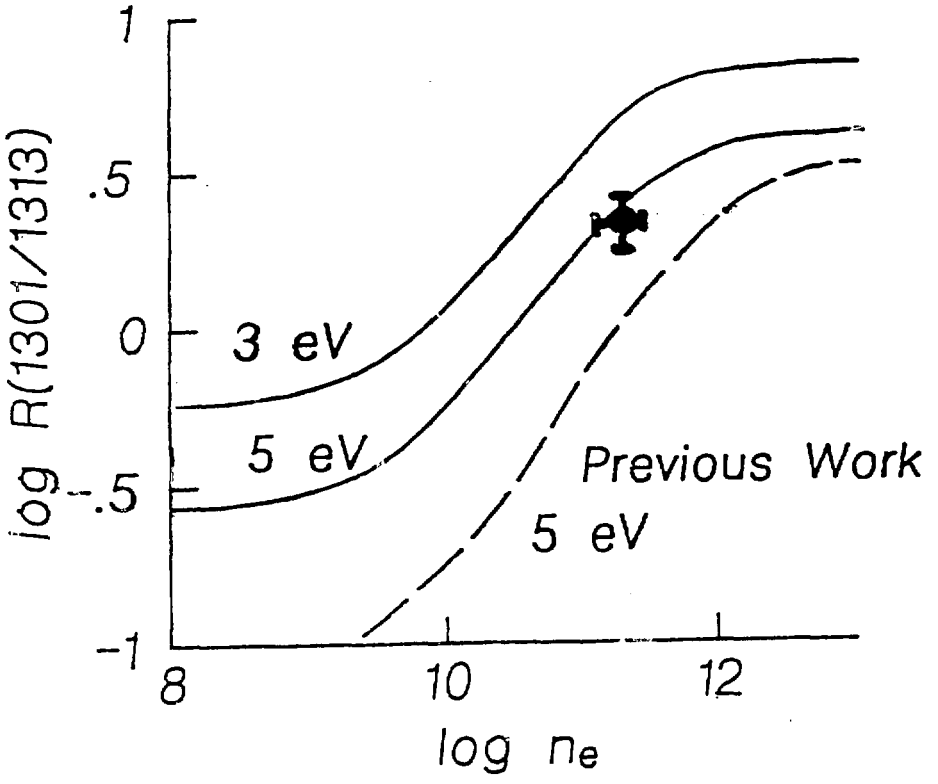

As one can see in figure 1, the difference between the two theoretical computations would lead to a difference of an order of magnitude in the infered electron density both for solar corona and flare. The experimental values of several line ratios,(discussed in detail in T.Yu et al. 1984), indicate that the effect of resonances is very important and must be taken into account in the collision strength computations.

(b) THE EFFECT OF INNER-SHELL IONIZATION PROCESSES ON THE LINE INTENSITY OF MgI - LIKE IONS IN TOKAMAK PLASMAS.

A persistent departure from the predicted 'resonance - intercombination' line ratios within the MgI like sequence (from Sc X to Mo XXXI has been observed in tokamak spectra (Finkenthal et al. 1982 a, Finkenthal et al. 1982 b). A model including 47 energy levels has been considered for the Se XXIII ion and a large discrepancy still subsisted between theory and experiment as seen in table 1.

Transition	λ (A)	Brightness (photons/cm^2-sec-sr)	Relarive Intensity meas.	calc.
$3s^2\ ^1S_0$ - $3s3p\ ^1P_1$	175.92	2.2(15)	100	100
$3s^2\ ^1S_0$ - $3s3p\ ^3P_1$	265.7	3.4(14)	15	6.5
$3s3p\ ^3P_2$ - $3s3d\ ^3D_3$	154.04	1.3(14)	6	2.2
$3s3p\ ^1P_1$ - $3s3d\ ^1D_2$	158.86	1.6(14)	7	5.7

Table 1.

The ionization from the AlI like ion (ground state $3s^2 3p$) by an inner shell ionization process has been included in the level population model. (One of the 3s electrons is eliminated, bringing thus the newly produced MgI like ions, directly into the excited 3s3p state). When the relative concentration of AlI/MgI like ions is close to two, the experimental results come in good agreement with those predicted by theory. A detailed discussion of this topic is currently under publication (Finkenthal et al 1984 b).

3. ASTROPHYSICS

Iron has been injected into the PLT tokamak (by the above mentioned technique) at two different central electron densities, 5×10^{12} cm^{-3} and 3.5×10^{13} cm^{-3}. The spectra obtained have been compared in the 90-140 Å region with a solar flare spectrum. Figure 2 shows the comparison of the three spectra. The first striking thing is the similarity of the low density tokamak and flare spectra. This would already indicate that both electron density and temperature conditions of the two emitting plasmas are fairly close. The next step was to analyze in detail the line brightness within different ionization states and compare their experimental density dependence with this predicted by the theoretical models (the spectrometer which recorded the tokamak spectra has been calibrated at the SURF facility at NBS). The results for Fe XVIII to Fe XXII ions have been presented elsewhere (Stratton et al. 1984 a) and first results of an extension of this work for other elements, from titanium to selenium is presented at this conference (Stratton et al. 1984 b). As a general conclusion one should remark the good agreement between theory and experiment in these cases, which indicates that the basic assumptions made in the models, concerning populating mechanisms, transition probabilities and collisional excitation rates, are correct. This kind of 'laboratory simulations' of astrophysical plasmas is extremelly valuable for astrophysical plasma diagnostics and will be further pursued in future experiments.

ACKNOWLEDGEMENTS

The author whishes to acknowledge the whole Plasma Spectroscopy Group at Johns Hopkins University headed by Prof. H.W. Moos for several years of fruitful cooperation on these subjects. The PLT tokamak group

and the TMX U team are thanked for enabling us to perform the experiments. The Plasma Spectroscopy Group at 'Racah' Institute of Physics, Hebrew University, Jerusalem, was involved both in theoretical and experimental aspects of the work.

This survey was made possible,in part,by funds granted by the Charles H. Revson Foundation.

References

Dufton, P.L., Hibbert, A., Kingston, A.E., Doschek, G.A. 1984, Astrophys. J. 274, 420.

Eubank, H. et al., 1979, Phys. Rev. Lett., 43, 270.

Finkenthal M., Bell, R.E., Moos, H.W. and TFR Group, 1982a, Phys. Lett. 88 A, 165

Finkenthal M. Hinnov, E., Cohen S., Suckewer, S. 1982b, Phys. Lett. 91 A, 284.

Finkenthal, M., Stratton, B.C. Moos H.W., Hodge, W.L., Mandelbaum, P., Klapisch, M., and Cohen, S. 1984a, to be published.

Finkenthal, M., Stratton, B.C., Moos H.W. and Bar-Shalom, A., Klapisch, M., 1984b to be published.

Furth H., 1981, 'The Tokamak', Fusion, Vol. I, ed. E. Teller, Academic press.

Hodge, W.L., Stratton, B.C., and Moos, H.W., 1984, Rev. Sci. instr., 55, 16.

Marmar, E., Cecchi, J., and Cohen, S., 1975, Rev. Sci. Instr., 46, 1149.

Nicolas, K.R. Bartoc, J.D.F., Brueckner, G.E., and Van Hoosier, M.E., 1979, Astrophys. J., 233, 741.

Schwob, J.L., Finkenthal, M., Suckewer, S., 1983, Proc. 7th International Conf. V.U.V. Radiation Phys., Jerusalem, Vol. 1, 54.

Schwob, J.L. Wouters, A.W., Suckewer, S. and Finkenthal, M., 1984 to be published.

Simonen, T.C., et al., 1983, Phys. Rev. Lett., 50 1668.

Stratton, B.C., Hodge, W.L. Moos, H.W., and Schwob, J.L. Suckewer, S. Finkenthal, M. Cohen, S., 1983, J. Opt. Soc. Am., 73 877.

Stratton, B.C. Moos, H.W., and Finkenthal, M., 1984a Astrophys. J. Lett., 279, L31.

Stratton, B.C., Moos H.W., Feldman U. Seely, J.F., Suckewer, S., Finkenthal, M. 1984b, to be published.

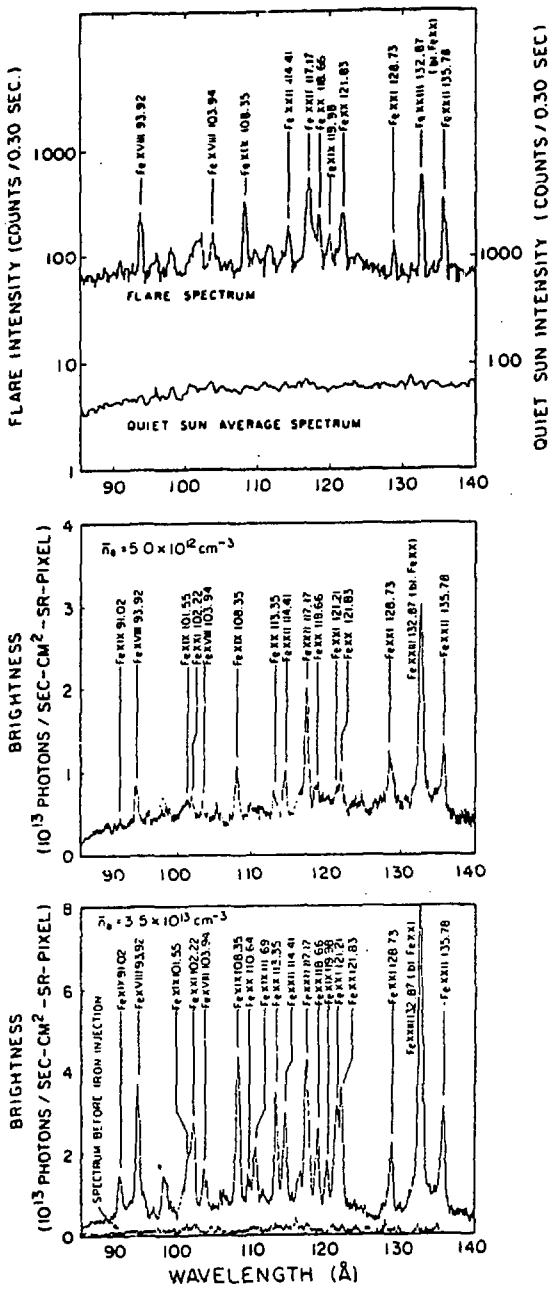

UPPER: SOLAR FLARE AND QUIET SUN AVERAGE SPECTRA (FLARE E IN S.O. KASTNER, W.M. NEUPERT, AND M. SWARTZ 1979, AP. J., 191, 261).

MIDDLE AND LOWER: PLT TOKAMAK IRON SPECTRA AT $\bar{N}_E = 5 \times 10^{12}$ CM^{-3} AND $\bar{N}_E = 3.5 \times 10^{13}$ CM^{-3} (B.C. STRATTON, H.W. MOOS, AND M. FINKENTHAL 1984, AP. J. (LETTERS), 279, L31)

INTENSITIES IN COMPLEX SPECTRA OF HIGHLY IONIZED ATOMS

M. Klapisch, A. Bar-Shalom and A. Cohen
Racah Institute of Physics
Hebrew University
Jerusalem 91904, Israel

We describe a package of programs for the implementation of the collisional-radiative model to complex configurations. The number of levels taken into account may be several hundreds. The heart of the package is a very efficient program for excitation cross sections in the Distorted Wave framework, using the Relativistic Parametric Potential wave functions. The basic jj coupling scheme actually simplified the computations, enabling a useful factorization into radial and angular parts. Intermediate coupling and configuration interactions are accounted for. We computed ratios of intensities of $3d^9 - 3d^8 4s$ (E2) to $3d^9 - 3d^8 4p$ (E1) transitions as functions of n_e and T_e in Xe XXVIII and other Co-like spectra. The atomic model involves all the levels of configurations $(3p^6)3d^9$; $-3d^8 4s$, $-3d^8 4p$, $-3d^8 4d$, $-3d^8 4f$, and $(3p^5) -3d^{10}$, $-3d^9 4p$. (275 levels) and all the transitions between them. Results compare very well with experimental spectra from TFR.

SUPRA THERMAL ELECTRON TAILS EFFECTS ON X-RAY LINE EMISSION IN A TOKAMAK PLASMA

R. Bartiromo, F. Bombarda and R. Giannella
Associazione EURATOM-ENEA sulla Fusione, CRE Frascati
Frascati, Italy

INTRODUCTION

The soft X-ray lines emitted by highly ionized impurities are one of the most prominent spectral features of today's tokamaks. In fact the hydrogen isotope plasmas produced in these devices attain temperature values ranging from about one to several keV. A great deal of information about the plasma conditions can be drawn, in particular, from the highly resolved spectra of medium-Z ions which are very rich in satellites excited via dielectronic recombination and innner shell excitation (Dubau and Volontè 1980, Bitter et al. 1979).

The intensity ratio between a dielectronically excited satellite and the resonance line of the parent ion is an example of a diagnostic tool useful for the electron temperature measurement of a thermal plasma. This ratio, in effect, is sensibly dependent upon that temperature because electrons of different energies are involved in the excitation of the two lines, the resonance one being excited by the electrons whose energy is greater than the threshold Eo and the satellite by those who resonate with its excitation energy Es that is usually lower than Eo by a few keV.

On the other hand the values of these ratios in plasmas where the electron distribution function deviates from a Maxwellian are expected to be sensibly different from thermal ones (Gabriel and Phillips 1979).

In this presentation the experimentally observed effects on these ratios in situations where supra-thermal electron tails are present are briefly described. It is also shown how quantitative information about the electrons in the tail can be deduced using this method.

THE EXPERIMENT

Our experiments have been performed on the Frascati Tokamak FT, a high toroidal magnetic field device. Such devices are characterized by a higher current density as compared to other tokamaks and their plasmas are therefore more easily affected by supra-thermal phenomena. The discharges studied are characterized by temperature profiles that are peaked at the plasma centre reaching peak values between 0.7 and 2 keV. The electron density profiles are peaked at the centre too and their peak values range from 0.5 to $5 \cdot 10^{14}$ cm^{-3}. In these discharges the soft X-ray line spectra of He-like Cr and Fe have been recorded. Their emission is estimated to come from a limited region about the plasma centre.

In a purely maxwellian framework a theoretical value $R_{th}=I_S/I_W$ can be worked out for the ratio between the

intensity I_s of a dielectronically excited satellite and the intensity I_w of the resonance line of the ions considered, starting from well established expressions for the two intensities (Dubau and Volontè 1980, Bely-Dubau et al. 1982). This ratio in the low density limit is only dependent on the electron temperature, and has been extensively checked in different tokamak experiments (Bitter et al. 1981, Apicella et al. 1983).

A good agreement of the experimental ratio R_{exp} and the theoretically expected value has been observed in our experiments at electron densities higher than $2.5 \cdot 10^{14}$ cm^{-3}. This has been found for Cr XXIII, using the d_{13} line as the dielectronic satellite, and for Fe XXV, using the close group of satellites A,B,d_{13} . But for densities decreasing below the mentioned value an increasingly important deviation of R_{exp} from R_{th} has been observed (figs. 1 and 2 referring respectively to Cr and Fe). This has been interpreted as due to the presence of a supra-thermal electron tail enhancing the excitation of the resonance line with respect to a maxwellian situation (Apicella et al. 1983).

INTERPRETATION OF RESULTS

To get quantitative information about the electrons in the tail from these observations a model expression should be assumed in principle for the tail distribution function, in order to evaluate the relative contribution of these electrons to the excitation rate coefficient of the resonance line $Q_w = \int f(E)\sigma_w v \, dE$. But in this case a favourable coincidence permits to get rid of this assumption.

To understand this it is useful to look at the fig. 3. The crosses there indicate the $\sigma_w v$ product versus the energy of the incident electron as deduced by recently published values of the excitation cross section σ_w for the Fe XXV resonance line (Mann 1984). These values are well fitted asymptotically by the dashed line, that has been computed by using the non relativistic Bethe expression for σ_w

$$\sigma_w = 4\pi a_0^2 \frac{E_H}{E_0} \frac{E_H}{E} f \cdot \left[\ln \frac{4E}{E_H} (K a_0)^2 \left(\frac{E_H}{E_0}\right)^2 \right].$$

Here the values f=0.744 and $K=11.7/a_0$ have been used for the oscillator strength and the cutoff wavenumber respectively, a_0 is the Bohr radius and E_H=13.6 eV is the Rydberg constant.

But at the energies we are speaking of, this description is no more correct because, as the electron energy E approaches the relativistic domain, a new effect starts playing an increasingly important role: this is the interaction with the ion through exchange of virtual photons (Fano 1963). In this case the relativistic expression has to be used for the cross section:

$$\sigma_w = \frac{8\pi a_0^2}{m v^2} \frac{E_H^2}{E_0} f \cdot \left[\ln \left\{ \frac{\beta^2}{1-\beta^2} (K a_0)^2 \left(\frac{E_H}{E_0}\right)^2 \frac{2mc^2}{E_0} \right\} - \beta^2 \right], \quad \left(\beta = \frac{v}{c}\right)$$

The $\sigma_w v$ product so deduced is represented in the figure by

the continuous line. It has to be considered as a fairly good approximation for energies greater than about 15 keV. Moreover up to energies of the order of the MeV and higher it has the pleasant feature not to depart more than a small percentage from its median value $\langle \sigma v \rangle$.

This occurrence permits us to interpret the increment in the resonance line intensity as simply proportional to the number of electrons in the tail through a coefficient that is independent of their distribution function, provided that the tail develops for energies sensibly greater than the threshold Eo=6.7 keV. Thus we are led to a simple expression for the density n_s of electrons that are in excess of the maxwellian number over the threshold energy:

$$n_s/n_e = \left(Q_s(T_e)/\langle \sigma v \rangle \right) \cdot \left(1/R_{exp} - 1/R_{th}(T_e) \right),$$

where n_e is the electron density and $Q_s(T_e)$ is the dielectronic satellite excitation rate coefficient.

SOME RESULTS

To show an example of application of this kind of analysis we present fig. 4. There the quantity n_s/n_e for a set of ohmic discharges is plotted versus the Dreicer parameter $\mathcal{E}/\mathcal{E}_c$, that is the ratio between the toroidal electric field in the plasma and the critical field $\mathcal{E}_c$. This is the field whose force would not be compensated by the collision frictional resistance for electrons whose energy is greater than kT_e. The boxes in the figure refer to discharges done at toroidal magnetic field of 8 Tesla and the dots at 4 Tesla. A clear dependence of the supra-thermal population on the Dreicer parameter can be seen. But an even more remarkable dependence upon the magnetic field appears from these data. This cannot actually be understood in terms of the collisional theories of runaway electrons generation in static electric fields. Probably more complicated effects involving the presence of waves in the plasma should be included in the picture in order to get a better insight in these phenomena.

REFERENCES

Apicella, M.L., Bartiromo, R., Bombarda, F. and Giannella, R. 1983 Phys. Lett., 98 A, 174.

Bely-Dubau, F., Dubau, J., Faucher, P., and Gabriel, A.H. 1982 Mon. Not. R. Astron. Soc., 198, 239.

Bitter, M., von Goeler, S., Horton, R., Goldman, H., Hill, K.W., Sauthoff, N.R., and Stodiek, W. 1979 Phys. Rev. Lett., 42, 304.

Bitter, M., von Goeler, S., Hill, K.W., Horton, R., Johnson, D., Roney, W., Sauthoff, N.R., Silver, E. and Stodiek, W. 1981 Phys. Rev. Lett., 47, 921.

Dubau, J., and Volontè, S. 1980, Rep. Prog. Phys., 43, 199.

Fano, U. 1963, Ann. Rev. Nucl. Sci., 13, 1.

Gabriel, A.H., and Phillips, K.J.S. 1979 Mon. Not. R. Astron. Soc., 189, 319.

Mann, J.B. 1984 Atom. Data and Nucl. Data Tables, 29,407.

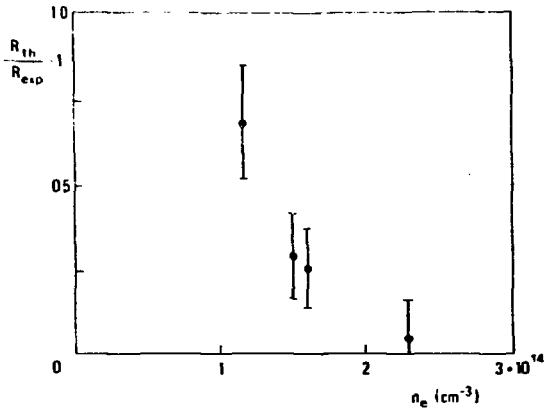

Figure 1

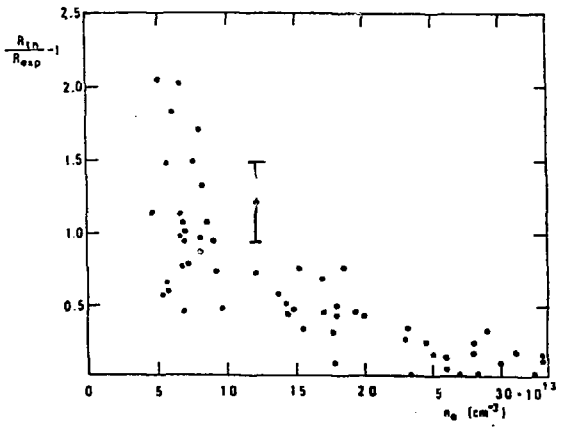

Figure 2

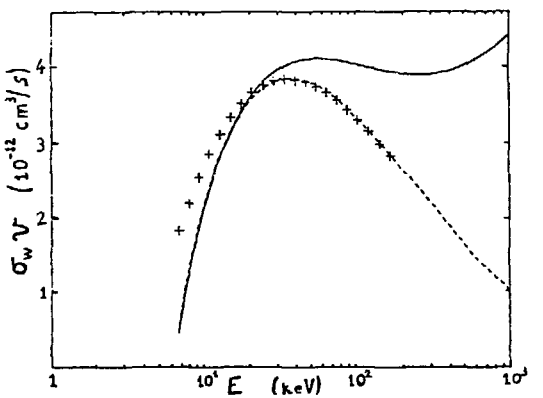

Figure 3

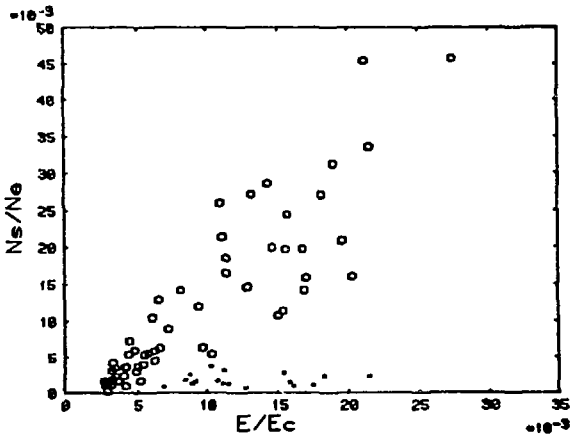

Figure 4

RECOMBINATION PROCESS FROM A METASTABLE STATE

T. Kato, K. Masai and K. Sato
Institute of Plasma Physics
Nagoya University, Nagoya 464, Japan

The level $2s2p^2(^4P)$ of OIV is a metastable state and the line intensity I_i $(2p^3(^4S) - 2s2p^2(^4P))$ is mainly generated by the excitation from the metastable state $2s2p^2(^4P)$ to $2p^3(^4S)$. Then the line intensity ratio is I_i to the resonance line intensity I_r $(2s2p^2(^2D) - 2s^22p(^2P))$ has a dependence on electron density until the metastable level is saturated. The ratio I_i/I_r obtained from the measurements of JIPPT-IIU Tokamak plasmas has been analyzed. It is found that the recombination from a metastable state of OV $2s2p(^3P)$ to the metastable state of OIV $2s2p^2(^4P)$ is appreciable in high temperature plasmas where the abundance of OV is larger than that of OIV. The recombination rate coefficient between metastable states is determined from the line intensity ratios; $I(2p^2(^3P) - 2s2p(^3P))/I(2s2p(^1P) - 2s^2(^1S))$ of OV, $I_r^{OV}(2s2p(^1P) - 2s^2(^1S))/I_r^{OIV}(2s2p^2(^2D) - 2s^22p(^2P))$ and I_i/I_r of OIV. This recombination process consists of dielectronic recombination and radiative recombination.

NEW CALCULATIONS OF INNER SHELL X-RAY LINES IN Ti, Cr, AND Ni AS DENSITY DIAGNOSTICS

J.R. Lemen
Mullard Space Science Lab
University College London
Dorking, Surrey, England

K.J.H. Phillips
Space and Astrophysics Division
Rutherford Appleton Lab
Chilton, Didcot, OXON OX11 0QX, England

G.A. Doschek
E.O. Hulburt Center for Space Research
Naval Research Laboratory
Washington, DC 20375-5000

R.D. Cowan
Los Alamos National Lab
Los Alamos, NM 87545

We present new calculations for 1s-2p transitions in C-, N-, and O-like Ti, Cr, and Ni for application to tokamak X-ray spectra. This extends our earlier work for the corresponding iron ions (Phillips et al. 1983, Ap.J. 265, 1120) in which a density dependence of line intensities was pointed out. These lines are principally formed by dielectronic recombination; the density effect arises due to the density-dependent populations of the fine structure levels in the ground configuration of the recombining ion. In the present work the calculations of the Ti, Cr, and Ni lines have been made for the wavelengths and the dielectronic recombination rates using a Hartree-Fock technique with statistical exchange. The density dependence of the collisionally excited transitions was also included. Density-dependent populations of the fine structure levels of the ground configuration were obtained from Feldman et al. (1980 J. Appl. Phys. 51, 190) and Bhatia et al. (1980, J. Appl. Phys. 51, 1464). In calculating the ionization fractions we have assumed coronal equilibrium; new ionization rate coefficients were calculated using the formalism given by Burgess and Chidichimo (1983). The spectra were synthesized with Voigt line profiles and typical tokamak radius-dependent temperature and density profiles were assumed. The N-like lines in particular show a strong dependence over the range: $<10^{11}$-3.10^{13} cm^{-3} (Ti XVI), $<10^{11}$-3.10^{14} cm^{-3} (Cr XVIII), 10^{12}-10^{15} cm^{-3} (Ni XXII). If a density profile across the torus is available from Thomson-scattered laser radiation, observations of these lines may serve to show where the N-like ions are formed in the tokamak plasma.

X-RAY SATELLITE LINES

J. Dubau
Observatoire de Paris
92195 Meudon, France

Satellite lines are typical features of X-ray spectra. They correspond to radiative transitions involving an inner-shell vacancy. The most studied satellite lines are of the K_α - type, i.e., (1s-2p) transition.

With the advent of Space Astronomy, X-ray spectra emitted by very hot solar plasma have been obtained. By a simple comparison of different spectra, it appears that, for highly ionized atoms, some satellite lines have intensities as large as resonance lines intensities and, more particularly, this is the case for the $1s^2 n\ell$ - $1s2pn\ell$ satellite lines of the $1s^2$ - 1s2p resonance lines.

The analysis of the different population mechanisms responsible for the satellite lines and resonance lines emission has shown that different spectroscopic diagnostics could be derived from line ratios only if atomic data of great accuracy were available. There exists nowadays different atomic data programs adapted to X-ray satellite lines. They have in common to give a great amount of data simultaneously : wavelengths, autoionization and radiative transition probabilities. They take into account correlation and relativistic effects.

After tackling the simple 3-electron system, the programs give now appropriate data for more complex systems but this required large computers because the lines become blended. It is therefore impossible to limit the calculation to the most intense lines.

SESSION 3. NON-SOLAR ASTROPHYSICS

ULTRAVIOLET SPECTROSCOPY OF COOL STARS FROM IUE

[+]C. Jordan, [+]P. Judge and [*]S. Johansson
[+]Department of Theoretical Physics, University of Oxford, UK.
[*]Fysiska Institutionen, Lunds University, Sweden

ABSTRACT

Observations of cool stars with the IUE satellite have shown that although main sequence stars have uv spectra similar to that of the sun, the spectra of the giants and supergiants are dominated by lines of neutral atoms and singly charged ions. The atmospheres of the low gravity stars are greatly extended and there is a large opacity in the stronger lines. This leads to multiple scattering and the appearance of many transitions through line 'leakage'.

A review is given of how high resolution IUE spectra have allowed line identifications to be established and some current problems are discussed.

The spectroscopic diagnostic techniques for the low gravity, low density atmospheres are also briefly outlined.

INTRODUCTION

Over the past six years the International Ultraviolet Explorer Satellite (IUE) has allowed extensive observations to be made of a variety of cool stars. In the first few years of operation the observations of cool stars were usually obtained at low (~ 6 Å) resolution in order to survey the general properties of line fluxes from a wide variety of stars. As a result of this early work (see for example Linsky and Haisch, 1979; Brown, Jordan and Wilson, 1979; Dupree, 1982), it was found that main-sequence dwarfs and other relatively high gravity stars have spectra between 1200 Å and 2000 Å which show essentially the same emission lines as does the solar spectrum. (Above 2000 Å the appearance of emission lines rather than absorption lines depends on the effective temperature). Analyses of such spectra show that the density regime is within an order of magnitude or so of that in the solar atmosphere and that the majority of the emission lines arise through ion-electron collisions, as in the sun. There have, therefore, been no surprising developments related to the spectroscopy of these stars. The interest has lain mainly in the quantitative analyses of the spectra to find the structure and energy requirements of individual stars and in systematic correlations of line fluxes to investigate trends which might be related to the processes underlying the existence of hot coronae.

On the other hand, even an early spectrum of the cool giant, α Boo (K2 III) obtained from a rocket by McKinney, Moos and Giles (1976) showed that the emission lines from intermediate stages of ionization, formed up to ~2 x 10^5K, which are common in the higher gravity stars are absent from the cool giants. Instead, lines from neutral atoms and singly charged ions dominate the spectra. Indeed, the spectrum obtained by McKinney et al. showed strong emission in the O I resonance lines around 1304 Å, which was accounted for by Haisch et al. (1977) in terms of fluorescence with H Ly β, following an early proposal by Bowen (1947). The IUE spectra

have now shown that such strong O I emission is a common feature of cool giants and supergiants. Also, more recent work, particularly using high resolution spectra, has shown that accidental fluorescent processes and photo-excitation and line-leakage through interlocked lines play a very important role in producing the observed spectra. (See review by Jordan and Judge, 1984). Collisional excitation is less important than in the sun, but is still relevant in the initial production of photons, though the stellar surface fluxes may be lower because of the reduced electron temperatures.

The low gravity stars are found to have electron densities $\leq 2 \times 10^{8} cm^{-3}$ (Stencel et al. 1981) and the spectroscopic diagnostic techniques developed for solar work are not appropriate. Instead new techniques become available. Although other low density objects such as planetary nebulae are reviewed elsewhere in these proceedings by Seaton, they are of interest also to stellar work through the limiting values they provide on line ratios. The ultraviolet emission line spectra of peculiar objects, such as that of the slow nova RR Tel (Penston et al. 1983) also have great potential for spectroscopic studies.

The sections below discuss recent work on line identifications, excitation mechanisms and spectroscopic diagnostic techniques and point out some areas where further work is required.

LINE IDENTIFICATIONS

When spectra of cool giants and supergiants were first obtained at low resolution with IUE it was found that although most high temperature lines were absent a feature still appeared at around 1640 Å, where He II Bα is expected and observed in the dwarf stars. Blending with Fe II was a possibility but it was not until high resolution spectra of α Tau (K5 III) and β Gru (M3 II) were obtained (Brown and Jordan, 1980) that the wavelength of the additional line (1641.3 Å) could be measured. Both S I and O I have semiforbidden lines close to this wavelength, sharing common upper levels with strong optically thick multiplets. Given the strength of the O I multiplet at 1304 Å, the O I identification, $2p^3 3s\ ^3S_1^o \rightarrow 2p^4\ ^1D_2$ seems the more likely (Brown, Ferraz and Jordan, 1981). Also, as discussed below the relevant upper level in S I has an alternative decay route. Other examples of line leakage in semiforbidden lines sharing common upper levels with very optically thick multiplets occur in C I producing lines at 1993.6 Å (Jordan, 1967) and perhaps 1537 Å (Jordan and Judge, 1984).

The high resolution spectra of cool giants and supergiants also allowed various sets of close blends to be resolved. Carpenter and Wing (1979) found that in α Ori (M2 Iab) the feature which appears at ~ 1814 Å at low resolution is composed both of Si II (mult. uv 1) and of S I (uv 2) and that the S I lines are stronger. Both multiplets are present in the K giants but there the Si II multiplet dominates. The contribution of S I to the blend can be detected at low resolution and probably accounts for the apparently anomalous ratio between the Si II 1808 Å and 1816, 1817 Å components which was noted early in the IUE mission (Linsky et al. 1978).

Examples of accidental fluorescence have also been found through high resolution observations. This type of process has been known for some time to be important in the production of emission lines in the near uv and optical spectrum of cool stars. Gahm (1974) gave an extensive finding list for fluorescent lines excited by the strong lines of H I, Mg II and Ca II, the majority of which were for $\gtrsim$ 2000 Å. The most striking example of fluorescence by Mg II is the excitation of Fe I (mult. 44) which was observed prior to IUE with the BUSS spectrograph (Van der Hucht et al. 1979) and has since been seen in other K and M low gravity stars.

As mentioned in the Introduction the excitation of the O I resonance lines by cascades, following a fluorescent excitation by H Ly β to a higher level, is now well-known. Early low resolution IUE spectra showed the presence of a blend to the short wavelength side of the O I multiplet (~ 1304 Å). The identification of this feature, suspected to be due to either S I or Fe II, was made through high resolution observations of α Tau and β Gru (Brown and Jordan, 1980) which showed clearly that S I was the origin. Moreover, it was found that two members of the S I (mult uv 9) coincide with the broad O I lines at 1302 Å and 1306 Å. The member of the multiplet which cannot be pumped by O I is absent, showing the importance of O I in the excitation. Thus photons originating in H Ly β escape eventually in both O I and S I.

One motivation for the high resolution observations of cool giants and supergiants has been to identify features present at low resolution where the poor wavelength accuracy and blending prevents unambiguous identification. From early spectra of α Tau and α Cet (M0 III) Brown, Jordan and Wilson (1979) suggested that lines of Fe II excited by H Ly α and the O I (1304 Å) lines might be present. Later work has shown other identifications for some of these features (eg the S I, O I lines discussed above) but a recent long exposure of β Gru (obtained in collaboration with Engvold and Stencel) shows some of the lines of Fe II as well (Johansson and Jordan, 1984). The upper levels of the observed lines are odd levels around 10 ev (levels of the 5p $^4D^o$, $^4F^o$, $^4P^o$, $^6F^o$ and 4p $^4P^o$, $^4G^o$ and $^4S^o$ terms) and are excited from a ^4D by Ly α photons. There are observed decays to a ^4P between 1291 Å and 1300 Å, perhaps to a ^4D around 1209 Å and 1220 Å, and to c^4F at 2506.7 Å and 2508.30 Å. These latter lines are observed also in α Tau and in the spectrum of the slow nova RR Tel. (Penston et al. 1983). In a wider investigation of Fe II Johansson has identified a new $^4G^o$ level at around 107700 cm^{-1} above the ground which can be pumped by H Ly α from the a ^4G levels and which accounts for quite strong emission lines in cool stars around 1870 Å at low resolution (Johansson and Jordan, 1984). This identification is particularly important since in stars such as α Ori H Ly α is not itself observable owing to extensive scattering and interstellar absorption. In general the pumping by H Ly α to the 10 ev levels can explain the strength of multiplets such as uv 399, 373, 380, 391, etc. which decay from them, and the absence of uv 402, 375 etc., which decay from slightly higher levels.

Johansson (1983) has identified further lines of Fe II in the uv spectrum of RR Tel, which are pumped by the strong C IV lines, and infrared decays from the same upper levels in the spectrum of V1016 Cyg. The uv

lines were identified in V 1016 Cyg by Nussbaumer and Schild (1981).

Mult. uv 191 of Fe II (at 1785 - 1788 Å) is proving to be of particular interest. This is a strong multiplet in a wide range of objects. Photoexcitation by continuum radiation at $\lambda \sim 1260$ Å has been suggested in systems including early type stars (eg Hagen et al. 1980, Stalio and Selvelli, 1980), photo-excitation by Si II (uv 4) at 1260.42 A via Fe II (uv 9) has been proposed by Viotti et al. (1980) but collisional excitation in the uv 191 itself was preferred by Nussbaumer et al. (1981) on the basis of the unfavourable branching ratio from the 1260 Å to the 1786 Å multiplets. The continuum photo-excitation process is favoured by Engvold, Jensen and Moe (1983). Johansson (1984) notes that recombination could be important in some objects. However, as Penston et al. (1983) point out it may also be significant that the upper term, x $^6P^o$, lies very close in energy to the e ^4D levels which are heavily populated by the cascades from levels excited by H Ly α and collisional population transfer could occur.

There are features in cool star spectra between 1200 Å and 2000 Å, some of which correspond to lines in the solar spectrum, which do not yet have a satisfactory identification. Given the dominance of radiative processes it is likely that they are transitions in neutral atoms or first ions which have levels which can be pumped by the strong lines of hydrogen or of O I. However, the upper levels may be rather high or be above the first ionization limit and further laboratory studies of such levels would be of value. Although coincidences with known lines can be found no satisfactory explanation emerges. The strongest lines are at 1347.08 ± 0.15 Å, 1360.18 ± 0.15 Å and 1366.42 ± 0.15 Å and occur in the spectrum of β Gru and also the solar spectrum (Jordan et al. 1978a).

A broad feature, or perhaps the combination of a broad and narrow feature occurs around 1309-1310 Å. Its possible origin in terms of Si II (uv 3) or S I ($3p^4\ ^1D_2$-$3p^3\ 3s\ ^1D^o_2$, Tondello, 1972) has been discussed by Brown et al. (1984) and Jordan and Judge (1984). The feature appears in stars as early as β Dra (G2 II) and as late as β Gru (M3 II) and is relatively stronger in the bright giants and supergiants than the giants. It is present only where there are other indications of a high opacity - eg through strong lines of O I (1641.3 Å) and C I (1993.6 Å). Given its proximity to O I and the way it reflects the O I line profile it could be a broad level, such as that in S I, above the first ionization limit, populated by photo-excitation by O I. The photoionization edge of S I from the $^1D_2$ level lies nearby. However, the whole feature could be understood in terms of excitation of Si II (1304.37 Å) by O I (1304.86 Å), the resulting profile of Si II (1309.27 Å) reflecting the asymmetry of the pumping process.

Given the presence of molecules in the photospheric spectra of cool stars it is at first sight surprising that there is not clear evidence of molecular fluorescence in the uv spectra. Fluorescent excitation of H_2 and CO by H Ly α and strong transition lines has been identified in the Naval Research Laboratory's spectra of sunspots, obtained with their High Resolution Telescope and Spectrograph (HRTS) (Jordan et al. 1978a, 1978b). Ayres, Moos and Linsky (1981) suggested that CO emission, excited by the O I lines could be present in the spectrum of α Boo (K2 III), at ~ 1340 Å,

1380 Å and 1420 Å; lines also appear at these wavelengths in low resolution spectra of α Tau. A high resolution spectrum of α Boo has been obtained recently to investigate this possible C O emission (Ayres et al. 1984) and weak broad patches of emission do seem to be present at the relevant wavelengths. The one object, other than the sun, from which H_2 fluorescence emission pumped by H Ly α has been definitely identified is the pre-main-sequence star T Tauri (Brown et al. 1979). The emission extends away from the star and is excited above the stellar atmosphere in the nearby gas cloud. The most likely explanation for the absence of stronger molecular emission in the cool giants and supergiant spectra is the high opacity between the source of excitation (eg H Ly α and O I) and the lower layers where the molecules exist.

Although space does not permit a full discussion there is evidence that photoionization or photo-excitation to high n states plays an important role in atoms such as S I and C I which have ionization limits near H Ly α. Judge (1984) has found that collisional excitation alone is not sufficient to account for the strength of the S I spectrum. Photo-excitation followed by cascades, radiative and di-electronic recombination also contribute to the observed emission in uv 1 and uv 3. The weakness of uv 5 relative to uv 2 can be caused by a high opacity in uv 5 transferring photons to uv 2 via the 4p ^3P term. This should give rise to strong emission at 1.89 μ.

SPECTROSCOPIC DIAGNOSTICS AT LOW DENSITIES

Having established line identifications in the cool giants and supergiants the subsequent modelling of the atmosphere from absolute line fluxes relies heavily on independent measurements of plasma parameters, particularly the electron density and total gas density. If strong turbulent motions or winds exist modelling from the emission measure using hydrostatic solutions gives only lower limits to the extent of the atmosphere.

Most of the density diagnostic techniques developed for solar work involve lines of at least doubly charged ions. The relative intensity of the intersystem line of C III, $2s^2\ ^1S_o - 2s2p\ ^3P_1$ to permitted lines remains sensitive to N_e down to $N_e \sim 10^9$ cm^{-3} and is still useful in the G bright giants. If one could be certain that the atomic data for level populations and ion populations were sufficiently accurate then the ratio of the Si III]/C III] lines at 1892 Å and 1909 Å provides a means of measuring departures from solar abundance ratios in evolved giants and supergiants. At the very low densities ($N_e \lesssim 10^6$ cm^{-3}) in planetary nebulae the ratio of the magnetic quadrupole transition $2s^2\ ^1S_o$-$2s2p\ ^3P_2$ to that of the corresponding ^1S_o-$^3P_1$ transition becomes density sensitive and the relevant atomic data are available (Nussbaumer and Schild, 1979, Keenan et al. 1984). This ratio places useful constraints on wind solutions for cool star atmospheres. The most sensitive and useful method to date for measuring N_e in low gravity stars cooler than ~ K 0 involves the C II] multiplet at ~ 2325 Å. Because of the range of A-values three pairs of relative intensities within the multiplet yield values of N_e (for the range 10^7-10^9 cm^{-3}). The atomic data available (Jackson, 1972; Dankwort and Trefftz, 1978; Nussbaumer and Storey, 1981) do not yield precisely the same values of N_e when applied but the discrepancies are not large (about a factor of two). Calculations of

the line ratios have shown that $N_e \sim 2 \times 10^8$ cm^{-3} at $T_e \sim 10^4$ K in the K and early M giants and bright giants but $\sim 10^7$ cm^{-3} in the M supergiant α Ori. The total flux in the C II multiplet relative to permitted lines is also density sensitive for $N_e \gtrsim 10^9$ cm^{-3}. But at $N_e \lesssim 10^9$ cm^{-3} the C II lines are more useful as a temperature diagnostic. Collision cross-sections for both the C II multiplet and the resonance lines at 1335 Å have recently been calculated by Hayes and Nussbaumer (1984) and their lower cross-section for the resonance lines resolves an anomaly in the apparent electron temperature derived from the 2325/1325 Å line ratio in α Tau and β Gru (Brown, Ferraz and Jordan, 1981).

At $T_e \lesssim 10^4$ K a measurement of the electron density does not also determine the total gas density since important species, eg hydrogen and helium, are not fully ionized. Opacity sensitive line ratios provide a valuable way of measuring the value of $\int N_H \, dh$ in the following way. The ideal case is where a strong resonance multiplet shares a common upper level with a semi-forbidden transition of substantially lower transition probability. Then, whilst the resonance lines become optically thick, the semi-forbidden line does not. A measurement of the line ratio, under assumptions concerning line profiles, allows the probability of escape and opacity in the resonance lines to be found, and hence $\int N_H \, dh$. Since the mean emission measure gives $\int N_e N_H \, dh$ an independent rough estimate of N_e can also be found. The lines of C I (1656 Å and 1994 Å) (Jordan, 1967) and O I (1302, 1305, 1306 Å and 1641 Å) (Brown, Ferraz and Jordan, 1981) are examples of this method. Although the branching ratios for C I have recently been measured and re-calculated (Tossi, Huber and Pauls, 1984) the transition probability used for the O I line at 1641.31 Å (Garstang, 1961; Müller, 1968) has not been re-examined in recent years.

DIRECTIONS FOR FUTURE WORK

Much of the high resolution spectroscopy of cool stars is now being carried out with exposures of up to ~ 22 hours. However it is still not possible to detect some of the unidentified emission seen at low resolution. Since the wavelength regions of interest have been established the Space Telescope high resolution spectrograph will be an ideal instrument for further work on cool stars. Similarly one could hope to improve and extend the observation of the density sensitive C II ratios which are not ideally placed regarding the sensitivity of the IUE long wavelength cameras.

Although neutral atoms are now well studied in laboratory sources and the situation for the singly charged metals has improved in recent years there is still a need for investigations of high levels near and above the first ionization limit.

ACKNOWLEDGEMENTS

Many of the high resolution spectra discussed in this review were obtained in collaborations between European observers (at Oxford and Oslo) using the ESA IUE ground-station at Villafranca, Madrid and US observers from the Center for Astrophysics, Cambridge, Mass. and JILA and LASP, University of Colorado, Boulder, using the NASA ground station at Goddard Space Flight Centre. Thanks are expressed to the staff at the ground stations.

REFERENCES

Ayres, T.R., Moos, H.W. and Linsky, J.L. 1981, Astrophys. J., 248, L137.

Ayres, T.R., Jordan, C., Judge, P., Brown, A. and Linsky, J.L. 1984, In preparation.

Bowen, I.S. 1947, Publ. Astr. Soc. Pacif., 59, 196.

Brown, A. and Jordan, C. 1980, Mon. Not. R. astr. Soc. 191, 37P.

Brown, A., Jordan, C. and Wilson, R. 1979, Proc. Symp. The First Year of IUE, UCL (Ed. A. Willis), p.232.

Brown, A., Ferraz, M.C. de M. and Jordan, C. 1981, Proc. Symp. The Universe at Ultraviolet Wavelengths: The First Two Years of IUE (Ed. R. Chapman) NASA C.P. 2171, p297.

Brown, A., Jordan, C., Millar, T.J., Gondhalekar, P. and Wilson, R. 1981, Nature, 290, 34.

Brown, A., Jordan, C., Stencel, R.E., Linsky, J.L. and Ayres, T.R. 1984, Astrophys. J. In press.

Carpenter, K.G. and Wing, R.F. 1979, Bull. Am. Astr. Soc. 11, 419.

Dupree, A.K. 1982, in 'Proc. Second Cambridge Workshop on Cool Stars; Stellar Systems and the Sun, SAO Special Rep. 392, Vol.II, p.3.

Engvold, O., Jensen, F. and Moe, O.K. 1983, Paper presented at Nordic Astronomy Meeting 15-17 August, Oslo.

Gahm, G.F. 1974, Astron. and Astrophys. Suppl. 18, 259.

Garstang, R.H. 1961, Proc. Camb. Phil. Soc. 57, 115.

Hagen, W., Black, J.H., Dupree, A.K. and Holm, A.V. 1980, Astrophys. J., 238, 203.

Haisch, B.M., Linsky, J.L., Weinstein, A. and Shine, R.A. 1977, Astrophys. J., 214, 785.

Hayes, M.A. and Nussbaumer, H. 1984, Astron. Astrophys. 134, 193.

Johansson, S. 1983, Mon. Not. R. astr. Soc. 205, 71P.

Johansson, S. 1984, Proc. 4th European IUE Meeting, Rome, In press.

Johansson, S. and Jordan, C. 1984, Mon. Not. R. astr. Soc. 210, 239.

Jordan, C. and Judge, P. 1984, Physica Scripta, T8, 43.

Jordan, C., Brueckner, G.E., Bartoe, J.D.F., Sandlin, G.D. and Van Hoosier, M.E. 1978a, Astrophys. J. 226, 687.

Jordan, C., Bartoe, J-D.F., Brueckner, G.E., Sandlin, G.D. and Van Hoosier, M.E. 1978b, Astrophys. J. 223, L51.

Judge, P. 1984, in 'Proc. Third Cambridge Workshop on Cool Stars'. Springer-Verlag (Ed. Baliunas, S.L. and Hartmann, L.) p.353.

Keenan, F.P., Berrington, K.A., Burke, P.G., Kingston, A.E. and Dufton, P.L. 1984, Mon. Not. R. astr. Soc. 207, 459.

Linsky, J.L. and Haisch, B.M. 1979, Astrophys. J., 229, L27.

Linsky, J.L. et al. 1978, Nature, 225, 19.

McKinney, W.R., Moos, H.W. and Giles, J.W. 1976, Astrophys. J., 205, 848.

Müller, D. 1968, Z. Naturforsch, 23a, 1707.

Nussbaumer, H. and Schild, H. 1979, Astron. Astrophys. 75, L17.

Nussbaumer, H. and Schild, H. 1981, Astron. Astrophys. 101, 118.

Nussbaumer, H., Pettini, M. and Storey, R.J. 1981, Astron. Astrophys. 102, 351.

Penston, M.V., Benvenuti, P., Cassatella, A., Heck, A., Selvelli, P., Macchetto, F., Ponz, D., Jordan, C., Cramer, N., Rufener, F. and Manfroid, J., 1983, Mon. Not. R. astr. Soc., 202, 833.

Stalio, R. and Selvelli, P.L. 1980, in 'The Universe at Ultraviolet Wavelengths: First Two Years of IUE', NASA CP 2171, p201.

Stencel, R.E., Linsky, J.L., Brown, A., Jordan, C., Carpenter, K.G., Wing, R.F. and Czyzak, S. 1981, Mon. Not. R. astr. Soc., 196, 47P.

Tondello, G. 1972, Astrophys. J. 172, 771.

Tossi, G.P., Huber, M.C.E. and Pauls, U. 1984, Astron. Astrophys. In Press.

Van der Hucht, K.A., Stencel, R.E., Haisch, B.M. and Kondo, Y. 1979, Astr. Astrophys. Suppl. 36, 377.

Viotti, R., Giagrande, A., Ricciardi, D., Altamore, A., Casatella, A., Friedjung, M., Muratorio, G., 1980, Proc. Second IUE European Conference, p39.

To appear in Proc. 8th Int. Coll. on EUV and X-ray Spectroscopy of Astrophys. and Lab. Plasmas, Washington, 27-29 Aug 1984.

SOFT X-RAY SPECTROSCOPY WITH EXOSAT

R. Mewe
Laboratory for Space Research
Utrecht, The Netherlands

Summary

With the 500 and 1000 l/mm transmission gratings aboard the *European X-ray Observatory SAT*ellite (*EXOSAT*) we have measured medium-resolution ($\Delta\lambda \approx$ 5 A at 100 A) spectra of some ten objects of various categories such as isolated white dwarfs, cool stars with convective mantles, cataclysmic variables (e.g. AM Her) and a high-luminosity X-ray source (Sco X-1).

The instrument configuration was mostly such that one low-energy telescope was used as a photometer, while the other telescope was used as a spectrometer with the 500 l/mm grating inserted.

The white dwarf spectra were measured between about 60 and 300 A. They show a continuum with no clear evidence of aborption and emission lines except for the He II absorption edge at 227 A in the spectrum of Feige 24. For the cooler (28 000 K) white dwarf Sirius B the emission is peaked between about 100 and 160 A and limited to about 200 A, which can be expected from atmospheric model spectra of DA white dwarfs. The soft X-ray emission of the hotter ($>$ 60 000 K) DA white dwarfs (HZ43, Feige 24) is also interpreted in terms of photospheric emission. In the HZ43 spectrum the absorption edge is apparently absent which sets a stringent upper limit to the abundance ratio He/H of about 10^{-5}. On the other hand the spectrum of Feige 24 shows a dominant absorption edge, implying He/H $> 10^{-3}$. Moreover, here the shape of the continuum may be indicative of a stratification of element abundances in the outer atmosphere.

The active late-type stars σ^2 CrB and Capella show in the spectral region between 90 and 140 A lines from Fe XVIII to Fe XXIII, indicative of the presence of hot ($\approx$ 10 MK) plasma like that in a Solar flare. On the contrary, the spectrum of the cooler corona of the star Procyon does not show the hot Fe XXII and Fe XXIII lines but instead a blend at 175 A of Fe IX, X and XI lines that are formed in a typically quiet corona of a temperature around 1.5 MK. Also the ratio of Fe XVI (65 A) and Si XII (48 A) lines is a good indicator of temperature in the spectra. From the spectral intensities and the additional results of the simultaneous multi-color photometry coronal temperatures and emission measures are derived. There are indications in the spectra that the emission should be interpreted in terms of differential emission measure distribution models.

1. Introduction

The first free-standing gold bar transmission gratings we made by holographic techniques (Dijkstra and Lantwaard 1975, Dijkstra 1976, Schnopper et al. 1977) were implemented in the objective grating spectrometer aboard the astronomical *EINSTEIN* X-ray observatory (see Seward et al. 1982). The gratings in the *European X-ray Observatory SAT*ellite (*EXOSAT*) were made by an improved lithographic technique of contact printing producing replica gratings from a master mask (Dijkstra et al. 1978). The grating line densities are 500 and 1000 lines per mm.

The use of transmission gratings allows the study of point-like cosmic soft X-ray sources like isolated white dwarfs, stellar coronae and cataclysmic variables with comparatively high efficiency combined with a moderate resolution ($\Delta\lambda$ typically ≅ 3 to 6 A from λ = 10 to 200 A for the 500 l/mm grating) in a large dynamic range that is measured simultaneously.

2. *Schematical design of EXOSAT spectrometer*

Fig. 1 gives a schematic layout of the optical arrangement showing convergent bundle from Wolter I telescope, transmission grating ring and one first-order focus at a given wavelength (a) and an enlarged view of two-loop focal curve for one grating ring (b), where p is the displacement from the first-order image (z_0) and a the total extent of the focal pattern determined by grating aberrations. Ray-tracing computer calculations for the double nested *EXOSAT* telescope (Dijkstra et al. 1978) give a more complicated pattern consisting of a superposition of four loops. The grazing incidence Wolter-type mirror has a net total geometric area of about 90 cm^2. The grating consists of 24 elements mounted on a ring 3 cm behind the mirror. The spectrum is imaged 85 cm behind the grating in the focal plane on a channel multiplier array (CMA) detector. For a point source on axis the zero-order image is in the center of the field of view, the plus and minus first and higher orders are formed perpendicularly to the grating lines symmetrically around the 0th order. There are two identical telescopes on board *EXOSAT*, one with the 500 l/mm grating and one with the 1000 l/mm grating. The wavelength coverage with the 500 l/mm grating is for an on-axis source ± 450 A and the first-order linear dispersion 42.5 μm/A. The resolution of the 500 l/mm grating is $\Delta\lambda$ ≅ 3 A for λ < 70 A (determined by effects of mirror and finite resolution of image detector) and $\Delta\lambda$ ≅ 0.04λ at longer wavelengths (dominated by grating aberrations, e.g. coma). Corresponding values for 1000 l/mm grating differ by a factor of about two.

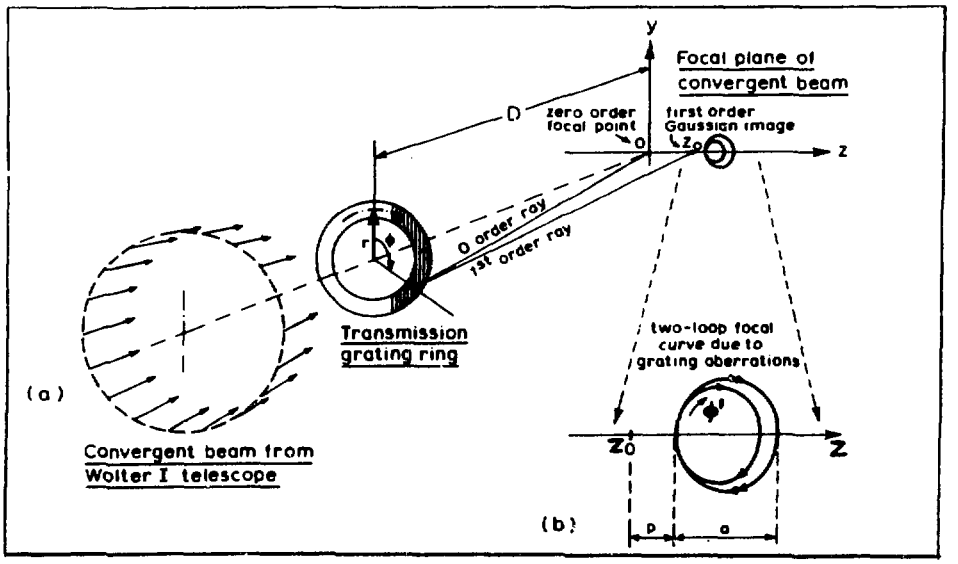

Fig. 1. Schematic layout of optical arrangement of *EXOSAT* objective grating spectrometer (see text).

The effective area of the spectrometer with the 500 l/mm grating is shown in Fig. 2 for various filter combinations (lex thin: thin (3000 A) lexan; lex thick: thick (4000 A) lexan; Al/P: Aluminum/Parylene; Ppl: Polypropylene; Boron: Boron). The efficiency of the 1000 l/mm grating spectrometer is comparable to this.

For a more detailed instrumental description see Brinkman et al. (1980).

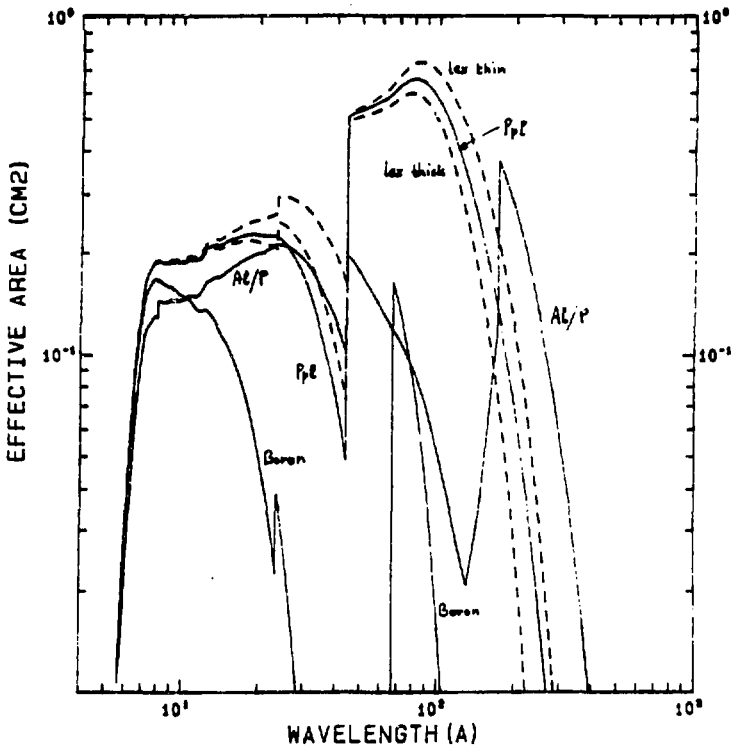

Fig. 2. Efficiency of 500 l/mm grating spectrometer (see text).

3. Observational results

3.1. Isolated white dwarfs

Observations with the *EINSTEIN* observatory have yielded a few new detections (Kahn et al. 1984) above the previously known sources such as Sirius B, HZ 43 and Feige 24.

Predictions on the basis of photospheric models (e.g. Wesemael et al. 1980) indicate that the bulk of the X-ray emission from hot (T_{eff} > 30000 K) white dwarfs falls in the XUV region. Therefore, the extension of the sensitivity towards longer wavelengths of *EXOSAT* compared to *EINSTEIN* makes it a suitable tool for studying the spectra of these objects. Indeed, recent *EXOSAT* results (Heise et al. 1984a) have demonstrated that isolated white dwarfs constitute a class of extreme soft X-ray emitters. Out of 12 pointings at least 8 are detected to be quite bright. They are mostly of spectral type DA or the hotter DB.

Spectra obtained with the *EXOSAT* grating spectrometer of the white dwarfs Feige 24, HZ 43 and Sirius B are shown in Fig. 3 and will be shortly discussed here. For further details I refer to a forthcoming paper by Heise et al. (1984b).

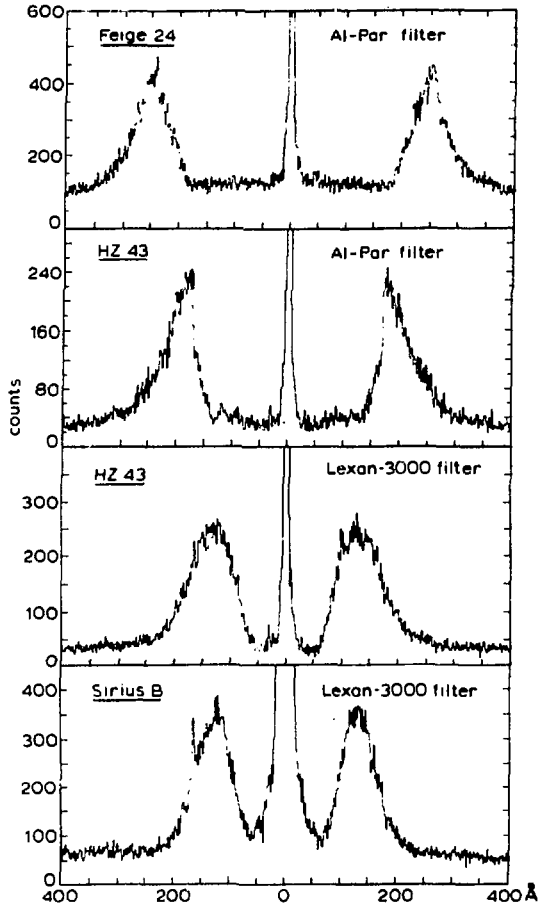

Fig. 3. *EXOSAT* 500 l/mm grating spectra of white dwarfs.

The spectrum of the comparatively cooler (≈28000 K) white dwarf Sirius B is peaked between 100 and 200 A, as is indeed predicted by the atmospheric model spectra of DA white dwarfs calculated by Wesemael et al. (1980). For the hotter dwarfs (> 40000 K) the models indicate an extension of the emission spectrum towards wavelengths above 200 A, which is indeed seen in the spectra of the hotter (T_{eff} near 60000 K) DA white dwarfs Feige 24 and HZ 43. In this case the *EXOSAT* observations provide the possibility of detecting the He II absorption feature. From the disappearance of helium lines in the optical spectra we know that the He/H abundance ratio should be lower than about 1% (e.g. Buess 1970), but model calculations predict already noticeable jumps at the He II Lyman absorption edge at 227 A for He/H abundance ratios above about 10^{-5}.

The spectrum of HZ 43 is everywhere well fitted by a pure hydrogen model spectrum. No jump at 227 A is observed, which implies a stringent upper limit of He/H $\leq 10^{-5}$. This contradicts the results obtained by Malina et al. (1982) which claim to find in a spectrum with a rocket-borne EUV imaging spectrometer a jump at the He II edge of a factor of 2, consistent with He/H abundance ratios in the range 1.5–6 10^{-5} for T_{eff}=45000–60000K. It should be remarked that most of their data points together with the measurements from Apollo-Soyuz and Voyager presented in their Fig. 2 can be reasonably fitted by a pure hydrogen model with T_{eff}=60000K and a hydrogen column density N_H=5 10^{17} cm^{-2}.

The spectrum of Feige 24 steeply declines below 230 A. It is neither fitted by a pure H model nor a pure He model. Reasonable fits require an abundance ratio He/H of at least about 10^{-3}, but still there are significant discrepancies on both sides of the peak. It will be investigated whether models with a stratification of element abundances give better agreement.

3.2. Stellar coronae

Grating spectroscopy has its most obvious application in the measurements of hot optically thin sources which are expected to display in their X-ray spectra many interesting emission line features from highly ionized elements.

The *EINSTEIN* observations have provided us with a picture of stellar coronae based on a lot of detections of X-rays from nearly every type of star (e.g. Vaiana et al. 1981, Mewe 1984), but at the same time they pose many questions concerning the structure of the sources and the nature of the X-ray generating mechanisms. It is interesting that the surface fluxes of late-type stars cover a range extending from 10^3 to 10^8 erg cm^{-2} s^{-1}, that is from more than ten times weaker than a Solar coronal hole up to ten times brighter than Solar active regions (Schrijver 1983)! Medium- to high-resolution spectroscopy is required to obtain accurate estimates of gas temperatures, emission measures and densities.

The few observations with the *EXOSAT* spectrometer are limited to some of the brighter stars for reasons of obtaining good statistics. We have chosen three late-type stars with widely different levels of intrinsic X-ray activity: Procyon (α CMi F5IV+DF), Capella (α Aur G6III+F9III) and σ^2 CrB (F6V + G1V) (underlined are the candidate X-ray emitters). The photometric *EXOSAT* observations (Brinkman et al. 1984) simultaneously with the grating measurements and earlier *EINSTEIN* observations (Schrijver et al. 1984) yield that these stars have increasing X-ray surface fluxes of about 2, 10 and 10^3 times that of the average Sun, respectively, consistent with the increasing rotation rates of these stars. Fig. 4 shows a composition of the spectra of these objects juxtaposed to each other on the same wavelength scale. The net observing times were 20 hrs for the two RS CVn stars and 6.5 hrs for Procyon. Various interesting line groups are indicated by letters a to g. Their temperature behaviour shown in Fig. 5 was calculated by folding theoretical spectra (Mewe et al. 1982, 1984) for an optically thin plasma with the instrumental response function.

A quick analysis (see also Brinkman et al. 1984) of these line blends shows for example that the "Solar flare" lines from $2s$-$2p$ transitions in Fe XXII (e) and Fe XXIII (f) are prominent for the RS CVn stars, but are absent in the Procyon spectrum, whereas in the latter spectrum a line blend around 175 A is present, which does not occur in the spectra of Capella and σ^2 CrB. These lines can be probably attributed to lines from Fe IX, X and XI ions which are formed in a cool quiet corona of about 1.5 MK, but which are comparatively faint in a hot corona of about 10 MK like those around the RS CVn stars. Furthermore, it is seen that the intensity ratio Fe XVI (c) / Si XII (b) decreases going from Procyon to σ^2 CrB. The photometric measurements indicate coronal temperatures of about 2, 5-10 and 6-12 MK for α CMi, α Aur and σ^2 CrB, respectively. Indeed from the temperature behaviour of the considered lines (compare Figs. 4 and 5) one can infer that the spectra from bottom to top indicate an increasing coronal temperature. The simultaneous appearance of lines from many different ionization stages in the spectra of the two hotter stars suggests that a differential emission measure distribution probably better fits the spectra than a single-temperature model does. However, further detailed analysis is still in progress to derive accurate physical parameters for the X-ray emitting structures.

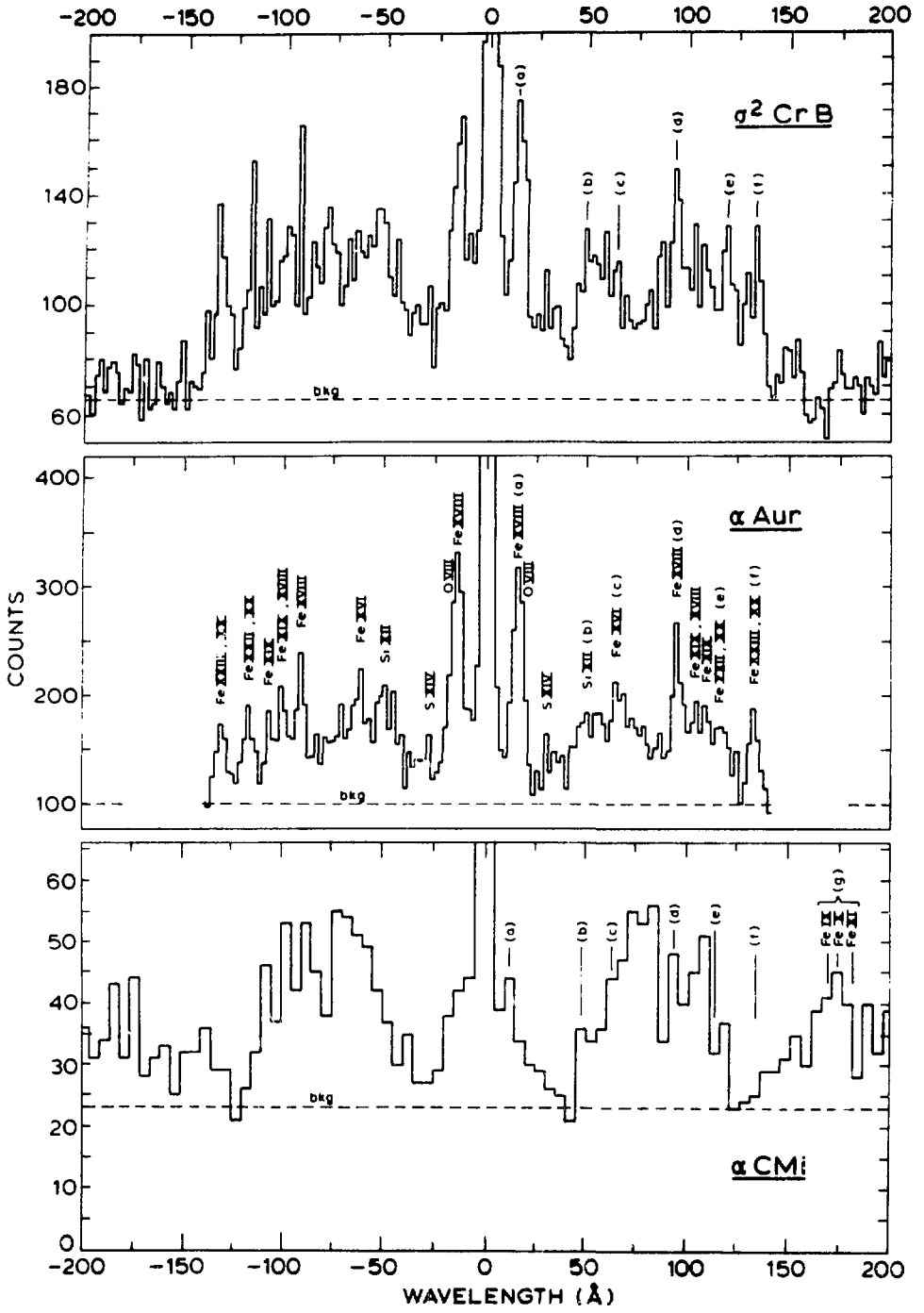

Fig. 4. *EXOSAT* 500 l/mm grating spectra of late-type stars. Letters a to g indicate line groups with different temperature behaviour (see Fig. 5). In all three cases the thin lexan filter was used.

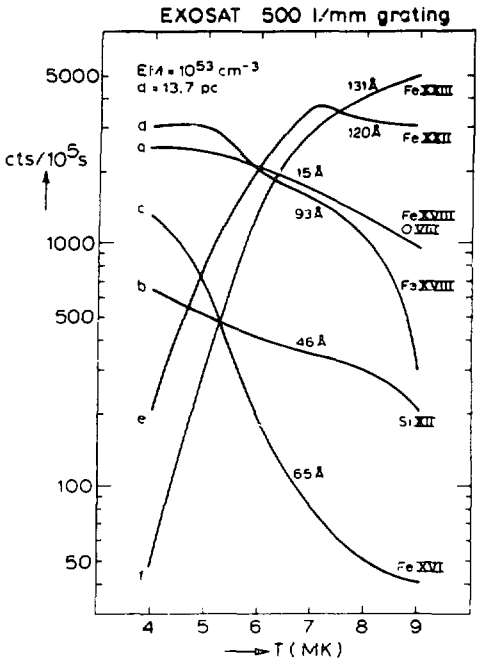

Fig. 5. Temperature behaviour of intensities of various line blends indicated in the spectra given in Fig. 4. The assumed widths of the blends correspond to about the spectral resolution. For each blend only the strongest line is indicated.

3.3. Miscellaneous sources

A few other sources such as the low-mass binary Sco X-1 and the magnetic white dwarf (polar) AM Her have been measured. The spectra of Sco X-1 (in both 500 and 1000 l/mm grating) contain features that are indicative of absorption edges and of line emission. During the observations these features varied strongly in time. The spectrum (detected with 500 l/mm grating) of AM Her comes from the optically thick soft X-ray component and can be fitted by blackbody radiation of temperature about 3 10^5 K and interstellar absorption with a column density $N_H = 8\ 10^{19}$ cm^{-2}. It is interesting that during the observations in summer 1983 the soft X-ray radiation was in anti-phase with the optically thin hard X-rays and this result will allow a critical discussion of the various models that exist for the generation of the soft X-ray component and the geometry of the emission region (see Heise et al. 1984c). Data analysis of these sources is still in progress.

4. Conclusions

These early results have demonstrated the potential of medium-resolution soft X-ray spectroscopy with transmission gratings in the study of astrophysical sources. We have seen that in the study of extreme soft sources like white dwarfs the main thrust of the *EXOSAT* spectrometer comes from the extension of the wavelength range. The extension towards longer wavelengths is also very important in studying the hot coronal sources which exhibit in their spectra groups of strong iron lines indicative either of hot (10 MK) plasma components (Fe XXII and XXIII lines around 130 Å) or the cooler (1.5 MK) quiet corona (Fe IX-XI at 175 Å). The analysis of these medium-resolution spectra already shows a glimpse of the enormous possibilities of next-generation spectrometers with one or two orders improvement in spectral resolution and throughput like in *AXAF*.

Acknowledgements Part of the research was made possible by the support of the Space Research Organization of the Netherlands (SRON). I am indebted to many of my colleagues for their efforts in the instrumental work, the preparation of the observations and the data analysis and I wish to thank also the staff of Resident Astronomers at ESOC for their help in acquiring the EXOSAT data.

References

Brinkman, A.C., Dijkstra, J.H., Geerlings, W.F.P.A., van Rooijen, F.A., Timmerman, C., de Korte, P.A.J.: 1980, Appl. Optics **19**, 1601.
Brinkman, A.C. et al.: 1984, to be publ. in COSPAR proc.
Bues, I.: 1970, Astron. Astrophys. **7**, 91.
Dijkstra, J.H., Lantwaard, L.J.: 1975, Opt. Commun. **15**, 3.
Dijkstra, J.H.: 1976, Space Sci. Instr. **2**, 363.
Dijkstra, J.H., Lantwaard, L.J., Timmerman, C.: 1978, in New Instrumentation for Space Astronomy (Eds. K.A. van der Hucht, G.S. Vaiana), Pergamon, London, p. 257.
Heise, J. et al.: 1984a, in preparation.
Heise, J. et al.: 1984b, to be publ. in COSPAR proc.
Heise, J. et al.: 1984c, to be publ. in proc. of Bologna (july) conf.
Kahn, S.M., Wesemael, F., Liebert, J., Raymond, J.C., Steiner, J.E., Shipman, H.L.: 1984, Astrophys. J. **278**, 255.
Malina, R.F., Bowyer, S., Basri, G.: 1982, Astrophys. J. **262**, 717.
Mewe, R., Gronenschild, E.H.B.M.: 1981, Astron. Astrophys. Suppl. Ser. **45**, 11.
Mewe, R.: 1984, Physica Scripta **T7**, 5.
Mewe, R., Gronenschild, E.H.B.M., Oord, G.H.J. van den: 1984, submitted to Astron. Astrophys. Suppl. Ser.
Schnopper, H.W., Van Speybroeck, L.P., Delvaille, J.P., Epstein, A., Källine, E., Babrach, R.Z., Dijkstra, J., Lantwaard, L.: 1977, Appl. Opt. **16**, 1088.
Schrijver, C.J.: 1983, Astron. Astrophys. **127**, 289.
Schrijver, C.J., Mewe, R., Walter, F.M.: 1984, Astron. Astrophys., in press.
Seward, F.D. et al.: 1982, Appl. Opt. **21**, 2012.
Vaiana, G.S. et al.: 1981, Astrophys. J. **245**, 163.
Wesemael, F., Auer, L.H., Van Horn, H.M., Savedoff, M.P.: 1980, Astrophys. J. Suppl. **43**, 159.

UV SPECTRA OF NEBULAE AND NOVAE

M.J. Seaton
Department of Physics and Astronomy
University College London
London WC1E 6BT
England

Optical spectra of nebulae and novae are dominated by recombination lines of H I, Be I and He II and by forbidden lines, such as those of [O III]. Their IR spectra show the fine-structure lines and continua due to dust. Most of the lines observed in the UV (say from 3000 to 1200 Å) are either due to resonance transitions (e.g. C IV 1549) or are of intercombination type (e.g. C III] 1908). Some elements do not have many lines in the optical - nitrogen gives only [N II] and there are no forbidden lines of ionized carbon - and for such elements much valuable information is provided by UV lines (e.g. N III], N IV], N V, C II], C III] and C IV). Carbon/oxygen abundance ratios deduced from combined UV and optical observations agree well with those deduced from IR continuum features (Seaton, 1983).

The nebular continua observed in the UV (Clegg et al. 1983) are mainly due to two-photon 2s-1s transitions in hydrogen. Some lines, such as C III 2297, appear with a strength which was unexpected and which has been explained in terms of the process of di-electronic recombination (Storey, 1981). For resonance lines, such as C IV 1549, scattered optical depths can be of order 10000 and radiation trapping can lead to absorption by dust even when the dust optical depth is small.

IUE observations of novae have enabled detailed abundance analyses to be made. Nova Cygni 1978 was found (Stickland et al., 1981) to have high abundances of C and O and a very high abundance of N, in accordance with predictions for thermo-nuclear run-away models. Two remarkable novae have been studied recently, Cra. 1981 (Williams et al., 1984) and Aql. 1982 (Snijders et al., 1984). Both have surprisingly high abundances of heavier elements - neon accounted for about one half of the mass in the gaseous envelope of Aql. 1982! Some gas-phase abundance anomalies are due to condensation of C, O, Mg and Si into dust grains. Others must be explained in terms of nuclear processing in the progenitors and during the outburst.

XR observations of nebulae and novae will be of great interest.

REFERENCES

Clegg, R.E.S., Seaton, M.J., Peimbert, M. and Torres-Peimbert, S., 1983. MN, 205, 417.
Seaton, M.J., 1983. IAU Symposium 103, p. 129.
Snijders, M.A.J., Batt, T.J., Seaton, M.J., Blades, J.C. and Morton, D.C. 1984. MN, submitted.
Stickland, D.J., Penn, C.J., Seaton, M.J., Snijders, M.A.J. and Storey, P.J., 1981. MN, 197, 107.
Storey, P.J., 1981. MN, 195, 27P.
Williams, R.E., Ney, E.P., Sparks, W.M., Starrfield, S.G., Truran, J.W. and Wyckoff, S., 1984. MN, submitted.

BROAD-BAND SPECTROSCOPY OF LATE-TYPE STARS WITH EXOSAT

M. Landini, B.C. Monsignori-Fossi, R. Pallavicini

Osservatorio di Arcetri, Florence, Italy

ABSTRACT

We analyze 6-300 Å observations of late-type stars obtained with EXOSAT. We discuss the problem of deriving source temperature and other physical parameters from broad-band EXOSAT observations.

1. INTRODUCTION

We have observed a number of late-type stars using the EXOSAT satellite. Our targets include active solar type stars of spectral types F8 to G5, as well as a group of flare stars of the BY Dra type. Preliminary results have been presented elsewhere (Landini et al. 1984a). In this paper we discuss the problem of deriving source temperatures from broad-band EXOSAT observations and we investigate whether an isothermal model can be used to adequately fit EXOSAT data.

2. OBSERVATIONS

The observations discussed in this report were obtained with the Low Energy Experiment LE1 on EXOSAT, using the Channel Multiplier Array (CMA) at the focal plane. Several filters were used in conjunction with the CMA. All targets were observed using the two softer filters 6 and 7 (Al/P and 3-Lexan, respectively), plus occasionally filter 3 (4-Lexan). For a few targets, we also detected weak signals using filter 8 (Boron), which has a harder spectral band, more similar to that of the EINSTEIN IPC. Background subtraction and source identification were performed using stardard procedures developed at ESOC.

The data have been analyzed using the model spectrum of Landini and Monsignori-Fossi (1984) which is appropriate for an optically-thin low-density plasma. The adopted spectrum has been proven to be in good agreement with similar calculations by Kato (1976), Mewe and Gronenschild (1981) and Gaetz and Salpeter (1983).

Since the Position Sensitive Detector (PSD) on EXOSAT was unavailable for our observations, source temperatures must be derived by comparing ob-

served CMA count rates through different filters. This provides a colour temperature for the isothermal plasma emitting the observed broad-band fluxes. The details of the procedure are given in the following section.

3. SOURCE TEMPERATURES AND EMISSION MEASURES

As all our targets were observed using at least filter 6 (Al/P) and filter 7 (3-Lexan), a temperature can be derived from the ratio of count rates in these two filters. This procedure, although simple, is quite crude and results in large uncertainties on the derived colour temperatures.

A more refined procedure is to construct for each CMA filter the locus of emission measure (EM) vs temperature (T) allowed by the observed count rates (including errors) and to search for regions of common interception. An example for the star 111 Tau is shown in Fig. 1. As seen from the figure, EM vs T curves for the softer EXOSAT filters (Al/P and 3-Lexan) cross at a temperature of $(4.5\pm1.0) \times 10^6$ K, corresponding to an emission measure of $(2.0\pm0.2) \times 10^{29}$ cm^{-5}. This solution however is not unique, and other regions exist for which the isothermal approximation gives an acceptable fit (once errors are taken into account). One such region is at $T \simeq 5 \times 10^5$ K and the other is at all temperatures between $\simeq 10^7$ and 10^8 K. This behaviour is typical for all stars observed in our program.

The ambiguity can be reduced if one has observations in substantially different spectral bands, such as the Boron filter on EXOSAT or the EINSTEIN IPC. In particular, the addition of IPC data allows us to exclude the solution at $T \simeq 5 \times 10^5$ K, while the Boron filter reduces the ambiguity at temperatures larger than $\simeq 10^7$ K.

Fig. 1 shows also the existence of a systematic effect. The IPC and Boron curves run lower than what expected from the crossing point of the Al/P and 3-Lexan filters, thus suggesting a somewhat lower source temperature. This effect is typical of all our observations. The agreement between the Boron filter and the IPC argues against temporal variability as the cause of the discrepancy. More likely, this effect may be due to one of the following causes. Either fluxes in the EXOSAT Al/P and 3-Lexan filters are overestimated, for instance owing to contamination by UV photons, or the assumption of an isothermal source is not very good. The first alternative is unlikely. We have estimated the degree of UV contamination of EXOSAT filters and we have found it to be negligible (less than 1%) for all stars in our program. More likely, a fraction of the fluxes measured by the Al/P and 3-Lexan filters (and also by the 4-Lexan filter) may be due to plasma at a much lower temperature than that responsible for the emission in harder spectral bands.

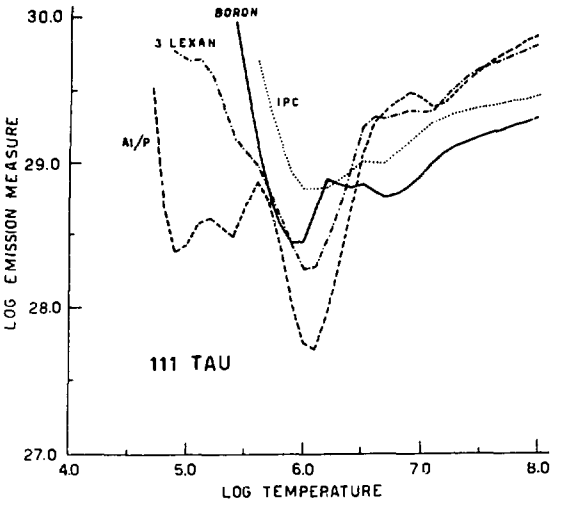

Fig. 1 - Loci of linear Emission Measure vs Temperature allowed by the observed EXOSAT and EINSTEIN X-ray fluxes.

Remaining in the limits of an isothermal approximation, we can derive a better estimate of the coronal temperature by using all available data and by determining the region of minimum deviation of all EM vs T curves from a common interception. When applied to 111 Tau, this procedure gives a temperature of 2.8×10^6 K, some 40% lower than the temperature derived using only the Al/P and 3-Lexan observations. The corresponding emission measure is 8×10^{28} cm^{-5}.

As a check of the goodness of the isothermal model, we have used the derived temperatures and emission measures to calculate expected count rates in various filters for comparison with observations. The results for 111 Tau are shown in Fig. 2. It appears that, within the errors, the isothermal model is able to give a sufficiently accurate fit to the observed count rates in all EXOSAT filters and in the IPC. However the systematic higher temperatures obtained using softer filters indicates the opportunity to investigate multi-temperature models.

Most stars in our program have temperatures around 3×10^6 K and linear emission measures in the range 3×10^{28} - 2×10^{29} cm^{-5}. For the flare star CC Eri we derive a temperature of $\simeq 10^7$ K and emission measure of 9×10^{29} cm^{-5} (cf. Landini et al. 1984a). The derived luminosities in the spectral band 0.04 - 2 KeV are in the range 4×10^{28} - 4×10^{29} erg s^{-1}, one to two orders of magnitude larger than for the Sun. This is consistent with the relatively high rotation rate and active nature of all stars in our program.

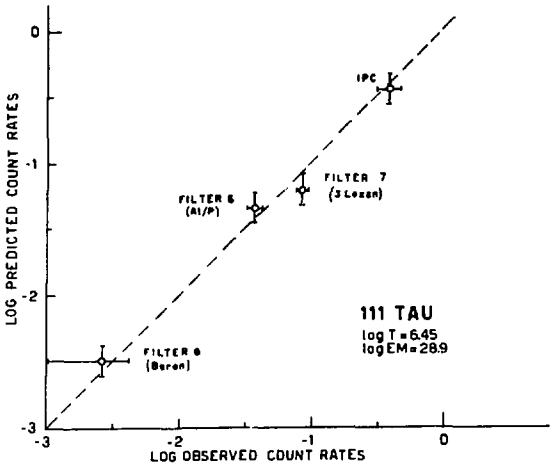

Fig. 2 - Observed and predicted EXOSAT and EINSTEIN count rates for an isothermal model of 111 Tau.

4. CONCLUSIONS

From the analysis above we draw the following conclusions:

a) An isothermal coronal model can be used as a first approximation to interpret EXOSAT observations of late-type stars.
b) Temperatures derived using softer EXOSAT filters (Al/P, 3-Lexan and 4-Lexan) are systematically higher by 30% to 50% than those obtained using also fluxes in harder spectral bands (Boron and/or IPC).
c) The systematically different temperatures obtained using different spectral bands suggest that a multitemperature model will probably fit better our EXOSAT observations.

We are exploring the latter possibility by using the loop model of Landini et al. (1984b). Results of this analysis will be published in a separate paper.

REFERENCES

Gaetz, T.J., and Salpeter, E.E. (1983) Ap. J. Suppl. 52, 155.
Kato, T. (1976) Ap. J. Suppl. 30, 397.
Landini, M., and Monsignori-Fossi, B.C. (1984) Physica Scripta T7, 53.
Landini, M., Monsignori-Fossi, B.C., and Pallavicini, R. (1984a) in X-Ray Astronomy '84, in press.
Landini, M., Monsignori-Fossi, B.C., Paresce, F., and Stern, R.A. (1984b) Ap. J., submitted.
Mewe, R., and Gronenschild, E.H.B.M. (1981) Astron. Astrophys. Suppl. 45, 11.

THE PROPOSED COLUMBUS MISSION: HIGH AND LOW RESOLUTION SPECTROSCOPY IN THE 100-2000 Å SPECTRAL REGION

Jeffrey L. Linsky[1,2]
Joint Institute for Laboratory Astrophysics
University of Colorado and National Bureau of Standards
Boulder, Colorado 80309 U.S.A.

For the past year a Joint Working Group of NASA and ESA scientists and engineers has been defining the scientific objectives and instrument parameters for a proposed satellite to obtain far and extreme ultraviolet spectra of stars, interstellar gas, solar system objects, and galaxies. The project, now called Columbus, incorporates the scientific goals of the previously proposed NASA Far Ultraviolet Spectrograph Explorer (FUSE) and ESA Magellan missions.

The prime spectral range of Columbus, 900-1200 Å, cannot be observed by IUE or Space Telescope. In this spectral range Copernicus was able to observe bright stars ($m_v \leq 6$) with high resolution and the Hopkins Ultraviolet Telescope (HUT) will observe faint sources at low resolution, but Columbus will be the first instrument capable of high spectral resolution observations of faint sources ($m_v \approx 17$). High resolution spectra in the 900-1200 Å region will permit studies of the Lyman lines of atomic H and D, the molecules H_2 and HD, resonance lines of C III and O VI, and other species listed in Table 1. Columbus also is being designed to observe the 1200-2000 Å spectral region at high resolution, permitting measurements of many stages of ionization for the same atom (i.e. N I, II, III, V; C II, III, IV; and S II, III, IV, VI). The broad coverage of ionization states is essential for the analysis of interstellar and stellar plasmas where the ionization balance can be quite complex.

Table 1. Important Spectral Lines Observable by Columbus

Species	log T_e	912-1216 Å Lines	Species	log T_e	100-912 Å Lines
H I, D I		1216, 1026, 973...912	Ne VII	5.8	465
H_2, HD		many lines 912-1120	Ne VIII	5.9	770, 780
N I		951, 964, 1133, 1200	Mg X	6.1	610, 625
A I		1048, 1066	Fe XII	6.3	187
N II	4.4	916, 1084, 1085	Si XII	6.4	499, 512
C III	4.8	977, 1175	Fe XV	6.5	284
N III	4.8	991	Fe XVI	6.6	335, 361
S III	4.8	1012, 1190	Fe XVIII	6.8	104
P IV	5.0	951	Fe XIX	6.9	108
S IV	5.0	1062	Fe XX	7.0	121
P V	5.2	1118, 1128	Fe XXI	7.2	103, 138, 150
O VI	5.5	1032, 1038	Fe XXIV	7.5	192, 225
S VI	5.5	933, 944			

[1]For the Columbus Joint Science Working Group.
[2]Staff Member, Quantum Physics Division, National Bureau of Standards.

Table 2. Prime Science Program of Columbus

Science objective	Spectral features to be observed	Astronomical targets
Primordial D/H ratio ratio in unprocessed gas	H, D Lyman lines H_2, HD	Interstellar gas in distant regions of galaxies
Morphology and kinematics of the hot component of interstellar matter	O VI, Fe XV, Fe XVI etc.	Disks and halos of galaxies
Hot (10^5–10^7 K) gas in active galactic nuclei	C III, O VI, Fe XV?, Fe XVI?	Quasars, Seyfert galaxies
Global energy balance of 10^4–10^7 K plasmas in outer atmospheres of stars	C III, O VI, Fe XV, Fe XVI, etc.	A-M main sequence, F-K giants, hot stars, binary systems
Energy balance of 10^4–10^7 K plasmas and physical processes during flares	O VI, Fe IX-XXIV	Transient stellar sources and binary systems
Evolution and winds of stars (mass loss, acceleration mechanisms, physical properties)	C III, O VI, Fe XV Fe XVI, etc.	Young and old hot stars, cool stars
Physical properties of hot evolved stars (temperature, luminosity, evolution, chemical composition)	EUV continuum, EUV absorption edges and lines	White dwarfs, subdwarfs, nuclei of planetary nebulae
Physical processes occurring in the magnetospheres of the giant planets and their satellites	H_2, S III-VI, O III, etc.	Neptune aurorae, Io torus

A novel feature of Columbus will be the capability for moderate resolution spectroscopy in the 100-900 Å region, which permits observations of plasmas hotter than 300,000 K (see Table 1) simultaneously with observations of the cooler plasmas. Since many types of stars, galactic nuclei, and the interstellar medium contain both cool and very hot plasmas, the ability of one instrument to observe all temperature regimes in the same object nearly simultaneously will be a powerful tool for solving many fundamental problems. Table 2 lists some of these scientific objectives; the types of astronomical objects to be studied; and the important spectral features to be observed. A more detailed description can be found in the Final Report of the Science Working Group for the Far Ultraviolet Spectroscopic Explorer.

Interstellar opacity will limit the number of objects which can be observed below the Lyman continuum limit at 912 Å. The opacity decreases as λ^3, however, and interstellar densities are very low ($n_H = 10^{-2}$-10^{-3} cm^{-3}) in the hot phase, which probably represents most of the volume of the interstellar medium. Thus, Columbus should be able to observe objects to considerable distances at 100-300 Å in some directions in the Galactic plane (see Fig. 1) and to larger distances perpendicular to the plane, perhaps even outside the Galaxy. In addition, many nearby objects can be observed above 300 Å.

The scientific goals and spectral features summarized in Table 2 are compatible with the tentative telescope and spectrograph parameters given in Table 3. The high resolution capability in the 900-1200 Å region (spectrograph A) is considered prime with a desired total effective area (telescope and spectrograph) of 100 cm^2. Coverage of the full spectral range at one time is highly desirable for each spectrograph. Work is now under way to develop more detailed designs for the scientific instrument, spacecraft, orbit, and operations.

The Columbus Joint Science Working Group is supported by NASA and ESA.

Table 3. Tentative Instrumentation

Telescope			
~1 m aperture grazing incidence optics 1 arcsec imaging long slit			
Spectrograph Capabilities			
Spectral Range (Å)	900-1200	1200-2000	100-2000
Spectral Resolution ($\lambda/\Delta\lambda$)	30,000	10,000	1,000
Spectrograph Type	Rowland?	Echelle	Grazing Incidence
Optical Surface Coatings	SiC, Aℓ, Os?	MgF_2	Au
Effective Area Specification	100 cm^2	---	---

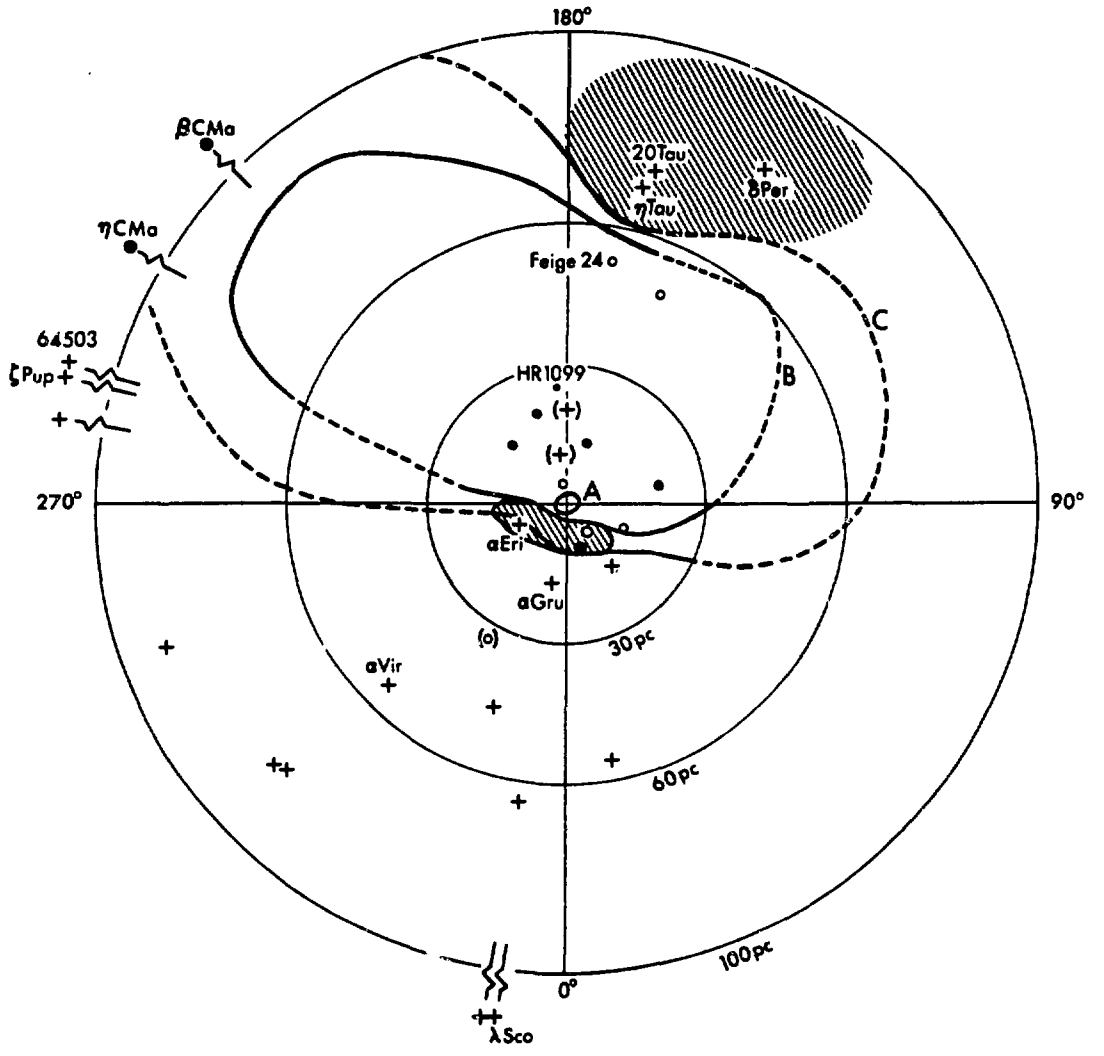

Fig. 1. Neutral hydrogen column density N_{HI} contours projected onto the plane of the galaxy (b = 0°). The Sun is at the center of the plot, distances out to 100 pc are indicated, and the direction toward the galactic center (ℓ = 0°) is at the bottom. Line A is the contour of $N_{HI} \sim 5 \times 10^{17}$ cm^{-2}, corresponding to $\tau_{500\ Å} = 1$, $\tau_{200\ Å} \approx 0.1$, and $\tau_{100\ Å} \approx 0.01$. Line B is the contour of $N_{HI} = 25 \times 10^{17}$ cm^{-2}, corresponding to $\tau_{500\ Å} = 5$, $\tau_{200\ Å} \approx 0.5$, and $\tau_{100\ Å} \approx 0.05$. Line C is the contour of $N_{HI} \sim 50 \times 10^{17}$ cm^{-2}, corresponding to $\tau_{500\ Å} = 10$, $\tau_{200\ Å} = 1$, and $\tau_{100\ Å} \approx 0.1$. All open circles are white dwarfs. Small circles represent stars with $N_{HI} \leq 5 \times 10^{17}$ cm^{-2}, medium circles represent stars with $5 \times 10^{17} < N_{HI} < 25 \times 10^{17}$ cm^{-2}, the large circles represent stars with $25 \times 10^{17} < N_{HI} < 50 \times 10^{17}$ cm^{-2}, and the crosses represent stars with $N_{HI} > 50 \times 10^{17}$ cm^{-2}. Stars with measured hydrogen column densities but which are located within 10 pc projected distance are not plotted. Data compiled by York and Frisch (from Final Report of the FUSE Science Working Group).

X-RAY SPECTROSCOPIC MEASUREMENTS OF NON-EQUILIBRIUM IONIZATION IN SUPERNOVA REMNANTS

T. H. Markert, C. R. Canizares, T. Pfafman and P. Vedder
MIT, Center for Space Research, Cambridge, MA 02139

P. F. Winkler
Dept. of Physics, Middlebury College, Middlebury, VT 05753

A. Pradhan
JILA, University of Colorado, Boulder, CO 80309

INTRODUCTION

When a cool plasma is shock-heated to X-ray temperatures, the ionization structure does not attain its final, equilibrium value immmediately, but proceeds toward it through electron-ion collisions with a timescale $\tau \equiv n_e t$ of order 10^{12} cm^{-3} sec. For supernova remnants (SNRs), where $0.1 \lesssim n_e \lesssim 10$ cm^{-3} typically, the time required to achieve collisional ionization equilibrium (CIE) can be greater than the age of the remnant. Even if the SNR is quite old, that part of the remnant which is emitting most of the X-rays may have been shocked relatively recently, so that the assumption of CIE may be inappropriate (see below).

The question of ionization equilibrium is of great astrophysical importance in the study of SNRs because it affects the deduced values of their masses and elemental abundances (e.g. Shull 1982). Mass determinations are affected because underionized plasma generally has a much higher emissivity in soft X-rays than equilibrium plasma. Unless this is accounted for, the deduced value of the density and therefore of the mass, will be considerably overestimated.

In this paper we will discuss a simple model for non-equilibrium ionization (NEI) that we have used to assist us in the analysis of high-resolution ($E/\Delta E \sim 50$ to 500) X-ray spectra obtained with the Focal Plane Crystal Spectrometer (FPCS) on the Einstein Observatory (Giacconi et al. 1979). Here we will apply this model to FPCS observations of 3 SNRs.

MODEL

We begin with a relatively cool plasma with cosmic abundances and shock-heat it to X-ray temperatures (i.e. we assign a value to the electron temperature T_e between 10^6 and several $\times 10^7$ K). The density of each ion (for a particular element) is given by

$$\frac{1}{n_e}\frac{dn_z}{dt} = n_{z-1}S_{z-1} - n_z(S_z + \alpha_z) + n_{z+1}\alpha_{z+1}$$

where z is the ionic charge, S_z is the electron collisional ionization rate for the process $n_z \rightarrow n_{z+1}$ and α_z is the total (radiative plus dielectronic) recombination rate for $n_z \rightarrow n_{z-1}$. These coefficients were taken from Mewe and Schrijver (1978) except for the case of iron,

where they were taken from Jacobs et al. (1977).

These ion balance equations were solved on the computer by a modified Euler's method and provide us with the ion structure of each element as a function of τ. An example appears in Figure 1.

Some of the most useful diagnostics for the determination of NEI parameters are the relative intensities of the lines of the n = 2 to n = 1 transitions of the helium-like ions (e.g. Pradhan and Shull 1981). We computed the ratios of the intensities of these lines in the low-density limit including the effects of electron impact excitation, inner-shell ionization of the Li-like ion, radiative and dielectronic recombination, and cascades. (The rate coefficients were determined by one of us [A.P.].)

When the ionization balance and relative line strengths for the helium-like ions have been determined for a set of τ and T_e, we prepared a set of graphs with line and ion ratios on the axes and an overlaid τ - T_e grid. Figure 2 is an illustration of the final output for a set of oxygen lines. In order to use these graphs we must have a measurement of the He-like lines and an estimate of the H to He-like ion population ratio for the element in question. This latter ratio can be obtained from any two lines of the same species for which electron impact is the dominant excitation mechanism. For the example in Figure 2 we selected the O VIII Ly α (n = 2 to n = 1) and the O VII He β lines (n = 3 to n = 1) at 654 and 666 eV respectively.

Once the set of ratios is determined and plotted, a corresponding range of τ and T_e is determined from the grid. In the example (Figure 2) we have used observations taken from the interior of Puppis A (Winkler et al. 1981) to find $\tau \sim 2.2 \times 10^{10}$ cm^{-3} s and $T_e \sim 6 \times 10^6$ K. Note that this plasma is well separated from CIE, which is represented by the log τ = 12.0 line. Also note that the temperature determined exclusively from the ion population ratio (assuming CIE) is log $T_e \sim 6.4$, much cooler than found by our NEI model (log $T_e \sim 6.8$). This indicates that the plasma is still ionizing and the H to He-like ratio is smaller than would be expected for a plasma in equilibrium at log $T_e \sim 6.8$.

EXAMPLES

We have applied our model to several SNRs and here present some of the results. All data were obtained with the FPCS.

A. Puppis A Knot

The highest X-ray surface brightness in Puppis A (as measured by the Einstein HRI) is from a knot of emission which lies just to the east of the Puppis A shock front (Petre et al. 1982). We have FPCS measurements of this knot for the He-like neon lines (He α n = 2 to n = 1 and Heβ n = 3 to n = 1) and H-like Lyman α, so that we are able to restrict the τ - T_e region. Furthermore, we have determined the H-like to He-like oxygen population ratio from the O VIII Ly α and O VII He β line strengths, and so can further restrict the allowed region of (τ, T_e) space. We find $T_e = (7 \pm 1) \times 10^6$ K and $\tau = (3 \pm 0.6) \times 10^{10}$ cm^{-3} s. (Note that our results are independent of the relative abundances of oxygen to neon).

Petre et al. (1982) interpreted the eastern knot to be a recently

shocked interstellar cloud with electron density $n_e \sim 10$ cm^{-3}. Our value of $\tau \simeq n_e \times t$ implies that the shock occurred approximately 3×10^9 s = 100 yr ago. The electron temperature implies a shock velocity of $\simeq 700$ km s^{-1} (assuming electron-ion equipartition)). In 100 years the shock would thus traverse ~ 0.1 pc, about the size of the bright features in the knot.

B. Cygnus Loop

We scanned an X-ray bright region in the NW of the Cygnus Loop with the FPCS. We observed the O VII He α and He β lines, the O VIII Ly α line and the Ne IX He α lines, enabling us to restrict the values of τ and T_e. We find $7.0 > \log T_e > 6.45$ and $9.9 < \log \tau < 11.4$, significantly far from CIE. Although the Cygnus Loop is $\sim 20{,}000$ yr. old (Ku et al. 1984), it is not necessary to require CIE. The observed X-ray emission may rise from a more recently shocked region. Even if the plasma was shocked 20,000 yr. ago, our results require only $n_e \lesssim 0.47$ cm^{-3}. Ku et al. (1984) find the mean density of the interstellar medium to be ~ 0.16 cm^{-3} or, assuming a hard shock $\langle n_e \rangle \sim 0.64$ cm^{-3}, not far from what we require.

C. N132D

N132D is a relatively young (age estimates range from 1000 to 3000 years) remnant of a Type II supernova in the Large Magellanic Cloud. Our observations of Ne IX He α and Ne X Ly α lines are sufficient to restrict (τ, T_e) space to a region centered about $\log \tau = 11.4$ and $\log T_e = 6.8$. Unlike our results for Puppis A and the Cygnus Loop, CIE is permitted for N132D, for temperatures between $6.65 \lesssim \log T_e \lesssim 6.80$. If N132D has attained CIE, then the mean n_e must be $\gtrsim 10$ cm^{-3} (this is the mean density for the entire remnant, since N132D fits within the FPCS viewing aperture). Such a density would be extremely high if we were viewing primarily the shocked interstellar medium. However, other FPCS observations of this object require a large overabundance of oxygen relative to iron, suggesting that most of the X-ray emission comes from the supernova ejecta, for which the oxygen has been greatly enriched by the Type II supernova explosion. The density of the ejecta can be considerably higher than the ambient medium and CIE could be attained in a few thousand years.

COMPARISON WITH OTHER MODELS

Our model provides a simple, but fairly accurate picture of several astrophysical situations. For SNRs, it is certainly appropriate for observations of recently shocked interstellar clouds (such as the knot in Puppis A) or a relatively small portion of a very extended object (such as the FPCS observations of the Cygnus Loop). In fact, it can be used for any situation where the plasma can be characterized by a single electron temperature and ionization time. Even in more complex situations, such as for N132D where there is a superposition of plasmas shocked over a long period of time at different temperatures, the X-ray spectrum is frequently dominated by plasma with a small range of T_e and τ. Hamilton and Sarazin (1984) have shown this to be true for a wide range of SNR models. We have recently begun to compare our model with

the more complex Sedov model developed by Hamilton, Sarazin and Chevalier (1983). We find considerable agreement between the two pictures if we interpret our T_e and τ as the mean electron temperature and ionization time of the material in the primary shock.

This work was supported in part by NASA Contract NAS-8-30752.

REFERENCES

Giacconi, R. et al. 1979, Astrophys. J., 230, 540.
Hamilton, A. J. S., Sarazin, C. L., and Chevalier, R. A. 1983, Astrophys. J. (Suppl.), 51, 115.
Hamilton A. J. S. and Sarazin, C. L., 1984, submitted to Astrophys. J.
Jacobs, V. L., Davis, J., Kepple, P. C. and Blaha, M. 1977, Astrophys. J., 211, 605.
Ku, W. H-M., Kahn, S. M., Pisarski, R. and Long, K. S. 1984, Astrophys. J., 278, 615.
Mewe, R. and Schrijver, J. 1978, Astron. Astrophys., 65, 99.
Petre, R., Canizares, C. R., Kriss, G. A. and Winkler, P. F. 1982, Astrophys. J., 258, 22.
Pradhan, A. K. and Shull, J. M. 1982, Astrophys. J., 249, 821.
Shull, J. M. 1982, Astrophys. J., 262, 308.
Winkler, P. F., Canizares, C. R., Clark, G. W., Markert, T. H. and Petre, P. F. 1981, Astrophys. J., 245, 574.

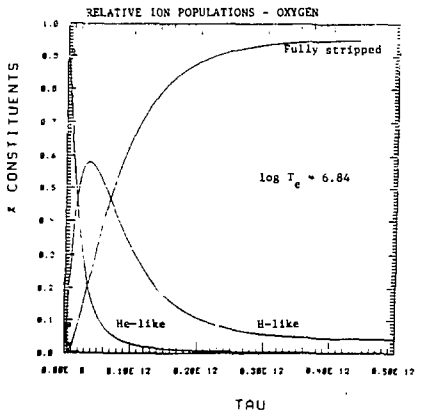

Fig. 1 (above) Solution to ionization balance equations for an oxygen plasma suddenly heated to log T_e = 6.84. Note that CIE is essentially established by $\tau = 3 \times 10^{11}$.

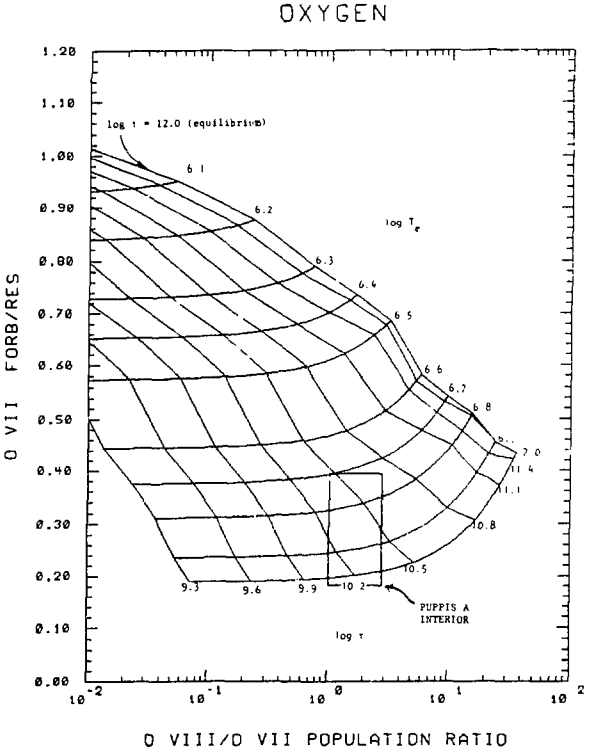

Fig. 2 (right) Determination of NEI parameters (T_e, τ) from observations of oxygen lines. The example is from FPCS observations of Puppis A.

OBJECTIVE GRATING SOFT X-RAY SPECTROSCOPY OF COMPACT BINARY X-RAY SOURCES

S.M. Kahn
Department of Physics
University of California
Berkeley, CA 94720

S.D. Vrtilek
Department of Astronomy
Columbia University
New York, NY 10027

L. Chiappetti and N.E. White
European Space Operations Centre
European Space Agency
Darmstadt, West Germany

INTRODUCTION

The presence of objective transmission gratings on the two recent X-ray telescope experiments, the Einstein and EXOSAT Observatories, has opened up a new avenue of research in X-ray astronomy by enabling us, for the first time, to obtain moderate-to-high resolution spectra of cosmic sources in the soft X-ray band ($\lambda \sim 5$-200 Å). Both experiments incorporated gold bar transmission gratings with line densities of 500 l/mm and 1000 l/mm which could be inserted into the X-ray optical path at the exit from a grazing incidence mirror. At short wavelengths, the resolution was determined principally by the spatial resolution of the detector-telescope combination. For Einstein, this was $\Delta\lambda \sim 0.4$ Å for the 1000 l/mm grating and ~ 0.8 Å for the 500 l/mm grating. For EXOSAT, the resolution was somewhat worse: $\Delta\lambda \sim 1.5$ Å for the 1000 l/mm grating, and ~ 3 Å for the 500 l/mm grating. (More complete descriptions of these instruments can be found in Seward et al. 1982 and de Korte et al. 1981.)

The peak effective area of the objective grating experiments was ~ 1 cm^2 in both cases. This is rather low by cosmic X-ray astronomy standards, and the spectroscopic observations performed thus gave useful results only for relatively bright sources. Compact X-ray binaries, which are among the brightest soft X-ray sources in the sky, were consequently the most common objects observed. These are believed to be interacting binary systems containing a relatively normal star which transfers matter onto a collapsed companion, either a neutron star, a black hole, or a white dwarf. The energy released by gravitational infall heats the accreting material to temperatures $\sim 10^8$ K thereby producing copious X-ray emission. Moderate-to-high resolution soft X-ray spectroscopy of such sources can be useful primarily as a probe of this circumsource accreting flow. The transfer of the intense X-radiation outward through the cooler, less dense, accreting gas can produce a number of observable spectral features in the soft X-ray band. K-shell lines and edges of partially ionized CNO and L-shell lines of partially ionized Fe are particularly important. Measurements of such features can yield sensitive constraints on the density, temperature, and geometry of the surrounding medium.

Here we present a brief review of some of the spectra of bright X-ray binaries that have been obtained with the objective grating instruments on Einstein and EXOSAT. The data are quite complex, and at this point, only general, qualitative conclusions can be drawn. However, the data do suggest the power of soft X-ray spectroscopic observations for this field, and provide an important impetus for the development of higher sensitivity, higher resolution grating experiments on future satellite facilities.

SCORPIUS X-1

We begin with the Einstein observations of Sco X-1. Four separate exposures were taken, each ∿ 5000 s long. The raw count spectra resulting from these observations are shown in Figure 1 below. As can be seen, the data do exhibit some obvious discrete spectral structure. In order to interpret such features however, it is useful to first model

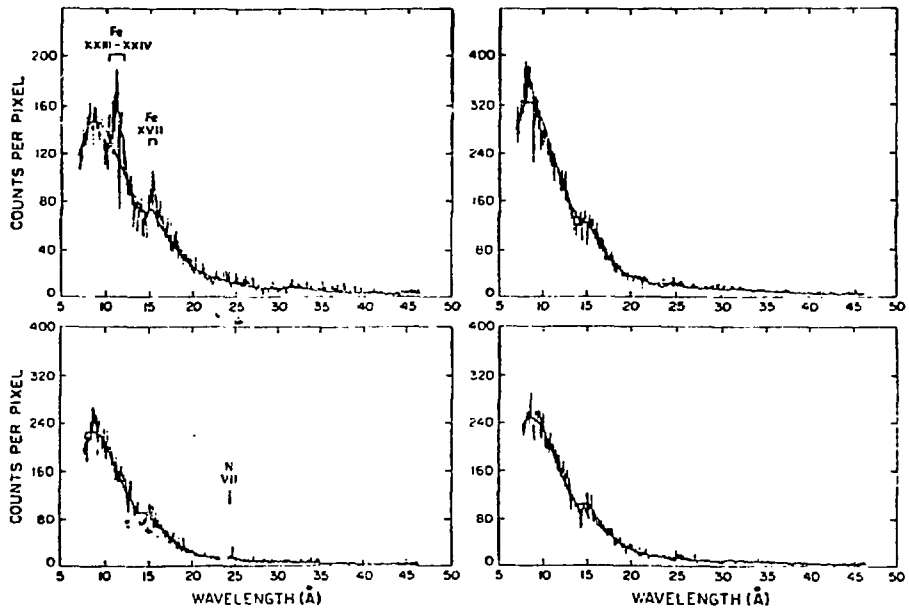

Figure 1. Raw Einstein objective grating spectra of Scorpius X-1. Obvious emission features are marked. The solid lines represent the best fit model continuum spectra.

the continuum; otherwise it is difficult to discriminate regions of true continuum from weak emission or absorption complexes. The model we have chosen to fit involves a slightly Compton-deformed bremsstrahlung continuum absorbed at long wavelengths by intervening material. Such a model has always been found to provide an acceptable fit to the low resolution spectra which have been obtained in the past.

When we perform these model fits, we find the first interesting fact about these spectra: even after allowing for the presence of discrete features, it is impossible to obtain near acceptable χ^2's without also allowing for abundance anomalies in the absorbing medium, an underabundance of oxygen and an overabundance of nitrogen with respect to cosmic

values. Such anomalous abundances are suggestive of CNO processing associated with hydrogen burning. This result is of interest for Sco X-1 since the secondary star in that system is thought to be evolved (Cowley and Crampton 1975). It is possible that processed material produced in the hydrogen burning layers of the evolved secondary could be dredged to the surface via convection, and then transferred to the compact object through the accreting flow. The abundance anomaly thus strongly suggests that the absorbing component in the spectra is associated with accreting material, which is local to the system.

The best fit continuum models (incorporating these anomalous abundances) are plotted as solid continuous lines in Figure 1. Discrete residuals to the fits, which are suggestive of emission features, are marked and line identifications are indicated where possible. Typical equivalent widths for these features are $\sim$ 0.1 Å. The range of ions observed is striking; it is indicative of a large spread in temperature, $\sim 10^5$-10^8 K. The N VII line visible in the third spectrum is particularly interesting. Note that it is not accompanied by O VII lines near 22 Å or an O VIII line near 19 Å. In most X-ray transfer situations where the N VII line is expected to be prominent, the oxygen lines would be at least of comparable intensity for a normal abundance medium. Thus, our observations suggest that the N/O ratio is high in the line emitting component as well. For a more complete discussion of these spectra, see Kahn, Seward, and Chlebowski (1984).

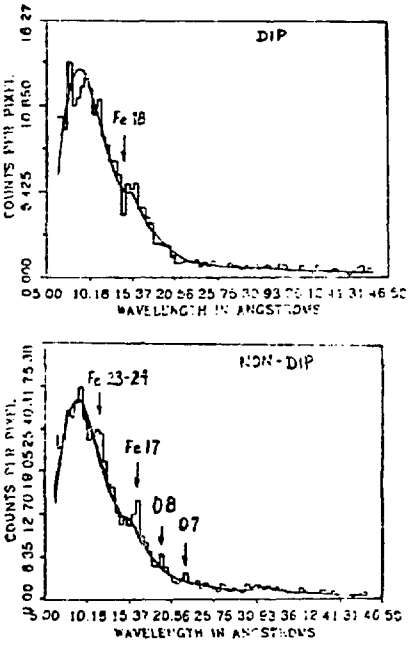

Figure 2. Einstein objective grating spectra of Cygnus X-2 acquired during "dip" and "non-dip" intervals. The smooth solid lines are model continua.

CYGNUS X-2

The Einstein grating study of Cyg X-2 is interesting because the source was quite variable during the course of the observation. In particular, the zero order countrate exhibited a series of recurrent dips involving reductions in flux by as much as 40%. The dip durations were $\sim$ 1000 s and they were separated by time scales of order several thousand seconds. The Monitor Proportional Counter (MPC) on Einstein, which observed the source simultaneously at higher energies (2-20 keV), also detected these dips, however the fractional reduction in flux was not as large for that instrument. Hence, the overall continuum spectrum of the source must have "hardened" during the dips.

In order to investigate the matter further, we compiled grating spectra of the source separately for the "dip" and "non-dip" intervals. The results are shown in Figure 2. Best fit model continua have been derived in the same manner as for Sco X-1. For Cyg X-2, we also require an underabundance of oxygen and an overabundance of nitrogen in the absorbing medium. That is, perhaps, not surprising since the companion star for Cyg X-2 is known to be evolved as well (Cowley, Crampton, and Hutchings 1979). Note that the spectra during "dip" and "non-dip" states are different.

The "non-dip" spectrum exhibits emission lines, most of which can be readily identified. These do not appear in the "dip" spectrum. Instead there is an apparent absorption line probably associated with Fe XVIII. The derived absorbing column density is also higher in the "dip" spectrum as expected form the spectral hardness variations.

This spectral behavior suggests an interpretation of the dips. If we imagine an obscuring blob passing in front of our line of sight, we expect an increase in the photoelectric absorption and may see absorption lines like Fe XVIII. As the blob moves away, the column density should decrease and the flux should increase. In addition, the irradiated face of the blob should become visible, and we might expect to see emission lines due to recombination by atoms which have been ionized by the incident X-ray flux. We are presently working to quantify this scenario and derive concrete constraints on the density of this blob and its location with respect to the central source (Vrtilek et al. 1984).

4U1543-47

4U1543-47 is an X-ray transient previously observed by experiments on several X-ray satellites. It was detected again in outburst by the Tenma Observatory in late August of 1983, and the EXOSAT Observatory team was quickly notified so as to facilitate an EXOSAT pointing while the source was still bright. The EXOSAT observation lasted ∿ 6000 s. Both the 500 1/mm and the 1000 1/mm gratings were used simultaneously together with higher energy experiments.

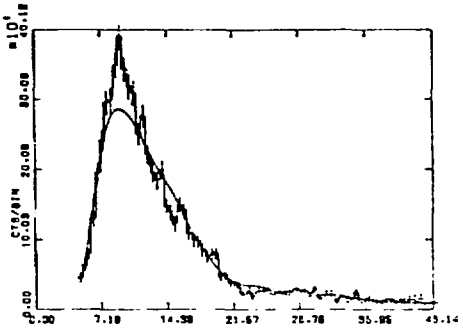

Figure 3. EXOSAT objective grating spectra of 4U1543-47 during outburst. The solid line is the best fit model continuum. Note the excess near 10 Å in the data.

The raw 1000 1/mm spectrum obtained during the first half of the observation is shown in Figure 4 along with the best fit model continuum. Interestingly enough, the model fits for this source also require a marked underabundance of oxygen. Even after allowing for abundance anomalies however, the fit is still poor, primarily because of a large excess at short wavelengths, $\lambda \sim 8\text{-}11$ Å. This is observed on both sides of the spectrum and with both gratings. If we explicitly add an emission line to the model, we can obtain a reasonable fit to the data, with a required line equivalent width ∿ 0.6 Å. However, the best fit wavelength, $\lambda \sim 9.8$ Å, does not correspond to any known transition expected to be prominent. The line is also unresolved; an upper limit to the intrinsic width is ∿ 0.2 Å. It is interesting to note though that the best fit continuum model parameters agree well with those derived from the higher energy data. These results are preliminary, but they do suggest that future grating observations of X-ray binaries may yield surprises.

References

Cowley, A.P. and Crampton, D., 1975, Ap. J., 201, L65.
Cowley, A.P., Crampton, D., and Hutchings, J.B., 1979, Ap. J., 231, 539.
Kahn, S.M., Seward, F.D., and Chlebowski, T., 1984, Ap. J., 283, 286.
de Korte, P.A.J. et al., 1981, Sp. Sci. Rev., 30, 495.
Seward, F.D., et al., 1982, Appl. Opt., 21, 2012.
Vrtilek, S.D., Kahn, S.M., Seward, F.D., and Grindlay, J.E., 1984, in prep.

HIGH RESOLUTION EUV & SOFT X-RAY SPECTROMETERS USING VARIABLE GROOVE SPACINGS

M. Lampton, M. C. Hettrick, and S. Bowyer
Space Sciences Laboratory
University of California
Berkeley CA 94720 USA

Introduction

Spectroscopic analysis is a powerful technique for the diagnosis of temperatures and compositions of astrophysical plasmas. The EUV (100-1000Å) and soft x-ray (10-100Å) bands contain hundreds of potentially useful diagnostic lines. Unfortunately, traditional types of grating spectrometer become inefficient or unwieldy when adapted to stellar spectroscopy onboard a spacecraft. At grazing incidence, the required length of a high-resolution plane-grating spectrometer can easily exceed the length of the telescope feeding it. For these reasons, we have systematically explored ways to introduce a reflection grating into the converging beam formed by a given objective optical system ahead of its first focus. A spectrometer of this type results in an optical train no longer than the telescope's existing prime-focus beam.

Varied-Groove-Spacing Gratings

If placed in a converging beam, the linear dispersion of a conventional uniformly-ruled plane reflection grating will vary from point to point over the entrance pupil of the beam. By varying the groove spacing over the face of the grating to satisfy the local grating equation at a given order, wavelength, and dispersion, this problem can be enormously reduced[1]. The general arrangement is shown in Figure 1, below.

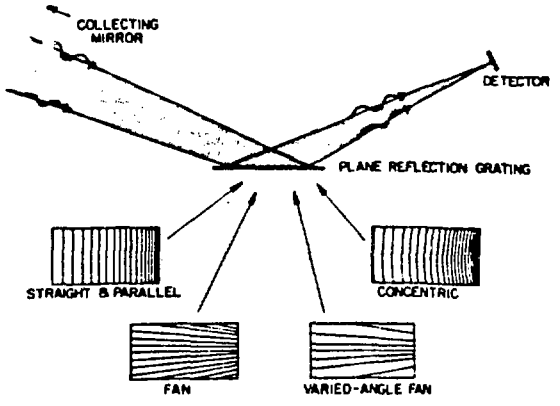

Figure 1.

Plane reflection gratings in converging light can be designed with a variety of groove illumination schemes and groove plans.

One important configuration is the in-plane mount, in which the incident and diffracted rays are approximately perpendicular to the grooves. The in-plane mount produces a straight linear spectrum and also offers the highest possible linear dispersion for a given spectral order. We have investigated a series of in-plane gratings with the goal of establishing

their performance in the areas of spectral resolution, throughput, and imaging (the ability to concentrate light in the direction perpendicular to the dispersion.)

Figure 2 is a set of spot diagrams illustrating the performance of four in-plane gratings having grooves optimally spaced for one wavelength, λ304Å, in the -1 order. The straight grooves (Figure 2a) and concentric grooves (2d) can be ruled by mechanical techniques. The hyperbolic groove plans, in contrast, must be created interferometrically. Figures 2b and 2c differ in their choice of recording wavelength, with (2c) being made practical[2] by the availability of argon ion lasers.

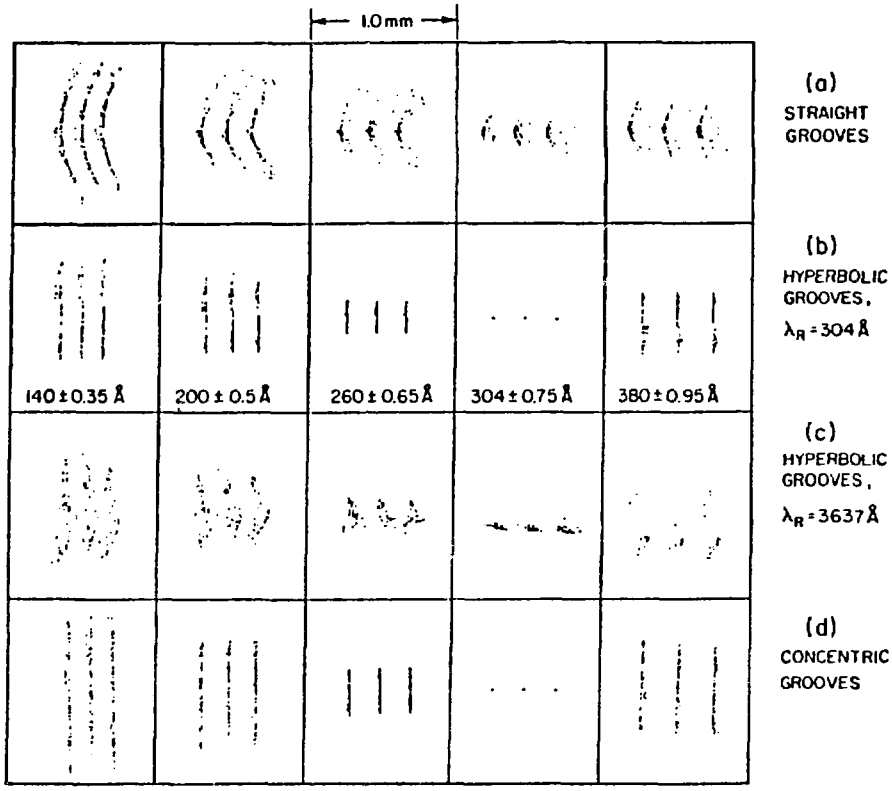

Figure 2. Performance of four in-plane grating designs using straight and curved grooves. The line separations shown are $\lambda/\Delta\lambda$ = 400, a design goal for the EUVE mission.

For comparison, each of these designs was chosen to intercept an f/6 × f/22 beam from a portion of the spectroscopy telescope[3] beam on the Extreme Ultraviolet Explorer mission[4]. The spectrometers traced here have a beam focal length of 136 cm, a distance separating the grating center from the focus equal to 48.5 cm, and a central groove spacing of 8294Å. The dispersion is 0.2 mm/Å at the detector. In all cases, the performance was optimized at λ304Å. These ray traces indicate that any of these ruling techniques can be effective for achieving the desired spectral resolution (~400) and that if other causes of blur were not factors, the concentric groove design would be able to do considerably better than this figure.

An alternative geometry is the out-of-plane "conical diffraction"[5,6,7] mount. In spectrometers of this kind, the incident and diffracted beams lie nearly parallel to the grooves. The grooves can remain fully illuminated even at grazing incidence, and high efficiency can consequently be obtained even at the very shortest wavelengths of interest. However, as the glancing angle is made small, only a small component of the incident wave vector is perpendicular to the groove direction, so a small dispersion is obtained for a given groove spacing. Two other complications are that the spectrum is formed along a circular arc, and that a circular "point" object becomes highly elongated upon undergoing conical diffraction. Both of these effects can lead to extreme requirements in the area of detector performance required to record high resolution spectra.

To adapt the extreme out-of-plane mount to converging-beam illumination, it is necessary to arrange for the grooves to converge. The resulting gratings resemble oriental fans; the groove spacing is proportional to the distance from a ruling focus[1] or "hub"[8]. In Figure 3, we present ray traces of a grating of this kind, for three mounting configurations. The wavelengths chosen for these traces are separated by $\lambda/\Delta\lambda = 100$. These traces assume a flat focal surface, for which wavelength aberrations grow rapidly away from the optimized wavelength (here, 150Å). However, by the use of a curved focal surface, maximum wavelength resolution (as in panels 3i and 3n) can be enforced over the entire spectrum.[9]

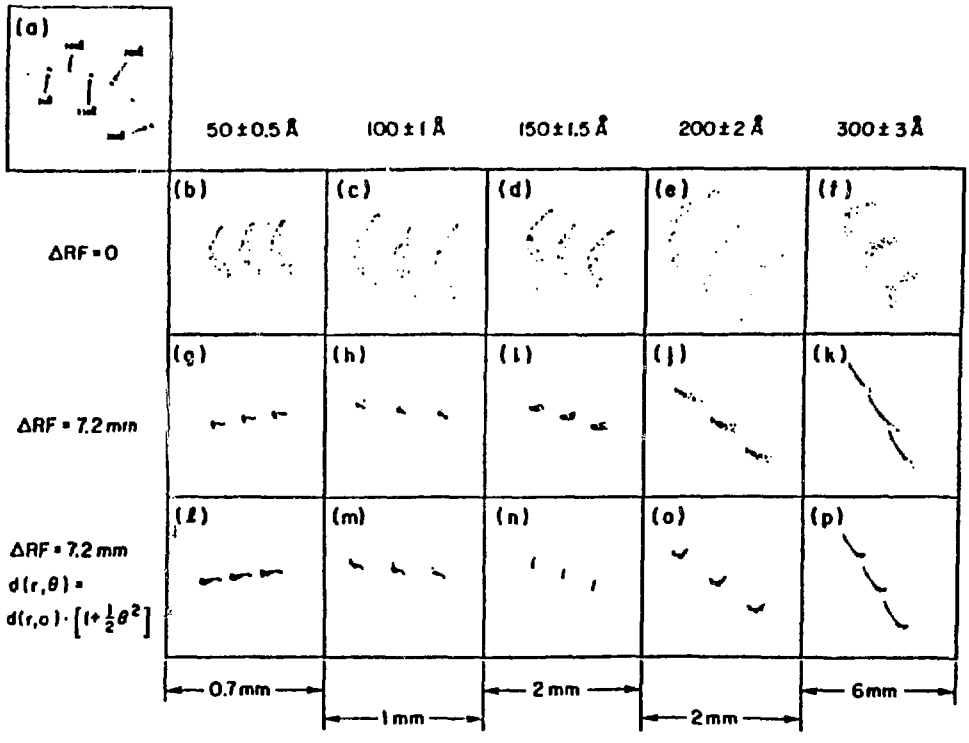

Figure 3. Oriental fan spectra. Here (a) is the gross wavelength map; ΔRF=displacement between image plane and ruling focus; (b)-(f) have ΔRF=0; (g)-(k) have ruling focus optimized 7.2mm behind focal plane; (l)-(p) have also an optimized angular variation in groove spacing.

After comparing the detailed characteristics of the in-plane and out-of-plane mounts, we have selected the in-plane mount for use in the spectroscopy experiment of the EUVE mission. In addition, we are developing a set of concentric-groove gratings for soft x-ray spectroscopy as one candidate instrument for the the AXAF mission. Each grating will accept about 20% of the converging beam from the AXAF objective, and provide useful throughput over a 2:1 wavelength band in the $\lambda\lambda$10-100Å region. The spectral resolution will be on the order of $\lambda/\Delta\lambda \sim 3000$ in each band.

Finally we mention that a high-dispersion concentric-groove grating can be combined with the oriental fan grating to form an echelle spectrometer well suited for feeding a two dimensional format detector. Such a combination offers high throughput and extremely high spectral resolution (~40000) over the $\lambda\lambda$900-1200Å wavelength range, and could form the basis of a spectrometer applicable to the Columbus mission. Figure 4 illustrates such an echelle spectrometer fed by a novel grazing incidence telescope[10] that allows a field-limiting aperture to be placed between primary and secondary.

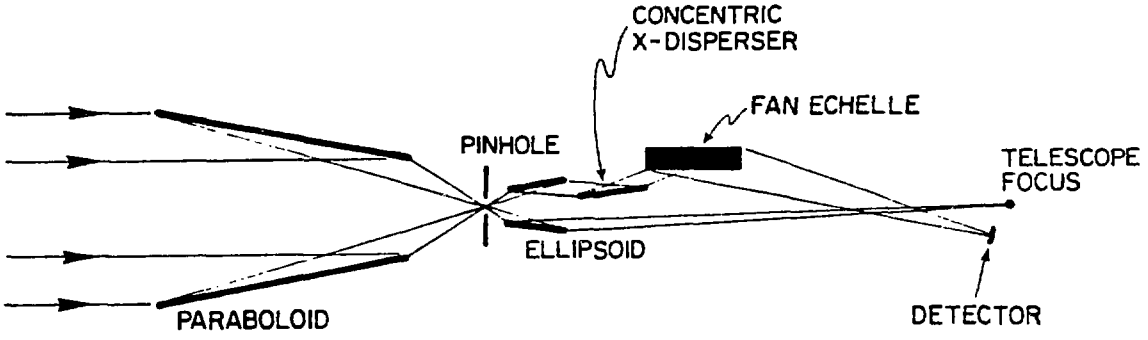

Figure 4. A grazing incidence telescope incorporating a slit feeds a grazing incidence echelle spectrometer; the combination offers high resolution and high throughput.

This work has been supported by contract NA5W-3636.

References

[1] M. C. Hettrick and S. Bowyer, Appl. Opt. 22#24, 3921, 1983.
[2] M. C. Hettrick and C. Martin, Proc. SPIE Symp. 28, San Diego, 1984.
[3] M. C. Hettrick, EUVE Report 321/81, Univ. Calif. Berkeley, 1982.
[4] S. Bowyer, R. Malina, M. Lampton, D. Finley, F. Paresce, & G. Penegor, Proc. Soc. Photo-Optical Instrum. Eng. 279 p. 176, 1982.
[5] W. Werner, Appl. Opt. 16#8, 2078, 1977.
[6] M. Neviere, P. Vincent, and D. Maystre, Appl. Opt. 17#6, 1978.
[7] M. Neviere, D. Maystre, and W. R. Hunter, J. Opt. Soc. Amer 68#8, 1106, 1978.
[8] W. Cash, Appl. Opt. 22#24, 3971, 1983.
[9] M. C. Hettrick, Appl. Opt. 23#18, 3221, 1984.
[10] M. Hettrick and S. Bowyer, Appl. Opt., 1 Nov. 1984.

THE STATISTICAL EQUILIBRIUM OF H AND He AND THE H/He RATIO IN WR STARS

A.B. Underhill and A.K. Bhatia
Laboratory for Astronomy and Solar Physics
NASA Goddard Space Flight Center, Greenbelt, MD 20771

INTRODUCTION

The mixed selection of strong emission lines present in the spectra of WR stars suggests that we are observing plasma with an electron temperature of the order of 10^5 K somewhere in the atmospheres of these rare stars. In the spectra of some WR stars emission lines of H are detected; this suggests that plasma with an electron temperature of the order of 10^4 K may be present also. Since the observations made in the last 30 years show that the masses, luminosities, effective temperatures, and general distribution in space of WR stars are similar to those of stars with spectral types in the range from about B2 to O9, a prime question is why are the spectra of WR stars so different from those of the B stars with which they are associated.

In this paper we present some new theoretical results which correct conclusions about the physical state of the atmospheres of WR stars which have been widely accepted even though a careful consideration of the theory used to interpret observed line strengths would have suggested caution. We are particularly concerned with correcting the deduction that the atmospheres of WR stars are deficient in H (Castor and van Blerkom 1970; Willis and Wilson 1978; Smith and Willis 1982, 1983).

The transfer of radiation through an outer atmosphere which contains a velocity gradient and which is optically thin except for the continua and lines of one ion has been studied by Castor (1970). This theory was used by Castor and van Blerkom (1970) to study the statistical equilibrium of He^+ in the atmospheres of WR stars. It has been used by Willis and Wilson (1978) and by Smith and Willis (1982, 1983) to interpret the strengths of He II lines and lines from the C and N ions in the spectra of WR stars. The conclusion reached as a result of these studies is that the composition of the atmospheres of WR stars corresponds to that of material which has been processed by nuclear burning in the center of the star. This has led to the postulate (see Conti 1982 and Maeder 1982) that WR stars are highly evolved objects. Conti has suggested that WR stars are the remnants of massive O stars which have lost their outer layers because of strong mass loss.

The spectrum analyses upon which these conclusions stand suffer from four grave errors: (1) Castor's theory has been applied for such typical lengths and electron densities that the model atmosphere is opaque in electron scattering, a condition contrary to one of the basic assumptions of Castor's theory. (2) No study was done of the statistical equilibrium of H. Instead it was assumed that the relative populations of the levels from which observed lines arise are in LTE ratios with respect to the density of H^+ ions. (3) The model He atom

used contains no levels of He I even though He I lines are quite strong in many WR spectra. (4) The statistical equilibrium of the selected C and N ions is studied taking account only of bound-bound transitions.

In the published work, the identification of the model atmospheres with the atmospheres of real stars was done in a cursory manner using only the relative strengths of He II lines in the visible range as criteria of fit. One result of this is that Willis and his colleagues claim that the electron temperatures in the atmospheres of WR stars are of the order of 30000 to 50000 K and that the electron density is of the order of 5×10^{11} cm^{-3}. They assume that hydrogen is completely absent, and they put the number density of He^+ equal to half the electron density.

MODEL ATOMS AND THE EQUATIONS OF STATISTICAL EQUILIBRIUM

We (Bhatia and Underhill 1984) have solved the equations of statistical equilibrium for a 70-level model He atom and for a 25-level model H atom in a plasma at temperature T and electron density N_e irradiated by a photosphere which emits a continuous spectrum $B_\nu(T_*)$. The model He atom contains singly and doubly excited states of He I; dielectronic recombination of He is considered as well as all the usual bound-bound and bound-free transitons driven by radiation and by electron collisions. We used the radiative transfer theory of Castor (1970) in the manner of Castor and van Blerkom (1970) to iterate to a final set of populations for 80 model atmospheres. We assume a normal composition for the atmosphere, that is N(H) = 10 N(He), and we calculate the fractional population of the levels of both model atoms by solving the equations of statistical equilibrium.

In order to relate our model atmospheres and model spectra to the real spectra of real stars we calculated the relative energies in the lines He I 5876, He II 1640, 3203, 4338, 4686, 5411, and Hα, Hβ, and Hγ, and we compared the theoretical results with observed energy ratios corrected for wavelength-dependent interstellar extinction.

The choice of $T_* = 2 \times 10^4$ K provides a continuous spectrum in the primary ionization continua of H, He I, and He II approximately like that of a star with $T_{eff} \sim 27000$ K. The choice $T_* = 3 \times 10^4$ K provides a continuous spectrum which mimics that from a star with $T_{eff} = 3.5 \times 10^4$ K.

It is necessary to restrict the choice of electron density to $N_e < 10^{10}$ cm^{-3} in order that the optical depth in electron scattering may remain negligible, as it must be for Castor's (1970) theory to be valid.

THREE SIGNIFICANT RESULTS

1. The departures from LTE of He I can be large; those of He II are modest. An electron temperature of the order of 10^5 K is required to account for the observed ratio of He I 5876/He II 5411 in HD 191765, HD 192103, and HD 192163. The relative energy in He I 5876 to that in He II 5411 is sensitive to the amount of dielectronic recombination. Only when T is high does the relative energy in He I 5876 approach what is observed. Neglect of the levels of He I in the studies by previous workers prevented the use earlier of this sensitive criterion for determining the electron temperature.

2. No matter what the values of T_* and T (within the range appropriate for WR stars), the departure coefficients of the levels from which the usually observed Balmer lines arise are of the order of 0.04. This fact accounts fully for the difficulty of detecting H emission lines in the spectra of many WR stars because the departure coefficients of the levels of He^+ from which the usually observed blending Pickering lines arise are of the order of or greater than 1 when T is of the order of 10^5 K. Typically at $T \sim 10^5$ K, the predicted energy ratio He II 4338/Hγ is greater than about 4. There is no reason to conclude that the atmosphere of any WR star is deficient in hydrogen. Ratios less than 1 can be obtained if $T < 3 \times 10^4$ K and if $N_e > 10^{10}$ cm^{-3}.

3. The relative energies in He II 4686, 3203, and 5411 are insensitive to the choice of T_*, T, and N_e. The relative energies in He II 1640 and 4686, however, are very sensitive to N_e and slightly sensitive to the choice of T_*. Agreement between observation and theory indicates that $T_* = 2 \times 10^4$ K and an electron density a little larger than 10^9 cm^{-3} is appropriate for the atmospheres of the WR stars HD 191765, HD 192103, and HD 192163.

Numerical results supporting these conclusions can be found in Bhatia and Underhill (1984). A few results are given in Tables 1 and 2.

REFERENCES

Bhatia, A. K. and Underhill, A. B. 1984, submitted to Ap.J. Suppl.

Castor, J. I. 1970, M.N.R.A.S., 149, 111.

Castor, J. I. and van Blerkom, D. 1970, Ap.J., 161, 485.

Conti, P. S. 1981, in Wolf-Rayet Stars: Observations, Physics, Evolution, eds. C.W.H. de Loore and A. J. Willis, (Reidel: Dordrecht), p.3.

Maeder, A. 1981, in Wolf-Rayet Stars: Observations, Physics, Evolution, eds. C.W.H. de Loore and A. J. Willis, (Reidel: Dordrecht), p.405.

Smith, L. J. and Willis, A. J. 1982, M.N.R.A.S., 201, 451.

Smith, L. J. and Willis, A.J. 1983, Astr. Ap. Suppl., 54, 229.

Willis, A. J. and Wilson, R. 1978, M.N.R.A.S., 182, 559.

Table 1

Predicted Relative Energies in He I 5876/He II 5411
Case $T_* = 2 \times 10^4$ K

T (10^4 K)	Case $N_e = 10^9$ cm^{-3}	Case $N_e = 10^{10}$ cm^{-3}	Observed Ratios
7.5	0.132	0.045	HD 191765: 0.3
10.0	1.07	0.367	HD 192103: 3.1
12.5	3.71	1.30	HD 192163: 0.4

Table 2

Predicted Relative Energies in He II Lines
Case $T_* = 2 \times 10^4$ K, $T = 10^5$ K

Ratio	Case $N_e = 10^9$ cm^{-3}	Case $N_e = 10^{10}$ cm^{-3}	Observed Ratios HD 191765	HD 192103	HD 192163
4686/5411	33.7	0.616	10.3	10.2	8.6
3203/5411	10.9	2.39	3.2	2.8	6.5
1640/4686	7.41	1.82 +5	7.4	>0.6*	8.2

*He II 1640 shows a strong central reversal.

SESSION 4. THEORETICAL SPECTROSCOPY

where C^e_{ij} is the collisional excitation rate coefficient from level i to j and is given by averaging over the Maxwellian distribution

$$C^e_{ij} = \frac{8.63\times10^{-6}}{\omega_i k T_e^{3/2}} \int_{\Delta E_{ij}} \Omega_{ij}\, e^{-E/kT_e}\, dE \qquad cm^{-3}\, s^{-1} . \tag{3}$$

T_e is the electron temperature. Collision strengths Ω_{ij}, dimensionless and symmetric in i and j, are related to the excitation cross section by

$$\Omega_{ij} = E\, \omega_i\, \sigma_{ij} \quad , \tag{4}$$

where E is the incident energy and ω_i is the statistical weight of the lower level i. The de-excitation rate coefficient C^d_{ji} is given by

$$C^d_{ji} = \frac{\omega_i}{\omega_j}\, C^e_{ij}\, e^{\Delta E_{ij}/kT_e} . \tag{5}$$

Other processes which can populate or depopulate the levels must be included in Eq. (2): photoexcitation by background radiation, as from the photosphere of the Sun, the rate for which is given by

$$F_{ij} = D(R)\, A_{ji} / \left(e^{\Delta E_{ij}/kT_R} - 1 \right) \quad , \tag{6}$$

where T_R is the temperature of the blackbody radiation and D(h) is the dilution factor. Stimulated emission, much smaller than spontaneous emission, and proton excitation rates[2] between the fine-structure levels should also be included.

A number of approximations have been made to calculate Ω_{ij}. The Coulomb Born approximation has been used extensively. This approximation overestimates collision strengths near the threshold for excitation. The Gaunt factor approximation based on the Bethe approximation, valid for allowed transitions, is not very reliable. The distorted wave approximation, which is valid when the coupling between the various channels is weak, has been widely used for the last few years. The total hamiltonian of the (N + 1) electron system is

$$H_{N+1} = -\sum_{i=1}^{N+1} \left(\nabla_i^2 + 2Z/r_i \right) + \sum_{i\neq j}^{N+1} 2/r_{ij} \quad , \tag{7}$$

where N is the number of target electrons and Z the nuclear charge. The total wave function is

$$\Psi_n = \mathcal{A}\, \Phi_n (1,2,\ldots, N)\, F_n (N+1) \quad , \tag{8}$$

where n is the initial or final state. F_n satisfies the equation

$$\left(\frac{d^2}{dr^2} - \frac{l_n(l_n+1)}{r^2} + V_{nn}(r) + k_n^2\right) F_n(r) = 0 \quad . \tag{9}$$

In the distorted wave programs[3] developed at University College London (UCL) V_{nn} is chosen to be a central potential and is given by a scaled Thomas-Fermi potential such that

$$\lim_{r\to\infty} V_{nn}(r) = 2(Z-N)/r \quad . \tag{10}$$

The functions $F_n(r)$ which have the usual limit for $r \to 0$ and ∞ are made orthogonal to the target orbitals having the same angular momentum. The reaction matrix is given by

$$\begin{aligned} K_{ij} &= -\langle \Psi_i | H_{N+1} - E_T | \Psi_j \rangle \\ &= -\langle F_i | V_{ij} + W_{ij} | F_j \rangle \quad , \end{aligned} \tag{11}$$

where V_{ij} and W_{ij} are the direct and exchange potentials. The short range correlations[3] can be improved by including quadratically integrable functions in the wave functions (8). The reaction matrix K_{ij} is modified then. The T matrix is given by

$$T = -\frac{2iK}{1+iK} \tag{12}$$

and the collision strength for a given parity and total angular and spin momenta L and S is given by

$$\Omega_{ij}^{\pi LS} = \frac{1}{2}(2L+1)(2S+1)\sum_{l_i,l_j} |T_{ij}|^2 \quad . \tag{13}$$

The total collision strength is given by

$$\Omega_{ij} = \sum_{\pi LS} \Omega_{ij}^{\pi LS} \quad . \tag{14}$$

In general, only the first few incident partial waves l_i are used in the calculation. The contribution for $l > l_i$, for allowed transitions, is included in the Coulomb Bethe approximation[4].

A better approximation is a close coupling approximation[5]. Though the calculations tend to be difficult and expensive, they have the advantage of including resonances.

The target wave functions Φ_n are calculated using the 'Superstructure' program[6], also developed at UCL. The radial functions are again calculated in a scaled Thomas-Fermi Potential. As pointed out by Lazer[7] that to obtain accurate wave function of highly ionized systems, it is necessary to include all configurations in the same complex of a given principal quantum number and parity. The configuration interaction type wave functions can be used in this program to calculate the energy levels, oscillator strengths and radiative transition rates in LS and intermediate couplings. The term

coupling coefficients are calculated in this program to transform LS coupling collision strengths to collisions strengths in intermediate coupling[8]. Since we require atomic data for high nuclear charge Z, the relativistic corrections are calculated using the Breit-Pauli Hamiltonian as a perturbation to the non-relativistic Hamiltonian. Atomic data have been calculated for a number of ions, and the level populations and intensity ratios have been calculated for diagnostic purposes by solving the statistical equilibrium equations (2) by assuming that the steady state $\frac{dN_i}{dt} = 0$ exists. We discuss some specific cases.

UV lines of Ca XVII have been observed by Doschek el al[9] in the August 9, 1973 solar flare by using NRL's slitless objective grating (171-630Å) aboard Skylab. Also X-ray lines have been identified by McKenzie and Landecker[10] in solar flares obtained from the Solex Bragg crystal spectrometer aboard the USAF P78-1 satellite. Bhatia and Mason[11] calculated the atomic data using three sets of configurations: Case A: $2s^2$, 2sp, $2p^2$; Case B: Case A + 2s3s, 2s3p, 2s3d; and Case C: Case B + 2p3s, 2p3p, 2p3d.

The energy values for Cases B and C are in good agreement with the observed values. The collision strengths are calculated using Case B configurations and scaled. The collision strengths are in good agreement with the close coupling calculations of Dufton el al[5].

The rates for electric dipole, electric quadrupole and magnetic dipole transitions are proportional to Z^4, Z^6 and Z^{10}, respectively. The rates for magnetic transitions at high Z become comparable to rates for the allowed transitionsand therefore, the transitions become very important in the observations of tokamak plasma. The collision strengths for the dipole allowed, spin-forbidden and non-dipole allowed transitions behave like logE, $1/E^2$ and constant, respectively, as $E \to \infty$. Also $Z^2\Omega_{ij} \to$ constant for a fixed E/Z^2. These limits are useful for interpolation or extrapolation of A_{ji} and Ω_{ij}.

The level populations and intensity ratios have been calculated for UV and X-ray lines. The observed[9] intensity ratio for the lines 192.86 and 232.83 Å corresponding to the transitions $2s2p\ ^1P_1 \to 2s^2\ ^1So$ and $2p^2\ ^3P_2 \to 2s2p^3P_2$ is 60. The calculated ratios are 87.6, 62.9 and 59.1 for log Ne = 12, 13, and 14 cm^{-3}, respectively. A comparison with the observed value of 60 would imply an electron density of 5×10^{13} cm^{-3} which is much higher than 3×10^{11} cm^{-3} at 6.3×10^6 K obtained by Dere et al[12] from the measurements of Ca XV and XVI. This would imply an uncertainty in the calibration or the 233Å line is blended. In the X-ray region, the line at 20.456A° ($2s3d\ ^3D_3 \to 2s2p\ ^3P_2$) is density sensitive. But the electron density was not determined as the measured intensities are weak. A line observed at 22.025Å can be associated with the calculated line 22.152A° ($2s3s\ ^1So \to 2s2p\ ^1P_1$). A similar calculation has been carried out for Fe XXIII by Bhatia and Mason[13]. Since then the identification of the lines in the X-ray region given by them has been

confirmed by McKenzie and Landecker[14]. The lines at 263.76 and 132.83Å due to the transitions $2s2p\ ^3P_1 \rightarrow 2s^2\ ^1S_o$ and $2s2p\ ^1P_1 \rightarrow 2s^2\ ^1S_o$ have been seen by Hinnov[15] in PLT tokamak. The line at 263.76Å obtained in NRL's spectroheliograph is an important line and has been used to study the energy release processes in solar flares. The most intense line of Fe XXIII in the UV region has been seen by Kastner et al[16] using the GSFC grating spectrometer on OSO-5.

The atomic data have been calculated for Mg VI, Si VIII, S X, Ar XII, etc by using the configurations $2s^22p^3$, $2s2p^4$ and $2p^5$ by Feldman el al[17]. The line ratios $(^2P_{3/2} \rightarrow {}^4S_{3/2})/(^2D_{3/2} \rightarrow {}^4S_{3/2})$ and $(^2D_{3/2} \rightarrow {}^4S_{3/2})/(^2D_{5/2} \rightarrow {}^4S_{3/2})$ are density sensitive but not temperature sensitive. These transitions are within the levels of the ground configuration $2s^2p^3$. S X lines have been observed in quiet and active regions of the Sun using NRL's spectrograph aboard Skylab. Using the observed ratios for the lines 1213.00 and 1196.26Å corresponding to the transitions $2s^22p^3$ $(^2D_{3/2} \rightarrow {}^4S_{3/2})$ and $2s^22p^3$ $(^2D_{5/2} \rightarrow {}^4S_{3/2})$ respectively, Feldman et al[17] inferred an electron density of 10^9 cm^{-3} at 1.3×10^6 K in quiet and active regions of the Sun. A similar calculation has been carried out for Fe XX. The line at 2665.1Å and 824.1Å corresponding to the transitions $2s^2p^3$ $(^2D_{5/2} \rightarrow {}^2D_{3/2})$ and $2s^22p^3(^2D_{3/2} \rightarrow {}^4S_{3/2})$ have been seen by Suckewer and Hinnov[18] in PLT tokamak.

Doschek et al[19] inferred the densities in the quiet sun and in coronal holes by comparing the intensities of the intersystem and allowed lines emitted by the ions formed in the transition zone. They used the lines at 1402.77Å $(3p\ ^2P1/2 \rightarrow 3s\ ^2S_{1/2})$ in Si IV, 1908.73Å $(2s2p\ ^3P_1 \rightarrow 2s^2\ ^1So)$ in C III, and 1666.15Å $(2s2p^3\ ^5S_2 \rightarrow 2s^2p^2\ ^3P_2)$ in O III. But the intersystem and allowed lines were not close in wavelength. Therefore, when comparing the intensities of the various lines, it was necessary to take into account the change in temperature of the emitting plasma as well as the variation of the instrument reflectivity with wavelength. Those problems can be avoided by using the line ratios of the S IV 1406Å intersystem line and the 1403Å resonance line in Si IV. These lines have been observed from Skylab. Bhatia et al[20] calculated the atomic data for S IV using the $3s^23p$, $3s3p^2$ and $3s3d^2$ configurations. But the density they inferred for December 17, and 21, 1973 and January 21, 1974 flares was four times that inferred from O IV measurements. Bhadra and Henry[21], and Dufton and Kingston[22] by using a larger set of configurations calculated the collision strengths in close coupling approximation. The latter calculations include resonances as well. Dufton et al[23] calculated the densities in the quiet sun, coronal holes, active region B and active region C and these are closer to the densities deduced by using other ions.

The intensity ratio of the allowed lines is temperature sensitive and it can be shown that

$$I_{ji}/I_{ki} \propto e^{-(\Delta E_{ij} - \Delta E_{ik})/kT_e} \quad . \tag{15}$$

This ratio is sensitive to changes to the electron temperature Te if $(\Delta E_{ij} - \Delta E_{ik})/kT_e \sim 1$. Feldman and Doschek[24] inferred the electron temperature = ion temperature using Mg II allowed lines. The intensity ratio of the satellite line to the resonance line is a function of electron temperature and can be used for temperature diagnostics[25].

The Bowen fluorescence mechanism takes place when the wave length of a transition coincides with the wavelength emitted by another ion. This radiation when absorbed will populate the upper levels preferentially and therefore will change the level populations and intensities of the emitted radiation. He II Lyman α (304 Å) coincides with the O III $2p^2\ ^3P_2 > 2p3d\ ^3P_2$ wave length. Bhatia et al[26] calculated the atomic data for O III by using $2s^22p^2$, $2s2p^3$, $2p^4$, 2p3s, 2p3p and 2p3d configurations. The photoexcitation by He II was taken into account by increasing the electron excitation rate coefficient C by PC where C is the rate coefficient for exciting the $2p3d\ ^3P_2$ from $2p^2\ ^3P_2$. The total excitation rate is, therefore, KC, where K = 1+P The level populations e.g. of $2p3d\ ^3P_2$ and $2p3p\ ^3S_1$, were found to be K dependent. Choosing K = 1000 to obtain agreement of the calculated intensity of 304Å line with the intensity observed by Behring et al[27], they calculate the intensities of other lines and multiplets and compare with the observation.

The calculated intensities of the non-photosensitive multiplets 508, 526, 703 and 835Å are in good agreement with the observations of Varanazza and Reeves[28]. Also, the intensities of multiplet components 508.18, 703.85, and 702.90Å agree very well with the observations of Behring et al[27]. The intensity of the multiplet 374Å is higher when photoexcitation is included but is lower than the observed intensity given by Raymond[29]. Dere[30] has pointed out that this line is blended, and according to Raymond (private communication), the observed intensity should be lower than that given in Ref. 29. Finally, the line at 644Å will not be observed at all if photoexcitation is not present and the calculated intensity in the presence of photoexcitation agrees very well with the observation of Veranazza and Reeves[28] (see Fig. 4 of Ref. 26 for more details). Furthermore, the observed multiplet 644Å is due to O III and not N II or O II as suggested by Veranazza and Reeves[28].

Though the bulk of the plasma is usually hydrogen or deuterium, other gases are added in controlled quantities for diagnostic purposes. Since the temperature in a tokamak is comparable to temperatures reached in solar flares, various stages of ionization of elements are present. Atomic data for various ions of interest have been calculated using UCL programs. The forbidden transitions, in particular magnetic dipole, are of special interest. These lines fall in the UV and EUV spectral regions and are due to transitions between the levels of the ground configurations $2s^2p^k$ of these ions. These lines are well separated in wave lengths and line blending is much less severe than in the case of allowed lines at shorter wave lengths. These transitions can be well observed to determine the line profiles. Ion temperatures can be inferred by measuring the full width at half maximum. Ion concentration and electron density can be determined from the intensities of these lines. Suckewer et al[31] observed lines from titanium ions and compared the observed intensities with the synthetic spectrum calculated by Bhatia et al[32] using the configurations $2s^2$, $2s2p^{k+1}$, $2p^{k+2}$. Suckewer el al[31] observed the Ti XIV 2115.3, Ti XV 2544.8, Ti XVII 3834.4 and 3371.5Å lines along with the allowed Ti XIX 169Å line and their intensity variation with time. The ion density can be calculated by noting that if the level population of the upper level does not vary with electron density, as for $2s^22p^4\ {}^3P_1$ of Ti XV, (see Fig. 3 of Ref. 32), then

$$I_{ji} = \frac{A_{ji}}{4\pi} \int N_j\, dV = \frac{n_j A_{ji}}{4\pi} \int N_T\, dV \quad , \tag{16}$$

where $n_j = N_j/N_t$ is the level of population of the level j. From the measured I_{ji} and the calculated n_jA_{ji} as indicated in Fig. 3 of Ref. 31, they obtained an ion density of 2.6×10^{10} cm^{-3}.

More recently Stratton et al[1] measured the intensity ratios of various lines in Fe XVIII to XXII and compared with intensity ratios inferred from the DW calculations. They conclude (See Table 1 of Ref. 1) that in general the agreement is within 30 percent, the expected accuracy of the distorted wave calculations.

REFERENCES

1. B.C. Stratton, H.W. Moss and M. Finkenthal, Ap. J. 279, L31 (1984).
2. S.O. Kastner and A.K. Bhatia, Astron. Astrophys, 71, 211 (1979).
3. W. Eissner and M. J. Seaton, J. Phys. B 5, 2187 (1972).
4. A. Burgess and V. B. Sheorey, J. Phys. B 1, 2403 (1974).
5. P. L. Dufton, A. E. Kingston and N. S. Scott, J. Phys. B 16, 3053 (1983).
6. W. Eissner, M. Jones and H. Nussbaumer, Comp. Phys. Comm. 8, 270 (1974).
7. D. Layzer, Ann. Phys. 8, 271 (1972).
8. H. E. Saraph, Comp. Phys. Comm. 3, 256 (1972).
9. G. A. Doschek, U. Feldman and K. P. Dere, Astron. Astrophs. 60, L11 (1977).
10. D. L. McKenzie and P. B. Landecker, Ap. J. 254, 309 (1982).
11. A. K. Bhatia and H. E. Mason, Astron. Astrophys. Suppl. Ser. 52 115 (1982).
12. K. P. Dere, H. E. Mason, K. G. Widing and A. K. Bhatia, Astron. Astrophys, Suppl. Ser. 50, 341 (1979).
13. A. K. Bhatia and H. E. Mason, Astron. Astrophys. 103, 324 (1981).
14. D. L. McKenzie and P. B. Landecker, Ap. J. 254, 309 (1982).
15. E. Hinnov. Ap. J. Lett. 230, L197 (1980).
16. S. O. Kastner, W. M. Neupert and M. Swartz, Ap. J. 191, 261 (1976).
17. U. Feldman, G. A. Doschek, J. T. Mariska, A. K. Bhatia and H.E. Mason, Ap. J. 226, 674 (1978).
18. S. Suckewer and E. Hinnov, Phys. Rev. Lett. 41, 756, (1978).
19. G. A. Doschek, U. Feldman, A. K. Bhatia and H. E. Mason, Ap. J. 226, 1129 (1978).
20. A. K. Bhatia, G. A. Doschek and U. Feldman, Astron. Astrophys. 86, 32 (1980).
21. K. Bhadra and R. J. W. Henry, Ap. J. 240, 368 (1980).
22. P. L. Dufton and A. E. Kingston, J. Phys. B 13, 4277 (1980).
23. P. L. Dufton, A. Hibbert, A. E. Kingston and G. A. Doschek, Ap. J. 257, 338 (1982).
24. U. Feldman and G. A. Doschek, Ap. J. 212, L147 (1977).
25. A. H. Gabriel Mon. Not, R. Astr. Soc. 145, 241 (1972).
26. A. K. Bhatia, S. O. Kastner and W. E. Behring, Ap. J. 254, 887 (1982).
27. W. E. Behring, L. Cohen, U. Feldman and G. A. Doschek, Ap. J. 203, 521 (1976).
28. J. E. Veranazza and E. M. Reeves, Ap. J. Suppl. 37, 485 (1978).
29. J. C. Raymond, Ap. J. 224, 259 (1978).
30. K. P. Dere, Solar Phys. 77, 79 (1982).
31. S. Suckewer, R. Fonck and E. Hinnov, Phys. Rev. A 21, 924 (1980).
32. A. K. Bhatia, U. Feldman, and G. A. Doschek, J. Appl. Phys. 51, 1464 (1979).

EFFECT OF TWO TYPES OF NON-MAXWELLIAN ELECTRON DISTRIBUTIONS ON TEMPERATURE SPECTROSCOPIC DIAGNOSTICS

C. Möller and M. Lamoureux
Laboratoire de Spectroscopie Atomique et Ionique,
Université Paris-Sud, 91405, Orsay, France

Continuum emission due to bremsstrahlung and direct radiative recombination is studied in two types of fusion-plasmas with non-Maxwellian electron distributions. The calculated emissivity coefficients $J_\omega(\hbar\omega)$ are shown to depart from the Maxwellian ones. The main consequence of the modification of the spectrum is to invalidate the usual electron temperature diagnostic which consits in equating $d\ln J_\omega(\hbar\omega)/\, d(\hbar\omega)$ to $1/kT_e$.

Case I corresponds to the critical density region of a laser-produced plasma (Langdon 1980, Mora and Yahi 1982). The distribution function is $c_m \exp(-v/v_{\circ,m})^m$ with m=5 for all values of the incident electron velocity $v_{\circ,m}$. Case II corresponds to very steep temperature gradients for which the spacial scale of the transport region is larger than the gradient scale itself (Albritton 1983, Luciani et al. 1984, Campbell 1984). On the higher temperature side of the heat front, the tail of the distribution is depleted with respect to the Maxwellian one . At a particular distance from it, this tail can be roughly described by the above analytical function but with m=3.

Universal emissivity curves (Lamoureux et al. 1984) were given in case I, for completely stripped ions, for bremsstrahlung and recombination separately, provided Kramers' atomic data are suitable. Another set of curves can be similarly established in case II as well. Results can be extended to less strongly ionized plasmas by employing an efficient degree of ionization (Kim and Pratt,1983), $(Z+Z_i)/2$, for the captures into each ion A^{Z_i+}. Results concerning bremsstrahlung are given in Fig. 1 ; the departure of the two non-Maxwellian curves from the Maxwellian straight line reflects the non-Maxwellian character of the distribution, and the variability of their slope points out the failure of the usual diagnostic in most regions of the spectrum.

We then evaluate as an example the total emissivity coefficient $J_\omega(\hbar\omega)_{21}$ produced at the kinetic temperature of 1 keV and the density of 10^{21} e/cc in an Aluminium plasma consisting of 25 % Al^{13+}, 50 % of Al^{12+} and 25 % of Al^{11+}.(See Fig. 2). In case II, non-Maxwellian effects are felt only at high photon energies. In case I, the non-Maxwellian character is more pronounced ; it is found over the entire spectrum, and especially right above the Al^{13+} Is threshold, as was observed experimentally (Matthews et al. 1983). The usual temperature diagnostic is then very mileading as is illustrated by the dotted curve of Fig. 2.

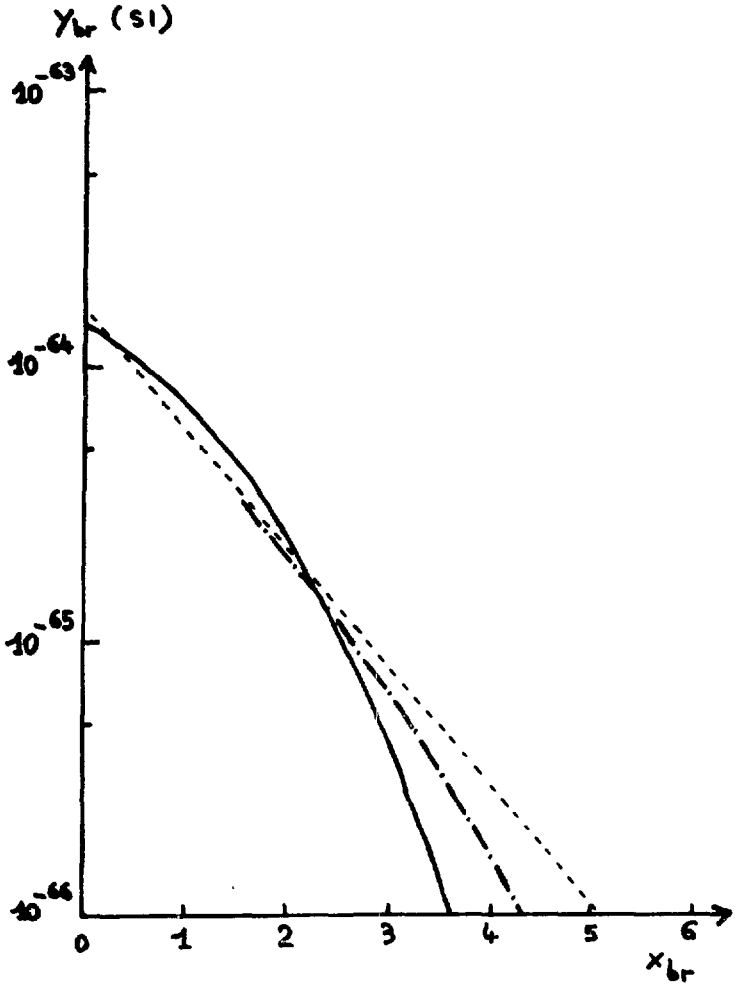

Fig. 1 : Reduced emissivity for bremsstrahlung y_{br} versus photon energy $x_{br} = \hbar\omega/kT_e$. y_{br} is related to the emissivity coefficient j_{br} by $y_{br}(\hbar\omega) = j_{br}(\hbar\omega)(kT_e)^{1/2} / (N_e N_i Z_i^2)$.
(- - -) : Maxwellian distribution, (—) : non-Maxwellian, case I;
(— . —) : non-Maxwellian, case II .

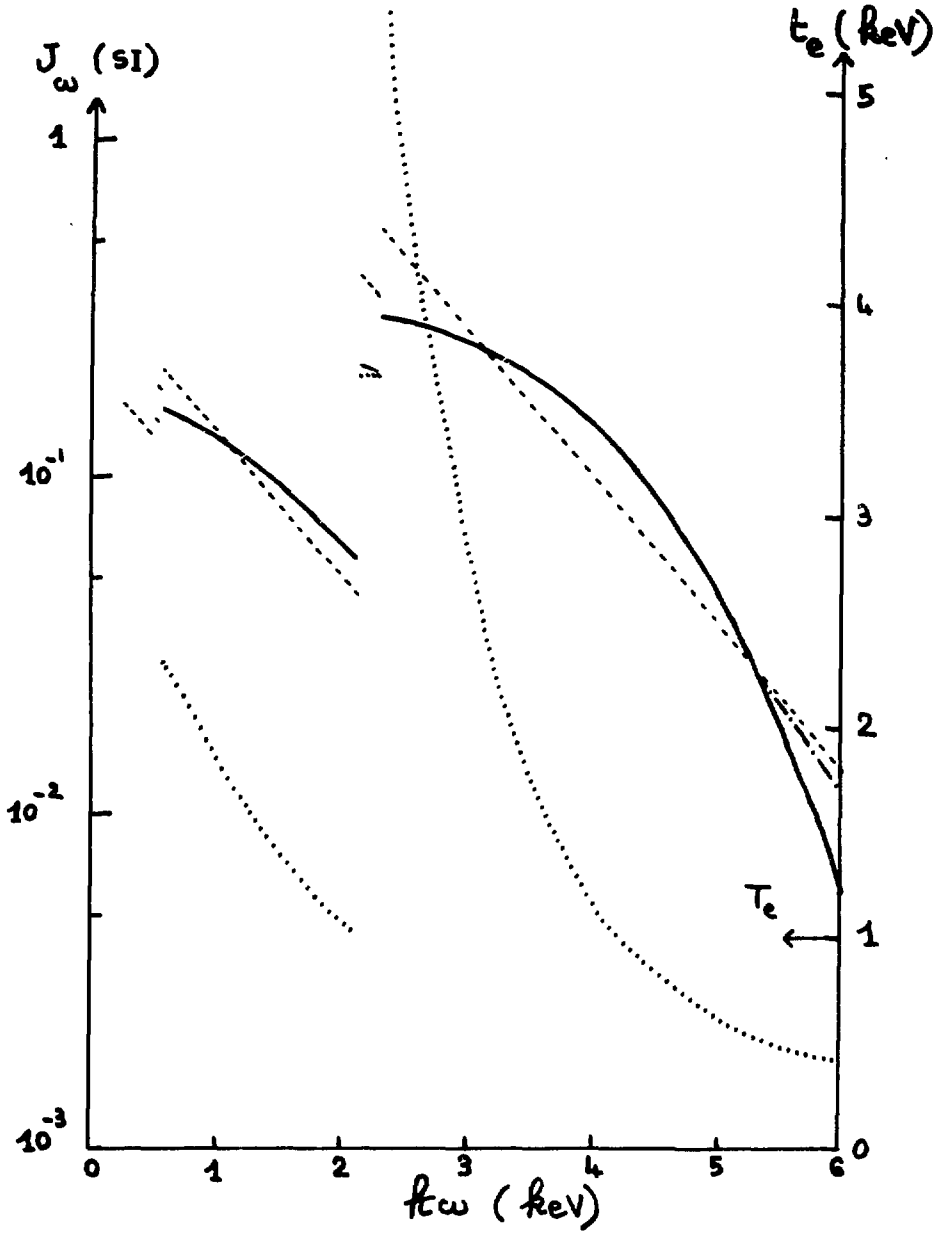

Fig. 2 : Total emissivity coefficient J_ω versus photon energy $\hbar\omega$ for an Al plasma, at T_e=1 keV and d = 10^{21} e/cc, consisting of 25 % Al^{13+}, 50 % Al^{12+} and 25 % Al^{11+}. (- - -) : Maxwellian distribution, (—) : non-Maxwellian, case I , (— . —) :non-Maxwellian, case II.

Misleading temperature t_e obtained from the diagnostic whereas the kinetic temperature is T_e, (....) : non-Maxwellian distribution, case I. (Dotted curves should be read on the right ordinate).

REFERENCES

Albritton, J.R. 1983, Phys. Rev. Lett., 50, 2078.

Campbell, P.M. 1984, Phys. Rev. A, 30, 365.

Young Soon Kim, and Pratt, R.H. 1983, Phys. Rev. A, 27, 2913.

Lamoureux, M., Möller, C., and Jaeglé, P. 1984, Phys. Rev. A, 30, 429.

Langdon, A.B. 1980, Phys. Rev. Lett., 44, 575.

Luciani,J., Mora, P., and Pellat, P., to be published, and private communication.

Mora, P., and Yahi, H. 1982, Phys. Rev. A, 26, 2259.

Matthews, D. L., Kauffmann, R.L., Kilkenny, J.D., and Lee, R.W. 1983, *Rutherford Appleton Laboratory Report* No. RL83-043.

Acknowledgement : We want to thank Dr. P. Jaeglé for encouragement in this work.

RADIATIVE CORRECTIONS TO INTENSITIES OF DIELECTRONIC SATELLITE LINES EMITTED FROM HELIUM- AND LITHIUM-LIKE ARGON*

V. L. Jacobs and J. E. Rogerson
Naval Research Laboratory, Plasma Physics Division,
Plasma Radiation Branch, Washington, D. C. 20375

The process of dielectronic recombination has been the subject of intense theoretical activity mainly because of the pioneering work by Burgess (1964), who demonstrated that this process can be the dominant recombination mechanism for multiply-charged atomic ions in low-density high-temperature astrophysical and laboratory plasmas. Recent attempts to measure dielectronic recombination cross sections and rate coefficients have renewed interest in the development of a rigorous quantum-mechanical theory of the resonant electron-ion recombination process. A precise theory is clearly required for the interpretation of the dielectronic satellite lines, which have been found to be of great value in the spectroscopic determination of temperatures, densities, and departures from ionization equilibrium.

In order to develop a rigorous quantum-mechanical theory of dielectronic recombination, it is necessary to treat the electron-ion collision and radiation processes in a unified manner by employing the methods of multi-channel scattering theory and quantum electrodynamics. Unified quantum-mechanical treatments of electron-ion recombination, which describe both the resonant and the non-resonant processes, have been developed by Davies and Seaton (1969) and by Shore (1969); but approximations to the scattering matrix are employed in these theories, leading to expressions in which the autoionization and radiative decay rates are additive. Armstrong, Theodosiou, and Wall (1978) were the first to investigate the effects of the electromagnetic interaction between the final continuum states which result from the autoionization and radiative decay modes. Using a two-level atom model, they demonstrated that the final-state interaction can alter the relative probabilities for an autoionizing state to decay into the two alternative continuum channels. They obtained approximate expressions for the Auger and fluorescence yields which they believed were valid only when the final-state continuum-continuum coupling is weak.

Recently, Haan and Cooper (1983) have rederived the results obtained by Armstrong, Theodosiou, and Wall (1978). By taking advantage of the separable form of the final-state interaction, they were able to obtain an exact closed-form solution for the two-level atom problem. Most significantly, they demonstrated that the approximate expressions for the Auger and fluorescence branching ratios first obtained by Armstrong, Theodosiou, and Wall (1978) remain valid even when the continuum-continuum coupling is strong and, therefore, have a wider region of validity than originally recognized.

In this investigation the two-level atom model has been extended to the case in which each of the atomic levels may consist of a set of degenerate magnetic sublevels. In the case where the final-state interaction involves only a single term in the partial-wave expansion for the electron-continuum state, the expressions obtained for the Auger and fluorescence yields are in agreement with those derived in the previous investigations. When several terms in the electron-continuum

partial-wave expansion are involved, the Auger and fluorescence branching ratios contain terms corresponding to the interference between different partial-wave components. Finally, the isolated-resonance approximation is employed to obtain the corrected expressions for the intensities of the dielectronic satellite lines resulting from the radiative decay of autoionizing states of multiply-charged ions in low-density plasmas. The modifications to the conventional expression for the satellite line intensities may be interpreted as terms corresponding to the interference between the direct radiative recombination and dielectronic recombination processes together with radiative corrections to the dielectronic recombination process.

In order to investigate the significance of the radiative corrections, we have evaluated the corrected expressions for the relative intensities of the dielectronic satellite lines emitted from autoionizing states of the type $2\ell\ 2\ell'$ in helium-like argon. In the total-electronic angular-momentum J representation, 24 electric-dipole radiative transitions are allowed between the doubly-excited states and the bound states. In addition to the autoionization and radiative decay rates, which are all the quantities that are required in the evaluation of the traditional expressions for the branching ratios, it is now necessary to obtain the photoionization cross sections of each bound level in order to incorporate the final-state interaction. The radiative corrections may also be expressed in terms of the Fano line-profile parameter Q_F. A selection of our preliminary results for helium-like argon, which were obtained using the relativistic atomic structure program of Cowan (1967), are presented in Table I and in Figure 1. The corrected rates we denoted by using the tilde. It is found that the effects of the final-state interaction are most important for radiative transitions with relatively small values of Q_F. However, the most intense satellite lines at low-densities correspond to very large values of Q_F. Calculations for autoionizing states of the type $1s2\ell\ 2\ell'$ in lithium-like argon are now in progress.

ACKNOWLEDGMENT

Work Supported by the Office of Naval Research*

REFERENCES

1. Armstrong, L., Jr., Theodosiou, C. E., and Wall, M. J. 1978, Phys. Rev. A18, 2538.
2. Burgess, A. 1964, Astrophys. J. 139, 776.
3. Cowan, R. D. 1967, Phys. Rev. 163, 54.
4. Davies, P. C. W., and Seaton, M. J. 1969, J. Phys. B2, 757.
5. Haan, S. L., and Cooper, J. 1983, Phys. Rev. A28, 3349.
6. Shore, B. W. 1967, Rev. Mod. Phys. 39, 439.

SELECTED RESULTS FOR ARGON XVII

RADIATIVE TRANSITION $a \rightarrow f$	FANO PARAMETER Q_F	RADIATIVE DECAY RATES (Sec^{-1})		DIELECTRONIC RECOMBINATION RATES ($cm^3\ sec^{-1}$) (K_BT_e = 1.6 Kev)	
		Ar	$\tilde{A}r$	α_{DR}	$\tilde{\alpha}_{DR}$
$2s2p\ ^1P_1 \rightarrow 1s^2\ ^1S_0$	0.74	2.3 (10)	4.7 (10)	1.5 (-17)	3.0 (-17)
$2s2p\ ^3P_1 \rightarrow 1s^2\ ^1S_0$	0.73	1.3 (8)	5.0 (9)	2.0 (-20)	7.5 (-19)
$2p^2\ ^3P_0 \rightarrow 1s2p\ ^1P_1$	4.4	6.3 (11)	3.0 (11)	1.4 (-18)	6.6 (-19)
$2p^2\ ^1D_2 \rightarrow 1s^2p\ ^3P_1$	1.7	8.9 (8)	7.9 (8)	9.3 (-19)	8.2 (-19)

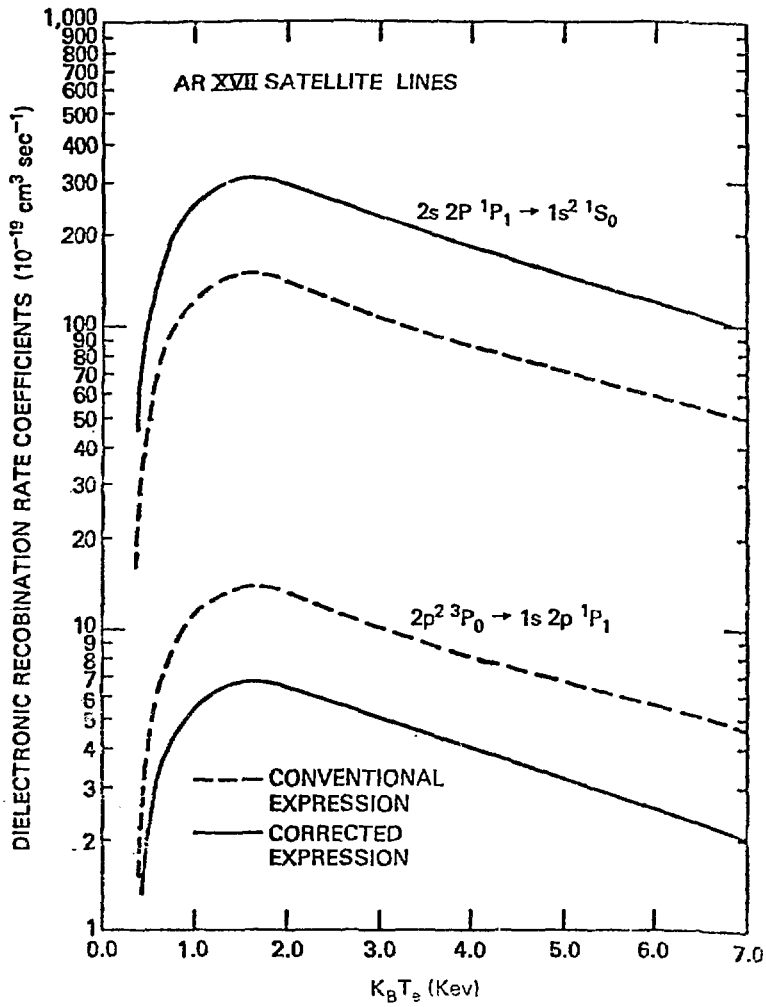
AR XVII SATELLITE LINES
2s 2P $^1P_1 \rightarrow 1s^2\ ^1S_0$
$2p^2\ ^3P_0 \rightarrow 1s\ 2p\ ^1P_1$
CONVENTIONAL EXPRESSION
CORRECTED EXPRESSION
DIELECTRONIC RECOBINATION RATE COEFFICIENTS (10^{-19} cm^3 sec^{-1})
$K_B T_e$ (Kev)
1,000
900
800
700
600
500
400
300
200
100
90
80
70
60
50
40
30
20
10
9
8
7
6
5
4
3
2
1
0.0
1.0
2.0
3.0
4.0
5.0
6.0
7.0

A COMPARISON OF VARIOUS NLTE CODES IN COMPUTING THE CHARGE-STATE POPULATIONS OF AN ARGON PLASMA

Sam R. Stone and Jon C. Weisheit
University of California, Lawrence Livermore National Laboratory
Livermore, California 94550

A comparison among nine computer codes shows surprisingly large differences where it had been believed that the computational physics was well understood. The codes simulate a plasma that is in steady state but not in local thermodynamic equilibrium (NLTE codes). In this study each code treats an "easy" problem, which is an argon plasma, optically thin and with no external photon flux; densities are varied from near-coronal to an intermediate 10^{21} electrons/cc and above. The temperatures are high enough that most ions have two or fewer bound electrons, which for this plasma means temperatures above about 300 eV.

The present study asks only if the codes compute similar charge-state populations (a surprising "no"), and, if not, why not. It does not claim accuracy for any code either by comparison to experiment or by appeal to a concensus.

A striking feature of the ionic populations computed by the various codes is their dissimilarity: The agreement varies from near exact to more than 2.5 orders of magnitude different, and if we ignore extremes, still the typical disagreement is about a factor of 2.

We seek clues to why the codes disagree by modifying bits of physics within a single code. What happens to the charge-state populations in the Ar plasma if a rate coefficient is arbitrarily cut in half or if the allowed number of excited states is reduced? It is found that populations computed by a single code vary by about a factor of 2 if

(i) electron-collisional excitation/de-excitation is cut in half; or
(ii) electron-collisional ionization/recombination is cut in half; or
(iii) the maximum principal quantum number n_{max} is reduced from 12 (allowed by continuum lowering) to only 5. See Figure 1.

The computed populations seem most at risk from n_{max} being set too small. This is because rate coefficients are computed with care (especially for H- and He-like ions), while continuum lowering and n_{max} are often set arbitrarily. For instance, we note that four formulae often used for e-collisional ionization/recombination vary by some 15% or less in the Ar problem. On the other hand, most codes do not compute n_{max} but fix it a priori.

Results of this study are being compiled in a LLNL internal report due to become available in the autumn of 1984.

Figure 1: Effect of n_{max} on populations. The code LINEZ computes the population fraction of charge-states with 0, 1, 2, and 3 bound electrons. The plasma is argon, optically thin, with particle temperature 1 keV and a density of 5.6×10^{19} ions/cc. For this figure LINEZ lowers the continuum by the Stewart-Pyatt algorithm, then fixes the maximum allowed principal quantum number at n_{max} for each ionic charge-state.

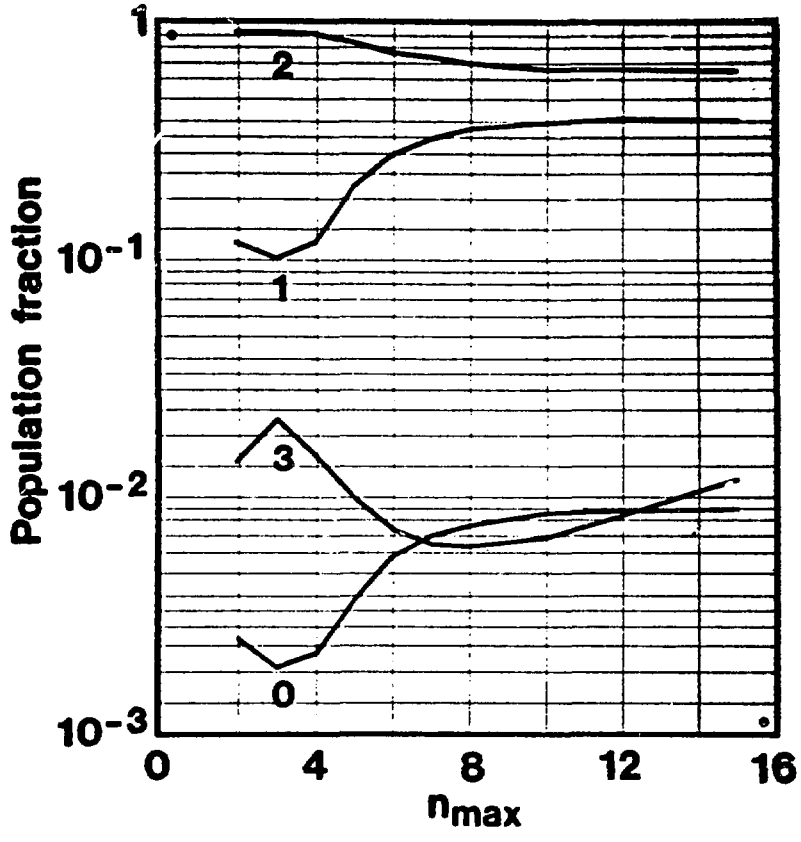

This work was performed under the auspices of the U. S. Department of Energy by the Lawrence Livermore National Laboratory under contract No. W-7405-ENG-48.

COLLISION STRENGTHS AND LINE STRENGTHS FOR TRANSITIONS FROM THE $1s^2 3\ell$ LEVELS TO THE $1s2\ell'3\ell''$ LEVELS IN LI-LIKE IONS*

D.H. Sampson, S.J. Goett† and G.V. Petrou
Department of Astronomy, The Pennsylvania State University
University Park, PA 16802

and

R.E.H. Clark
Los Alamos National Laboratory, Applied Theoretical Physics Div.
X-7, Los Alamos, NM 87545

It is well known that radiation from the levels of the $1s2\ell2\ell'$ and $1s2\ell3\ell'$ configurations of Li-like ions form satellites of spectral lines from He-like ions that are of high interest for plasma diagnostic purposes. Recently Sampson et al (1984) have made calculations of the collision strengths for innershell excitation to these upper levels from the $1s^2 2s$ and $1s^2 2p$ levels for a large number of Li-like ions using a Coulomb-Born-exchange method. Here we consider the alternative mechanism for populating the $1s2\ell3\ell'$ levels by collisional excitation from the $1s^2 3s$, $1s^2 3p$ and $1s^2 3d$ levels. Although the populations of the $1s^2 3\ell$ levels are lower than those of the $1s^2 2\ell$ levels, this is at least partially compensated for by the fact that the collision strengths for the $1s^2 3\ell$ - $1s2\ell'3\ell''$ transitions are considerably larger on the average than those for the $1s^2 2\ell$ - $1s2\ell'3\ell''$ transitions. The method of calculation is the same as that used by Sampson et al (1984), where all possible configuration mixing, parentage mixing and intermediate coupling type mixing among the states in a complex (the states having the same n values, parity and J values) was included. Also the present application is sufficiently simple that after summation over J values for the initial level the results for the collision strength Ω can be expressed in a simple manner in terms of the Z scaled hydrogenic collision strengths $Z^2\Omega_H$ and $Z^2\Omega_H^e$ analogous to Eqs (8)-(15) of Sampson et al (1984). The appropriate formulae and the numerical results for both excitation to upper fine structure levels and to upper energy terms for 19 Li-like ions have been submitted for publication to Atomic Data and Nuclear Data Tables. Here we give only the pertinent formula and sample numerical results for transitions between energy terms in Li-like iron. This formula is

$$\Omega[1s^2 3\ell\ {}^2L\text{-}(1s2\ell_a\ {}^{2S''+1}L'')3\ell''\ {}^{2S'+1}L'] = \frac{1}{(Z-\sigma)^2} A(1s\text{-}2\ell')Z^2\Omega_H(1s\text{-}2\ell') + \frac{1}{(Z-\sigma^e)^2} A^e(1s\text{-}2\ell')Z^2\Omega_H^e(1s\text{-}2\ell'),$$

where due to configuration mixing neither ℓ need equal ℓ'' nor ℓ_a need equal ℓ'. The recommended values for σ and σ^e are zero for transitions involving 1s-2s and are -0.5 and 0.3, respectively, for transitions involving 1s-2p. Numerical values for the coefficients A and A^e for Li-like iron are given in Tables I-III. Values for $Z^2\Omega_H$ and $Z^2\Omega_H^e$ for impact electron energies up to 15 times threshold are given in Golden

et al (1981) and Clark et al (1982) and are repeated in Table IV for convenience. Finally we note that the line strengths S for transitions involving 1s-2p are obtained by multiplying the corresponding value for A(1s-2p) by the scaled hydrogenic line strength 1.665 and dividing by $(Z-\sigma)^2$.

*Work supported by the U.S. Energy Department under contract DE-AC02-76ET53056.

†Present address: Bell Telephone Labs, 190 River Road, Summit, NJ 07901

REFERENCES

Clark, R.E.H., Sampson, D.H., and Goett, S.J. 1982, Astrophys. J. Suppl. 49, 545.

Golden, L.B., Clark, R.E.H., Goett, S.J., and Sampson, D.H. 1981, Astrophys. J. Suppl. 45, 603.

Sampson, D.H., Goett, S.J., Petrou, G.V., Zhang, H., and Clark, R.E.H. 1984, Atom. Data Nucl. Data Tables (in press).

TABLES

TABLE I. Values for the Coefficients A (Upper Entries) and A^e (Lower Entries) for Determining Ω for Innershell Excitation from $1s^2 3s^2 S$

Transitions Involving 1s-2s			Transitions Involving 1s-2p		
Upper Level	ΔE (Z^2Ryd)	A(Upper) A^e(Lower)	Upper Level	ΔE (Z^2Ryd)	A(Upper) A^e(Lower)
$(1s2s^3S)3s^4S$	7.206(-1)	0.0 1.928(0)	$(1s2s^3S)3p^4P$	7.227(-1)	5.718(-3) 1.384(-2)
$(1s2s^3S)3s^2S$	7.220(-1)	1.413(-3) 9.481(-1)	$(1s2s^3S)3p^2P$	7.231(-1)	7.128(-2) 9.883(-2)
$(1s2s^1S)3s^2S$	7.244(-1)	3.755(0) -2.816(0)	$(1s2s^1S)3p^2P$	7.262(-1)	5.168(-2) 1.367(-1)
$(1s2s^3S)3d^4D$	7.243(-1)	3.667(-3) -2.690(-3)	$(1s2p^3P)3s^4P$	7.256(-1)	1.479(-1) 1.726(0)
$(1s2s^3S)3d^2D$	7.251(-1)	0.0 3.539(-5)	$(1s2p^3P)3s^2P$	7.274(-1)	1.928(-1) 5.557(-1)
$(1s2s^1S)3d^2D$	7.280(-1)	0.0 2.783(-4)	$(1s2p^1P)3s^2P$	7.291(-1)	3.266(0) -2.380(0)
$(1s2p^3P)3p^4D$	7.270(-1)	6.479(-3) -1.600(-3)	$(1s2p^3P)3d^4F$	7.283(-1)	1.040(-3) -5.515(-4)
$(1s2p^3P)3p^2D$	7.287(-1)	0.0 8.160(-3)	$(1s2p^3P)3d^2F$	7.298(-1)	0.0 1.219(-2)
$(1s2p^1P)3p^2D$	7.308(-1)	0.0 7.721(-5)	$(1s2p^1P)3d^2F$	7.326(-1)	0.0 1.429(-5)
$(1s2p^3P)3p^4P$	7.281(-1)	6.391(-2) -3.283(-2)	$(1s2p^3P)3d^4D$	7.295(-1)	1.033(-2) -1.785(-3)
$(1s2p^3P)3p^2P$	7.281(-1)	5.217(-3) 2.437(-2)	$(1s2p^3P)3d^2D$	7.282(-1)	1.236(-1) -7.960(-2)
$(1s2p^1P)3p^2P$	7.311(-1)	3.749(-2) -2.466(-2)	$(1s2p^1P)3d^2D$	7.322(-1)	4.233(-3) -2.919(-3)

TABLE I - continued

$(1s2p^3P)3p^4S$	7.266(-1)	0.0	$(1s2p^3P)3d^4P$	7.302(-1)	3.464(-3)
		3.035(-2)			8.374(-3)
$(1s2p^3P)3p^2S$	7.298(-1)	8.281(-3)	$(1s2p^3P)3d^2P$	7.308(-1)	1.115(-1)
		1.676(-2)			-8.028(-2)
$(1s2p^1P)3p^2S$	7.319(-1)	1.187(-1)	$(1s2p^1P)3d^2P$	7.330(-1)	1.074(-2)
		-7.816(-2)			-6.277(-3)

TABLE II. Values for the Coefficients A(Upper Entries) and A^e(Lower Entries) for Determining Ω for Innershell Excitation from $1s^2 3p^2P$

Transitions Involving 1s-2p			Transitions Involving 1s-2s		
Upper Level	ΔE (Z^2Ryd)	A(Upper) A^e(Lower)	Upper Level	ΔE (Z^2Ryd)	A(Upper) A^e(Lower)
$(1s2s^3S)3s^4S$	7.186(-1)	4.693(-4)	$(1s2s^3S)3p^4P$	7.207(-1)	9.995(-3)
		2.358(-2)			5.835(0)
$(1s2s^3S)3s^2S$	7.200(-1)	3.598(-4)	$(1s2s^3S)3p^2P$	7.212(-1)	1.420(-1)
		1.648(-2)			2.307(0)
$(1s2s^1S)3s^2S$	7.224(-1)	6.888(-2)	$(1s2s^1S)3p^2P$	7.242(-1)	8.760(0)
		-4.902(-2)			-6.401(0)
$(1s2s^3S)3d^4D$	7.223(-1)	1.158(-2)	$(1s2p^3P)3s^4P$	7.236(-1)	1.130(-1)
		1.654(-1)			1.326(-1)
$(1s2s^3S)3d^2D$	7.231(-1)	7.456(-3)	$(1s2p^3P)3s^2P$	7.254(-1)	2.293(0)
		7.611(-2)			-1.561(0)
$(1s2s^1S)3d^2D$	7.260(-1)	2.322(-1)	$(1s2p^1P)3s^2P$	7.272(-1)	3.796(-1)
		1.867(-2)			-2.471(-1)
$(1s2p^3P)3p^4D$	7.250(-1)	4.463(-1)	$(1s2p^3P)3d^4F$	7.264(-1)	9.162(-3)
		2.696(0)			-5.712(-3)
$(1s2p^3P)3p^2D$	7.268(-1)	4.094(-1)	$(1s2p^3P)3d^2F$	7.278(-1)	0.0
		1.194(0)			2.395(-2)
$(1s2p^1P)3p^2D$	7.288(-1)	5.688(0)	$(1s2p^1P)3d^2F$	7.306(-1)	0.0
		-4.107(0)			7.540(-5)
$(1s2p^3P)3p^4P$	7.261(-1)	1.214(-1)	$(1s2p^3P)3d^4D$	7.275(-1)	2.559(-2)
		1.719(0)			3.481(-3)
$(1s2p^3P)3p^2P$	7.262(-1)	2.350(-1)	$(1s2p^3P)3d^2D$	7.262(-1)	2.414(-2)
		7.475(-1)			1.168(-2)
$(1s2p^1P)3p^2P$	7.291(-1)	3.246(0)	$(1s2p^1P)3d^2D$	7.302(-1)	7.441(-3)
		-2.257(0)			-3.112(-3)
$(1s2p^3P)3p^4S$	7.246(-1)	1.117(-1)	$(1s2p^3P)3d^4P$	7.283(-1)	2.026(-3)
		5.334(-1)			4.823(-2)
$(1s2p^3P)3p^2S$	7.278(-1)	4.920(-1)	$(1s2p^3P)3d^2P$	7.289(-1)	4.622(-2)
		-1.670(-1)			-4.702(-3)
$(1s2p^1P)3p^2S$	7.299(-1)	9.294(-1)	$(1s2p^1P)3d^2P$	7.310(-1)	1.880(-1)
		-6.095(-1)			-1.395(-1)

TABLE III. Values for the Coefficients A(Upper Entries) and A^e(Lower Entries) for Determining Ω for Innershell Excitation from $1s^2 3d\,^2D$

Transitions Involving 1s-2s			Transitions Involving 1s-2p		
Upper Level	ΔE (Z^2Ryd)	A(Upper) A^e(Lower)	Upper Level	ΔE (Z^2Ryd)	A(Upper) A^e(Lower)
$(1s2s\,^3S)3s\,^4S$	7.176(-1)	4.234(-8) 9.408(-8)	$(1s2s\,^3S)3p\,^4P$	7.197(-1)	8.342(-4) 3.138(-2)
$(1s2s\,^3S)3s\,^2S$	7.190(-1)	0.0 7.965(-7)	$(1s2s\,^3S)3p\,^2P$	7.201(-1)	1.077(-3) 1.249(-2)
$(1s2s\,^1S)3s\,^2S$	7.214(-1)	0.0 1.584(-3)	$(1s2s\,^1S)3p\,^2P$	7.232(-1)	7.964(-2) -5.438(-2)
$(1s2s\,^3S)3d\,^4D$	7.213(-1)	5.605(-3) 9.462(0)	$(1s2p\,^3P)3s\,^4P$	7.226(-1)	4.293(-3) 3.993(-2)
$(1s2s\,^3S)3d\,^2D$	7.221(-1)	4.113(-1) 4.338(0)	$(1s2p\,^3P)3s\,^2P$	7.244(-1)	2.463(-3) 4.990(-3)
$(1s2s\,^1S)3d\,^2D$	7.250(-1)	1.676(1) -1.251(1)	$(1s2p\,^1P)3s\,^2P$	7.261(-1)	2.311(-2) 4.721(-2)
$(1s2p\,^3P)3p\,^4D$	7.240(-1)	1.963(-1) 3.723(-1)	$(1s2p\,^3P)3d\,^4F$	7.253(-1)	5.318(-1) 4.133(0)
$(1s2p\,^3P)3p\,^2D$	7.257(-1)	5.587(-2) 1.249(-1)	$(1s2p\,^3P)3d\,^2F$	7.268(-1)	1.558(0) 7.549(-1)
$(1s2p\,^1P)3p\,^2D$	7.278(-1)	9.582(-1) -6.991(-1)	$(1s2p\,^1P)3d\,^2F$	7.296(-1)	7.089(0) -4.756(0)
$(1s2p\,^3P)3p\,^4P$	7.251(-1)	1.546(0) -1.097(0)	$(1s2p\,^3P)3d\,^4D$	7.265(-1)	4.263(-1) 2.889(0)
$(1s2p\,^3P)3p\,^2P$	7.251(-1)	9.008(-4) 2.181(-2)	$(1s2p\,^3P)3d\,^2D$	7.252(-1)	3.452(-1) 1.266(0)
$(1s2p\,^1P)3p\,^2P$	7.281(-1)	5.593(-2) -3.643(-2)	$(1s2p\,^1P)3d\,^2D$	7.292(-1)	6.019(0) -4.355(0)
$(1s2p\,^3P)3p\,^4S$	7.236(-1)	9.072(-3) 2.532(-2)	$(1s2p\,^3P)3d\,^4P$	7.272(-1)	1.033(-1) 1.868(0)
$(1s2p\,^3P)3p\,^2S$	7.268(-1)	0.0 1.612(-4)	$(1s2p\,^3P)3d\,^2P$	7.278(-1)	3.227(-1) 6.322(-1)
$(1s2p\,^1P)3p\,^2S$	7.289(-1)	0.0 2.890(-6)	$(1s2p\,^1P)3d\,^2P$	7.300(-1)	3.493(0) -2.514(0)

TABLE IV. Values for $Z^2\Omega_H$ and $Z^2\Omega_H^e$ as a Function of Impact Electron Energy ε in Threshold Units

ε	$Z^2\Omega_H$(1s-2s)	$Z^2\Omega_H^e$(1s-2s)	$Z^2\Omega_H$(1s-2p)	$Z^2\Omega_H^e$(1s-2p)
1.0	3.614(-1)	1.554(-1)	1.478(0)	8.770(-1)
1.2	3.674(-1)	1.276(-1)	1.599(0)	6.651(-1)
1.5	3.747(-1)	9.804(-2)	1.827(0)	4.634(-1)
1.9	3.824(-1)	7.236(-2)	2.147(0)	3.082(-1)
2.5	3.912(-1)	4.945(-2)	2.595(0)	1.866(-1)
4.0	4.051(-1)	2.427(-2)	3.494(0)	7.494(-2)
6.0	4.152(-1)	1.250(-2)	4.355(0)	3.294(-2)
10.0	4.250(-1)	5.154(-3)	5.548(0)	1.145(-2)
15.0	4.307(-1)	2.472(-3)	6.550(0)	4.936(-3)

NEW RESULTS OF THE UNRESOLVED TRANSITION ARRAYS METHOD

M. Klapisch, A. Krasnitz, P. Mandelbaum
Racah Institute of Physics
Hebrew University
Jerusalem 91904

C. Bauche-Arnoult, J. Bauche
Lab.-Aime Cotton
91405 Orsay

The formulas for mean wavelengths and widths of Unresolved Transition Arrays (UTA)[1,2], have been extended to include spectator electrons and jj transitions. These were used to interpret several sorts of satellite spectra, e.g., $3d^{10}\,n\ell^{q} - 3d^{9}\,4f\,n\ell^{q}$ transitions in atoms Tm thru W from laser produced plasmas, and $3d^{m}4s - 3d^{m-1}\,4p4s$ in Mo and Pd spectra. The Unresolved Character of the UTA will be discussed thanks to an evaluation of the number of lines in the array. This will be applied to 4d-4f transitions in Ionized Rare Earths.

REFERENCES

(1) C. Bauche-Arnoult, J. Bauche and M. Klapisch, Phys. Rev. A 20, 2424 (1979) and Phys. Rev. A 25, 2641 (1982).
(2) M. Klapisch, E. Meroz, P. Mandelbaum, A. Zigler, C. Bauche-Arnoult and J. Bauche, Phys. Rev. A 25, 2391 (1982).

SESSION 5. EXPERIMENTAL ATOMIC PHYSICS

DISTORTED WAVE CALCULATIONS: APPLICATION TO ASTROPHYSICS AND TOKAMAK PLASMA

A. K. Bhatia
Laboratory for Astronomy and Solar Physics
NASA/Goddard Space Flight Center
Greenbelt, Maryland 20771 USA

During the last few years, observations of solar phenomena have been carried out by rocket flights, manned satellites like Skylab, unmanned satellites like Orbiting Solar Observatories and more recently Solar Maximum Mission. The wavelengths, line intensities and line profiles in UV and X-ray regions of the solar spectra have been measured. The spectroscopic data obtained are of high spatial and spectral resolution. The goal is to understand the physical properties of the emitting plasma and determine the electron temperatures, densities and volume of the emitting plasma from UV and X-ray spectra.

Since emission lines are seen, this would imply plasma is hot and ionized. The lines are produced when the higher states of the positive ions excited by electron impact decay to the lower states. Therefore, it is necessary to understand the line forming processes and calculate the relevant atomic data for the interpretation of the spectroscopic data. Since the tokamak spectra are similar[1] to the flare spectra, the same atomic data can be used to interpret the tokamak spectra.

The intensity of the line due to the transition from j to i is given by

$$I_{ji} = N_j A_{ji} \frac{hc}{\lambda_{ij}} , \qquad (1)$$

where λ_{ij} is the wavelength of the line, A_{ji} is the transition rate and N_j is the population of the upper level. In the solar corona and in flares the electron densities are of the order of 10^9 to 10^{12} cm^{-3} which are not high enough to maintain a Saha-Boltzmann distribution of level populations. These must be obtained by solving the statistical equilibrium equations.

We assume that the collisional and radiative processes are much faster than the ionization and recombination processes so that the calculation of the level populations can be carried out separately by including only collisional and radiative processes. Therefore, we can deal with one ion at a time and assume that ionization equilibrium exists. This is a good approximation for the lower excited states but not for the higher excited states. We would also assume that the plasma is optically thin.

The level populations N_i are given by the rate equation

$$\frac{dN_i}{dt} = -N_e N_i \sum_{j>i} C^e_{ij} + \sum_{j>i} N_j A_{ji} - N_i \sum_{j<i} A_{ij} + N_e \sum_{j>i} N_j C^d_{ji} , \qquad (2)$$

RECENT LABORATORY STUDIES OF DIELECTRONIC RECOMBINATIONS

G.H. Dunn
Joint Institute for Laboratory Astrophysics
University of Colorado, Boulder, CO 80309

The breakthrough in 1978 by Brooks et al.[1] and by Breton et al.[1] provided the first plasma rate measurements on dielectronic recombination (DR), and their basic technique has been followed up on in a few other investigations. An important new plasma technique was introduced[2] in 1982. Another breakthrough in 1982-1983 led to colliding beams cross section measurements[3] for DR and to more direct comparisons with theory. Experiment/theory disagreements and agreements have led to follow-up experimental and theoretical efforts which are pointing to better understanding of DR and which emphasize issues that should be paid attention to by plasma modelers. An overview will be given with strong emphasis on the beams experiments and the implications.

* Staff Member, Quantum Physics Diivsion, National Bureau of Standards.

REFERENCES

[1] R.L. Brooks et al. Phys. Rev. Lett. 41, 107 (1978); C. Breton et al. Phys. Rev. Lett. 41, 110 (1978).
[2] M. Bitter et al. Bull. Am. Phys. Soc. 27, 1083 (1982).
[3] J.B.A. Mitchell et al. Phys. Rev. Lett. 50, 335 (1983); B.S. Belić et al. Phys. Rev. Lett. 50, 339 (1983); P.F. Dittner et al. Phys. Rev. Lett. 51, 31 (1983); J.F. Williams, Phys. Rev. A 29, 2936 (1984).

VUV HIGH RESOLUTION ABSORPTION SPECTRA OBTAINED WITH SYNCHROTRON LIGHT, AND INTERPRETATIONS

A.M. Baig, J.P. Connerade, W.R.S. Garton, J. Hormes,
C. Mayhew, G. Noldeke and K. Sommer
Physikalisches Inttitut, der Universitat Bonn & Blackett Laboratory
Imperial College, London

For over ten years an expanding collaborative programme of experimental work on the absorption spectra of neutral atomic and simpler molecular gases and vapours, and on similar species "matrix-isolated" in rare-gase solids, has been in progress. The experimental work has centered on use of background continua from the 0.5 and 2.6 GeV synchrotrons in Bonn, - high resolution work being based mainly on the smaller machine. The instrumentation includes - most significantly for the work reported here - a 3-metre Eagle-style vacuum spectrograph equipped with "holographic" gratings of 5,000 - 6,000 1/mm spacing, and usable over the range 200 - 2,000Å.

As regards absorption spectroscopy of neutral atoms in the VUV, the objective is to extend understanding of the atomic mechanics involved in inner-shell photoexcitation. The work in Bonn has produced a very large amount of new information on inner-shell and double- or multiple-excitations, of about half of the periodic system up to Bi I. This work has stimulated attempts at better theoretical interpretations, which have now become elaborate. A few cases in Figs. 1-4 illustrate the performance of the "holographic 3m".

1. Ba I - From earlier work 14 series attaching to 12 limits were identified by 1979. Most recently the spectrum was re-examined with the 3m instrument, giving a dispersion increase by a factor of 15 (see Baig et al., 1984 for interim report). Spectra were obtained in second order (0.27A/mm), by using a column of Hg vapour to suppress the first order of the background continuum in the range below 1178Å. In addition to improving and extending previous classification two further unexpected limits have been identified. Fig. 1 shows a portion of spectrum.

2. Rare Gases - Figure 2 shows the spectrum of Ne I, in first order. Second-order spectra have also been obtained by use of the Hg I - order-sorter mentioned above. This spectrum has previously been studied by others, but the Bonn instrument has given improved resolution by a factor of about 10. Though He I is generally recognized as being the exception among the rare gases, Ne I is more subtly unique in not being followed by growth of a d-subshell. This fact makes the Ne I autoionization structure between the levels of the ground doublet of the ion quite different from that in the cases of the heavier inert gases. Thus, as can be seen in Fig. 2, autoionization widths are small and - in contrast to A,Kr,Xe, - the ns transitions are broader than the nd.

3. Yb I - This spectrum has been the subject of a number of papers over the last few years. Figure 3 shows a portion of a higher resolution plate near 1400Å, from which recognition of a new series due to excitation of a 4f electron mixed with double-electron transitions has followed.

The foregoing are a few examples of work concerned with "internal

field" effects in atoms, i.e., effects ascribable to interactions/ correlations of the electrons of several shells or subshells. Other important cases (e.g., the alkalis or the Zn I - Hg I group) have been recently reported or are in course of interpretations. We are left in this area of work with the challenge of the three rows of transition elements - the important C, N, O, and halogen groups and a few likewise important cases of light elements like Al I. The wide-open field concerns proper quantitative absorption cross-section measurements. Accordingly, replacement of photography by linear-diode arrays ("reticons") is being initiated.

4. Molecular Spectra - The 3-meter spectrograph and the 0.5 GeV machine have been used by one of us (C.M.) for a comprehensive exploration of the dihydrides and deutrides of the oxygen group (i.e., H_2O to D_eTe). The spectra have produced a number of new Rydberg series in the range 900-1700Å. A nice example is shown in Fig. 4 where the Rydberg bands of H_2Te can be followed to n=30. Figure 5 shows the variation of rotational structure of the first member of the so-called E-series of this group of triatomics.

5. Zeeman Patterns - The first objective here has been to extend work on magnetic effects in long Rydberg series and adjacent continua, so far confined to the alkalis and alkaline-earth elements and above 2,000Å, into the VUV. Initial experiments were performed with a solenoid on temporary loan from ANL (Dr. F.S. Tomkins). A larger similar solenoid is just being commissioned in Bonn. However, use of the Argonne solenoid led to an unexpected bonus, in the shape of a promising method for VUV oscillator strength measurement, based essentially on magnetic rotation of plane polarized light (Faraday effect). Figure 6 illustrates.

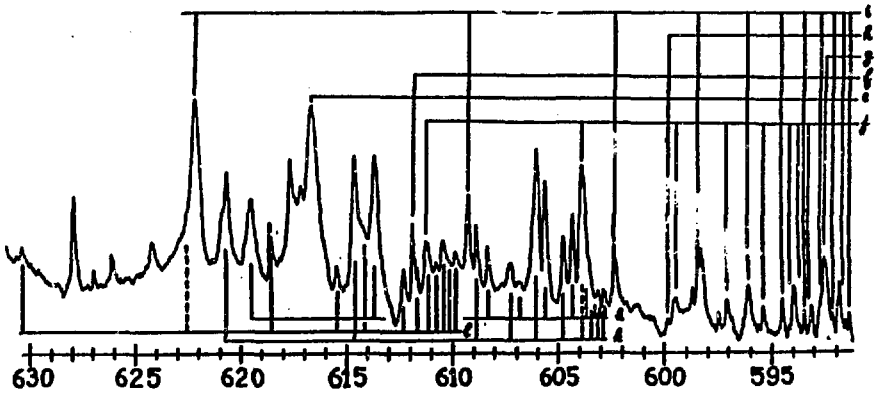

Fig.1.

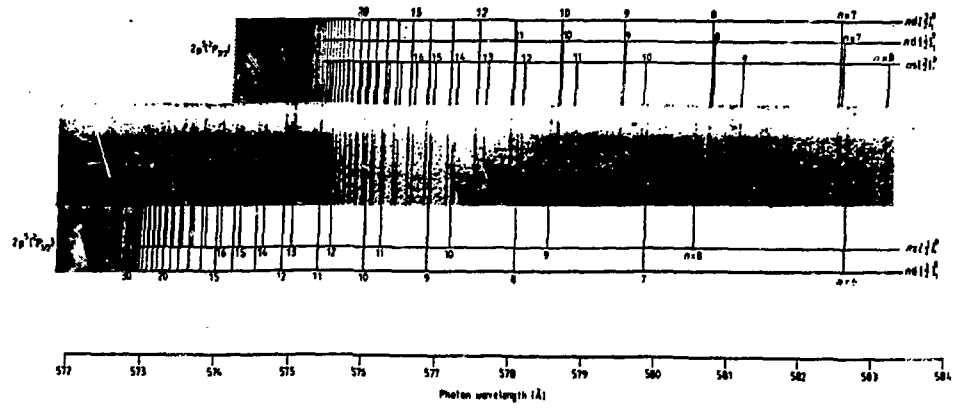

Fig.2.

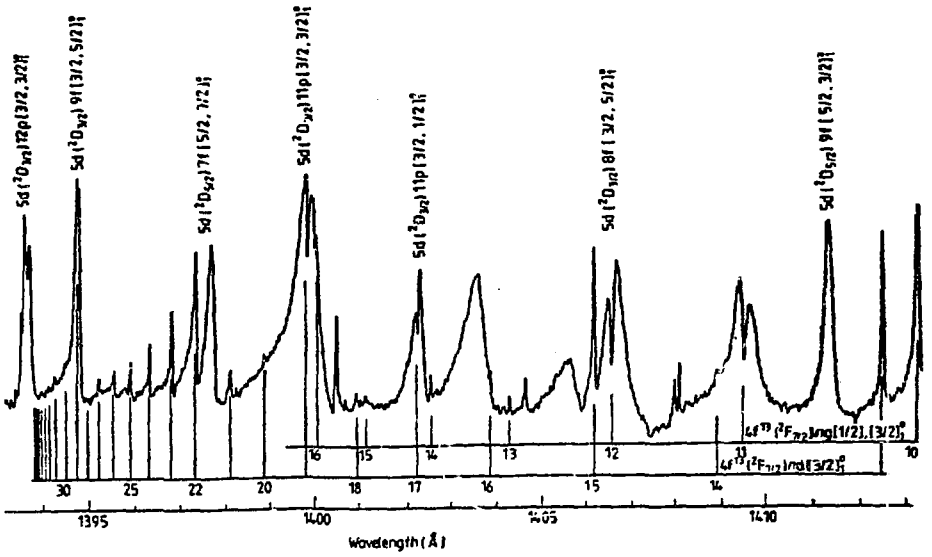

Fig.3. Densitometer trace of photoabsorption spectrum of Yb I showing the high members of the series due to single excitation from the 4f subshell. Note how sharp the lines remain except in the immediate vicinity of the strong perturber.

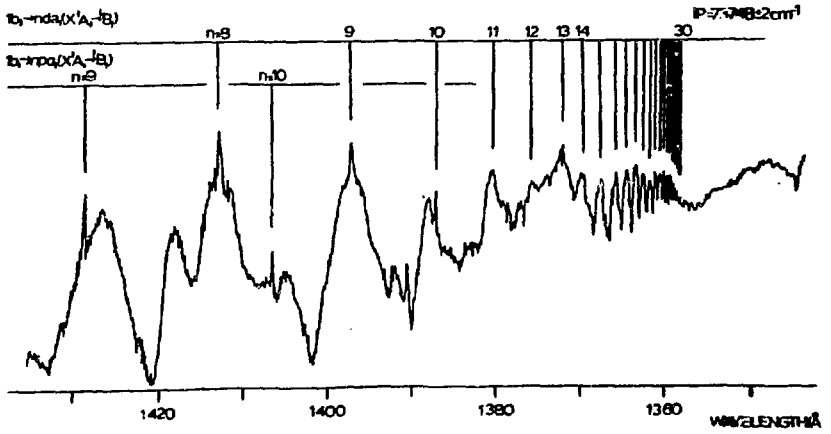

Fig.4.

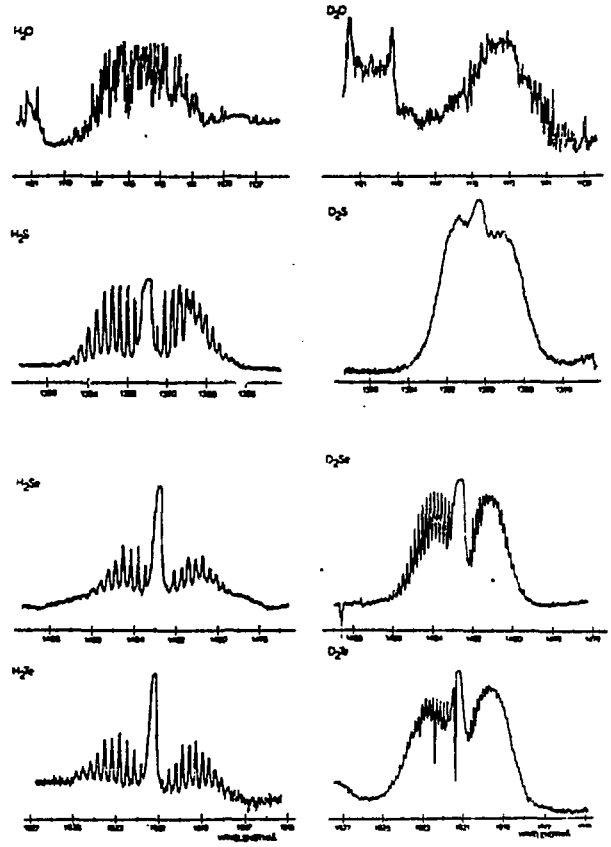

Fig.5.

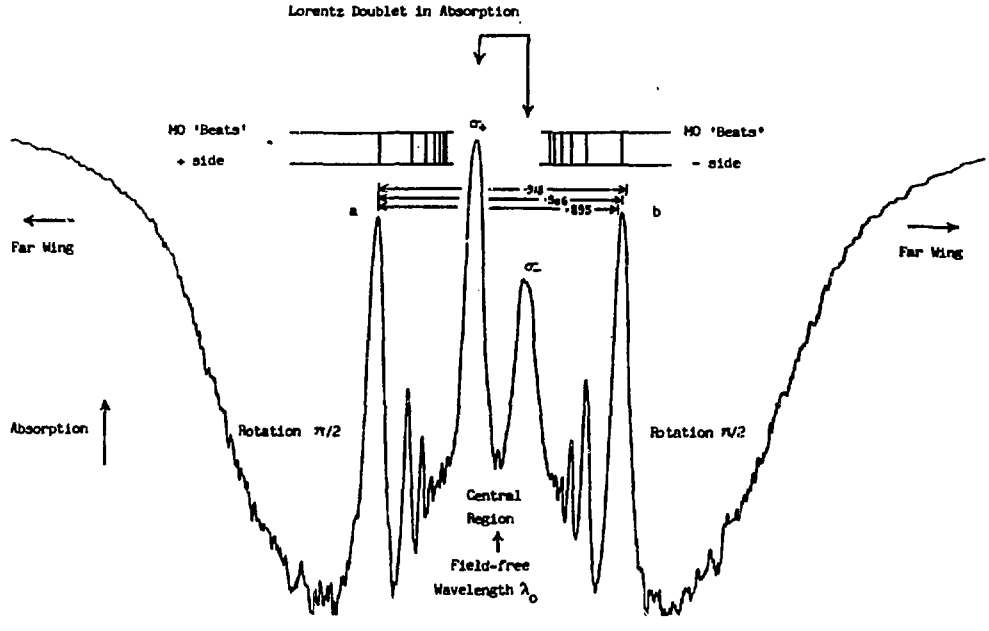
Lorentz Doublet in Absorption
MO 'Beats'
+ side
MO 'Beats'
- side
a
b
Far Wing
Far Wing
Absorption
Rotation π/2
Rotation π/2
Central
Region
Field-free
Wavelength λ0

Fig.6.

DETERMINATION OF ABSOLUTE X-RAY WAVELENGTH WITH THE DOUBLE REFLECTION METHOD

Benjamin S. Fraenkel
Laboratory of X-ray and Far Ultra-Violet Spectroscopy
Plasma Research Center
Racah Institute of Physics
The Hebrew University, Jerusalem, Israel

It has been shown[1,2] that is is possible to determine absolute wavelength values of X-ray radiation emitted as a result of electron transitions in ions or atoms, without precise Spectrometers and without reference "lines". Knowledge of the lattice constants of the diffracting crystal is sufficient for the determination of the wavelengths. Here the first experiment describing the feasibility of the method is shown.

Usually spectra are obtained in form of "lines". In the X-ray case, however, it is possible to obtain spectra in form of points, ordered along lines. The lines represent the white radiation [Fig. 1].

A point spectrum along a line may intersect another point spectrum presenting the same transitions, which is reflected by other crystal planes. In the setting to be described the intersection point has the same wavelength in the two spectra. The intersection wavelength is a constant of the crystal[2], taking also into account the indices of the crystal planes involved. It turns out that such intersections may be found near any wavelength in the soft X-ray range. The intersections may be looked upon as absolute wavelength reference values, they appear simultaneously with the point spectra, and the intersection wavelength may be computed to the accuracy with which the crystal lattice constants are known.

Two kinds of crystal reflection planes are connected with the production of these point spectra, ordinary reflection planes and "forbidden" reflection planes. A forbidden reflection plane does not reflect X-rays because of extinction. However, certain forbidden reflection planes in a distinct group of crystals reflect along special directions on the forbidden reflection cone[3]. Here the forbidden reflection is simulated through a pair of planes, the sum of the indices of them being equal to the indices of the forbidden reflection. For instance, the forbidden reflection [2,0,0] of a diamond lattice may be simulated by the pair $\{[1,1,1,]\ \ [1,-1,-1]\}$, in a very specified direction on the cone of reflection of [2,0,0]. This happens when the incoming radiation beam, for a given wavelength, will fulfill Bragg's law simultaneously for the [2,0,0] and [1,1,1] planes. The radiation reflected by the allowed reflection planes [1,1,1] will be in position to be re-reflected by the [1,-1,-1] plane into the "forbidden" direction. This is a simple description of a complicated, dynamical process.

Experimentally one uses an X-ray point source. The radiation impinges upon the crystal in form of an expanding cone [Fig. 1]. The surface of the crystal is ground and etched parallel to a suitable forbidden reflection plane. The crystal is set so that the central ray

of the beam hits, roughly, the central point of the crystal, with a Bragg angle for the central wavelength of the wavelength range of interest. The incoming and reflected central ray define a plane. In order that the double reflection of interest takes place, the azimuthal position of the crystal must also be set. This involves rotating the crystal in its own plane, so that a crystal axis in the forbidden reflection plane makes a predetermined angle with the plane of reflection, involving the indices of the double reflection and the wavelength.

No fine setting is involved. No collimator is used. The crystal reflects only the doubly reflected radiation.

The radiation which is not reflected is scattered into all directions. Each wavelength of the X-ray radiation coming from a point source will be reflected by an appropriate point on the surface of the crystal, in the double reflection process. For a strictly monochromatic wavelength the reflected radiation will be an infinitely thin ray, and intensity will not do gown with distance from the crystal. However, as practically each electronic transition exites radiation of finite wavelength width, the point reflected turns into a thin streak, in the direction of dispersion.

The intensity of a "point" will be proportional to $1/r$ where r is the distance from the source, while the background intensity will be proportional to $1/r^2$. The farther away the film, the better the signal to noise ratio.

Figure 2 shows the results of the experiment.

Two wavelengths are involved, the $L_{\alpha_{1,2}}$ Gold "lines" at 1.27639 and 1.28777Å. A fine focus X-ray tube is used as point source. It has practically the dimensions of $0.1mm^2$. The crystal involved is Ge. The forbidden reflection is [6,0,0], involving a Bragg angle of about 43°. The distance of the film from the source, through the crystal, is 1.7m.

Three double reflections are involved.

The two strong spots, on a nearly horizontal line of Fig. 2, belong to the double reflection $\{[3,-1,3]\ [3,1-3]\}$. This spectrum is intersected by the other spectra $\{[1,-7,-1]\ [5,7,1]\}$ and $\{[7,-3,1]\ [-1,3,-1]\}$.

The intersection wavelengths can be shown to be 1.287829 and 1.280169 $\pm$ 0.00002Å. The accuracy is given by the accuracy with which the crystal lattice is known - the crystal constant being 5.6576Å. Refraction of the radiation in the crystal does not change the results in a significant way at this accuracy.

Measuring the distances involved, and interpolating for AuL_{α_1}, yields a wavelength consistent with the known wavelength value, within the accuracy of 2.10^{-3}Å.

It should be noted that all points in Fig. 2 representing the L_{α_1} wavelength are ordered in a vertical direction, one above the other, as do also the L_{α_2} points. This is consistent with constant Bragg angle for each of the wavelengths. The inclination varies with the different double reflection, and their relative place above the $\{[3,-1,3]\ [3,1,-3]\}$ double reflection varies according to the azimuthal angle of the various double reflections.

The purpose of the method is to obtain accurate wavelengths for "lines" emitted in the X-ray range by highly ionized atoms in Tokamak or Laser produced plasma. A point source for Tokamak may be obtained by using a pin hole opening facing a Be window on the wall of the Tokamak. A system containing the pin hole, the crystal and the film is independent of the vibrations in the Tokamak, so that any number of discharges may be used to produce the spectrum without detriment to accuracy.

Intersection wavelength is obtained[2] by solving the equations:

$$r_x h_i + r_y k_i + r_z l_i = 1/2\ [h_i^2 + k_i^2 + l_i^2]/a; \quad i = 1,2,3$$

where r_x, r_y, r_z are the coordinates of the center of the sphere of reflection in the reciprocal lattice, and h_i, k_i, l_i are the indices of the forbidden reflection and of the two first reflections of the two pairs of double reflections involved.

Then $\lambda_{intersection} = [r_x^2 + r_y^2 + r_z^2]^{-1/2}$.

Relative values of wavelength may be absolutely determined by this method. For the [2,0,0] of Ge this covers the range from 1Å to about 5Å. Also relative values of lattice constants of various appropriate crystals may be determined by this method, and probably change of crystal lattice values with temperature.

REFERENCES

1. B.S. Fraenkel, Appl. Phys. Lett., 41, 234 (1982).
2. B.S. Fraenkel, VUV VII Proceedings, Ann. Israel Phys. Soc. 6(1) 63, (1983).
3. M. Renninger, Z. Phys. 106, 141 (1937).
4. International Tables for X-ray Crystallography, III, 64 (1968).

Fig. 1 - A beam of X-rays impinges on a crystal from a point source. The crystal reflects the image of the beam at two different wavelengths. The reflection takes place through two pairs of planes. The image of the source is obtained on a film DR by double reflection. The two images of each spectrum are joined by a line of white radiation. These lines intersect at a wavelength dependent only on the crystal structure and planes involved.

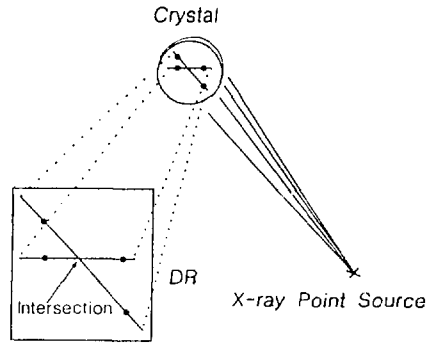

Fig. 2 - Double reflection spectra of Au $L_{\alpha 1}$ and $L_{\alpha 2}$. Two intersections are seen, the strong one between the two points, and the other one on the $L_{\alpha 2}$ point. The wavelengths of the two points are 1.276198Å and 1.28777Å. The wavelengths of the intersections are 1.287829Å, and 1.280269Å. The longish shape of the points is the result of the wavelength not being strictly monochromatic.

HIGH-RESOLUTION PHOTOABSORPTION SPECTRUM OF Cs+ ($5p^6\ ^1S_0 + 5p^5 ns,nd$) BETWEEN 504A AND 600A USING A LASER IONIZED Cs VAPOR COLUMN

T.J. McIlrath,[a] V. Kaufman, J. Sugar,
W.T. Hill, III[a], and D. Cooper
National Bureau of Standards
Gaithersburg, MD 20899

Rapid ionization of Cs vapor in a heat pipe at 0.05 torr was achieved by pumping the $6s\ ^2S_{1/2} - 7p\ ^2P_{1/2}$ transition (f=0.007)[1] with a flash-pumped dye laser at 4593.2A and 1 MW power output. Photoabsorption initiated at the end of the laser pulse (≃ 0.5μs) showed the $5p^5 ns$ and nd series below and above the $5p^5\ ^2P_{3/2}$ threshold at 535.4A. Broad Beutler - Fano resonances appeared in the d series above threshold. The spectrum was recorded photographically on a 10.7m grazing incidence spectrograph using a continuum background generated by a BRV high-voltage spark source with a uranium anode. We will compare the line-shapes and the quantum defect (Lu-Fano)[2] plot with the predictions of a relativistic random phase calculation.

[a]Permanent Address: Institute for Physical Science and Technology, University of Maryland, College Park, MD 20742.

[1]P.M. Stone, Phys. Rev. 127, 1151 (1962).

[2]W.T. Hill, K.T. Chang, W.R. Johnson, T.B. Lucatorto, T.J. McIlrath, and J. Sugar, Phys. Rev. Lett. 49, 1631 (1982).

THE MEASUREMENT OF BRANCHING RATIOS OF SPONTANEOUS RADIATIVE TRANSITION PROBABILITIES FOR Be-LIKE IONS N IV AND O V

J. Lang, R.A. Hardcastle and P.H. Spurrett
Space and Astrophysics Division, Rutherford Appleton Laboratory, Chilton, Didcot, Oxfordshire OX11 0QX, UK

In an experiment to measure emission line intensities from the Be-like ion Ne VII (Lang 1983), the intensity ratio $I(2s3s\,^3S\text{-}2s3p\,^3P)/I(2p^2\,^3P\text{-}2s3p\,^3P)$ was found to be a factor six larger than predicted from the ratio of the theoretical spontaneous radiative transition probabilities (A values). Indeed, to reconcile the Ne VII experiment and theory in several respects it was suggested also that in Be-like C III the theoretical ratios $I(2s3s\,^1S\text{-}2s3p\,^1P)/I(2p^2\,^1D\text{-}2s3p\,^1P)$ was about a factor three too low.

The same apparatus was used to measure A value ratios in Be-like N IV and O V. Briefly the 40 kJ θ-pinch plasma source was viewed radially using a 1½ m Ebert and a 1 m grazing incidence photoelectric spectrometer. The 1½ m Ebert was intensity calibrated from 7300 Å to 3600 Å using a tungsten filament lamp, and from 3800 Å to 2500 Å using a deuterium lamp, both lamps having been calibrated by NPL. As described fully by Lang (1983), the branching-ratios method was used to calibrate the front exit slit of the grazing incidence instrument in the wavelength range 88 Å to 500 Å. Only Li-like line pairs of those listed in that paper were used with the addition of the C IV doublets $2s^2S\text{-}3p^2P$ (312.4 Å) and $3s^2S\text{-}3p^2P$ (5801.33 Å, 5811.98 Å). The H-like ion He II 1-4 transition (243.0 Å) and 3-4 transition (4685.7 Å) were used to cross-check the calibration. As shown in the figure, the He II result agrees excellently with the calibration as defined from the Li-like lines.

A comparison of the measured ratios with the theoretical ratios is given in the table. Theoretical ratios are the average of values obtained from the references numbered 1 to 6 and 9 to 11. The uncertainty quoted includes both that from the measured ratios (typically ± 20%) and the standard deviation of the mean of the theoretical values. The $2s2p^3P\text{-}2s3d^3D$ transitions are the most liable to be affected by opacity (i.e. radiation trapping) since they have high oscillator strengths and the majority of the ion population is in the $2s2p^3P$ metastable term (Keenan et al. 1984, Lang 1983). Experimental checks showed that the results quoted here are not affected by opacity.

Consider the first three rows of the table, involving transitions with a single electron jump. Two of the five ratios are unity to within the quoted uncertainty. The other 3 ratios differ from unity, in one case by a factor 2.3. Although the theoretical oscillator strengths (f) as given in the table are of the same order of magnitude, the A value for the 2-3 transition is approximately three orders of magnitude greater than that for the 3-3 transition. The 2-3 transition contributes > 90% of the total decays from the upper level. Thus, although the theoretical papers quote agreement between theoretical lifetimes and those measured by

the beam foil method, the 3-3 transition A values could well be causing the discrepancies found.

For measured ratios involving $2p^2$-2s3p transitions, the discrepancies between theory and experiment are much larger and are attributed to the theoretical A values for these transitions. The calculations are difficult as the transitions depend on configuration mixing for their existence and have small oscillator strengths. Perhaps experiments of this type are the best way of obtaining reliable A values for such transitions.

REFERENCES

(1) Fawcett, B.C., 1984, Atomic Data and Nuclear Data Tables, 30, 1.

(2) Glass, R., 1979, J.Phys.B: At.Mol.Phys., 12, 1633.

(3) Glass, R., 1981, Z.Phys.A - Atoms and Nuclei, 299, 15.

(4) Hibbert, A., 1976, J.Phys.B: At.Mol.Phys., 9, 2805.

(5) Hibbert, A., 1980, J.Phys.B: At.Mol.Phys., 13, 1721.

(6) Hummer, D.G. and Norcross, D.W., 1974, Mon.Not.R.astr.Soc., 168, 263.

(7) Keenan, F.P., Berrington, K.A., Burke, P.G., Kingston, A.E. and Dufton, P.L., 1984, Mon.Not.R.astr.Soc., 207, 459.

(8) Lang, J., 1983, J.Phys.B: At.Mol.Phys., 16, 3907.

(9) Laughlin, C., Constantinides, E.R. and Victor, G.A., 1978, J.Phys.B: At.Mol.Phys., 11, 2243.

(10) Malinovsky, M., 1975, Astronomy & Astrophysics, 43, 101.

(11) Nussbaumer, H., 1972, Astronomy & Astrophysics, 16, 77.

RESULTS FOR EXPERIMENTAL BRANCHING-RATIO/ THEORETICAL BRANCHING-RATIO

RATIO	N IV	O V	f(O V)
$\frac{A(2s3s\,^1S-2s3p\,^1P)}{A(2s^2\,^1S-2s3p\,^1P)}$	-	1.6±0.3	0.214 *0.389*
$\frac{A(2s3p\,^1P-2s3d\,^1D)}{A(2s2p\,^1P-2s3d\,^1D)}$	1.6±0.4	2.3±0.6	0.210 0.561
$\frac{A(2s3p\,^3P-2s3d\,^3D)}{A(2s2p\,^3P-2s3d\,^3D)}$	1.2±0.4	1.3±0.3	0.116 0.644
$\frac{A(2s3s\,^1S-2s3p\,^1P)}{A(2p^2\,^1D-2s3p\,^1P)}$	-	3.4±1.0	0.214 0.020
$\frac{A(2s3s\,^3S-2s3p\,^3P)}{A(2p^2\,^3P-2s3p\,^3P)}$	0.05±0.02	-	0.576 0.0004

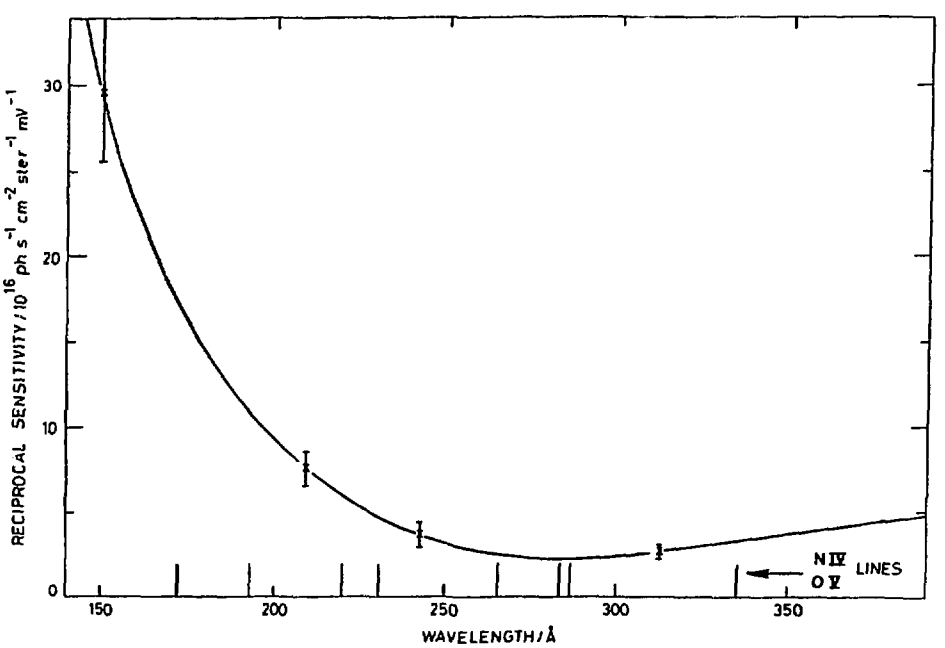

OBSERVATION OF IONIZATION OF LASER EXCITED ATOMS BY SYNCHROTRON RADIATION

J.M. Bizau, F. Wuilleumier, P. Gerard, P. Dhez
Laboratoire de Spectroscopie Atomique et Ionique and
Laboratoire pour l'Utilization du Rayonnemet Electromagnetique
Universite Paris-Sud, Orsay, France 91405

B. Carré, G. Spiess
Service de Physique des Atomes et des Surfaces
CEN, Saclay, France 91191

D.L. Ederer
Radiation Physics Division
National Bureau of Standards
Gaithersburg, MD 20899

J.L. Picqué, J.L. LeGouet, J.C. Keller
Laboratoire Aimé Cotton
CNRS, Orsay, France 91405

P. Koch
Physics Dept.
State University of New York
Stony Brook, NY 11790

We have begun a program to measure oscillator strengths of autoionizing resonances that result from a transition in the VUV between a laser excited initial state and a final state in which a core electron is promoted. These measurements demonstrate a new technique to combine synchrotron radiation, laser pumping, and photoelectron spectroscopy.

Measurements of the energy positions of autoionizing resonances have been honed to a fine art over the past 50 years.[1] Total cross section measurements and the parameters that describe autoionizing resonances have been determined.[2] Most of these studies have been made from the dipole allowed ground state. Recently autoionizing resonances have been observed from excited initial states[3] and from ion initial states.[4] We have heard several talks[5],[6] at this meeting which described some of this type of research. In the measurements to be described in this paper, laser radiation is combined with synchrotron radiation, as shown schematicaly in Figure 1, to study the photoionization from excited initial states to continuum final states or to autoionizing final states. Continuum radiation from the Aneau de Collisions d'Orsay (ACO), which is installed at the Universite de Paris-Sud,in Orsay France, is monochromatized by a toroidal grating monochromator (TGM)[7] and is focused by a toroidal output mirror on to a weakly collimated sodium beam emanating from a furnace mounted on the axis of a cylinderical mirror analyzer (CMA). This electron spectrometer is used to study the kinetic energy distribution of the ejected photoelectrons produced by the interaction of the photon beam with the focused synchrotron radiation.

This arrangement has been used to study atoms[8] and molecules[9] in the ground state.
To extend this research to excited states[10], we have mounted a ring dye laser (maximum intensity at the sodium D lines 9w/cm^2) so that its beam traverses the CMA in a direction perpendicular to the CMA axis at the focus of the synchrotron radiation. The laser is stabilized to 20 MHz by locking it to the $3^2S_{1/2}(F=2) \rightarrow 3\ ^2P_{3/2}(F=3)$ transition in an auxiliary collimated sodium beam also shown schematically Figure 1. The size of the laser beam is adjusted so that it just fills the source volume, V. Electrons emanating from this volume at the magic angle (54°48') can be detected.

We have chosen to determine the oscillator strength of a group of autoionizing resonances in sodium[11] with the same parity as the ground state.

The area $N(h\nu)$ of the photoelectron peak from 2p ionization of the laser-excited atoms is proporational to the product of the excited state density and the photoionization cross section $\sigma(h\nu)$[12]:

$$N(h\nu) = K \cdot I(h\nu) \cdot E(h\nu) \cdot n(3p) \cdot \int_{\Delta E} \sigma(h\nu') \cdot W(h\nu - h\nu') d(h\nu') \qquad (1)$$

where K is the spectrometer constant, $I(h\nu)$ is the photon flux at photon energy $h\nu$; $E(h\nu)$ is th kinetic energy of the photoelectron; $n(3p)$ is the density of laser-excited atoms; ΔE is the monochromator band pass, and W is the photon monochromator window function. Similarly, the integrated area $N(h\nu_R)$, of the photoelectron peak for the autoionizing resonance is given by:

$$N(h\nu_R) = K_R \cdot I(h\nu_R) \cdot E \cdot (h\nu_R) \cdot n(3p) \cdot f'_R \qquad (2)$$

where $I(h\nu_R)$ is the photon flux at the resonance excitation energy, $E(h\nu_R)$ is the kinetic energy of the decay electron and ΔE_R is the monochromator bandpass. In our experiment, the monochromator bandpass (about 0.1eV in first order) was much larger than the width of the resonance, and the integral over the oscillator strength density in Eq(2) can be replaced by the oscillator strength of the resonance. The oscillator strength can be obtained from the ratio of Eq(2) to Eq(1), yielding:

$$f_R = \frac{N(h\nu_R)}{N(h\nu)} \cdot \frac{K}{K_R} \cdot \frac{I(h\nu)}{I(h\nu_R)} \cdot \frac{E(h\nu)}{E(h\nu_R)} \cdot \Delta E \cdot \sigma(h\nu) \qquad (3)$$

This ratio is independent of the excited state density, one of the more difficult quantities to determine experimentally. All the terms on the right of Eq(3) can be determined experimentally, but one can obtain a

very good approximate value of f_R by assuming $\sigma(h\nu)$, the excited state continuum cross section, is equal to the photoionization for the ground state.[13]

In Figure 3 we plot Eq(3) as a function of photon energy for some autoionizing resonances in sodium vapor. Photoionization cross sections from an excited ground state in lithium and barium have also been obtained.

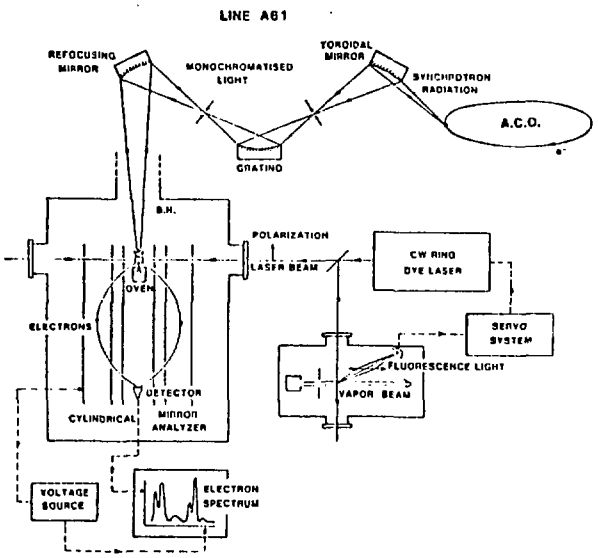

Fig. 1

A schematic representation of the apparatus used for synchrotron radiation studies of laser-exacited states. XUV radiation from the ACO storage ring at the Laboratoire pour l'Utilization du Rayonnement Electro-magnêtique (LURE) is monochromatized and is focused on the axis of a cylindrical mirror electron energy analyzer (CMA). An oven located on the CMA axis produces an effusive cloud of sodium which is excited by the stabilized laser beam traversing the CMA perpendicular to its axis. the beam from the ring dye laser (9 Wcm^2 max power) is stabilized to 20 MHz by using fluorescence from the $3\ ^2S_{1/2}(F=2) \rightarrow\ ^2P_{3/2}(F=3)$ transition in a well collimated sodium beam.

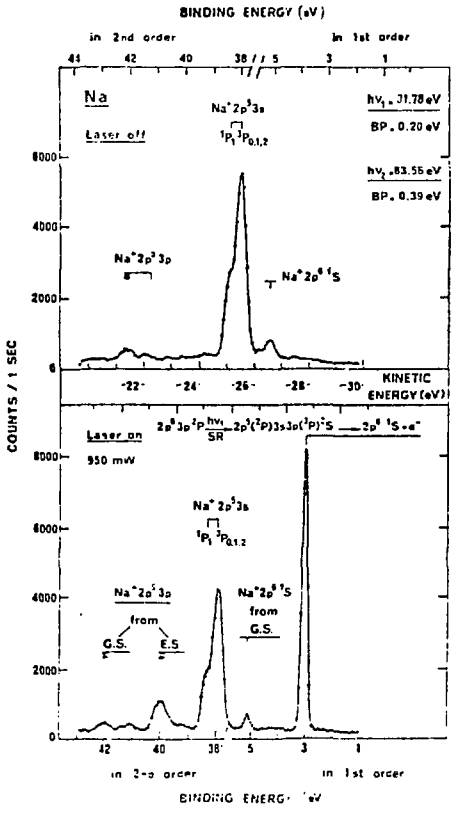

Fig. 2

Photoelectron energy spectrum taken with the TGM set at 31.78 eV. The intense peak at about 29eV kinetic energy (KE) corresponds to the autoionizing decay of the resonance excited by the inner subshell transition indicated in the figure. The small peak at 26.5 eV KE is due to the direct ionization of the 3s electron by the 31.78 eV photons. The structures at 25.5 eV, 22.1 eV, and at 21.4 eV KE are due to the direct ionization of the $2p^63s$ subshell. by 63.56 eV radiation (2nd order radiation diffracted by the TGM). The structure in the lower frame at 23 eV KE is due to the ionization of a 2p electron in the laser excited sodium

Fig. 3

Excitation function of laser excited sodium as a function of photon energy for a TGM band pass of 0.10 eV (BP in figure). The configuration and terms of the autoionizing resonance in the spectral range shown in the figure are indicated according to Ref. 11. The energy position of the $2p^5(^2P)3s3p(^1P)^2D_{3/2}$ differs by 0.022 eV from that of Ref. 11. The width of the structure Γ = 0.11 includes the resonance widths plus the TGM bandpass.

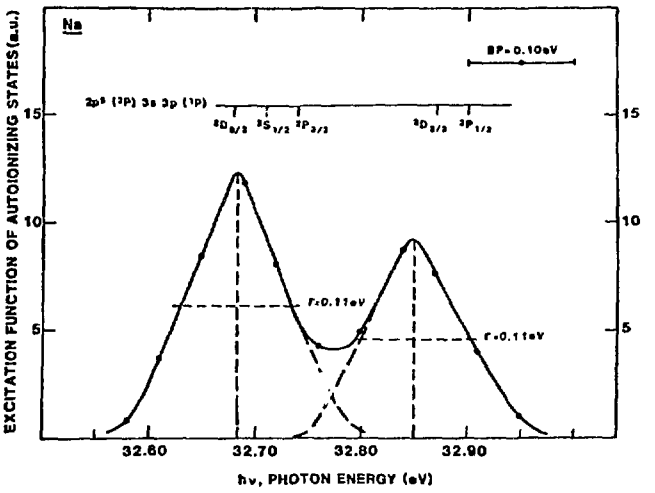

References

1. H. Beutler, Z. Physics 93, 177 (1935); K. Codling, Rep. Prog. Physics 36, 541 (1973).

2. M.O. Krause, F. Cerrina, and T. Fahlman, Phys. Rev. Lett. 50, 118 (1983); J.A.R. Samson, Phys. Lett. 28C 303 (1976).

3. W. Hill, III, K.T. Cheng, W. Johnson, T.B. Lucatorto, T.J. McIlrath, and J. Sugar, Physical Rev. Lett. 49, 1634 (1982).

4. T.J. McIlrath and T.B. Lucatorto, Phys. Rev. Lett. 38, 1390 (1977).

5. M.A. Baig, J.P. Connerade, W.R.S. Garton, J. Hornes, C. Mayhew, G. Noldeke, and K. Sommer, these proceedings.

6. T.J. McIlrath, C. Cromer, V. Kaufman, J. Sugar, W.T. Hill, III, and D. Cooper, these proceedings.

7. P.K. Larsen, W.A.M. van Bers, J.M. Bizau, F. Wuilleumier, V. Schmidt, and D.L. Ederer, Nucl. Instrum. Meth. 195, 245 (1982).

8. S. Krummacher, V. Schmidt, J.M. Bizau, D.L. Ederer, P. Dhez, and F. Wuilleumier, J. Phys. B. 15, 4363 (1982).

9. S. Krummacher, V. Schmidt, F. Wuilleumier, J.M. Bizau, and D.L. Ederer, J. Phys. B. 16, 1733 (1983).

10. J.L. LeGouët, J.L. Picqué, F. Wuilleumier, J.M. Bizau, P. Dhez, P. Koch, and D.L. Ederer. Phys. Rev. Lett. 48, 600 (1982).

11. J. Sugar, T.B. Lucatorto, T.J. McIlrath, A.W. Weiss, Opt. Lett. 4, 109 (1979).

12. M.O. Krause, Chem. Phys. Lett. 10, 65 (1971).

13. T.N. Chang and Y.S. Kim, J. Phys. B. 15, L835 (1982).

STUDY OF ELECTRON CAPTURE IN THE N^{5+}-He, H_2 COLLISIONS BY UV SPECTROSCOPY

M. Druetta and P.H. Cotte
Laboratoire de Spectrométrie Ionique et Moléculaire/AGRIPPA
Université Lyon I 69622 Villeurbanne France

The physics of multicharged ions has considerably developped during the last few years. Aside from its fundamental interest and its motivation for fusion research with Tokamak devices where charge exchange involving highly charged impurities are important, this new effort in this direction is due to the development of new sources of highly charged ions.

We report results concerning spectroscopic study of radiative transitions observed during the collision between multicharged N^{5+} ions with a helium or molecular hydrogen target. N^{X+} ions are produced with the E.C.R. ion source in Grenoble (Geller and Jacquot 1981). The N^{5+} ions are then selected with two 168° bending magnets and finally sent into the target chamber where they collide either with He or H_2 gas. Spectra are observed with a grazing incidence (82°) spectrometer equipped with photon detection.

NV SPECTRA

With a He target, the NV spectra shows a nearly selective capture into the n=3 levels from which decay via the 2s-3p (209Å), 2p-3d (247Å) and 2p-3s (266Å) transitions are recorded. Transitions from the n=4 levels are very weak, apart from 3d-4f.

With H_2 as a target, the n=3 to 2 transitions are always intense but the 3-4 and 2-4 transitions are present in the spectrum, and the 3-5, 4f-6g and 4d-6f transitions are also identified. The electron capture is in this case predominantly into the n=3,4 levels.

Part of the spectra are displayed in figures 1(He) and 2(H_2).

The relative intensity measurement of the 2s-2p transition between He and H_2 is compatible with the total cross section ratio value deduce from Crandall *et al.* 1977. So far we have based cross section calibration on the total charge exchange cross section measurement of Crandall *et al.* 1977. The results for a 50 keV N^{5+} beam are reported in table I.

TABLE I

NV level cross section measurements (in 10^{-16} cm^2) at 50 keV

	σ_{3s}	σ_{3p}	σ_{3d}	σ_{4s}	σ_{4p}	σ_{4d}	σ_{4f}
He target	5	2.5	2.5	-	-	-	0.1
H_2 target	3	8	7	0.6	0.9	1.3	1.9

$\sigma_{n=5}$ estimated (with H_2) : 0.3
$\sigma_{n=6}$ estimated (with He) : 0.15 .

Cross section variation with energy has also been measured with a helium gas target. Results are displayed in figure 3.

TWO ELECTRON CHARGE EXCHANGE: N IV SPECTRA

Some line of N IV appear in the spectra. Two processes may be considered: $N^{5+} \rightarrow N^{4+} \rightarrow N^{3+}$

$$N^{5+} \rightarrow N^{3+} \quad .$$

The first mechanism may be called a double collision process, and the second, a double capture process. The intensity variation with pressure of these N IV lines shows a nearly quadratic dependence with the H_2 target characteristic of the first mechanism and a linear variation with He characteristic of the second one.

The double electron capture is well established during the N^{5+}+He collision and shown with the very strong $2s^2\ ^1S$-$2s2p\ ^1P$ N III-transition (figure 1).

REFERENCES

Geller, R. and Jacquot, B., Nucl. Instrum. Methods, 184, 293, 1981

Crandall, D.H., Mallory, M.L. and Kocher, D.C., Phys. Rev. A, 15, 61, 1977.

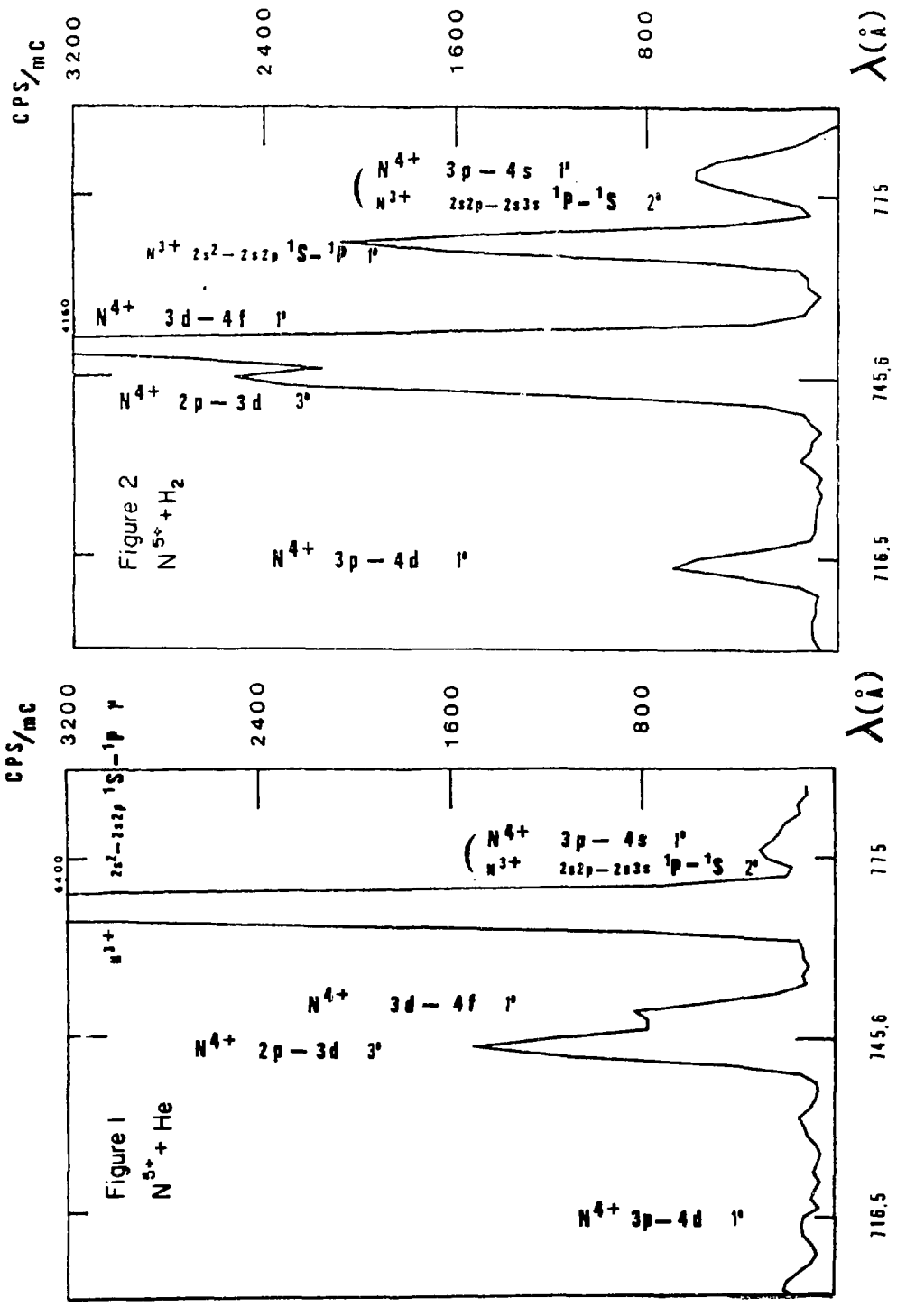
CPS/mC
3200
2400
1600
800
λ(Å)
N4+ 3p – 4s 1°
N3+ 2s2p – 2s3s 1P – 1S 2°
N3+ 2s2 – 2s2p 1S – 1P 1°
N4+ 3d – 4f 1°
N4+ 2p – 3d 3°
N4+ 3p – 4d 1°
775
745,6
716,5
Figure 2
N5+ + H2
CPS/mC
3200
2400
1600
800
λ(Å)
N3+ 2s2 – 2s2p 1S – 1P 1°
N4+ 3p – 4s 1°
N3+ 2s2p – 2s3s 1P – 1S 2°
N3+
N4+ 3d – 4f 1°
N4+ 2p – 3d 3°
N4+ 3p – 4d 1°
775
745,6
716,5
Figure 1
N5+ + He

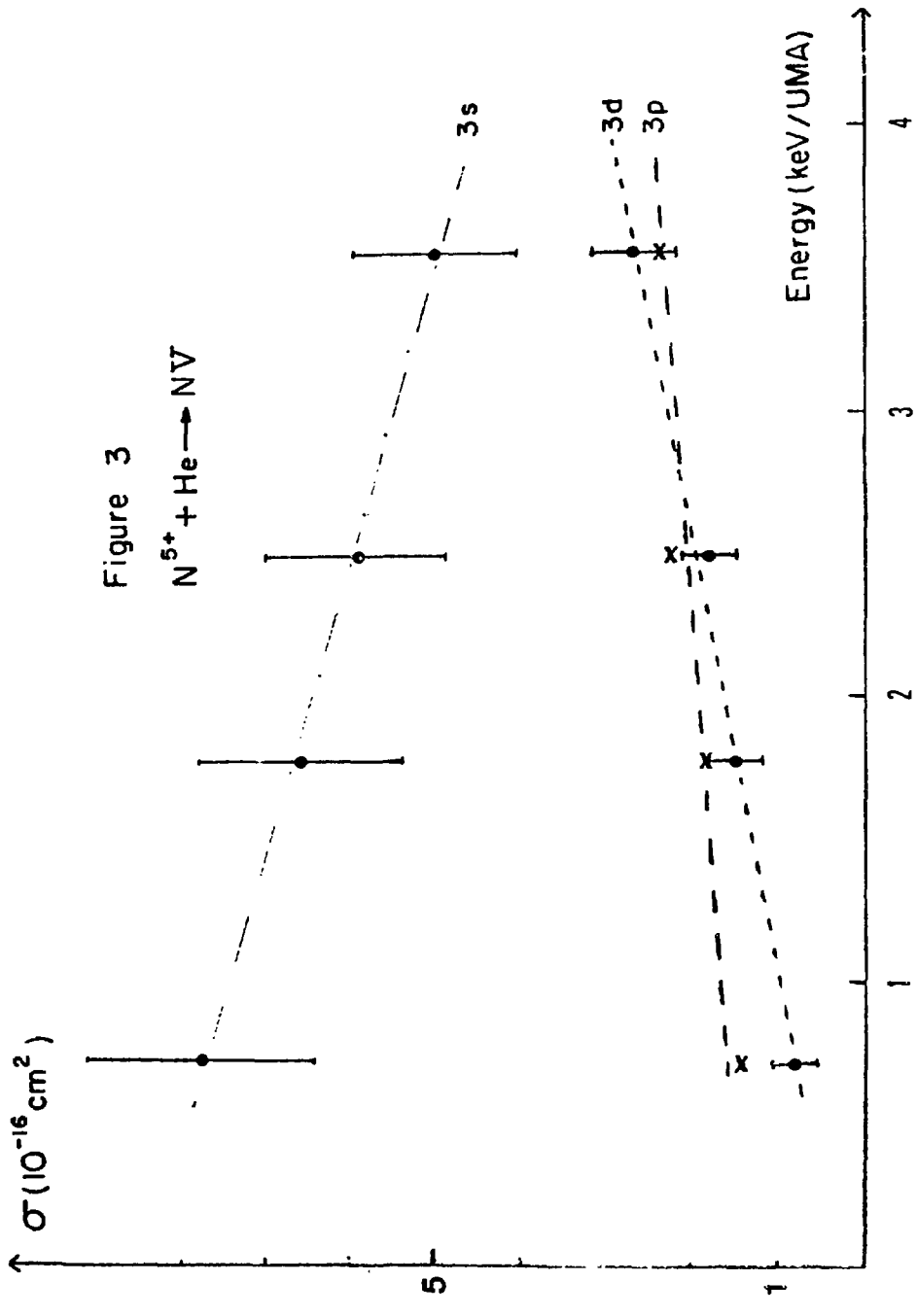
Figure 3
$N^{5+} + He \longrightarrow NV$
$\sigma (10^{-16} cm^2)$
5
1
3s
3d
3p
1
2
3
4
Energy (keV/UMA)

SESSION 6. POSTER PAPERS

SOLAR CORONAL Fe XVII X-RAY LINE RATIOS

H. R. Rugge and D. L. McKenzie
Space Sciences Laboratory
The Aerospace Corporation
Los Angeles, CA

The SOLEX bragg crystal spectrometer experiment on the P78-1 satellite (Landecker, McKenzie and Rugge, 1979) has been used to determine accurate flux ratios of several strong solar Fe XVII x-ray emission lines in the $\sim$15 to $\sim$17 Å wavelength region. The ratios chosen were selected because the lines used permitted an accurate determination of the ratios both from the aspect of counting statistics as well as the lack of interference from other lines of comparable strength. Observations for a variety of conditions of solar activity, ranging from quiet conditions to large solar flares, are presented. For these observations intensity variations of a factor of about 60 were observed for the Fe XVII lines. Variations of a factor of almost 800 were observed for the Fe XVIII line at 14.2 Å. The observed ratios of the Fe XVII lines are compared to the theories of Loulergue and Nussbaumer (1975) and Smith, Raymond, Mann and Cowan (1984).

Agreement between the observed values of the ratios and the mean theoretical values is, in general, acceptable. However agreement between observation and theory for the ratios as a function of solar activity is not good. The observations further show that ratios involving the 15.01 Å Fe XVII resonance line show greater variability than predicted by theory or than observed in other ratios. This may be evidence for resonance absorption of this line in the active region producing it.

The values and variability of the important line ratios are presented below as a function of parameters involving Fe XVII and Fe XVIII lines and line ratios used to characterize solar activity. There is little systematic dependence on solar activity in these ratios as characterized by flux in a resonance line of Fe XVIII (14.2 Å) or the Fe XVIII (14.2 Å)/Fe XVII (17.04 Å) flux ratio.

REFERENCES

Landecker, P.B., McKenzie, D.L., and Rugge, H.R., 1979, Proc. S.P.I.E., 184, 285.

Loulergue, M. and Nussbaumer, H., 1975, Astron. and Astrophys. 45, 125.

Smith, B.W., Raymond, J.C., Mann, J.B. and Cowan, R.D., 1984, Los Alamos Preprint-LA-UR-84-1355.

FIGURE CAPTIONS

Fig. 1 A typical spectrum used to determine line intensities and ratios. Most active region spectra (14.2 Å flux $\lesssim 150 \times 10^3$ ph $cm^{-2}s^{-1}$) used sums of about 10 scans. Flare ratios were determined using individual scans.

Fig. 2 16.77 Å to 17.04 Å intensity ratios for 46 observations. Figs. 2, 3 and 4 use the same scales so that the variability of the ratios can be easily compared.

Fig. 3 17.04 Å to 15.01 Å intensity ratios for 46 observations. Note the substantially greater variation in the ratios as compared to Figures 2 and 4.

Fig. 4 17.04 Å to 17.09 Å intensity ratios for 46 observations. There is essentially no change in the ratio with solar activity.

Fig. 5 A comparison of the observed ratios with those predicted by two independent theoretical calculations.

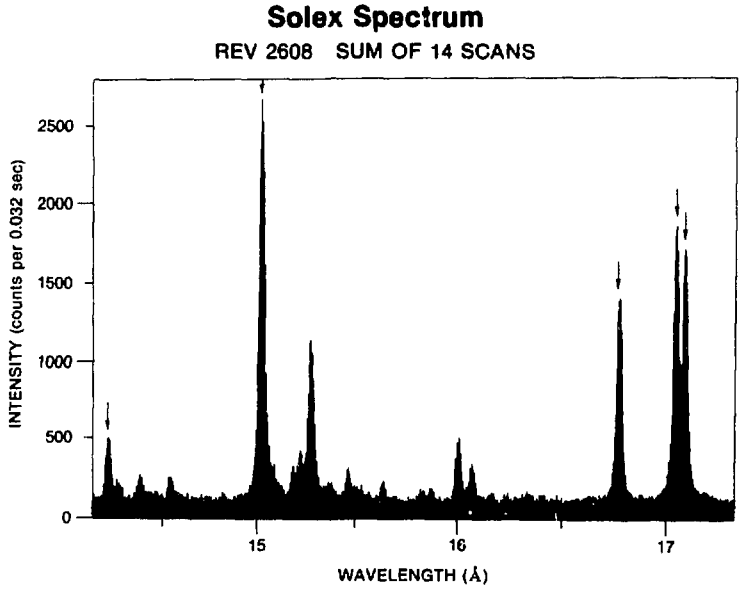

Figure 1

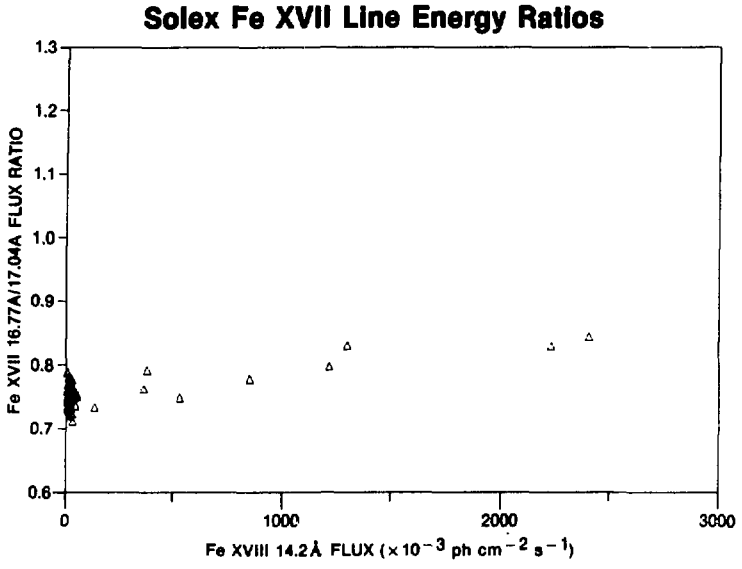

Figure 2

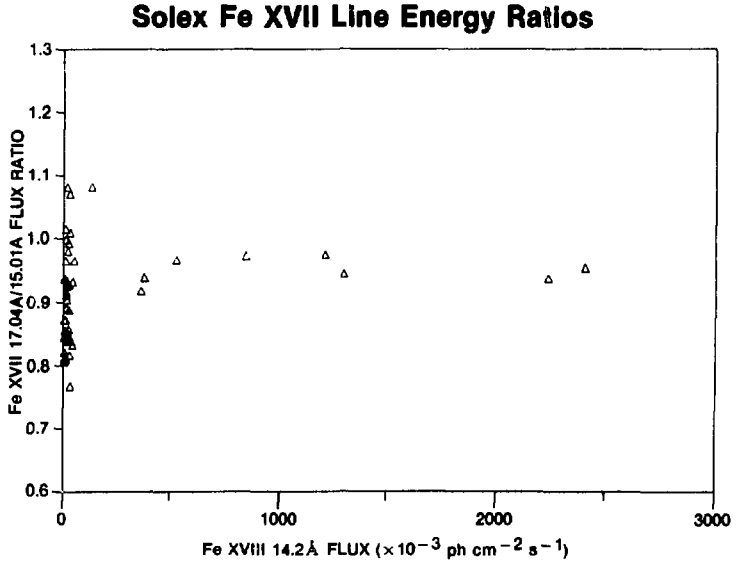

Figure 3

Solex Fe XVII Line Energy Ratios

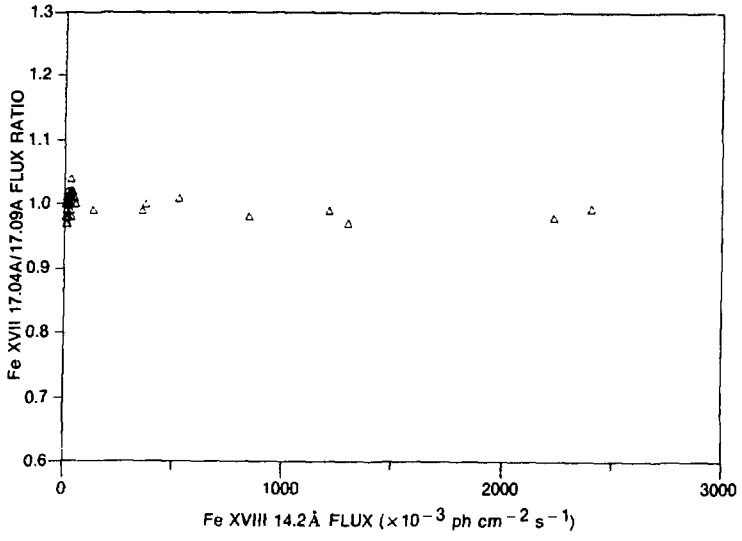

Figure 4

Comparison of Theory and Observations

AUTHORS	ENERGY RATIOS		
	16.77A/17.04A	17.04A/17.09A	17.04A/15.01A
RUGGE and MCKENZIE THIS WORK (1984)	0.75 → Δ	1.00 → Δ	0.91 → Δ
LOULERGUE and NUSSBAUMER* As. Ap. 45, 125 (1975)	0.64+ → Δ	1.29 → Δ	0.86+ → Δ
SMITH, RAYMOND, MANN and COWAN* LANL PREPRINT (1984)	1.02+ → Δ	1.32 → Δ	0.61+ → Δ

Fe XVII TRANSITIONS

15.01A	$1s^2 2s^2 2p^6\ {}^1S_0 - 1s^2 2s^2 2p^5 3d\ {}^1P_1$
16.77A	$1s^2 2s^2 2p^6\ {}^1S_0 - 1s^2 2s^2 2p^5 3s\ {}^1P_1$
17.04A	$1s^2 2s^2 2p^6\ {}^1S_0 - 1s^2 2s^4 2p^5 3s\ {}^3P_1$
17.09A	$1s^2 2s^2 2p^6\ {}^1S_0 - 1s^2 2s^2 2p^5 3d\ {}^3P_2$

*CALCULATION FOR $T = 5 \times 10^6$ °K

+ "17.04A" FLUX USED = (17.04A + 17.09A FLUX) ÷ 2

Δ ARROWS INDICATE TREND WITH INCREASING TEMPERATURE

Figure 5

ATOMIC CALCULATIONS FOR THE HIGHLY IONIZED IRON IONS PRODUCED IN SOLAR FLARES

H. E. Mason
Department of Applied Mathematics and Theoretical Physics
Silver Street
Cambridge CB3 9EW, GB

A. K. Bhatia
NASA/Goddard Space Flight Center
Laboratory for Astronomy and Solar Physics
Greenbelt, Maryland, 20771, USA

The XUV (90-150 Å) and X-ray (10-25 Å) spectra of solar flares are rich in lines from the highly ionized iron ions. Atomic data have been calculated for Fe XVIII (Bhatia, unpublished), Fe XIX (Loulergue et al., 1984, Bhatia and Mason, 1984), Fe XX (Mason and Bhatia, 1980, 1983), Fe XXI (Mason et al., 1979), Fe XXII (Mason and Storey, 1980), Fe XXIII (Bhatia and Mason, 1981), Fe XXIV (Hayes, 1979). The University College London computer package was used. This consists of an atomic structure code (SUPERSTRUCTURE, Eissner et al., 1974); a 'distorted wave' electron scattering program (COLLDW, Eissner and Seaton, 1972); a 'Bethe' approximation electron scattering program (Burgess and Shoerey, unpublished); a program for obtaining electron collision strength in pair coupling from R matrices in LS coupling (JAJOM, Saraph, 1972); a proton scattering program (Bely and Faucher, 1970) and a program for obtaining level populations and intensity ratios.

The transitions $2s^2 2p^n - 2s2p^{n+1}$ fall into the wavelength region 90-150 Å. There are few solar lines in this wavelength region in the absence of flare activity. The only solar flare spectra covering this wavelength region were obtained by the Goddard Space Flight Center's grating spectrometer on OSO-5 (Kastner et al., 1974). An analysis of one of these spectra using recent atomic data has been published by Mason et al. (1984). A steep, positive slope in the emission measure between $10^{6.5}$ and $10^{7.3}$ K was found. An electron density of $\simeq 4 \times 10^{11}$ cm^{-3} at 10^7K was deduced from the line intensity ratios of FE XXI. Theoretical intensity ratios for the Fe XIX lines (Loulergue et al., 1984) agree well with the solar flare spectra and also with recent tokamak spectra published by Stratton et al., 1984. Consistent values are obtained between the theoretical and tokamak intensity ratio I(91.02Å/I(108.37Å) as a function of electron density. The variation in this intensity ratio is due to the enhancement of the $2s^2 2p^4\ ^1D_2$ population relative to that of $2s^2 2p^4\ ^3P_2$ with increasing electron density.

The $2s^2 2p^n - 2s^2 2p^{n-1} 3d$ transitions fall into the wavelength region 10-25 Å. The highest resolution solar flare spectra have been obtained with the X-ray polychromator-flat crystal spectrometer (XRP-FCS) on the Solar Maximum Mission (SMM) (Phillips et al., 1982). The Fe XIX lines fall around 13.5 Å and are partially blended with the lines from Ne VIII and Ne IX. Atomic structure and electron scattering calculations have been carried out for the configurations $2s^2 2p^4$ > $2s^2 2p^3 3s$ and $2s^2 2p^3 3d$ of Fe XIX

(Bhatia and Mason, 1984). To obtain accurate energy level separations for the excited configurations, it was necessary to consider configuration interaction with $2s2p^4 3p$, $2p^5 3s$, $2p^5 3d$. The wavelength identifications have been re-examined by Fawcett and Mason (1984). There is good agreement between the theoretical and solar flare intensity ratios for Fe XIX.

REFERENCES

Bhatia, A.K., and Mason, H.E. 1981, Astron. Astrophys., 103, 324.
Bhatia, A.K., and Mason, H.E. 1984, Preprint
Bely, O., and Faucher, P. 1970, Astron. Astrophys., 6, 88.
Eissner, W., Jones, M., and Nussbaumer, H. 1974, Comp. Phys. Commun. 8, 270.
Eissner, W., and Seaton, M.J. 1972, J. Phys. B., 5, 2187.
Fawcett, B.C. and Mason, H.E. 1984, Preprint.
Hayes, M.A. 1979, Mon. Not. R. Astr. Soc., 189, 55p.
Kastner, S.O., Neupert, W.M., and Swartz, M. 1974, Astrophysics J, 191, 261
Loulergue, M., Mason, H.E., Nussbaumer, H., and Storey, P.J. 1984, Preprint.
Mason, H.E., and Bhatia, A.K. 1980, Astron. Astrophys., 83, 380.
Mason, H.E., and Bhatia, A.K. 1983, Astron. Astrophys. Suppl. Ser., 52, 181.
Mason, H.E., and Bhatia, A.K., Kastner, S.O., Neupert, W.M., and Swartz, M. 1984, Solar Phys., 92, 199.
Mason, H.E., Doschek, G.A., Feldman, U., and Bhatia, A.K. 1979, Astron. Astrophys., 73, 74.
Mason, H.E. and Storey, P.J. 1980, Mon. Nat. R. Astr. Soc., 191, 631.
Phillips, K.J.H., Leibacher, J.W., Wolfson, C.J., Parkinson, J.H., Fawcett, B.C., Kent, B.J., Mason, H.E., Acton, L.W., Culhane, J.L., and Gabriel, A.H. 1982, Astrophys. J., 256, 774.
Saraph, H.E. 1972, Comp. Phys. Commun., 3, 256.
Stratton, B.C., Moos, H.W., and Finkerthal, M. 1984, Astrophys. J., 279, L31.

HIGH SPECTRAL RESOLUTION OBSERVATIONS OF CORONAL X-RAY EMISSION FROM THE RS CVn BINARY SIGMA CORONA BOREALIS

G. R. RIEGLER*
Jet Propulsion Laboratory, Pasadena, CA 91109,
P. C. AGRAWAL*
Tata Institute of Fundamental Research, Bombay, India
and T. H. MARKERT
Massachusetts Institute of Technology, Cambridge, MA 02139.

Results of a high spectral resolution observation of the RS CVn binary σ Cr B, made with the Focal Plane Crystal Spectrometer (FPCS) on the Einstein Observatory, are reported. A spectral scan in the 800-840 eV interval shows clear presence of an X-ray emission line at 826 eV identified with the $^1S_0$-$^1P_1$ transition of Fe XVII. A prominent peak at 1007 eV in the scan band 987-1013 eV is attributed to a blend of lines due to Fe XVII and Fe XXI. Using the observed line fluxes and the Raymond-Smith model, best fit values of corona temperature and volume emission measure, with associated 90% confidence level uncertainties, are derived to be $(6.9 \pm 0.8) \times 10^6$ K and $(1.7 \pm 0.7) \times 10^{53}$ cm^{-3}, respectively. Pressure and density of the X-ray emitting plasma and loop length are deduced by applying a Constant Pressure Coronal Loop Model.

INTRODUCTION

Sigma Corona Borealis (σ Cr B), a visual binary located at a distance of 21 pc, consists of the primary star HD 146361, (m_v = 5.76, spectral type F8V) and the secondary HD 146362, with an angular separation of 5.6". The primary HD 146361 itself is a double-line spectroscopic binary with a period of 1.14 day (Batten, Fletcher and Mann 1978). Strong chromospheric and transition region lines with surface fluxes comparable to those observed in RS CVn binaries, have been observed with the IUE from HD 146361, thus confirming its RS CVn-like nature (Tarafdar and Agrawal 1983). X-ray emission from σ Cr B was detected with the HEAO A-2 experiment (Agrawal, Riegler and Garmire 1980) and confirmed subsequently with Einstein observations (Walter 1981). Moderate spectral resolution observations carried out with the Solid State Spectrometer (SSS) on Einstein showed presence of X-ray emission lines due to ions of magnesium, silicon, iron etc. in its spectrum (Agrawal, Riegler and White 1981). This implied that the X-ray emission in σ Cr B originated in a corona which is most likely associated with the RS CVn binary HD 146361. The SSS spectrum required a two temperature Raymond-Smith plasma fit, a dominant low temperature component with a temperature $T=6 \times 10^6$ K and a high temperature component with $T > 3 \times 10^7$ K. The iron L-emission lines were not resolved in the SSS spectrum so that it was not possible to identify the dominant iron ions responsible for emission in the 0.8-1.0 keV band.

The FPCS is a curved crystal Bragg spectrometer designed for high spectral resolution ($E/\Delta E$ in the range 50-500) studies of X-ray sources in the 0.2 - 3.3 KeV band (Canizares et al. 1977). The spectral bands 12.24 - 12.56 A and 14.76 - 15.50 A were scanned with an exposure of about 2×10^4 s for each band on August 17, 1980.

*Guest Investigators with the Einstein Observatory

ENERGY SPECTRA

In fig. 1 we show plots of observed count rate vs. energy in the 987-1013 eV and 800-840 eV bands, corrected for exposure time and instrumental efficiency. The principal X-ray emission lines and their energies expected from a corona with log T = 6.84 (best fit value of T discussed below) from calculations of Raymond and Smith (1977) are marked by arrows in both graphs. The dashed horizontal lines show the average background from off-source observations. We identify the peak at 826 eV with the $^1S_0$ $^1P_1$ transition of Fe XVII. Counts detected in the 807-820 eV band are almost certainly due to the $^1S_0$ - $^3P_1$ (803 eV) and $^1S_0$ $^3D_1$ (813 eV) multiplets of Fe XVII. A prominent peak visible at 1007 eV is most likely due to a blend of Fe XXI and Fe XVII lines. We have shown the calculated spectrum from Raymond-Smith and Mewe-Gronenschild (1981, 1982) emissivities for the best fit value of log T = 6.84 by the continuous curves in fig. 1.

CORONA TEMPERATURE AND VOLUME EMISSION MEASURE

The observed flux values of the identified lines due to Fe XVII and Fe XXI ions are converted to line luminosities (L_X) using a distance of 21 pc for σ Cr B. Using these L_X values and the coronal emissivities in these energy bands taken from the calculations of Raymond and Smith as well as Mewe and Gronenschild we estimate the volume emission measure (VEM) for the various lines as a function of the corona temperature (T) separately for the 800-820 eV, 820-832 eV and 987-1013 eV bands. We find that the three VEM vs. T curves overlap, which demonstrates that all the lines can be explained as originating from a single-temperature corona. A χ^2-minimization analysis, using the criterion of Avni (1976), was used to generate 90% confidence contours for log VEM vs. log T. We obtain best-fit values of T = (6.7 ± 0.8) x 10^6 K and VEM = (1.7 ± 0.7) x 10^{53} cm^{-3} at χ^2/d.o.f. = 0.83 for the Raymond-Smith model and T = ($6.5^{+0.6}_{-1.2}$) x 10^6 K and VEM = (4.8 ± 2.8) x 10^{53} cm^{-3} at χ^2/d.o.f. = 2.0 for the Mewe-Gronenschild model. The corresponding low-temperature component value of the SSS data fit were T = (5.9 ± 0.5) x 10^6 K and VEM = 1.8 x 10^{53} cm^{-3}.

DISCUSSION

X-ray emission lines due to ions of Fe XVII and Fe XXI detected in the FPCS spectra confirm the coronal nature of the X-ray emission from σ Cr B. The values of T and VEM derived from FPCS observations are in excellent agreement with those obtained earlier with the SSS observations for the dominant low temperature component using the Raymond-Smith model (Agrawal, Riegler and White, 1981). The IUE observations strongly suggest that the spectroscopic binary HD 146361 is the X-ray source in σ Cr B. Since the two component stars of HD 146361 have nearly the same magnitude and mass and similar spectral type and Mg II emission (Tarafdar and Agrawal 1983) we assume that the observed X-ray emission arises due to equal contribution from the coronae of the two stars.

The constant pressure coronal loop model of Rosner, Tucker and Vaiana (1978) has been used to explain coronal X-ray emission from RS CVn binaries (Walter et al. 1980). We obtain a loop length L = 1.2 x 10^9 cm for fill-

ing factor $F_c = 1$, pressure $P = 97$ dynes cm^{-2} and electron density $n_e = 5 \times 10^{10}$ cm^{-3}.

ACKNOWLEDGEMENTS

One of us (PCA) would like to thank Prof. B. V. Sreekantan, Director of T.I.F.R., for support and encouragement during this work. We thank Peter Vedder and Megan Donahue for assistance with the analysis and Prof. Claude Canizares for helpful comments. This work was supported in part by contract NAS 8-30752 from NASA at MIT and by contract NAS 7-100 from NASA at JPL.

REFERENCES

Agrawal, P. C., Riegler, G. R., and Garmire, G. P. 1980, Mon. Not. R. Astr. Soc., 190, 853.

Agrawal, P. C., Riegler, G. R., and White, N. E. 1981, Mon. Not. R. Astron. Soc., 196, 73 p.

Avni, Y. 1976, Astrophys. J., 210, 642.

Batten, A. H., Fletcher, J. M., and Mann, P. J. 1978, Pub. Dominion Astrophys. Obs., 15, 121.

Canizares, C. R., Clark, G. W., Bardas, D., and Markert, T. 1977, Proceedings of Soc. of Photo-optics Inst. Engineers (SPIE), 106, 154.

Mewe, R. and Gronenschild, E. H. B. M. 1981, Astr. Ap. Suppl., 45, 11.

Mewe, R., Gronenschild, E. H. B. M., Westergaard, N. J., Heise, J., Seward, F. D., Chlebowski, T., Kuin, N. P. M., Brinkman, A. C., Digkstra, J. H., and Schnopper, H. W. 1982, Ap. J., 260, 233.

Raymond, J. C. and Smith, B. W. 1977, Ap. J. Suppl., 35, 419.

Rosner, R., Tucker, W. H., and Vaiana, G. S. 1978, Astrophys. J., 220, 643.

Tarafdar, S. P. and Agrawal, P. C. 1984, Mon. Not. R. Astron. Soc., in press.

Walter, F. M. 1981, Astrophys. J., 245, 677.

Walter, F. M., Cash, W., Charles, P. A., and Bowyer, C. S. 1980, Astrophys.J., 236,212.

FIG. 1 SPECTRAL PLOT OF THE FPCS 987-1013 eV AND 800-840 eV SCANS OF THE X-RAY EMISSION LINES DUE TO Fe XVII AND Fe XXI FROM σ Cr B. THE HORIZONTAL DASHED LINES INDICATE THE BACKGROUND LEVEL.

SPECTROSCOPIC DIAGNOSTICS OF THE UV EMITTING PLASMAS IN SOLAR FLARES OBSERVED FROM SMM

Chung-Chieh Cheng
E.O. Hulburt Center for Space Research
Naval Research Laboratory
Washington, DC

E. Tandberg-Hanssen
NASA Marshall Space Flight Center
Huntsville, AL

INTRODUCTION

The transition region exhibits dynamic changes during solar flares. To understand the energy release and transport processes in solar flares, it is important to determine observationally the physical conditions in the flare transition region plasmas, which emit in the UV wavelength ranges. During the Solar Maximum Mission (SMM) we observed many flares in the UV emission lines of Si IV (1402 Å) and O IV (1401 Å) using the Ultraviolet Spectrometer and Polarimeter (Woodgate et al. 1983). In this paper we present the Si IV/O IV flare observations, in particular the dynamic evolution of the transition zone plasmas ($\sim 10^5$ K). We also studied the temporal and spatial correlations between the impulsive UV and hard X-ray bursts.

DIAGNOSTICS OF THE FLARE TRANSITON-ZONE PLASMAS

The O IV 1401.2 Å line is an intersystem line and the Si IV 1401.8 Å line is a resonance line. Their intensity ratio is sensitive to densities $> 5 \times 10^{10}$ cm^{-3}, and is particularly useful for density determination in the flare transition zone plasmas of temperatures $\sim 10^5$ K (for details, see Cheng et al. 1982). Figures 1 and 2 show the application of the Si IV/O IV plasma diagnostics to the 8 April and 22 November 1980 flares respectively, using the raster-through-the line (RL) mode of the UVSP. Use of the RL mode consists of making spectroheliograms in a number of wavelength positions successively for the two lines so that line profiles can be constructed for each individual pixel in the raster. We find that the Si IV/O IV burst in the 8 April flare occurred in a low-lying transition-zone temperature loop. At the onset of the flare, the footpoints, particularly the eastmost one, brightened up impulsively. The density at this flare footpoint increased from its preflare value of $\sim 10^{11}$ cm^{-3} to 3×10^{12} cm^{-3}, and the plasma there had a downflow velocity of 20-40 km s^{-1}. The situation was the same for the 22 November 9180 flare, which was located outside the main sunspot regions. The Si IV/O IV emission was concentrated in small kernels, located at the footpoints of interacting loops, one of which was a large loop observed in soft X-rays (Cheng and Pallavicini 1984). At the flaring UV bright points, the density increased to $\sim 2 \times 10^{12}$ cm^{-3}, and there was a downflow of ~ 20 km s^{-1}.

FIG. 1

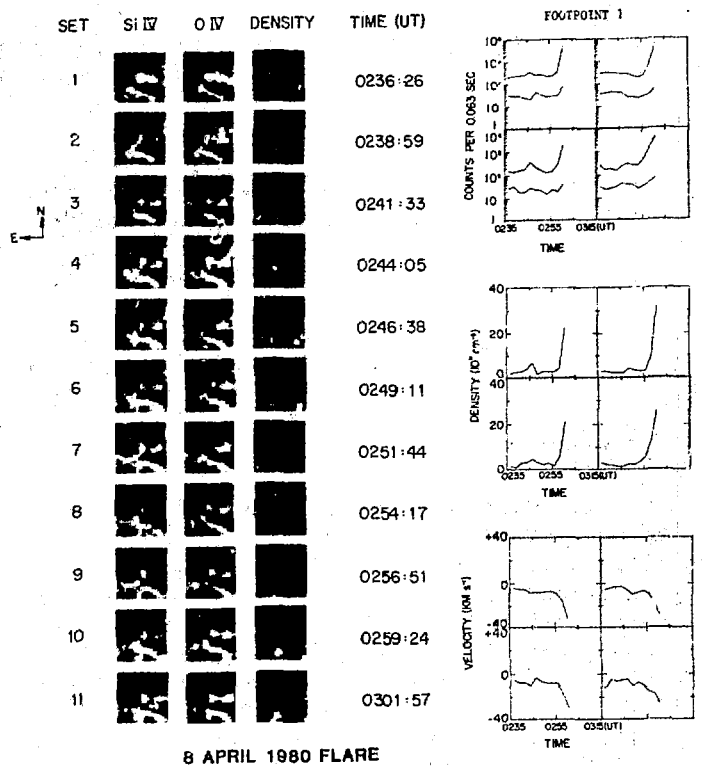
SET
Si IV
O IV
DENSITY
TIME (UT)
1
0236:26
2
0238:59
3
0241:33
4
0244:05
5
0246:38
6
0249:11
7
0251:44
8
0254:17
9
0256:51
10
0259:24
11
0301:57
E
N
FOOTPOINT 1
COUNTS PER 0.063 SEC
TIME
DENSITY
VELOCITY
8 APRIL 1980 FLARE

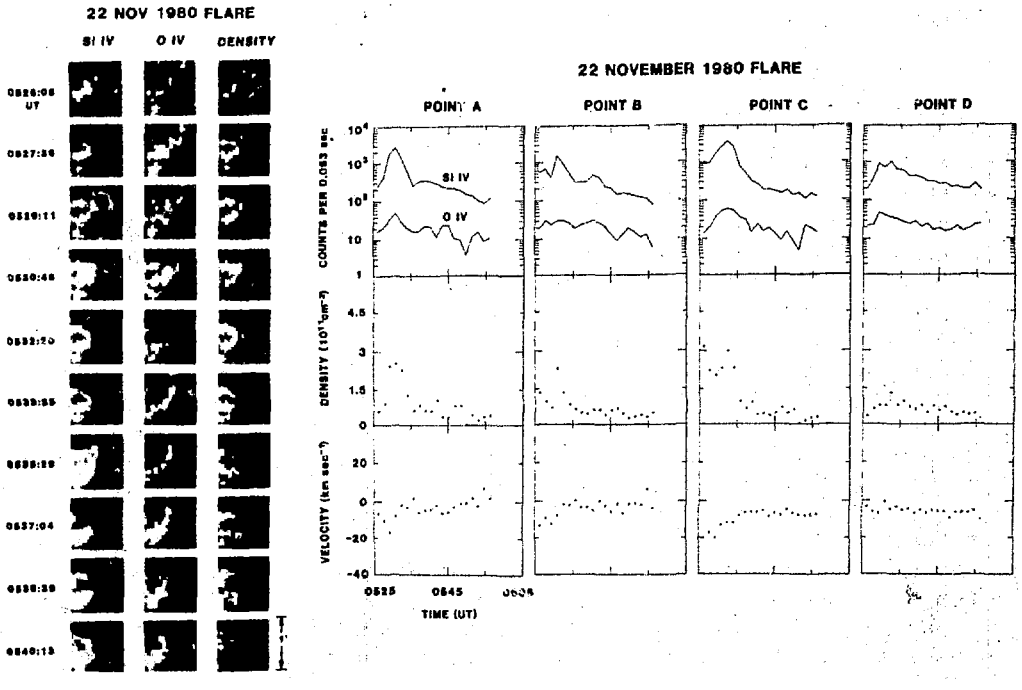
22 NOV 1980 FLARE
SI IV
O IV
DENSITY
22 NOVEMBER 1980 FLARE
POINT A
POINT B
POINT C
POINT D
COUNTS PER 0.063 sec
SI IV
O IV
DENSITY
VELOCITY
TIME (UT)

FIG. 2

TEMPORAL AND SPATIAL STRUCTURES OF IMPULSIVE UV AND HARD X-RAY BURSTS

Correlations between the impulsive hard X-ray bursts and the spatially-resolved Si IV/O IV observations enable us to deduce the spatial structures of the impulsive hard X-ray bursts. Figure 3 shows one example of Si IV/S IV observation of the impulsive phase in solar flares (Cheng et al. 1981). As can be seen from the figure, the Si IV/S IV bursts occurred at discrete kernels of size 3"-4". The impulsive UV and hard X-ray bursts were temporally correlated, and individual hard X-ray peaks were associated with brightenings in individual UV kernels. Sometimes, however, one hard X-ray peak may correspond to many UV brightenings in different kernels. These observations show that the impulsive UV and hard X-ray bursts originate in small regions of high density, and that the emission regions have considerable spatial structure (Cheng, Tandberg-Hanssen, and Orwig 1984).

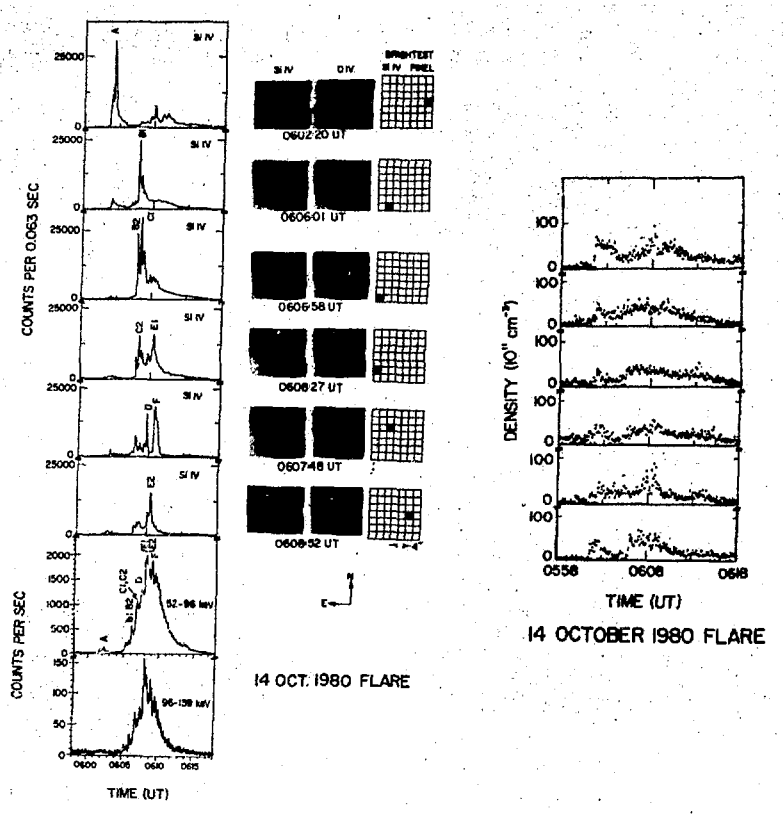

FIG. 3

CONCLUSIONS

The Si IV and C IV lines proved to be useful diagnostic tools for studying the flare transition zone plasmas. As a result of these observations, we now know more about the temporal and spatial structures of the impulsive UV and hard X-ray bursts. The observations show that there is considerable spatial structure in the emission regions of these impulsive components. For a proper understanding of the energy release and transport processes in flares, it is necessary to include the spatial structure in modeling the impulsive bursts.

We sincerely thank all the people who have contributed to the successful operations of SMM. The work was supported in part by NASA under contract DPR W-15367.

REFERENCES

Cheng, C.-C. et al. 1981, Ap. J., (Letters), 248, L39.
Cheng, C.-C. et al. 1982, Ap. J., 253, 353.
Cheng, C-C. and Pallavicini, R. 1984, Solar Phys., (in press).
Cheng, C.-C., Tandberg-Hanssen, E., and Orwig, L.E. 1984, Ap. J., 278, 853.
Woodgate, B.E. et al., 1980, Solar Phys., 65, 73.

MEASUREMENT OF WAVELENGTHS AND ABUNDANCES FROM SOLAR FLARE X-RAY SPECTRA

J.F. Seely, U. Feldman, and G.A. Doschek
E.O. Hulburt Center for Space Research
Naval Research Laboratory
Washington, DC 20375-5000

INTRODUCTION

The measurement of transition energies in highly charged ions represents an important test of quantum electrodynamics (QED) in strong fields. The QED contributions to the hydrogenic transition energies increase as $(\alpha Z)^4$, where α is the fine structure constant and Z is the atomic number. Transitions in hydrogenic ions of sulfur, chlorine, argon, and iron have previously been measured to a precision of 100 ppm or better. These measurements are in satisfactory agreement with accurate calculations of the energy levels, and this confirms the calculation of the QED contributions to the energy levels of one-electron ions.

In the case of highly charged two-electron ions, the situation at the present time is far from satisfactory. Precision measurements of the energies of several transitions in sulfur, chlorine, argon, and iron have been performed using beam foil techniques. These measurements have been compared to recent calculations, but there is not general agreement on the theoretical treatment of the QED contributions to the transition energies in two-electron ions. In three-electron ions, only the $1s^2 2s\ ^2S_{1/2} - 1s^2 2p\ ^2P_{3/2}$ transition has been measured and calculated to high precision.

We report here the measurement of wavelengths and abundances from solar flare spectra. Solar flares are bright sources of X-ray lines, and high-resolution spectra can be obtained in about 30 sec of observation time. Since the high-temperature phase of a flare typically persists for at least several minutes, spectra can be accumulated and added together to improve the signal to noise ratio. The statistics can also be improved by making measurements using data from a large number of flares.

WAVELENGTH MEASUREMENTS

Transitions in ions of argon, potassium, calcium, and iron with one, two, and three electrons have been identified. The wavelengths of the transitions in two-electron and three-electron ions are measured by using the hydrogenic transitions as references. The wavelengths are compared to recent high precision calculations, and the QED contributions to the transition energies can be determined. This work greatly expands the number of precision measurements of transitions in highly charged two-electron ions that are available for comparison with theory.

The data were recorded by the Naval Research Laboratory crystal spectrograph on the Air Force P78-1 spacecraft. The spectrograph consists of four crystals mounted on a common rotating shaft. The wavelength regions that are covered (and the strongest resonance lines in each wavelength region) are 1.80 to 1.98 Å (Fe XXV), 2.96 to 3.10 Å (Ca XX), 3.13 to 3.25 Å (Ca XIX), and 8.23 to 8.52 Å (Mg XII). The first three wavelength regions are covered by Ge crystals (2d = 4.00068 Å), and the fourth wavelength region is covered by an ADP crystal (2d = 10.6416 Å). Dielectronic satellite lines and inner-shell transitions from lower stages of ionization generally fall on the long wavelength side of the resonance lines. These highly charged ions are produced in the hot (1.0×10^7 to 2.5×10^7 K) plasmas associated with solar flares.

On each spectral scan, the shaft rotates 450 steps in one direction and then 450 steps in the opposite direction. Both halves of the scan are over the same wavelength region, and the two halves are folded and added together to improve the signal to noise ratio. The two spectra are folded so that the centroids of the Ca XIX resonance lines in the two spectra are aligned. This eliminates any possible misregistration of the spectra due to the motion of the flare plasma. The wavelength scales are also stretched to account for the angular rotation of the shaft on each of the 900 steps. These angular displacements were measured to a precision of 1 arc sec in the laboratory before launch.

For this study, which is still in progress, we have selected for analysis the data from five flares with good signal to noise ratios. The signal to noise ratio is improved by adding together several scans near the time of peak emission for each flare.

The wavelengths of six isolated transitions in Ar XVII, K XVIII, and Fe XXV of the type $1s^2\ {}^1S_0 - 1snp\ {}^1P_1$ (n=3-8) are measured. The line profiles of these isolated transitions are found to be nearly Gaussian in shape and with full widths at half maximum of 1 to 3 mÅ. Gaussian profiles are expected when thermal Doppler broadening is the dominant broadening mechanism. The wavelengths are measured by fitting Gaussian profiles to the spectral features. For each flare spectrum, the precision of the Gaussian fit to a spectral feature is typically 0.05 mÅ. The standard deviation of the wavelength measurements of a given spectral feature in the five flare spectra is typically between 0.05 and 0.5 mÅ. The Ca XIX and Fe XXV transitions to the $1s^2\ {}^1S_0$ level from the $1s2p\ {}^1P_1$, $1s2s\ {}^3S_1$, $1s2p\ {}^3P_1$, and $1s2p\ {}^3P_2$ levels (transitions designated w,x,y, and z respectively) are blended with dielectronic satellite lines from lower stages of ionization. Using theoretical line intensities, these dielectronic satellite lines are numerically removed from the data, and the wavelengths of the w,x,y, and z transitions are measured in the resulting spectra. A synthetic satellite spectrum is produced by using the theoretical wavelengths and by convolving the theoretical intensities with Gaussian profiles. The wavelength and intensity scales of the synthetic spectrum are normalized to the data, and the synthetic spectrum is subtracted from the spectral data.

We have compared the measured transition energies with the calculated values for five transitions of the type $1s^2\ ^1S_0 - 1snp\ ^1P_1$ (n=2-5) in argon, potassium, calcium, and iron. Ermolaev and Jones (1974) have calculated all of these transitions, and Safronova (1981) has calculated the n=2 transitions. For n>2, we also compare the measurements to the transition energy obtained by using Safronova's ground state energy and the excited state energy of Ermolaev and Jones. Drake (1984) has calculated the transitions from the n=2 and 3 levels. For four of the five transitions, the measurements agree best with the calculations of Safronova and of Drake.

ABUNDANCES

In addition to providing accurate wavelengths, the intensities of lines of Fe XXV, Ca XX, Ca XIX, K XVIII, and Ar XVII can be used to determine their relative solar abundances. This can be done because Fe XXV and Ca XX are formed at nearly the same temperature, and a similar comment applies to the lines of Ca XIX, K XVIII, and Ar XVII. The relative intensities of these lines therefore depend primarily on the relative abundances, assuming that ionization equilibrium occurs in the flare plasma. Accurate collisional excitation rate coefficients and other necessary atomic data for the lines are available in the literature. Preliminary values of the relative abundances are: A(K)/A(Ca) = 0.11, A(Ar)/A(Ca) = 0.73, and A(Ca)/A(Fe) = 0.10. A more detailed discussion will be published elsewhere.

ACKNOWLEDEMENTS

Steven W. Daniels wrote the computer program that corrects for the nonlinearity in the angular rotation of the crystals during a spectral scan and that folds and adds the scan data. We would like to thank Dr. W.C. Martin for helpful discussions. We also thank Dr. G.W.F. Drake for communicating recently calculated transition energies. A detailed description of this work will be published in the Astrophysical Journal.

REFERENCES

Drake, G.W.F. 1984, private communications.

Ermolaev, A.M., and Jones, M. 1974, J. Phys. B 1, 199, and unpublished supplement.

Safronova, U.I. 1981, Phys. Scripta 23, 241.

ANALYSIS OF INTENSITY RATIO FOR MgXII Lyα COMPONENTS FROM INTERCOSMOS 7 OBSERVATIONS

J. Sylwester and B. Sylwester
Space Research Center
Polish Academy of Sciences

J. Jakimiec and M. Tomczak
Wroclaw University
Poland

S.L. Mandelstam, I.A. Zhitnik and V.V. Korneev
P.N. Lebedev Phys. Institute
Moscow

We discuss the Mg XII Lyα line profile measurements obtained by means of Bragg crystal spectrometer aboard INTERCOSMOS 7 satellite. The design of this spectrometer allows to clearly resolve both components ($\alpha_{1/2}$ and $\alpha_{3/2}$) of the Lyα spin doublet. The intensities of each of these components we derived by means of fitting two Voigt profiles to the measured Mg XII Lyα shape. More than 100 spectra were analyzed in this way providing the statistical information on the value of intensity ratio $\underline{a} = \alpha_{1/2} / \alpha_{3/2}$. Derived average value of $\underline{a}$ is close to the theoretically expected 0.5, but in many cases the value of $\underline{a}$ is significantly different from 0.5 (both lower and higher values occur). We present examples of the fit and the histograms showing correlations of a value with the values of other flare parameters. Present analysis consist the observational part of the larger paper under the preparation with Prof. R.W.P. McWhirter theoretical group.

THE SOLAR AND HELIOSPHERIC OBSERVATORY

Giancarlo Noci
Institute of Astronomy, Padua University, and
Arcetri Astrophysical Observatory

In the past years several space missions have been proposed for the study of the Sun and of the Heliosphere. These missions were intended to clarify various different aspects of solar physics. For example, the GRIST (Grazing Incidence Solar Telescope) mission was intended as a means to improve our knowledge of the upper transition region and low corona through the detection of the solar EUV spectrum with a spatial resolution larger than in previous missions; the DISCO (Dual Spectral Irradiance and Solar Constant Orbiter) and SDO (Solar Dynamics Observatory) missions were proposed to gat observational data about the solar oscillations better than those obtained from ground based instruments; the SOHO (Solar and Heliospheric Observatory) mission was initially proposed to combine the properties of GRIST with the study of the extended corona (up to several radii of heliocentric distance) by observing the scattered Ly-alpha and OVI radiation, which was also the basis of the SCE (Solar Corona Explorer) mission proposal; the development of the interest about the variability of the Sun, both in itself and for its consequences in the history of the Earth, led to propose observations of the solar constant (included in DISCO).

It has become apparent, at a certain stage, that the purposes of all these missions could be accomplished by a single spacecraft with the appropriate orbit and that this spacecraft could also accomplish extended measurements of the physical parameters of the interplanetary plasma and therefore include the concept of interplanetary missions (like, for example, IPL (Interplanetary Plasma Laboratory)). This led to the concept of the present SOHO mission.

The SOHO mission is therefore the product of a considerable process of criticism and synthesis accomplished on several previous projects.

A process of this kind has also been accomplished on a larger basis by a reconsideration of all the space projects proposed in the field of solar-terrestrial physics. This has led to the formulation of the International Solar-Terrestrial Physics (ISTP) Program as a collaborative effort of the American, European and Japanese space agencies. The present plans envisage a "core" ISTP program which consists of 6 spacecraft: of these SOHO would investigate solar oscillations and coronal features and monitor the solar wind; WIND, GEOTAIL, EQUATOR and POLAR would measure the plasma in the regions of origin and storage near the Earth; and CLUSTER (an ensemble of 4 close spacecraft) would observe the small scale structure of the plasma in the polar and middle magnetosphere and in the solar wind. This is considered at present the minimum requirement for the study of solar-terrestrial physics in the 1990's. Beyond this core program, and coordinated with it, other spacecraft, balloon and ground based observations are expected to take place.

Therefore, although originally proposed within ESA, where a phase A study on it is now under way, the SOHO mission will very likely become a joint ESA-NASA effort in the frame of the ISTP program.

The scientific aims of the mission, which sum up the purposes of several previously proposed missions, as said above, can be divided into 4 categories:

(a) constitution of the solar interior;
(b) high resolution structure of the transition region and low corona;
(c) structure of the extended corona and acceleration of the solar wind;
(d) structure of the heliosphere.

To fully meet the requests of the coronal observations and to avoid any phase problem caused by an observational window in the oscillation observations, the orbit should stay permanently in sunlight. The study of the variations of the solar constant requires an observation time of the order of a few years, and a similar period of time is needed by the study of the solar oscillations, to enhance the signal to noise ratio. An observation time as long as this is highly desirable by the other investigations.

An orbit close to L1 (1.5×10^6 km from Earth) satisfies all these requirements. (A positioning exactly at the libration point must be avoided because of solar interference on radio links.)

Therefore SOHO is planned as a three-axis stabilized spacecraft to be placed in a halo orbit around the Lagrangian point L1. It has a payload module dedicated to Sun pointing instruments and a "housekeeping" module carrying not only spacecraft subsystems but also some solar wind instruments. The spacecraft is pointed toward the Sun with an accuracy of 10 arcsec and the payload module is designed as a rigid lightweight structure in order to provide accurate mutual alignment between the various scientific instruments. The mission is planned to last 2 years.

(a) The solar interior will be studied by SOHO by means of the following instruments:

1. High resolution spectrometer (HRS)
2. Solar oscillation imager (SOI)
3. Solar irradiance monitor (SIM)

The first two instruments permit to probe the solar interior by seismological techniques. These consist in the observation of the oscillations of the entire Sun through their photospheric effect. The quantity observed is the periodic wavelength shift of a photospheric spectral line, which is measured by comparing the signals from a double pass band obtained by the Zeeman effect from the resonance absorption line of a vapour. The observations of the oscillations of the global Sun (HRS) give information on the solar core, while two dimensional observations (SOI) should permit the identification of oscillatory modes of intermediate spherical harmonic degree which give information on the intermediate solar layers.

With ground based instruments, oscillations with periods from several minutes to hours have been detected by these Doppler techniques. Most of these oscillations have velocity amplitudes as small as a few cm/sec or less. Observations from SOHO will be a considerable improvement over ground based observations because free from the noise due to the Earth atmosphere and rotation. Therefore photospheric oscillations with speeds of less than 1 mm/sec are expected to become observable, since the orbit properties include a sufficiently small motion towards or away from the Sun and the possibility of uninterrupted observation, to enhance the signal to noise ratio.

The third instrument (SIM) is devoted to the study of the time variations of the solar irradiance. It includes a high precision radiometer measuring the total solar irradiance and 5 photometers operating at different wavelengths, having a relative precision of 10^{-6}. It also includes a combination of two absolute radiometers which will achieve an absolute accuracy of better than 0.2% over the duration of the mission.

The Solar Maximum Mission has shown that the solar constant is in fact a varying quantity, and that its decreases are associated with the appearance of sunspot groups and may be explained by blocking of the output by the sunspots. Variations with longer time scales (for example associated to the solar cycle) are possible. The study of these variations would give information upon the dynamics of the convective zone and other internal solar layers.

(b) The instruments proposed for SOHO for the study of the solar chromosphere, transition region and low corona are the following:

	Wavelength range (A)	Spectral res. (mA)	Spatial res. (arcsec)
4. Grazing incidence spectrometer (GIS)	65-500	40	1
	138-998	65	
	514-1277	65	
	719-1750	100	
5. Normal incidence spectrometer (NIS)	584-625	14	1
	770-835	14	
	900-1300	10	
6. EUV imaging telescopes (EIT) (2)	284(FeXV),304(HeII)		10
7. Soft X-ray telescope	2-100		1,5

These instruments would permit the study of the solar atmosphere with continuous observations and long term coverage, as required by the evolving phenomena. It would be possible not only to study the geometry of the features, but also to determine the physical parameters in all the layers from the chromosphere to the low corona with high spatial resolution. Electron density and temperature can be obained by looking at the density and temperature sensitive line ratios; hence the emission measure can be deduced, and thus the ion abundance by the line total intensity, if the geometry of the emitting region is known by means of the scanning capability of the spectrometers and from the images provided by the EUV and soft X-ray telescopes. Temperature and emission measure can also be obtained from the X-ray telescope, the former by comparing the continuous emission in different spectral regions, the latter from the temperature and the absolute emission.

Beyond having the capability of determining these physical parameters, SOHO has also that of measuring the velocity field, by means of the normal incidence spectrometer, with high sensitivity (3 km/sec at 1000 A). This is very important because it has become more and more evident, in recent years, that the solar chromosphere, transition region and corona are highly structured and have complicated velocity patterns. It is therefore essential, for the understanding of many basic problems, to take this character into account and thus to make continuous observations with high spatial resolution and velocity sensitivity in all the layers from the chromosphere to the low corona. Other important information that can be

provided by the normal incidence spectrometer concerns the turbulent motions, since line profiles can be measured, given the spectral resolution of this instrument.

(c) The study of the outer solar atmosphere by SOHO continues at higher levels by means of the following two instruments:

	Wavelength range (A)	Spectral res. (mA)	Spatial res. (arcsec)
8. UV coronal spectrometer (UVCS)	1216(Ly α),1025(Lyβ) 1032, 1037 (OVI)	80	10-60
9. White-light coronagraph (WLC)	w.l. plus selected spectral regions		48

Recent rocket observations with a combination of coronal instruments similar to those which are planned for SOHO have shown that density, temperature and outflow speed can be determined by the observation of the white light intensity, the Ly-alpha intensity and profile and by the intensity of the OVI doublet at 1032 and 1037 A. Furthermore the Hanle effect method of magnetic field diagnostics would permit the determination of the magnetic field in some (higher field) coronal regions. Since, at present, the Doppler dimming technique, employed by SOHO, appears to be the only technique that can be used to determine the coronal outflow speed in the heliocentric distance range 1.2-5 solar radii, and since, furthermore, determinations of physical parameters above 1.4 solar radii are very scanty, except for the electron density, the importance of SOHO observations of this region is evident.

The main interest appears at this moment to lie in the determination of the outflow speed, temperature and density in the coronal holes, i.e. in the regions where the high speed wind originates. The height interval studied by SOHO will be particularly important because there the wind suffers its main acceleration. The determination of the physical parameters, as a function of the heliocentric distance, would be a powerful constraint on solar wind models, capable of strong information on the mechanisms of deposition of energy and momentum in the wind.

Besides strongly increasing our knowledge of these solar regions, also the knowledge of the regions of slow outflow--the streamers--can be greatly enhanced by the determination of density, temperature and magnetic field by the SOHO instruments.

(d) The SOHO instruments are also intended to continue the study of the solar wind at a much higher heliocentric distance by probing the interplanetary plasma with in situ measurements. These will add the necessary constraints to solar wind models. The instruments devised to this aim in the model payload will only be quoted here: 10. Solar wind analyzer; 11. Suprathermal particle analyzer; 12. Energetic particle analyzer; 13. Magnetometer; 14. Plasma wave analyzer.

REFERENCES

See the ESA publication SCI (83) 3, September 1983.

ATOMIC DATA IN ASTROPHYSICS

N.G. Bochkarev
Sternberg State Astronomical Institute, Moscow, USSR

Abstract

A short review of the atomic and molecular data which are necessary for astrophysics researches is presented. A list of atomic data is described which was chosen by first Soviet colloquiuum on atomic data in astrophysics.

Introduction

Almost all information is gotten by astrophysicists form observed electromagnetic radiation. More part of observed objects is plasma formations which are strongly different in their characteristics. Radiation reaching observers is usually emitted by relatively low-density outer layers of cosmical bodies. Physical conditions in the places of emission are usually far from thermodynamical equilibrium. Therefore for quantitative analysis of spectra of cosmical objects it is necessary very often to use analysis based upon detailed balance of atomic and molecular processes in plasma. Thus, atomic data are the foundation without which astrophysical researches are practially impossible.

Modern astrophysics covers all wavelengths. There are observations of radiations with differences of wavelength by the factor 10^{20}, from many kilometric radio waves to gamma-photons with energy 10^{12}–10^{14} eV. On continuum spectrum there are spectral lines. The longest wavelength line has $\lambda \approx 18$m and is transition on the level with number 732 in atomic hydrogen or carbon (Konovalenko and Sodin, 1981). The shortest wavelength lines are located in gamma-range and are radiated by excited atomic nuclei.

The principal structure unit of the Universe is stars. They radiate most of the energy in near IR, optical and UV ranges. These ranges are the most informative. Most observations are in these ranges. It is possible to get information about matter with low temperature ($T \approx 5$–300 K mainly in far IR and radio radiation, and about the most hot objects ($T > 10^6$K) by use of X-rays. Cold parts of matter are practically neutral and consist mainly of molecules, dust grains and atoms. Hot parts contain ions with charges until approximately 30 (see, e.g., Gibson, 1973).

Thus in modern astrophysical researches it is necessary to have data on elementary processes with atoms, molecules, atomic and molecular ions and sometime with solid bodies (dust grains).

Atoms and Atomic Ions

Atoms and ions of different elements play different roles in astrophysics which are connected with the different abundances of elements in space. Chemical composition of atmospheres of most stars and other astrophysical objects is almost universal (Aller, 1961). The most abundant are atoms of H and He (90% and 10% in quantity of atoms). Among others the most abundant are atoms from C to Fe with even-even nuclei (abundance on 3–5 decades less than H). Together with atoms H and He they form physical conditions in cosmical plasma. Therefore it is necessary to have the most full and various data on them. Other isotopes and atoms are present in small quantities (10^{-6}–10^{-14} relatively H). Nevertheless they give very interesting information on nuclear evolution of matter and therefore they are intensively studied.

In several groups of objects strong deviations from "standard cosmical" chemical and isotop abundance are observed, up to 3–5 orders of magnitude in both directions (higher or lower abundance). Peculiar Ap-stars show, e.g., overabundance of rare earth elements on factor 10^{3}–5 (Pikel'ner, Kokhlova,

1972). In the interstellar medium strong depletion of elements was found (Spitzer and Jenkins, 1975). Therefore quantitative chemical and isotope analysis continues to be an important astrophysical problem.

Stars. In spite of faint brightness of stars it is possible now to get very detailed spectra: in the range of hundreds or thousands angstrom spectrum resolution can reach ~0.3-0.03Å. In such spectra there are thousands of spectral lines. For some of the lines it is possible to get forms of contours. Stars with different temperature and chemical composition of atmospheres have different lines.

In stellar spectra, lines of all elements were found, including radioactive elements such as techecium. For th determination of abundances typically several dozen lines of each ion of each element (mainly I-VI ionizations) are necessary. Therefore for quantitative analysis of the spectrums it is necessary to have a lot of spectrosopic data: energy levels, wavelengths and oscialltor strengths for hundereds, thousands or millions of lines. Kurucz (1971, 1981) calculates, e.g., the catalog of oscillator strengths for several million lines. But this catalog needs to be revised because in a number of cases strong lines are missed.

For detailed analysis it is necessary to know data on collision broadening lines (particulary for rare earths), and data on collisonal and radiative processes, which determine populations of levels and ionization in condition of stellar atmospheres (mainly $T=(2-50)10^3$K, $N=10^{11}-10^{16}$cm^{-3}, I-V ionizations; for white dwarfs N is higher and sometimes T can be higher).

Chomospheres, transition regions and coronae of sun and stars show higher temperature until 10^8K and full collection of ions until $z\approx30$. They radiate mainly in UV and X regions.

Parameters of ~10^5 spectrum lines including highly-ionized elements are necessary for calculations of opacity of stellar matter in inner parts of stars (Cox, 1965).

Stellar objects show often strong magnetic fields. The sun and other "ordinary" stars have magnetic fields from ~1 Gs to 5000 Gs, Ap-stars until 10^5Gs, white dwarfs up to 10^8Gs, and on neutron stars fields of $10^{11}-10^{13}$Gs. Therefore, it is necessary to have, also, data on magnetic field influence on atoms and ions.

Important mechanisms of opacities of stellar atmospheres are bf and ff processes with negative ions (H^-, He^-, sometimes C^- and several molecular negative ions, see, e.g., Gray, 1976). Data on formation and destruction in collision and radiative processes and on radiation of them are needed.

Diffuse mediums. In stellar atmospheres conditions are usually not far from local thermodynamic equilibrium (LTE). In more diffuse media, such as gas nebula, interplanetary, interstellar, intergalactical media, nuclei of galaxies and quasars, in circumstellar envelopes etc. conditions are usually far from LTE. Analysis of radiation of such objects demands calculations of level populations and ionization, taking into account a large variety of atomic processes. Physical conditions in such objects cover a wide range: T from 4-6 K to many billion K in shock waves, N from $< 10^{-6}$ cm^{-3} to $\geq 10^{12}$cm^{-3}. These media are pierced by cosmical and X-rays, which produce strongly non-equilibrium ionization with coexistence in one place I-VI ions and, probably, sometimes I-XII ions (Bochkarev, 1979).

At the first Soviet meeting on systematization of atomic data, which are necessary for astrophysical researches (Bochkarev, 1983) was suggested the next list of principal data, which are necessary for research on the physics

of rarified media in astrophysical objects.

The most important are data on the most abundant elements: H, He, C, N, O, Ne, Mg, Si, S, Fe, including all stages of ionization for them. Data about other observable I-VI ions of Na, Al, Ar, Ca, Ni are also necessary. For all these ions it is necessary to have data on radiative and dielectronic recombinations in a wide interval of temperatures (e.g. formation of neutral atoms for T< 10-100 K). Full rates of recombinations are needed, as for several ions with observed recombination spectra (H, He, CII, NII, OIII etc.) also data on recombination populations of individual levels. As a result of low density of cosmical plasmas there are important dielectronic recombinations not only through permitted levels but also through forbidden ones. In the last case, dependence of recombination coefficients on density is required.

There are important data on ionization of atoms and ions: photoionization of outer and inner electronic envelopes (photon energy $h\nu$< 10-30 KeV) and a number of cases of metastable levels; collisional ionization by thermal electrons of ground and the most important metastable levels; ionization of nonrelativistic particles of cosmic rays. Actual problem is collecting data on charge-transfer reactions II-XII ions of C-Fe with HI for kT< 2eV, with HeI for kT<3-5 TeV and with HeII for kT<10-15 TeV.

It is necessary to have information on excitation of thin structure of main terms of atoms and several ions (e.g. CII, OIII, SiII, SII, FeII) by collisions of electrons, protons, atoms and molecules of hydrogen ($T=10-10^4$ K), data on collisional excitations of low terms of atoms and ions without variations of main quantum number n and for a number of ions for collisional excitation with variation of n for several low levels, which are not hydrogen like. Developing of observational technics in millimeter range demands more accurate data on energetic splintering of ground levels of atoms and above mentioned ions.

For collision processes it is necessary to have dependencies of cross-sections on energy and rates of the processes as functions of temperature.

Finally, it is necessary to have Einstein coefficients of one-electron transitions between above metnioned levels and terms, including forbidden, (intercombinational etc.) transitions, and also probabilities of non-radiative filling of vacancies in inner envelopes of atoms and ions (Auger effect), including cascades of transitions in inner envelopes.

Total data bank, discussed in this section, must consist of several thousand numbers and functions of energy and temperature. Above mentioned meeting states that it would be very likely to complete such bank of date.

Moleculars and dust grains

At present about 100 different molecules and molecular ions have been found in spectra of astrophysical objects. They are found in atmospheres of planets and cold stars (T<6000 K), in comets, interstellar medium and circumstellar envelopes. For stellar spectra there are oxides and hydrides of metals. The main problem is identification of faint molecular bands in optical and UV ranges. In comets there are visible optical fluorescence of CH, CH^+, NH, OH, OH^+, CN, C_2, CO^+, N_2^+, NH_2, H_2O^+, C_3, CO_2^+ in solar radiation. Here it is important to know constants of fluorescence and photodestruction (ionization, dissociation) of the molecules. In planetary atmospheres there are visible numerous IR bands of CO, N_2, O_2, HF, HCl, H_2O, DOH, CO, SO_2, HCN, NH_3, PH_3, CH_4, C_2H_2, C_2H_6, which are formed in a medium where T is hundreds of Kelvins and pressure from 10^{-3} atm. and higher.

The greatest quantity and variety of molecules are observed in the interstellar medium and circumstellar envelopes, especially in the most cold

(T=5-30K) and dense ($N=10^3-10^7 cm^{-3}$) parts of them. To the end of 1982 approximately 60 molecules and molecular ions in ~100 isotopic variant were found (Rudnitsky, 1983): 15 two atomic, 15 three-atomic molecules and multi-atomic, consisting until 13 atoms ($HC_{11}N$). All molecules, excluding NaOH, consist of H, C, N, O, Si, S; about 2/3 of them have carbon, among them H_2CO, HCOOH, methil and ethyl-alcohol, dimetilether. Cyclical molecules are not found. A real problem is to search 6-10 atomic molecules, mainly organical (simplest amino acids of glycin type etc.).

Most molecules were found from radio spectra of radiation, mainly in millimeter range. It is rotational transitions with J< 20-40, and also thin effects (K- and Λ-splitting, inversional transitions etc.). For reliable identification of lines it is necessary to have an accuracy of frequencies no worse than 0.5-1 MHz mainly in ranges 22-23 GHz, 35-37 GHz, 88-90 GHz, 110-116 GHz for which receivers exist.

In the next 10 years the submillimeter range will become more familiar.

The most important collision processes are exitation mainly of rotational and vibrational levels by thermal electrons, H, H_2 and He for $T=10-10^3K$ for molecules with observed maser effect (OH, H_2O, SiO, CH_3OH, H_2CO) and also for H_2,H_2^+, CO, CS, NH_3, etc.

It is necessary also to have data on rates of chemical reactions in low density and cold ($T=10-10^3K$) media, both on gas-phase reactions (mainly ion-molecular, including reactions of isotopic fractions) and on surfaces of dust grains (probability of absorption and desorption, interaction between molecules on the surface, desorption as the result of chemical reaction etc.). Knowledge of properties of dust grains, which is poor now, must be improved (Huffman, 1977; Martin 1978).

It is necessary to know optical and spectral properties of dust grains of different sizes from 0.005 to 5-10 μm in UV, optical and IR ranges, for grains with a large quantity defects of structure, admixtures and for heteogeneous grains (see Huffman 1977, Martin 1978).

References

Aller L.H., 1961, The abundance of the elements, New York, Int.

Bochkarev N.G., 1979, Issled. Geomagn. Aéron. Fiz. Solntsa (Moscow), No. 48, 195; Sov. Astron. Lett; 6, 160, 1980.

Bochkarev N.G., 1983, Sov. Astron., 27, No.6.

Cox A.N. 1965, in Stars and Stellar Systems, v.8, eds L.H. Aller, D.B. McLaughlin, Chicago: Univ. of Chicago Press.

Gibson E.G., 1973, The quiet Sun., NASA SP-303.

Gray D.F., 1976, The observation and analysis of stellar photospheres, New York, Wiley and Sons.

Huffman D.R., 1977, Adv. Phys, 26, 129.

Konovalenko A.A., Sodin L.G., 1981, Sov. Astron. Lett., 7,

Kurucz R.L., 1971, Spec. Rep. SAO No. 306-308.

Kurucz R.L., 1981, Spec. Rep. SAO No. 390.

Martin P.G., 1978, Cosmic dust. Its impact on astronomy, Clarendon, Oxford.

Pikel'ner S.B., Khokhlova V.L., 1972, Uspekhi, fiz. nauk., 107, 389 (Sov. Phys. Usp.)

Rudnitskij G.M., 1983, Molecules in Astrophysics, Ser. Cosmical Researches 20, Moscow, VINITI.

Spitzer L., Jenkins E., 1975, Ann. Rev. Astron. Astrophys. 13, 133.

MEASUREMENT OF THE A-VALUE OF THE $3s^2\ {}^1S_0$ -- $3s3p\ {}^3P^o_1$ INTERSYSTEM TRANSITION IN Al II AT 2670 Å: A PROGRESS REPORT

B. Carol Johnson and H.S. Kwong[1]
Harvard-Smithsonian Center for Astrophysics
60 Garden Street
Cambridge, MA 02138

INTRODUCTION

Ratios of intensities of spectral lines produced in the radiative decay of collisionally-excited levels of atomic ions are versatile indicators of electron density in astrophysical plasmas when one of the lines involves a metastable level (see the review by Feldman 1981 and references therein). Radiative transition probabilities (A-values) and electron excitation cross sections are necessary for accurate, quantitative analyses of these plasmas. The work reported here is part of a program of measurements of astrophysically interesting A-values and radiative lifetimes (see the review by Smith et al. 1984); until we began, such anaylyses of astrophysical plasmas depended upon unconfirmed calculated A-values.

Here we report preliminary laboratory study of the intersystem line at 2670 Å in Al II. This line is seen in pre-main sequence stars and symbiotic stars. Brown, de M. Ferraz, and Jordan (1984) observed the Al II] line in T Tauri and included the line in their derivation of the emission measure distribution. They predict line ratios involving Al II] and resonance lines will be density sensitive for $n_e \geq 10^{11}$ cm^{-3}. Recent calculations of the A-value for the $3s^2\ {}^1S_0$ -- $3s3p\ {}^3P^o_1$ transition in Al^+ are 2680±50% s^{-1} and 3450 s^{-1} by Cowan, Hobbs, and York (1982) and Laughlin and Victor (1979), respectively.

EXPERIMENTAL METHOD

In our measurements, radiative lifetimes are determined by monitoring the time dependence of the radiative decay from metastable ions stored in a cylindrical, radio frequency (rf) ion trap. In previous work (see, for example, Johnson, Smith, and Knight 1984 or Kwong et al. 1983), metastable ions were created by electron bombardment on source gases. In this measurement, Al^+ ions are produced in a laser plasma, generated by focussing the output of a Q-switched Nd:YAG laser onto a target mounted on the ring electrode of the rf ion trap. Knight (1981) demonstrated that singly charged metal ions produced using this technique were stored in an electrostatic ion trap.

The components of the experiment are indicted in Figure 1 and a timing diagram detailing the sequence of events for each laser pulse is given in Figure 2. The Nd:YAG laser is operated at 10 Hz. The 1.06 μ

---

1. Permanent Address: Department of Physics, University of Nevada, Las Vegas, 4505 Maryland Parkway, Las Vegas, NV 89154.

laser output is focussed, by a lens external to the vacuum system, onto an Al target after passing through the ion trap. The laser power delivered to the target area of ~ 2×10^{-4} cm^2 in the ~ 10 ns wide pulse is 1.0 to 2.5 MW. The threshold for plasma production is observed at a power density of ~ 3 $GWcm^{-2}$.

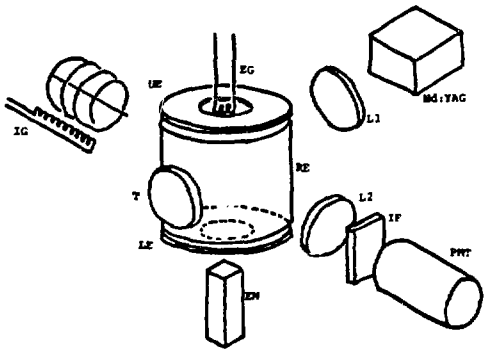

FIGURE 1. Schematic of the experiment. EG = electron gun, Nd:YAG = laser, L1 = lens to focus laser output onto target, T = target, IG = nude ionization gauge, UE = upper electrode, RE = ring electrode, LE = lower electrode, L2 = lens to focus stored ion fluorescence onto PMT, IF = interference filter, PMT = photomultiplier tube, EM = electron multiplier.

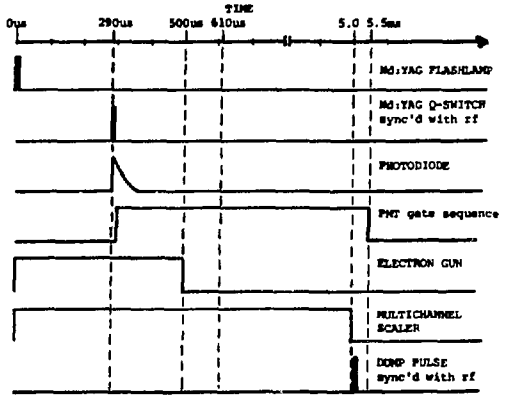

FIGURE 2. Timing sequence for each laser shot. The sequence repeats at 10 Hz. The gain on the PMT becomes constant at the location marked 610 μs.

The plasma is monitored by observing the voltage generated by the collector current of a nude ionization gauge. The temporal behavior of the neutral and ionized component of the plasma is estimated from these data. The plasma-produced stored ions are monitored by "dumping" the ions out of the trap onto an electron multiplier.

Emission from the Al plasma is studied using a 0.3 m scanning monochromator with a RCA 1P28 photomultiplier tube on the exit slit; a prism spectrograph and spectroscopic plates; or a 1P28 photomultiplier tube. For radiative lifetime measurements, (in Al II this corresponds to a measurement of the A-value for the $3s^2\ ^1S_0$ -- $3s3p\ ^3P^o_1$ transition, since there is only one decay channel for the $^3P_1$ level), fluorescence from trapped, metastable Al^+ is detected using a solar blind EMR 541Q-05M photomultiplier tube (PMT). A 55 Å FWHM filter centered on 2660 Å with 16 % transmission at 2670 Å limits the bandpass of the system.

Preliminary work indicates emission associated with the laser plasma is strong enough to damage the PMT. Therefore, the PMT is protected by gating the photocathode off during plasma production. Photon counts representing Al II 2670 Å fluorescence are time analyzed using a multichannel scaler with 10 μs resolution.

RESULTS

Temporal studies of the plasma using the ionization gauge indicate that the plasma velocity is approximately 10^6 cms^{-1}; the ions travel faster than the neutrals; and the vacuum system recovers to the base pressure of $1x10^{-8}$ Torr about 10 μs after plasma production. The plasma production efficiency, as determined by the resonance emission lines, the signal observed on the ionization gauge, and the stored ion signal, increases if the laser is focussed to a fresh target area by adjusting the lens external to the vacuum chamber approximately every 1000 laser shots. Spectroscopic studies of the plasma indicate that there is very little continuum from 2000 to 5000 Å. Resonance lines in Al I and Al II have been identified; the strongest emission occurs at 3082 and 3092 Å (the $3p\ ^2P^o$ -- $3d\ ^2D$ multiplet in Al I), 3586 Å (the $3d\ ^3D$ -- $4f\ ^3F^o$ multiplet in Al II), and 2632 Å (the $3p^2\ ^1D$ -- $4f\ ^1F^o$ multiplet in Al II). This latter emission passes through the bandpass filter that is used to isolate the Al II] 2760 Å fluorescence, however it is separated temporally from the intersystem fluorescence by the multichannel scaler.

Ions are trapped following plasma production. The threshold for the stored ion signal is coincident with the threshold for plasma production as determined from the ionization gauge signal. The charge-to-mass ratio of the stored ions inferred from the trap potentials (see Wineland, Itano, and Van Dyck 1983 for a discussion of the stability diagram for rf ion traps) and time-of-flight measurements on the stored ion signal indicates the ions are Al^+ and Al^{++}. Fluorescence within the bandpass of the detection system from stored ions is observed (see Figure 3). The fluorescence is not present if the trap is made to be unstable for storage of Al^+ ions while holding all other conditions fixed. The fluorescence seems to increase if the laser produced plasma is crossed with an electron beam of ~ 200 eV energy, ~ 50 μA current, and 500 μs duration. The data in Figure 3 give a decay rate that is consistent with calculations of the A-value of the intersystem transition in Al^+. However, the data are preliminary and it is premature to quote a measured decay rate.

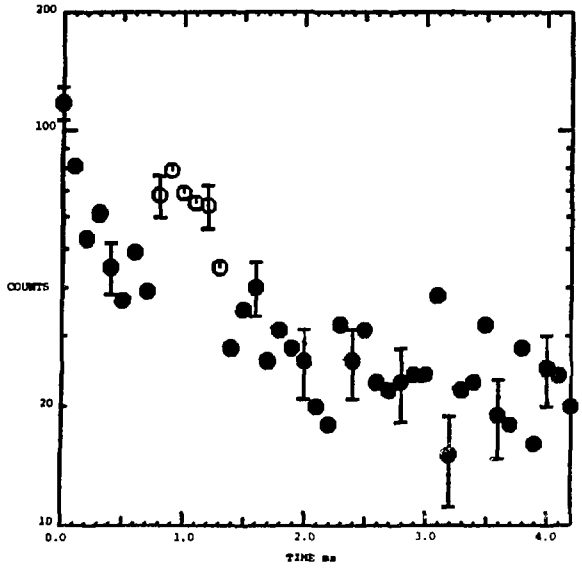

FIGURE 3. Time behavior of fluorescence observed for stored Al^+ ions. The data have been binned in 100 μs channels. Data plotted using open circles are contaminated by noise from the laser.

ACKNOWLEDGEMENTS

The authors thank Peter L. Smith for suggesting this measurement, and W.H. Parkinson for his advice and support. They also thank B.L. Cardon, L.D. Gardner, R.D. Knight, J. Kohl, G.P. Lafyatis, and K. Yoshino for their many useful suggestions concerning laboratory procedures. This work was supported in part by grants from NASA (NGL 22-007-006 and NSG-7304) and NSF (AST-82-17936) to Harvard College and by the Smithsonian Institution.

REFERENCES

Brown, A., de M. Ferraz, M.C., and Jordan, C. 1984, Mon. Not. R. astr. Soc., 207, 831.

Cowan, R.D., Hobbs, L.M., and York, D.G. 1982, Astrophys. J., 257, 373.

Feldman, U. 1981, Physica Scripta, 24, 681.

Johnson, B.C., Smith, P.L., and Knight, R.D. 1984, Astrophys. J., 281, 477.

Knight, R.D. 1981, Appl. Phys. Lett., 38, 221.

Kwong, H.S., Johnson, B.C., Smith, P.L., and Parkinson, W.H. 1983, Phys. Rev. A, 27, 3040.

Laughlin, C. and Victor, G.A. 1979, Astrophys. J., 234, 407.

Smith, P.L., Johnson, B.C., Kwong, H.S., Parkinson, W.H., and Knight, R.D. 1984, Physica Scripta, T8, 88.

Wineland, D.J., Itano, W.M., and Van Dyck, R.S. 1983, in Advances in Atomic and Molecular Physics, eds. D.R. Bates and B. Bederson (New York: Academic Press), 135.

PHOTODISSOCIATION OF NEUTRAL FREE RADICALS OF ASTROPHYSICAL INTEREST

L.D Gardner, M.M. Graff and J.L. Kohl
Harvard-Smithsonian Center for Astrophysics
Cambridge, MA 02138

The necessity for understanding molecular formation and destruction processes occurring in astrophysical environments is well known. Accurate molecular data are of critical importance in formulating models of such diverse regions as interstellar clouds and planetary and stellar atmospheres. With this in mind we have devised an experimental method and constructed an apparatus for the determination of cross sections as well as the kinetics for photodissociation processes in chemically unstable neutral molecules. Similar experimental methods have been independently developed by de Bruijn and co-workers and by Chen et al. (1).

A schematic of our apparatus is shown in Figure 1. We produce the negative ion of the species of interest in a discharge ion source. The ions are extracted and electrostatically accelerated to velocities greater than 10^7 cm/sec. To insure beam purity they are mass analyzed using a magnetic sector which also deflects them onto the primary axis of the apparatus, where they are subsequently collimated. The beam from a pulsed laser is also directed along this axis. The energy of the photons in this beam is chosen to be just sufficient to induce photodetachment of the negative ions, and the intensity is chosen to be high enough to induce the photodetachment of a very large fraction of the ions in the beam. The remaining negative ions are electrostatically swept out of the beam, and the now neutral molecular beam is allowed to pass into the next section of the apparatus. Here ultraviolet light from a second pulsed laser crosses the neutral beam at right angles. Absorption of photons from this laser causes photodissociation of some of the molecules. Part of the energy of the absorbed photon is converted into kinetic energy of the photofragments. The fragments therefore move away from each other and also from the axis as they continue their flight along the beam line. If the collimation angles are small enough, some of the fragments will leave the cone of the parent molecular beam and form a "halo" (not necessarily circular) around it. Since they are moving at high velocity, they may be detected with secondary electron multiplying devices such as channelplates. If the detection system records the fragment impact positions and arrival times relative to the firing of the dissociation laser, then individual fragment kinetic energies can be deduced and angular distributions determined.

We have carried out experiments on the photodissociation of excited states of H_2^+ in order to assess the performance of the apparatus (see Figure 2). Light from a flashlamp-pumped (rhodamine 6G) dye laser was directed along the beam axis, and it induced dissociation from states of vibrational quantum number $v' = 7$ and above. H^+ fragments were directed onto a channel electron multiplier and H fragments were allowed to strike a channelplate electron multiplier fitted with a coarse annular multianode array. The data we have obtained are shown in Figure 3. Note that the channeltron preferentially detects H^+ ejected along the beam axis, while the channelplate preferentially detects H ejected perpendicular to the

beam axis. The number of fragments ejected at a given angle to the axis (i.e., the angular distribution) is related to the laser beam polarization and to details of the initial and final quantum mechanical states (2). For this experiment large angles are expected (3) and observed.

Experiments on the astrophysically important free radical CH have been initiated. The C $^2\Sigma^+$ state can be excited from the X $^2\Pi$ ground state with 3140 Å light from a frequency doubled dye laser. It is inferred from spectroscopic evidence (4) that all vibrational-rotational substates of this electronic state predissociate, and this resonant process is considered to be the primary photodestruction mechanism for interstellar CH (5). We intend to study this predissociation by observing directly the H fragments. The apparatus can also be used to study the dissociation of CH through higher lying repulsive Σ and Π states and the dissociation of OH through predissociating substrates of the A $^2\Sigma^+$ state (6) and through the repulsive 1 $^2\Sigma^-$ state (7). This last process is expected to be a major loss mechanism for interstellar OH (7).

This work was supported by the Office of Naval Research under Contract N00014-84-K-0134 and the Smithsonian Institution through its Scholarly Studies and Postdoctoral Fellowship Programs.

REFERENCES

1. D.P. de Bruijn and J. Los, Rev. Sci. Ins. 53, 1020 (1982); H. Helm, D.P. de Bruijn and J. Los, post deadline paper at the Annual Meeting of the Division of Electron and Atomic Physics of the American Physical Society, Storrs, CT, May 30-June 1, 1984; Y.S. Chen, J.H. Newman, K.A. Smith, and R.F. Stebbings, Bull. Am. Phys. Soc. 29, 801 (1984).

2. R.N. Zare, Ph.D. thesis, Harvard University, 1964.

3. G.H. Dunn, Phys. Rev. 172, 1 (1968); M. Tadjeddine and G. Parlant, Molec. Phys. 33, 1797 (1977).

4. J. Hinze, G.C. Lie, and B. Liu, Ap. J. 196, 621 (1975); J. Brzozowski, P. Bunker, N. Elander, and P. Erman, Ap. J. 207, 414 (1976).

5. A. Dalgarno, in Atomic Processes and Applications, P.G. Burke and B.L. Moiseiwitsch, eds. (North-Holland Publishing Company, 1976) p. 109, and references therein.

6. J.Czarny, P. Felenbok, and H. Lefebvre-Brion, J. Phys. B 4, 124 (1971)

7. E.F. van Dishoeck and A. Dalgarno, J. Chem. Phys. 79, 873 (1983).

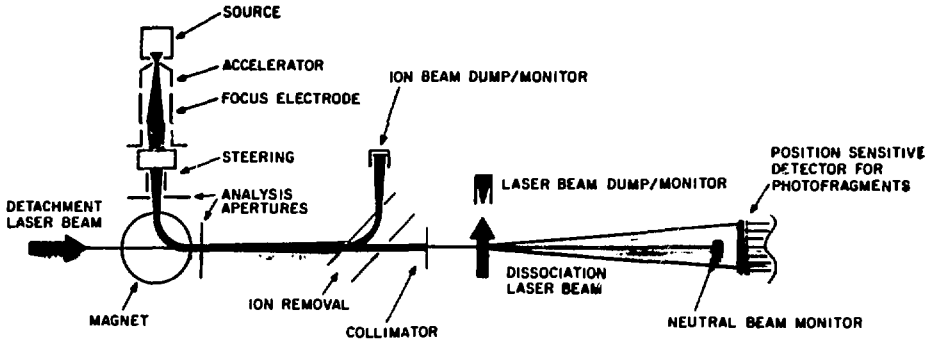

Figure 1. Schematic of Apparatus.

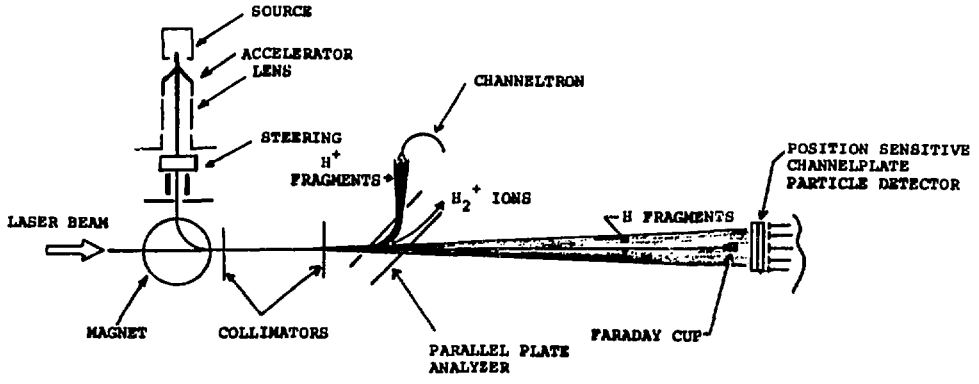

Figure 2. Schematic of Apparatus as Used for H_2^+ Photodissociation Experiment.

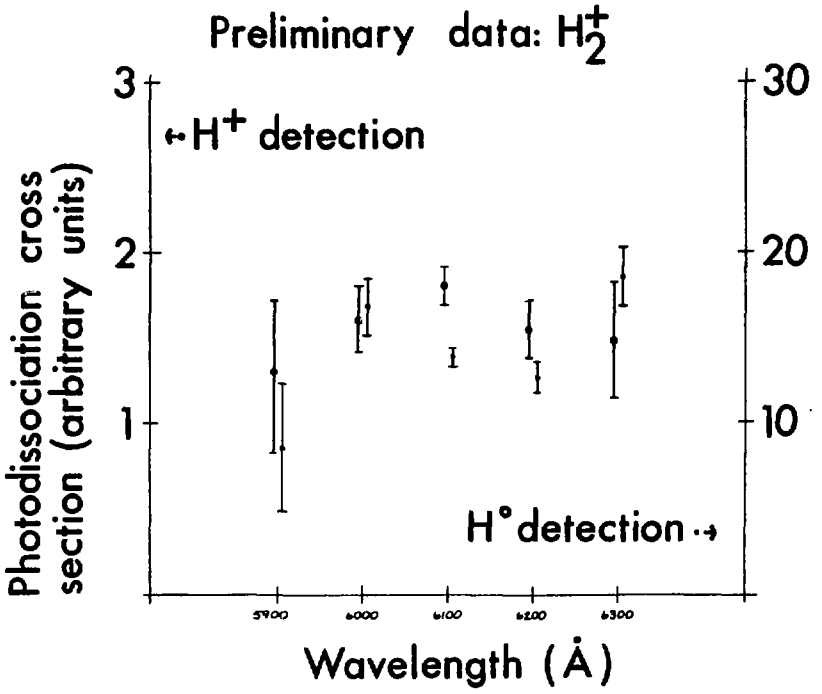

Figure 3. Preliminary Data for H_2^+ Photodissociaton Experiment

TIME-RESOLVED SPECTRA IN THE 5-330 Å REGION EMITTED FROM THE PLT AND TFTR TOKAMAK PLASMAS*

J.L. Schwob,† A.W. Wouters, S. Suckewer, F.P. Boody
Plasma Physics Laboratory, Princeton University
Princeton, N.J. 08544
and M. Finkenthal
Racah Institute of Physics, Hebrew University
91904 Jerusalem, Israel

1. INTRODUCTION

The analysis of impurity radiation from Tokamak plasmas is one of the most important diagnostics, allowing the measurement of the impurity concentrations, radiation losses and particle transport studies. This study requires simultaneous time-resolved observation of spectral lines from many ionization states for each element. The most intense and important lines are the He and H-like resonance transitions of Oxygen and Carbon and $\Delta n = 0, 1$ transitions of highly ionized metallic impurities. These emmissions have been recorded on PLT and TFTR tokamaks by means of a soft X-ray multichannel spectrometer (SOXMOS).

2. SOFT X-RAY MULTICHANNEL SPECTROMETER

The basic instrument is a high resolution, interferometrically adjusted, 2m extreme grazing incidence (between 89.3° and 87.5°) duochromator, built by Schwob and Fraenkel at the Hebrew University of Jerusalem (Filler et al. 1977). It is equipped with two interchangeable gratings: 2400 l/mm and 600 l/mm. With the less dispersive grating used in the present work, the instrument covers the 5-330 Å spectral range. In the multichannel version (Schwob et al. 1983) one of the 2 channel electron multipliers is replaced by a 50mm long, funneled MgF_2 coated microchannel plate (MCP). This detector is interferometrically adjusted and can be moved along the Rowland Circle. The MCP is associated with a phosphor screen image intensifier and coupled by a flexible fiber optic conduit to a 1024-element photodiode array. The photodiode array is controlled and read out via an optical multichannel analyzer. The instrument offers a simultaneous coverage of 20 Å at short wavelength (Al XIII lines at 7 Å were clearly observed) and 70 Å at the long wavelength limit. A high spectral resolution: 0.12 Å FWHM at 20 Å, with a low background over the whole range covered, has been achieved. This allows a good line separation and accurate line brightness measurements.

3. IDENTIFICATION OF Ag XXIX-XXXIV LINES IN THE 50-80 Å RANGE

Silver has been introduced in the PLT tokamak plasma by a laser blow off technique (Marmar et al. 1975). The target plasma parameters were $n_e(o) \sim 3.10^{13}$ cm^{-3} and $T_e(o) \sim 2.5$ keV, and the particle injection occurred during the steady-state phase of the

*Work supported by U.S. DOE Contract No. DE-AC02-76-CHO-3073.
†Permanent address: Hebrew University of Jerusalem, Israel.

ohmically heated tokamak discharge. Spectra emitted by silver ions belonging to NiI-NaI like sequences have been recorded between 25-150 Å. The present work discusses only the 50-80 Å range where a very large number of lines originating from $3p^6 3d^k$ - $3p^5 3d^{k+1}$ and $3p^k$ - $3p^{k-1} 3d$ transitions are emitted within many ionization states.

The brightest lines in this domain are classified in the present work (Fig. 1). They belong to KI, ArI, ClI, and SiI like ions. These ions have relatively simple ground configurations and the number of high intensity lines emitted within transitions between the low lying excited levels and the ground state is small. Identifications are based on comparison of the experimental data with extrapolated energy level values along the isoelectronic sequences from Z = 20 to Z = 42 elements (Stratton et al. 1983, Finkenthal et al. 1984). It is important to mention that in tokamak spectroscopic experiments the assignment of a line to a given ionization state can be inferred from its time behavior and the radial position of the emitting ion in the plasma.

4. FIRST SPECTROSCOPIC OBSERVATIONS ON THE TFTR TOKAMAK

The Tokamak Fusion Test Reactor (TFTR) in Princeton is (together with the JET in Europe) the largest operating tokamak. The plasma diameter is varying from 82 to 166 cm, plasma currents of 1-1.4 MA and discharge duration of about 4 seconds were obtained. The chord integrated electron density is $1-3 \times 10^{13}$ cm^{-3} and central electron and ion temperatures, without auxiliary heating, are 2-3 keV.

Understanding the origin and the behavior of the impurities in this experiment is of paramount importance for its success. A few examples of spectroscopic analysis of the TFTR plasma behavior are presented. The HeI and HI like carbon (introduced from the limiter) and oxygen emission from TFTR has been compared with that of PLT, using the SOXMOS spectrometer. Preliminary results show that the carbon/oxygen concentration ratio inferred from these spectra appears to be similar in the two devices at intermediate densities for TFTR and typically 2:1.

A very interesting example of the importance of spectroscopic observation is illustrated in Fig. 2. In some discharges, during the plasma current ramping phase a very high bolometric signal indicated large radiation losses accompanied by an electron temperature drop. A few such discharges were ended by disruptions. Analysis of spectra recorded by SOXMOS between 25-150 Å showed that a large amount of Zirconium was entering the plasma and radiating strongly as Zr XVI to Zr XXX ions. The time history of the Zirconium emission as presented in Fig. 2 agrees with the bolometer signal, indicating that the strong increase of radiation losses was due to a Zirconium influx. Zirconium has been introduced when the plasma interacted with the Al-Zr gettering system.

The impurity radiation has been studied at two plasma current values as a function of the electron density. Data show that the emission from metallic impurities (Ni and Fe) is decreasing as the gas density increases while Oxygen radiation is enhanced. This correlation between high Z and low Z impurity behavior, which is quite a general feature related to plasma density limits and disruptions will be discussed.

REFERENCES

Filler, A. S., Schwob, J. L., and Fraenkel, B. S. 1977, Proc. 5th Int. Conf. on VUV Radiation Physics, M.C. Castex, M. Pouey, and N. Pouey, Editors, CNRS Paris, Vol. 3, 86.

Finkenthal, M., Stratton, B. C., Moos, H. W., Hodge, W. L. Mandelbaum, P., Klapisch M., and Cohen, S. 1984, to be published

Marmar, E., Cecchi, J., and Cohen, S. 1975, Rev. Sci. Instrum., 46, 1149.

Schwob, J. L., Wouters, A., Suckewer, S., and Finkenthal, M. 1983, Bull. Am. Phys. Soc., 28, 1252.

Stratton, B. C., Hodge, W. L., Moos, H. W., Schwob, J. L., Suckewer, S., Finkenthal, M., and Cohen, S. 1983, J. Opt. Soc. Am., 73, 877.

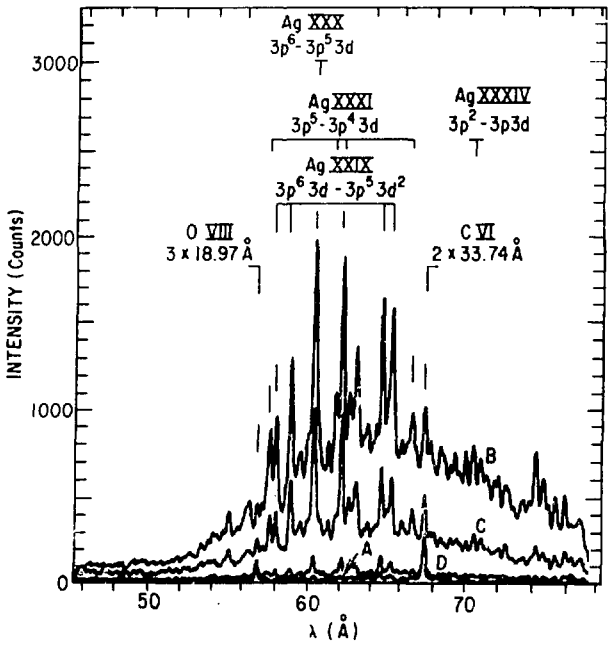

FIG. 1. Spectra from PLT, around 60 Å, showing the silver emission decay after injection:
A. before Ag injection t = 400 ms
B. after Ag injection t = 480 ms
C. at t = 560 ms
D. at t = 640 ms.

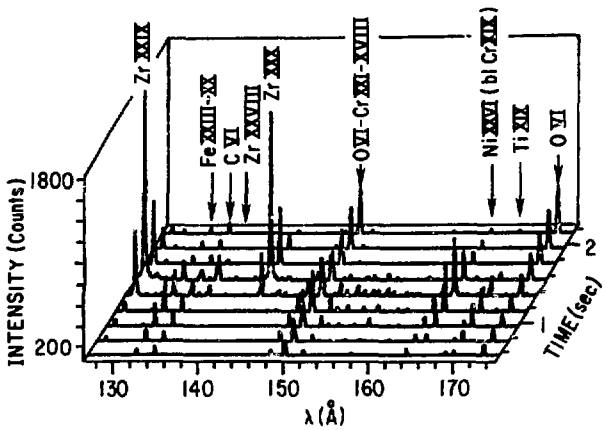

FIG. 2. (a) Time-resolved spectra from TFTR showing Zirconium emission due to plasma-getter interaction.

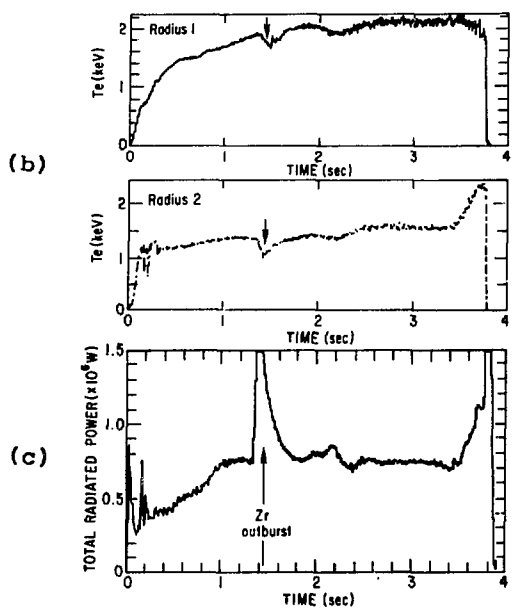

FIG. 2. (b) Electron temperature time histories (at different radii) in TFTR (courtesy of P. Efthimion and G. Taylor), and (c) bolometric signal (courtesy of J. Schivell) showing Zirconium outburst.

RELATIVE INTENSITIES OF LINES IN F I- B I-LIKE Ti, Cr, Fe, Ni, and Ge: A COMPARISON OF THEORY AND EXPERIMENT

B.C. Stratton and H.W. Moos
Department of Physics and Astronomy
Johns Hopkins University
Baltimore, Maryland

U. Feldman and J.F. Seely
E.O. Hulburt Center for Space Research
Naval Research Laboratory
Washington, D.C.

S. Suckewer
Plasma Physics Laboratory
Princeton University
Princeton, N.J.

M. Finkenthal
Racah Institute of Physics
Hebrew University
Jerusalem, Israel

INTRODUCTION

Allowed $2s^2 2p^k - 2s2p^{k+1}$ transitions in the F I- B I-like ions of elements with $Z \geq 20$ are often observed in spectra of high-temperature ($T_e \geq 10^7$ K) laboratory and astrophysical plasmas. Calculations of level populations in these ions are important in the interpretation of measured intensities of these lines for plasma diagnostics. Impurity ion densities and radiated power losses in tokamak plasmas, and the emission measure of astrophysical sources, can be derived from spectroscopic measurements using level population calculations. Certain line-intensity ratios can be used to measure the electron density in astrophysical plasmas; this technique may also be useful in some low-density laboratory plasmas. It is therefore important to experimentally check the level populations in high-Z ions using spectra from a well-diagnosed laboratory plasma, such as that of a tokamak. This has been previously done only for some transitions in Fe XVIII - Fe XXII (Suckewer and Hinnov 1979).

In the present work, measured relative intensities of many allowed $2s^2 2p^k - 2s2p^{k+1}$ transitions (60-200 Å) in the F I- B I-like ions of Ti, Cr, Fe, Ni, and Ge are compared with values from level population calculations (Bhatia, Feldman, and Doschek 1980; Feldman et al. 1980; Feldman, Seely, and Bhatia 1984). Spectra of all the elements were obtained from Princeton Large Torus (PLT) tokamak plasmas with line average electron densities ($\bar{n}_e$) near 2.5×10^{13} cm^{-3}; for Ti and Cr, spectra were also obtained at $\bar{n}_e \cong 5 \times 10^{12}$ cm^{-3}. Comparison of PLT iron spectra at $\bar{n}_e = 5 \times 10^{12}$ cm^{-3} and $\bar{n}_e = 3.5 \times 10^{13}$ cm^{-3} demonstrates that certain line-intensity ratios can be reliably used for density diagnostics. These spectra strongly resemble published spectra of high-temperature regions of solar flares.

The measurements were made with a grazing incidence time-resolving spectrograph (Hodge, Stratton, and Moos 1984) which covers the 15-360-Å region with 0.7-Å resolution. The spectrograph was absolutely calibrated from 60 to 360 Å using synchrotron radiation from the National Bureau of Standards SURF II facility. The measured relative intensities are therefore reliable. This was confirmed by comparison of 12 measured and calculated branching ratios: 10 of the measured ratios agreed with the calculations within 30%. Thus, the accuracy of the measurements is taken to be 30%. Small amounts of the impurity elements were introduced into the current plateau periods of ohmically-heated deuterium plasmas using the laser-blowoff technique.

RELATIVE INTENSITIES OF Ti, Cr, Fe, Ni, and Ge LINES

The peak brightness of each line was measured and converted to a relative intensity by taking its ratio with the brightness of a line due to a transition observed in all five elements. Of the 58 lines observed at $\bar{n}_e \cong 2.5 \times 10^{13}$ cm^{-3}, the measured relative intensities of 47 agree with the predicted values within 30%. In most cases, the exceptions can be reasonably attributed to problems with the measurements, such as blended lines. Thus, it appears that the level population calculations at this density can be used with some confidence for plasma diagnostics. In the C I-like ions, there is evidence that proton collisional excitation and de-excitation between the levels of the ground configuration should be included in the calculations: the $2s^22p^2\ ^3P_2 - 2s2p^3\ ^3D_3/2s^22p^2\ ^3P_0 - 2s2p^3\ ^3D_1$ intensity ratios calculated including proton collisions are in better agreement with the measurements in Fe XXI, Ni XXIII, and Ge XXVII than the values calculated not including proton collisions.

For Ti and Cr at $\bar{n}_e \cong 5 \times 10^{12}$ cm^{-3}, agreement between the measured and calculated relative intensities is not as good: the measured relative intensities of 16 out of 33 of the observed lines agree with the calculated values within 30%. Again, many of the exceptions can be traced to problems with the measurements. The remaining discrepancies are probably due to the fact that the low-density calculations do not include proton collisions. Calculations which include proton collisions are being performed and will be used to test this hypothesis.

COMPARISON OF TOKAMAK AND SOLAR-FLARE IRON SPECTRA

Fig. 1 shows PLT iron spectra in the 90-140 A region at $\bar{n}_e = 5 \times 10^{12}$ cm^{-3} and $\bar{n}_e = 3.5 \times 10^{13}$ cm^{-3} and a solar-flare spectrum of the same region obtained in 1969 by the Goddard Space Flight Center grating spectrometer on the OSO 5 satellite (Flare E in Kastner, Neupert, and Swartz 1974). The similarity between the tokamak and flare spectra is clear, especially in the low-density case, indicating that the density and temperature of the flare and low-density tokamak plasmas are approximately the same. (These tokamak spectra are discussed in detail in Stratton, Moos, and Finkenthal 1984).

In order to check the reliability of line-intensity ratios in Fe XIX - Fe XXII for density diagnostics, measured values of seven

density-dependent ratios were compared at both densities with values from level population calculations (Feldman et al. 1980; Bhatia and Mason 1980; Mason et al. 1979; Mason and Storey 1980). The ratios are Fe XIX 108.35 Å/119.98 Å, Fe XIX 108.35 Å/91.02 Å, Fe XX 121.83 Å/110.64 Å, Fe XXI 121.21 Å/128.73 Å, Fe XXI 102.22 Å/128.73 Å, Fe XXII 114.41 Å/117.17 Å, and Fe XXII 114.41 Å/135.78 Å. With the exception of the Fe XXII 114.41 Å/135.78 Å ratio at the low density, the measured and calculated values agree within 30%. Thus, these ratios can be reliably used to measure the density in solar flares, other astrophysical plasmas, and laboratory plasmas.

REFERENCES

Bhatia, A.K., Feldman, U., and Doschek, G.A. 1980, J. Appl. Phys., 51, 1464.

Bhatia, A.K., and Mason, H.E. 1980, Astr. Ap., 83, 380.

Feldman, U., Doschek, G.S., Cheng, C.C., and Bhatia, A.K. 1980, J. Appl. Phys., 51, 190.

Feldman U., Seely, J.F., and Bhatia, A.K. 1984, Atomic Data and Nuclear Data Tables, in press.

Hodge, W.L., Stratton, B.C., and Moos, H.W. 1984, Rev. Sci. Instr., 55, 16.

Kastner, S.O., Neupert, W.M., and Swartz, M. 1974, Ap. J., 191, 261.

Mason, H.E., Doschek, G.A., Feldman, U., and Bhatia, A.K. 1979, Astr. Ap., 73, 74.

Mason, H.E., and Storey, P.J. 1980, M.N.R.A.S., 191, 631.

Stratton, B.C., Moos, H.W., and Finkenthal, M. 1984, Ap. J. (Letters), 279, L31.

Suckewer, S., and Hinnov, E. 1979, Phys. Rev. A., 20, 578.

ACKNOWLEDGEMENTS

The authors would like to thank the PLT group, headed by J. Hosea, for supporting these measurements; S. Cohen, J. Timberlake, and T. Bennett for providing the impurity injection; and A.K. Bhatia of the Goddard Space Flight Center for useful discussions. This work was supported by Department of Energy Contract No. DE-AS02-76ET53006.

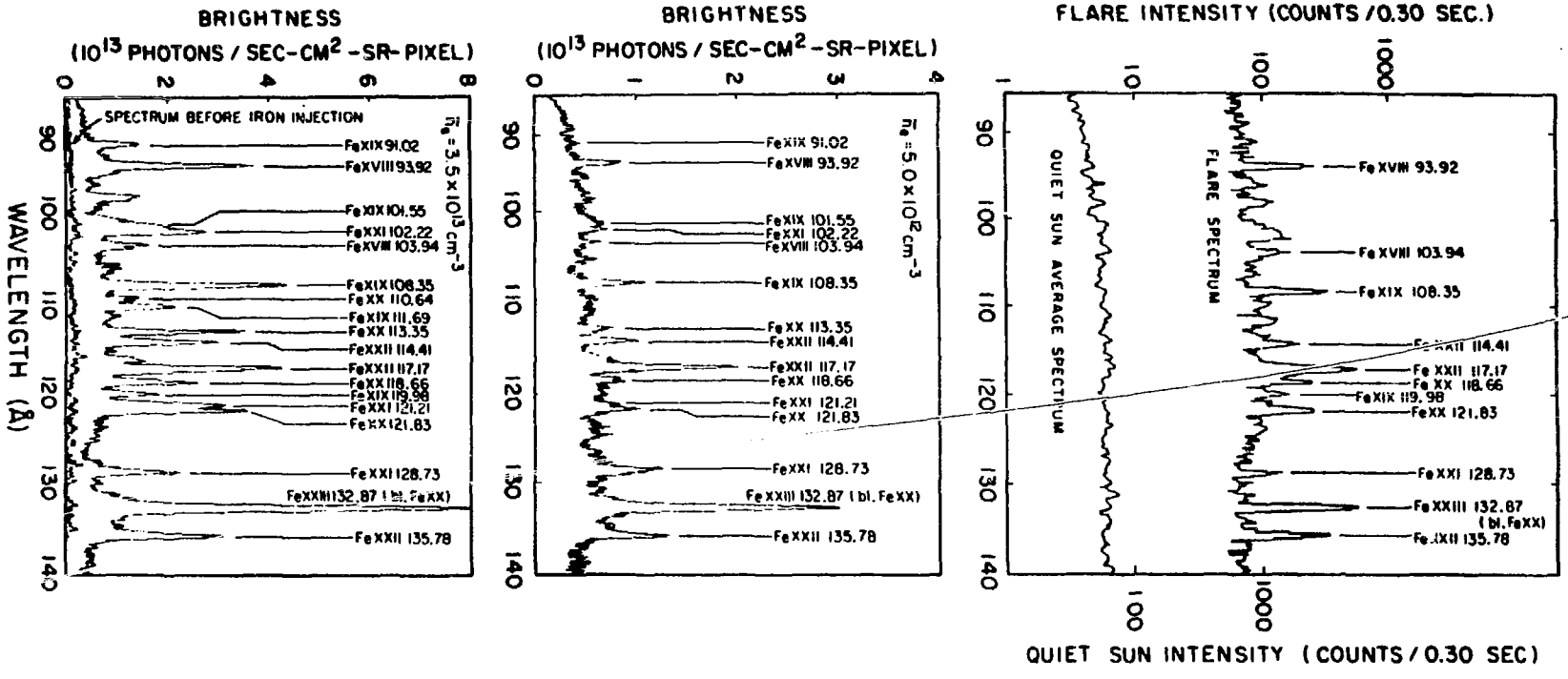

Fig. 1. Solar flare and quiet sun average spectra (upper). Tokamak spectra at $\bar{n}_e = 5 \times 10^{12}$ cm^{-3} (middle) and $\bar{n}_e = 3.5 \times 10^{13}$ cm^{-3} (lower). (From Stratton, Moos, and Finkenthal 1984).

MEASUREMENTS OF ABSOLUTE COLLISIONAL CROSS SECTIONS AT HARVARD-SMITHSONIAN CfA

J.L. Kohl, L.K. Deutsch, L.D. Gardner, G.P.Lafyatis and A.R. Young
Harvard-Smithsonian Center for Astrophysics
Cambridge, MA 02138

The major goal of this research program is to determine, experimentally, accurate absolute cross sections for dielectronic recombination (DR) in multiply and singly charged atomic ions. Our initial measurements of DR in C^{3+} are designed to provide a "bench mark" cross section for a simple atomic system. The experiment determines energy averaged DR cross sections for a well defined process involving a specific stabilizing transition. The fields in the region where dielectronic recombination occurs can be made small ($\lesssim$ 0.25 V/cm) in order to minimize the effect of Stark mixing which is expected to enhance the DR process [1]. We are presently adding the capability to apply known mixing fields up to 5 V/cm in the electron-ion interaction region of our apparatus.

Our experiment tests the basic theoretical formulation of the dielectronic recombination process, and it also virtually provides a separate test of the theoretical formulation of the enhancement as a function of the mixing field strength.

The field free dielectronic recombination process in C^{3+} that we are studying is illustrated in Figure 1 and in the following:

$$C^{3+}(2s) + e^- \rightarrow C^{2+}(2p,n\ell) \rightarrow \begin{cases} C^{2+}(2s,n\ell) + h\nu \\ \rightarrow C^{3+}(2s) + e^- \\ \rightarrow C^{2+}(2s^2) + \sum h\nu \end{cases}$$

where the incident electron excites the 2s electron and is captured in a high Rydberg state (HRS). Relaxation of the excited 2p core through emission of a satellite of the C^{3+}(2s - 2p) resonance line completes the dielectronic recombination process into the $C^{2+}(2s,n\ell)$ state. In the absence of external fields, this system would then relax to the $C^{2+}(2s^2)$ ground state through a cascade of radiative decays. However, external fields in the experiment can ionize $C^{2+}(2s,n\ell)$ yielding C^{3+} and a free electron.

The cross section itself exists as a series of narrow resonances which approach the threshold for electron impact excitation (EIE) of C^{3+}(2s - 2p). Our experiment measures the cross section averaged over the spread in the electron energy distribution. Figure 2 illustrates the theoretically predicted energy averaged cross section for C^{3+} of McLaughlin and Hahn [2]. The shaded portion of the histogram identifies an energy averaged cross section appropriate for the present experiment.

Our experimental approach [3] determines the dielectronic recombination event rate at the intersection of inclined ion and electron beams by measuring delayed coincidences between the stabilizing photons and the recombined C^{2+} ions. The coincidence technique discriminates against other processes such as charge transfer with residual gas molecules or electron impact excitation; they produce only one of these products. In an experiment, recombined ions that survive the applied external electric fields (e.g. charge state analyzer fields) can be detected directly, while recombined ions that undergo field ionization can be detected indirectly by detecting the field ionized electrons.

Recent experiments by Belic et al. [4] and Williams [5] have used the coincidence technique to measure DR in Mg^+ and Ca^+, respectively. Merged beam experiments have been used to measure DR in C^+ and B^{2+} [6] and in C^+ [7]. All of these experiments have determined DR cross sections that are substantially larger than the predicted values for zero mixing fields. LaGattuta and Hahn [8] have reported calculations for Mg^+ in small applied electric fields that tend to bring the experimental results for Mg^+ into much clearer agreement with theory. Hahn [9] and Griffin [10] have reported ongoing theoretical efforts to account for the other large experimental cross sections in terms of applied field enhancement.

Initial photon-ion coincidence results from this laboratory suggest that for dielectronic recombination (DR) in C^{3+} the energy averaged cross section in a mixing field of about 1.1 V/cm is apparently smaller than that measured in larger mixing fields at the Oak Ridge National Laboratory (ORNL). This result is qualitatively consistent with theoretical predictions of field enhanced DR brought about by the decrease in the autoionization probability of high Rydberg states with increasingly larger ℓ quantum numbers. Comparison of results from the two experiments is complicated by differences in electron energy distributions and because our experiment measures only the DR process which involves stabilization via radiative 2s-2p core relaxation while the ORNL experiment might conceivably include other recombination channels (e.g. radiative recombination). Although our present results only provide evidence for an upper limit on the C^{3+} cross section, additional data accumulation with the present experimental conditions is expected to yield actual values for DR cross sections at several energies near the 2s-2p threshold.

This work was supported by the U.S. Department of Energy under Contract DE-AC02-80ER10631 to the Smithsonian Institution.

References

1. V.L. Jacobs, J. Davis, and P.C. Kepple, Phys. Rev. Lett. 37, 1390 (1976).
2. D.J. McLaughlin and Y. Hahn, Phys. Rev. A 27, 1389 (1983).
3. G.P. Lafyatis and J.L. Kohl, Bull. Am. Phys. Soc. 24, 1181 (1979).
4. D.S. Belic, G.H. Dunn, T.J. Morgan, D.W. Mueller, and C. Timmer, Phys. Rev. Lett. 31, 339 (1983).
5. J.F. Williams, Phys. Rev. A 29, 2936 (1984).
6. P.F. Dittner, S. Datz, P.D. Miller, C.D. Moak, P.H. Stelson, C. Bottcher, W.B. Dress, G.D. Alton, N. Neskovic, and C.M. Fou, Phys. Rev. Lett. 51, 31 (1983).
7. J.B.A. Mitchell, C.T. Ng, J.L. Forand, D.P. Levac, R.E. Mitchell, A. Sen, D.B. Miko, and J.W. McGowan, Phys. Rev. Lett. 50, 335 (1983).
8. K. LaGattuta and Y. Hahn, Phys. Rev. Lett. 51, 558 (1983).
9. Y. Hahn, NBS Workshop on Atomic Spectra and Collisions in External Fields, Gaithersburg, MD, Oct. 1984.
10. D. Griffin, NBS Workshop on Atomic Spectra and Collisions in External Fields, Gaithersburg, MD, Oct. 1984.

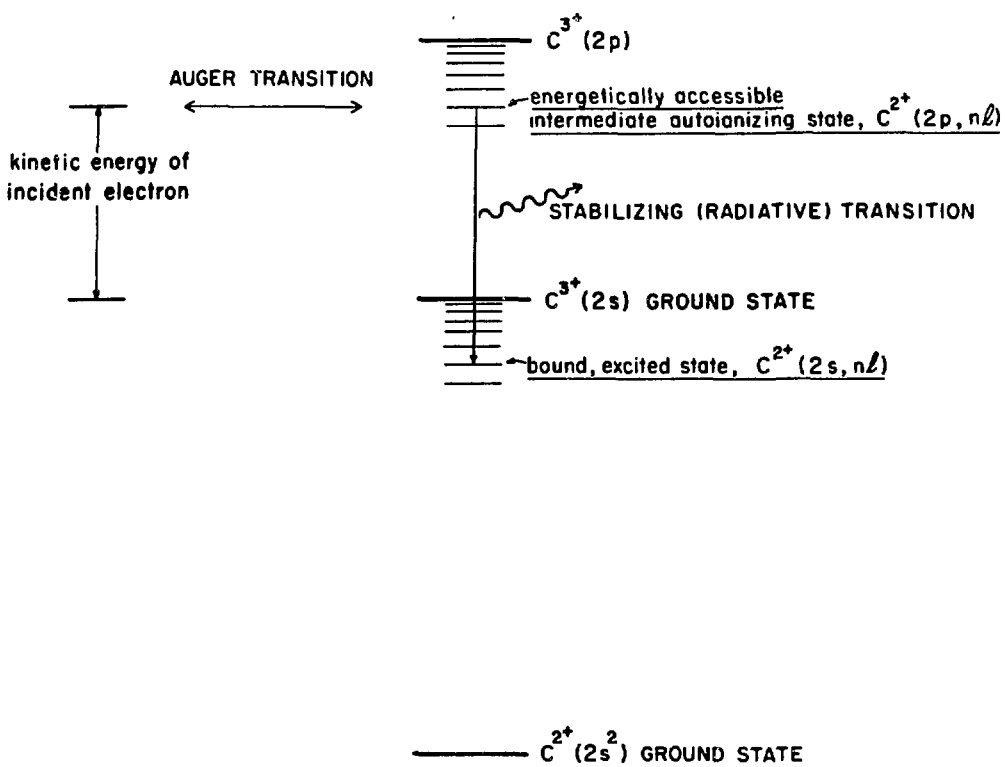

Figure 1. Energy levels for dielectronic recombination in C^{3+}.

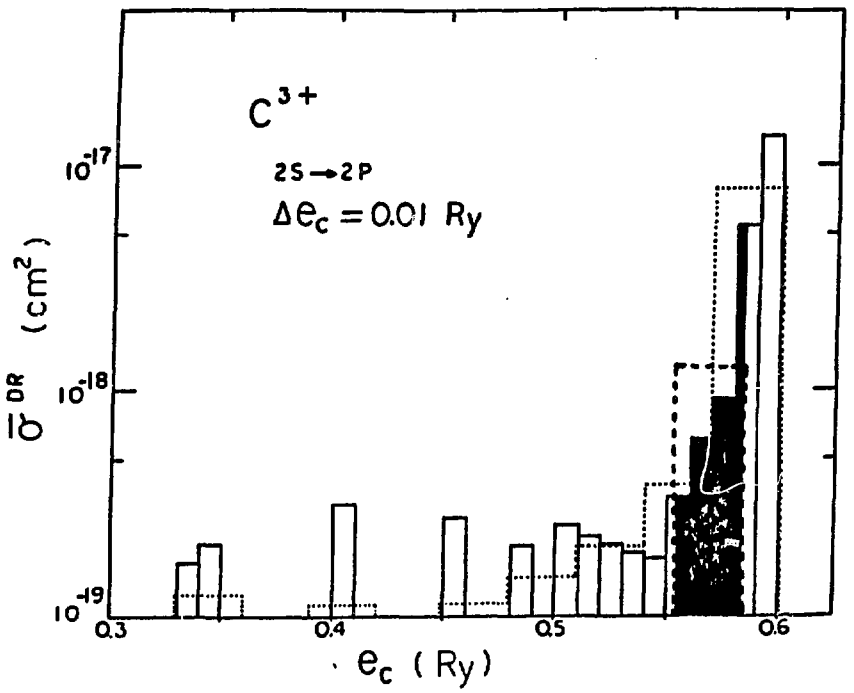

Figure 2. A theoretical dielectronic recombination cross section for C^{3+} averaged over a bin size $\Delta e_c = 0.01$ Ry. The shaded section illustrates the energy averaged cross section to be expected in the present experiment (from McLaughlin and Hahn, 1983).

ATOMIC POTENTIALS IN VERY DENSE ALUMINUM PLASMAS

R. Cauble and U. Gupta
Berkeley Research Associates
Springfield, VA

and

J. Davis
Plasma Radiation Branch, Plasma Physics Division
Naval Research Laboatory
Washington, D.C.

The calculation of atomic properties is plasma is critically dependent on the form of the ion-electron interaction potential. In the case of weak collisions in a low density ionized gas, the screening of the ion under consideration by surrounding plasma is adequately described by the Debye-Hückel potential (see, e.g., Weisheit, 1983). If the plasma is very dense, the perturbation approximations leading to the Debye form break down and other techniques must be employed to incorporate additional correlative effects. The transition from classical to this strongly coupled plasma occurs when the parameter $\Gamma = (\bar{Z})^2 e^2 \beta / r_o$, where $\bar{Z}$ is the mean charge per ion, $\beta = (k_B T)^{-1}$, and r_o is the ion-sphere radius, is greater than about one.

Correlations can be introduced by a method that provides accurate particle density distribution functions in ionic systems. The hypernetted chain (HNC) approximation (see, e.g., Hansen and McDonald, 1976) to the hierarchy of equations for the distributions has been shown to closely reproduce data from computer simulations of strongly coupled plasmas (Hansen and McDonald, 1981). The method utilizes a semiclassical form for the bare two-body interaction (Deutsch, 1977) to generate charge distributions which are employed in the Poisson equation to provide the HNC effective potential (Cauble, Blaha, and Davis, 1984).

A method capable of solving for the effective potential in a quantum mechanical way is density functional theory --DFT (Gupta and Rajagopal, 1982). Since the free energy of the system is a unique functional of the charge distributions, minimization of the free energy with density profiles found from the Schrodinger equation with exchange and correlation for the free and bound electrons and a form for the ion distribution, either with (Dharma-wardana and Perrot, 1982; Perrot and Dharma-wardana, 1984) or without (Gupta, Blaha, and Davis, 1984) ion-ion correlations, leads to a unique effective ion-electron potential via a self-consistent solution of the equations.

Fig. 1 displays the ion and electron distributions around an aluminum ion located at the origin in an aluminum plasma. The plasma conditions are $n_e = 10^{25}$ cm^{-3} and T = 500 eV ($\bar{Z}$ = 10.1 and Γ = 4.75), the most extreme case considered here. The quantum mechanical DFT and the semiclassical HNC methods give very similar results except: for $\rho_i(r)$ near $r/a_o \sim 2$ and $\rho_e(r)$ near $r/a_o \sim 1$, the HNC's better treatment of ion correlations reveals the onset of spatial structure (not evident

in the DFT) as well as plasma screening; and for $\rho_e(r)$ very close to the origin, where DFT handles the electron distribution more accurately, the curves are somewhat distinct. The Debye $\rho_i(r)$ is included for comparison; it is sigificantly in error throughout the entire range.

The remaining figures display the effective potentials for aluminum plasmas under various strongly coupled conditions. In all cases the DFT and HNC potentials are very similar, HNC ion correlations creating minor differences at large radius. The Debye potential shows excessive screening throughout. The Debye screening can be reduced by not including ions in the calculation of the Debye length, but too much of the screening effect is removed; the resulting exponential potential falls off far too slowly. The "ion-sphere" model (no ion-ion interactions at all and a uniform neutralizing electron density close to the ion being studied), thought to be valid at extremely high densities, is somewhat better than the Debye form, but is quite inaccurate even at 10^{25} cm^{-3}.

From effective potentials such as these, atomic properties of an average plasma ion can be obtained (Davis, et al, 1983). These include atomic energy levels, wavefunctions, equation of state properties (Gupta, Blaha, and Davis, 1984), photoionization cross sections (Cauble, Blaha, and Davis, 1983), and bremsstrahlung cross sections (Lamoureux, et al, 1984). These calculations show that considerable errors can be made when an inappropriately approximated potential (such as the Debye-Huckel or ion-sphere) is used. In general for atomic calculations in dense plasmas such as these considered here,the Debye-Hückel potential predicts results that have significantly greater error than those provided by the ion-sphere potential. It is quite easy, however, to use an effective interionic potential such as DFT or HNC/Poisson to account for the additional many-body effects that must be included when the plasma is close to being strongly coupled.

REFERENCES

Cauble, R., M. Blaha, and J. Davis 1983, Proceedings of the 2nd Int'l. Conference on the Radiative Properties of Hot Dense Matter, Sarasota (to be published in J. Quant. Spectros. Rad. Transf.).

Cauble, R., M. Blaha, and J. Davis 1984, Phys. Rev., A 29,3280.

Davis, J., M. Blaha, R. Cauble, and U. Gupta 1984, NRL Memo Report 5311.

Deutsch, C. 1977, Phys. Lett.,60A, 317.

Dharma-wardana, M.W.C. and F. Perrot 1982, Phys. Rev., A 26, 2096.

Gupta U., M. Blaha, and J. Davis 1984, J. Phys. B, to be published.

Gupta, U. and A. K. Rajagopal 1982, Phys. Rep., 87, 259.

Hansen, J.P. and I. R. McDonald 1976, Theory of Simple Liquids (Academic Press, New York).

Hansen, J.P. and I. R. McDonald 1981, Phys. Rev., A 23, 2041.

Lamoureux, M., R. Cauble, L. Kim, F. Perrot, and R. Pratt 1984, Proceedings of IAU Colloquium No. 86, Washington, D.C., this volume.

Perrot, F. and M.W.C. Dharma-wardana 1984, Phys. Rev., A 29, 1378.

Weisheit, J.C. 1983, in Applied Atomic Collision Physics, edited by H. S. Massey (Academic Press, New York), Vol. II.

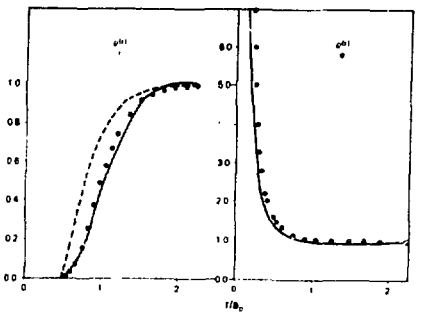

Fig. 1: Ion and electron charge distributions in Aℓ at $n_e = 10^{25}$ cm^{-3} and T = 500 eV DFT: circles; HNC: solid; and DH: dashed curve.

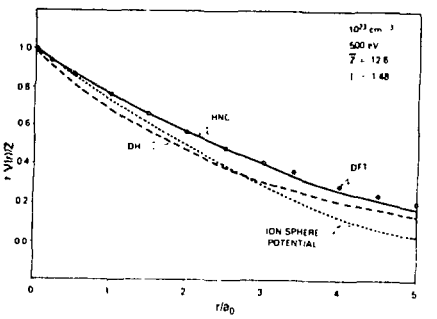

Fig. 2: Effective electron-ion potentials in Aℓ for various models. $n_e = 10^{25}$ cm^{-3}, T = 500 eV.

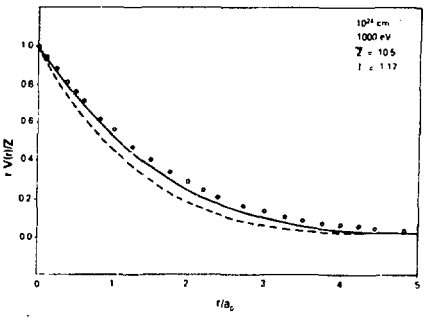

Fig. 3: Effective electron-ion potentials in Aℓ for various models. $n_e = 10^{24}$ cm^{-3} and T = 1000 eV.

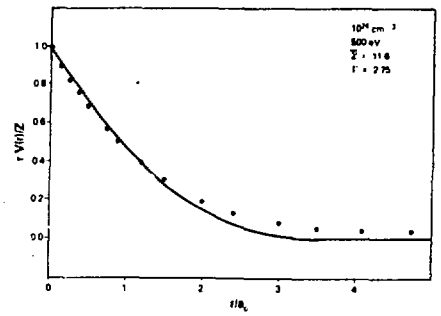

Fig. 4: Effective electron-ion potentials in Aℓ for various models. $n_e = 10^{23}$ cm^{-3} and T = 500 eV.

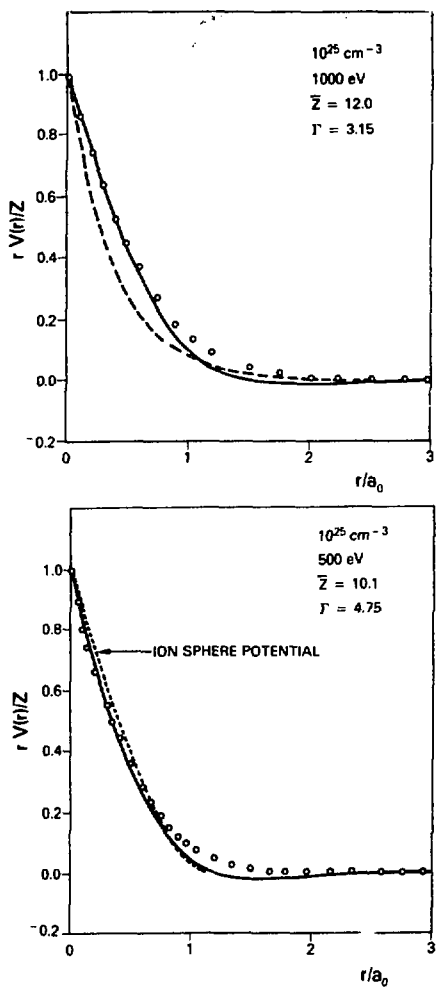

Fig. 5: Effective electron-ion potentials in Aℓ for various models. $n_e = 10^{25}$ cm^{-3}, T = 1000 eV and 500 eV.

COMPARATIVE STUDY OF ELECTRON BREMSSTRAHLUNG IN VARIOUS HIGH ρ - T POTENTIALS

M. Lamoureux
LSAI, University of Paris-Sud
91405 Orsay France

R. Cauble
Berkeley Research Associates
Springfield, VA 22151 USA

L. Kim
University of Pittsburgh
Pittsburgh, PA 15260 USA

F. Perrot
CEA Limeil
94190 Villeneuve St. Georges France

and

R. H. Pratt
University of Pittsburgh
Pittsburgh, PA 15260 USA

In order to calculate bremsstrahlung cross sections in plasmas, an atomic potential which includes the effects of the surrounding plasma is required. For the high ρ - T conditions we are considering ($n_e = 10^{25}$ cm^{-3}, T = 500 eV), plasma correlative effects are important. In these strongly coupled plasmas, the Debye-Hückel potential is irrelevant and not considered here. The statistical Thomas-Fermi (TF) potential (Feynmann, Metropolis, and Teller, 1949) is known to be correct at very high densities but does not contain correlation information. A semiclassical treatment of correlations that accurately reproduces results of numerical simulations of strongly coupled plasmas is the hypernetted chain (HNC) approximation to the hierarchy of equations describing density distributions (Hansen and McDonald, 1981). The method generates many-body distributions using an analytic two-body interaction that successfully approximates quantum effects at short distances. These distributions are used in the Poisson equation to find the effective potential (Cauble, Blaha, and Davis, 1984). An alternative method (Gupta and Rajagopal, 1982) of including correlations is to treat them in a quantum mechanical manner, taking into account ion correlations as well as electron exchange and correlation; this is done in density functional theory (DFT), where electron wavefunctions and the effective potential which is used here are obtained self-consistently (Dharma-wardana and Perrot, 1982; Perrot and Dharma-wardana, 1984). Comparison of these methods can be found elsewhere (Cauble, Gupta, and

Davis, 1984). These potentials for aluminum at 10^{25} cm^{-3} and 500 eV are displayed in Fig. 1.

Electron bremsstrahlung Gaunt factors are obtained from the three types of potentials described above by three different atomic physics methods (Pratt, 1983). The most sophisticated method is the multipole relativistic partial wave expansion model, which has been used for plasmas only recently (Feng, et al). The other two methods are much simpler (and consequently require much less computer time). The Born-Elwert form factor approximation, which is known to be best suited for high energies, overestimates the Gaunt factors at low energies. On the contrary, the classical mechanics approach (Lamoureux and Pratt, 1983), which is not valid at high energies, is more appropriate in the low energy range (see Fig. 2). As expected, the more screened the ion, the smaller the Gaunt factor; thus the TF potential leads to smaller Gaunt factors than the other two potentials. To further explain the influence of the choice of the potential, it is useful to recall that the range of radius probed by the bremsstrahlung process is estimated by the inverse of the momentum transferred. This accounts for the (somewhat accidental) similarity of the Gaunt factors obtained from the TF and DFT potentials in the example illustrated in Fig. 2 (The radius of interest here is about 1.2 a.u.).

In the high ρ - T case considered here, the relative discrepancies between the Gaunt factors obtained from the various atomic methods, all of them taking screening into account, can be as large as 50%. The type of average atom potential used to describe the plasma appears to be less influential (< 10%) than the choice of atomic method.

REFERENCES

Cauble, R., M. Blaha, and J. Davis 1984, Phys. Rev. A 29, 3280.

Cauble, R., U. Gupta, and J. Davis 1984, Proceedings of IAU Colloquium No. 86, Washington, D.C., this volume.

Dharma-wardana, M.W.C. and F. Perrot 1982, Phys. Rev. A 26, 2096.

Feng, I.J., M. Lamoureux, R.H. Pratt, and H.K. Tseng 1983, Phys. Rev. A 27, 3209.

Feynmann, R.F., N. Metropolis, and E. Teller 1949, Phys. Rev. 75, 1501.

Gupta, U. and A.K. Rajagopal 1982, Phys. Rep. 87, 259.

Hansen, J.P. and I.R. McDonald 1981, Phys. Rev. A 23, 2041.

Lamoureux, M. and R.H. Pratt 1983, Proceedings of the 2nd Int'l. Conference on the Radiative Properties of Hot Dense Matter, Sarasota (to be published in J. Quant. Spectros. Rad. Trans.).

Perrot, F. and M.W.C. Dharma-wardana 1984, Phys. Rev. A 29, 1378.

Pratt, R.H. 1983, Fundamental Processes in Energetic Atomic Collisions, ed. by H.O. Lutz, J.S. Briggs, and H. Kleinpoppen (Plenum Press, New York).

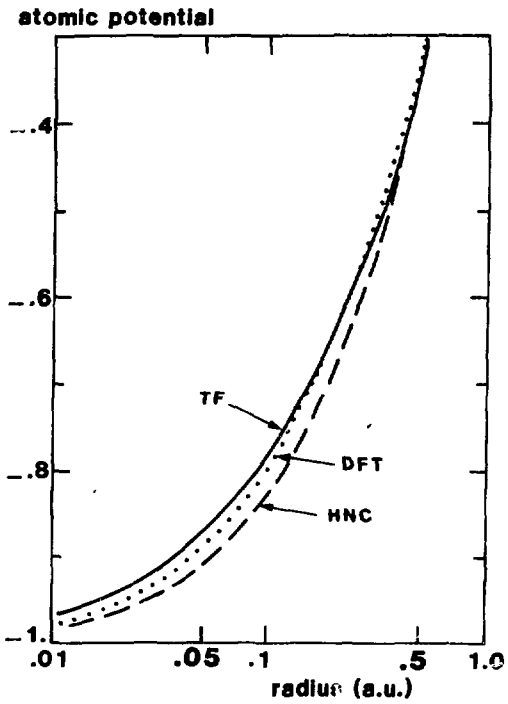

Fig. 1: Average atom potential (rV(r)/Z) for an Aℓ plasma at the temperature of 1 keV and the electron density of 10^{25} e/cc in models of increasing complexity. (-): TF; (---): HNC-Poisson; (···): DFT.

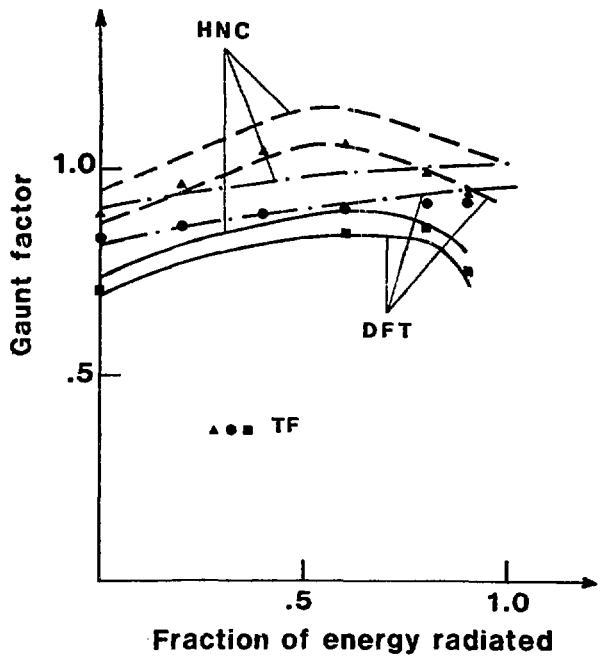

Fig. 2: Electron bremsstrahlung Gaunt factors obtained from the potentials of Fig. 1, for incident electrons of 1 keV, and using three atomic methods of increasing complexity. (-·-●): classical mechanics approach; (---▲): Elwert Born form factor; (——■): Multiple relativistic partial wave expansion model.

INVERSE INELASTIC SCATTERING THEORY

Cao xuan Chuan

Institut de Physique , Université de Constantine
B.P. 260 , Constantine , Algerie

For inverse scattering theories , it is well known that in order to guarrantee the existence and uniqueness of the solution , drastic restrictions must be imposed on the scattering potential or on the scattering data collected from experiments (see for example Newton I966) . The existing theories in their original form such as the Geldfan Levitan or the Marchenke equations therefore cannot be used in a straightforward manner and some further steps toward simplifications have to be considered .

In inelastic scattering problems where many coupled channels must be taken into account to construct various elements of the scattering matrix the problem become much more complicated both from thetheoretical and experimental point of view , The present work deal only with the energy fixed case and show that a solution can nevertheless be obtained by using on one hand the conventional technique of the Abelian transformation which has been extensively applied in the JWKB approach to the one channel problem (see for example a general review by Buck I97I) with on the other , some results obtained recently concerning a system of coupled differential equations (Cao I982 I) .

The case of two states approximation which may be interesting for its possible applications is investigated starting from the results of the direct problem (Cao I984 II) but its possible extension to the general case of a finite number of coupled channels will be emitted for space limitation .

The mathematical description of the 2 states problem for simplicity , is assumed to be , in matrix notation :

$$(L+U)Y = 0$$

$$Y = \begin{pmatrix} y_0 \\ y_1 \end{pmatrix} \qquad L = \begin{pmatrix} L_0 & 0 \\ 0 & L_1 \end{pmatrix} \qquad U = \begin{pmatrix} U_{00} & U_{01} \\ U_{10} & U_{11} \end{pmatrix}$$

$$L_i = \frac{d^2}{dr^2} + k_i^2 - \frac{l(l+1)}{r^2} \qquad i = 0,1$$

where we continue to keep the notations and conventions of Ref II . The interaction matrix U is generally symmetric so that we may set

$U_{01} = U_{10} = B$; B will be referred to as the coupling function of the system .

Let $\delta_\ell^\pm$ be the proper phase schift i.e. the phase schift one would have after separation of the coupled equations With the fellowing definitions :

$$I_\pm(S_\pm, E) = \log \frac{r(S_\pm)}{S_\pm}$$

$$S_\pm^2 = r^2 \left\{ 1 - \frac{1}{2E} \left[\tfrac{1}{2}(U_{00}+U_{11}) \pm \tfrac{1}{2}\left[(\Delta k^2 + \Delta U)^2 + 4B^2 \right]^{1/2} \right] \right\}$$

$$\Delta k^2 = k_1^2 - k_0^2 \qquad \Delta U = U_{11} - U_{00}$$

E : incident energy

and using the technique of Abelian transformation we obtain :

$$I_\pm - \alpha_\pm = \frac{2}{K\pi} \int_{S_\pm}^{\infty} \frac{1}{(b^2 - S_\pm^2)^{1/2}} \frac{d\delta_\ell^\pm}{db}\, db$$

$$K^2 = \tfrac{1}{2}(k_0^2 + k_1^2) \qquad b = \frac{1}{K}(\ell + 1/2) \qquad \alpha_\pm = \log \frac{E}{E \mp \Delta k^2}$$

The various elements U_{ij} of the interaction matrix U are therefore related to the quantities $I_\pm$ by a system of 2 equations :

$$U_{00} + U_{11} = \frac{1}{2E} \left\{ 2 - \left(e^{-2I_-} + e^{-2I_+} \right) \right\}$$

$$(\Delta k^2 + \Delta U)^2 + 4B^2 = \frac{1}{4E^2} \left[e^{-2I_-} - e^{-2I_+} \right]^2 \qquad (1)$$

In the one channel case , the diagonal terms U_{ii} are often referred to as the interaction potential of the ith channel which is described by an equivalent homogeneous equation . They can usually be inferred by other means , for example for sufficiently strong attractive forces , U_{ii} can yield a discrete energy spectrum . Therefore they can be evaluated from the wave function corresponding tochannel i . Particularly , it is reasonable to assume that the U_{oo} term which is related to the ground state can be attained by this way . The two equations in (1) are then sufficient in principle to lead to the unknowns U_{ii} and B provided that $d\delta_\ell^\pm/dk$ can be determined from experimental data .

In order to simplify the presentation , we shall limit ourselves to the case of "near resonance " (i.e. $\Delta k^2 \simeq 0$)for which $\alpha_\pm$ is set equal to zero . Assuming then that the elastic and inelastic partial cross section Q^o_ℓ , Q^i_ℓ are known , it can be shown that $\delta^\pm_\ell$ are given by the following equations:

$$\delta^+_\ell = \Gamma_1 + \delta^-_\ell \qquad (2) \qquad \Gamma_1 = \sin^{-1}\left[\frac{2k_o}{[(2\ell+1)\pi]^{1/2}}\frac{Q_{i\ell}^{1/2}}{\sin 2\varepsilon}\right]$$

$$\sin^2\varepsilon = \frac{d^2}{c^2+d^2} \qquad \cos^2\varepsilon = \frac{c^2}{c^2+d^2} \qquad f_o = \frac{k_o^2}{4\pi(2\ell+1)}\frac{Q_{i\ell}+Q_{e\ell}}{\cos^2\varepsilon}$$

$$(\cos 2\Gamma_1 + tg^2\varepsilon)\sin^2\delta^-_\ell + \tfrac{1}{2}\sin 2\Gamma_1 \sin 2\delta^-_\ell + (\sin^2\Gamma_1 - f_o) = 0 \qquad (3)$$

The quantities $d\delta^\pm_\ell/dl$ needed in the determination of $I_\pm$ are then given by :

$$d\delta^+_\ell/dl = 2(\sin 2\delta^+_\ell + tg^2\varepsilon \sin 2\delta^-_\ell)^{-1}\left[g_o - \frac{g_1}{(1-f_1)^{1/2}}\sin 2\delta^+_\ell\right]$$

$$d\delta^-_\ell/dl = 2(\sin 2\delta^+_\ell + tg^2\varepsilon \sin 2\delta^-_\ell)^{-1}\left[g_o + \frac{g_1}{(1-f_1)^{1/2}}tg^2\varepsilon \sin 2\delta^+_\ell\right]$$

$$g_o = -\frac{k_o^2}{4\pi(2\ell+1)^2}\frac{1}{\cos^2\varepsilon}\left[(2\ell+1)\left(\frac{dQ_{i\ell}}{dl}+\frac{dQ_{e\ell}}{dl}\right) - (Q_{i\ell}+Q_{e\ell})\right]$$

$$g_1 = \frac{1}{2}\frac{k_o}{[(2\ell+1)\pi]^{1/2}}\frac{1}{\sin 2\varepsilon}\frac{1}{Q_{i\ell}^{1/2}}\left(\frac{1}{2}\frac{dQ_{i\ell}}{dl} - \frac{1}{2\ell+1}Q_{i\ell}\right); \quad f_1 = \frac{k_o^2}{(2\ell+1)\pi}\frac{Q_{i\ell}}{\sin^2 2\varepsilon}$$

The quantity ε is related to an arbitrary parameter α (see Ref II) which must be chosen according to the validity condition of the theory :

$$\frac{B}{\Delta k^2 + \Delta U} \ll \frac{1}{\alpha^2 \tau(n)} \left(2n + 1/4\right) \qquad (4)$$

Assume first that the element U_{11} is known a priori . The following algorithm is needed to solve the problem :

(i) Let $\{n\}$ be the set of positive values of real number . To each element of this set correspond an element of the set $\{ I_\pm(E, n) \}$

(ii) Let $\{n_j\}$ be a subset of $\{n\}$ such that the first equation of system (1) is verified .

(iii) Corresponding to each n_j we can now compute the element of the set $\{B(n_j)\}$ from the second equation of (1) and for each case check the validity condition (4) . The appropriate value n_o is then the one for which this condition is satisfied best . The non existence of such n_o mean on the other hand that we must go over to the second order separation of the equations as indicated in Ref I .

The case where both U_{11} and B are unknown is obviously more complicated but nevertheless tractable , the results are summarised below : Define

$$V_\pm = \frac{1}{2}\left\{ U_{11} \pm \left[(\Delta k^2 + \Delta U)^2 + 4B^2 \right]^{1/2} \right\} \; ; \quad A\pm_\ell = \left(\frac{\epsilon}{\mu}\right)^{1/2} \left(\delta_\ell^\pm - \delta_\ell^{(c)} \right)$$

in which μ is the reduced mass , $\delta_\ell^{(0)}$ is the conventional JWKB phase schift corresponding to the potential $\frac{1}{2} U_{oo}$. We find then

$$V_\pm(r) = \frac{2}{\pi} f(U_{oo}) \int_r^\infty \frac{1}{(s^2 - r^2)^{1/2}} \frac{dA\pm_\ell}{ds} ds$$

$$V_+ - V_- = \frac{1}{2E} \left(e^{-2I_-} - e^{-2I_+} \right) \qquad (5)$$

where the expression of $f(U_{oo})$ is (Zerarke 1984)

$$f(U_{oo}) = E - \frac{1}{2} U_{oo} - \frac{1}{4} r \frac{dU_{oo}}{dr}$$

The above algorithm remains valid , the first equation of (5) can be used to evaluate V_+ , V_- while the second one serving to define the subset $\{n_j\}$ of the second step (ii) .

The non resonance case ($\Delta k^2 \neq 0$, $\alpha \pm \neq 0$) is more complicated in the sense that the quantities $\delta^\pm_\ell$ have to be reinterpreted and the relations (2) , (3) must be modified accordingly . It can be shown that the problem can nevertheless be made

tractable on the same basis .

To conclude , we may point out that the above results are derived in the frame of a JWKB treatment which imply strict limitations inherent to a short wave lenght approximation . We find however that it is also possible to generalise the theory to the case where such an approximation does not apply by including to the above approach some properties of non linear differential equations .

Buck U. 1974 , Rev Mod Phys 46 2 .
Cao x. Ch. 1982 J. Phys. A Math Gen. 15 2727
Cao x. Ch. 1984 J. Phys. A Math Gen. 17 609
Newton R. G. 1966 " Scattering of waves and particles "Mc Gr H.
Zerarka M. 1984 These Univ. Constantine

THE EFFECT OF RESONANCES ON THE EXCITATION RATES FOR THE IONS OF THE HE-LIKE ISOELECTRONIC SEQUENCE

P. Faucher, F. Bely-Dubau
Observatoire de Nice B.P. 139, 06003 Nice Cedex, France

J. Dubau
Observatoire de Meudon, 92195 Meudon Principal Cedex, France

The Helium-like resonance, intercombination and forbidden lines ($1s^2\ ^1S\text{-}1s2p\ ^1P$, $1s^2\ ^1S\text{-}1s2p\ ^3P$, $1s^2\ ^1S\text{-}1s2s\ ^3S$ respectively) can be observed from hot, low density plasmas such as coronal or tokamak plasmas. They can be used either to measure the electron temperature from the ratio of their intensity to that of the corresponding satellite lines ($1s^2 n\ell' - 1s2\ell n\ell'$) as described by Gabriel (1972) or directly as a density diagnostic (Gabriel and Jordan, 1972). The soft X-ray spectra obtained from these plasmas have been observed from space satellite experiments such as the Solar Maximum Mission (Acton et al., 1980), Hinotori (Tanaka et al., 1982) and P78-1 (Doschek et al., 1982) or from tokamaks such as PDX, PLT (Princeton, USA), TFR (Fontenay-aux-Roses, France). The analysis of some of these spectra, for example, Mg XI (Faucher et al., 1983), Ti XXI (Bely-Dubau et al., 1982b) and Ca XIX (Bely-Dubau et al., 1982a, Jordan and Veck 1982) show that these diagnostics are sensitive to the accuracy of the atomic data and demonstrate the need for improved calculations of the excitation rates for the He-like ions.

The doubly excited states of the Li-like ions which give rise to the satellite lines can either autoionize to a He-like continuum or decay radiatively. Thus, when these states are above the $2\ ^3S$, $2\ ^3P$ or $2\ ^1P$ thresholds, they produce resonances in the ($1\ ^1S\text{-}2\ ^3S$), ($1\ ^1S\text{-}2\ ^3P$) and ($1\ ^1S\text{-}2\ ^1P$) collision strengths which are numerous enough to enhance the effective rate coefficients. However, as these states can also decay radiatively with transition probabilities scaling as Z^4, it is clear that their effect decreases for increasing Z.

Previous calculations were carried out for the effect of resonances on the intensity of the forbidden line for various He-like ions: O, Mg, Ca, Fe (Steenman-Clark and Faucher, 1984). This line is the most sensitive to this effect, $2\ ^3S$ being the lowest-lying level in the n=2 complex. Results were obtained using the quantum defect theory developed by Gailitis (1963) and Seaton (1969) including the possibility for the resonant states to decay radiatively. The effect of the $1s2\ell' n\ell$ resonances on the excitation rate coefficients has been estimated by comparing the rates derived from the direct collision strengths computed in intermediate coupling with the D.W. method with those obtained similarly but including the resonant states. At the temperatures of maximum abundance of each ion, the effect of resonances was estimated to be 37% for O VII (10^6K), 17% for Mg XI (4.10^6K), 6% for Ca XIX (15.10^6K) and 5% for Fe XXV (20.10^6K).

Recent investigations of Pradhan (1983) and Tayal and Kingston (1984) emphasize the importance of the resonances due to the autoionizing states $1s3\ell' n\ell$ ($n \geq 3$). To estimate the effect of these

resonances we used the method developed for the autoionizing states $1s2\ell\,'n\ell$ and found it to be negligible (Steenman-Clark and Faucher, 1984). However, such a method is valid only for large values of n as the corresponding collision strengths are calculated averaging over all the resonances within a small energy interval where the reactance matrix is assumed to be constant.

New calculations are presented here to estimate the effect of the resonances due to the autoionizing levels $1s3\ell\,'n\ell$ with $n \lesssim 5$. As these resonances are well separated and situated in a limited energy range, their contribution over the direct excitation rates were calculated from the following process:

$$1s^2\ ^1S + e \rightarrow 1s3\ell\,'n\ell \rightarrow 1s2\ell\,'' + e' \quad . \tag{1}$$

The corresponding excitation rate C can be expressed as:

$$C\ (cm^3\ s^{-1}) = F_1(T_e) \times F_2^*(s) \tag{2}$$

where

$$F_1(T_e) = 3.27\ 10^{-24} \left(\frac{E_H}{kT_e}\right)^{3/2} \exp(-E_s/kT_e) \tag{3}$$

$$F_2^*(s) = \frac{g_s}{g_1} \frac{A_a^1(s)\ \ A_a^2(s)}{\sum_i A_a^i(s) + \sum_j A_r^j(s)} \quad . \tag{4}$$

E_s is the energy difference between the autoionization state s and the ground state of the He-like ion of statistical weight $g_1=1$. $A_a^1(s)$ and $A_r^j(s)$ are respectively the autoionization and radiative probabilities with

$$A_a^1(s) = A_a\ (s \equiv 1s3\ell\,'n\ell\ ^{2s+1}L_J \rightarrow 1 \equiv 1s^2\ ^1S_o) \tag{5}$$

$$A_a^2(s) = A_a\ (s \equiv 1s3\ell\,'n\ell\ ^{2s+1}L_J \rightarrow 2 \equiv 1s2\ell\,''\ ^{2s+1}L'_{J'}). \tag{6}$$

The summations over $A_a^i(s)$ and $A_r^j(s)$ are extended respectively to all the possible continua from the autoionizing level s and to all radiatively allowed lower states.

We can express the excitation rate for a given transition as the summation of three contributions:

$$C = C_1 + C_2 + C_3 \tag{7}$$

where C_1 is the direct excitation rate
C_2 is the excitation rate due to the autoionizing levels $1s2\ell\,'n\ell$ $(n > n_c)$
C_3 is the excitation rate due to the autoionizing levels $1s3\ell\,'n\ell$ $(n = 3, 4, 5)$.

Table 1 shows the results obtained for Fe XXV for the resonance and forbidden lines w and z respectively at three temperatures of interest for this ion.

TABLE 1. Relative Importance of the Different Contributions to the Excitation Rates for the Resonance (w) and Forbidden (z) Lines in Fe XXV.

	w			z		
T_e (10^6K)	C_1	C_2	C_3	C_1	C_2	C_3
10	.303(-14)	0	.886(-16)	.396(-15)	.391(-16)	.108(-15)
20	.119(-12)	0	.192(-14)	.116(-13)	.633(-15)	.230(-14)
30	.398(-12)	0	.413(-14)	.310(-13)	.123(-14)	.494(-14)

The effect of the autoionizing levels $1s3\ell'n\ell$ ($n \lesssim 5$) is very important for the z-line with respect to the contribution due to the $1s2\ell'n\ell$ ($n > 16$) autoionizing levels.

Table 2 shows, for the z-line, that this contribution decreases rapidly with n, thus confirming that the contribution due to the $1s3\ell'n\ell$ autoionizing states for large values of n is negligible.

TABLE 2. Contributions of Each N to the Excitation Rate C_3 Obtained for Fe XXV at 20.10^6K ($C_3 = C_3^3 + C_3^4 + C_3^5$)

T_e (10^6K)	C_3^3	C_3^4	C_3^5
20	1.383(-15)	6.966(-16)	2.224(-16)

REFERENCES

Acton, L.W., et al. 1980, Solar Phys. 65, 53.
Bely-Dubau, F., et al. 1982a, Mon. Not. R. astr. Soc. 201, 1155.
Bely-Dubau, F., et al. 1982b, Phys. Rev. A 26, 3459.
Doschek, G.A., et al. 1981, Astrophys. J. 249, 372.
Faucher, P., et al. 1983, Astron. Astrophys. 118, 147.
Gailitis, M. 1963, Sov. Phys. JETP 17, 1328.
Gabriel, A.H. 1972, Mon. Not. R. astr. Soc. 160, 99.
Gabriel, A.H., Jordan, C. 1972, Case Studies in Atomic Collision Physics, Vol. 2
Jordan, C., Veck, N.J. 1982, Solar Phys. 78, 125.
Pradhan, A.K. 1983, Phys. Rev. 28A, 2128.
Seaton, M.J. 1969, J. Phys. B 2, 5.
Steenman-Clark, L., Faucher, P. 1984, J. Phys. B 17, 73.
Tanaka, K., et al. 1982, Astrophys. J. Lett. 245, L59.
Tayal, S.S., Kingston A.E. 1984, J. Phys. B 17, L145.

PROTON-INDUCED FINE-STRUCTURE TRANSITIONS*

B. Zygelman and A. Dalgarno
Harvard-Smithsonian Center for Astrophysics
Cambridge, MA 02138

Experimental studies of the intensity of the (2p1/2-1s1/2) and (2p3/2-1s1/2) lines of SXVI in the Alcator Takamak show large departures from the statistical ratio of 0.5 (Källne et al. 1982). Similar enhancements in the intensity ratio have been reported in solar observations (Grineva et al. 1973, Phillips et al. 1982) for the Mg XII lines and in laser produced plasmas (Boiko et al. 1977). Theoretical calculations of the intensity ratio have been carried out by Vinogradov et al. (1977), Beigman et al. (1979) and Ljepojevic et al. (1984). We suspect that proton-impact induced transitions play a crucial role which depends sensitively on the conditions of temperature and density in the Plasma. In this abstract we will present some preliminary results of proton-impact excitation cross section calculations, for the n=2 sub levels of hydrogenic ions.

FORMALISM

We can express the total wavefunction for the H^+-ion system by the expansion,

$$\psi_\Gamma(\vec{R},\vec{r}) = \sum_{\Gamma'} \frac{F_{\Gamma',\Gamma'}(|R|)}{|R|} |\Gamma'\rangle \quad ,$$

$$|\Gamma'\rangle \equiv |JM\ell\lambda jn\rangle \tag{1}$$

where $\vec{R},\vec{r}$ are the proton and electron coordinates respectively. The expansion kets $|\Gamma'\rangle$ are specified by, the total angular momentum JM, the proton angular momentum ℓ, the total and orbital electronic angular momenta j,λ, and the atomic radial quantum number n. We are interested in the transitions among the n=2 levels only. We can then restrict the expansion (1) to the $|JM\ell\lambda j\ n=2\rangle$ channels. The Schrödinger equation for the scattering amplitudes becomes,

$$\left(\frac{d^2}{dR^2} - \frac{\ell(\ell+1)}{R^2} \right) F_{\Gamma,\Gamma'} + \kappa_{nj}^2 F_{\Gamma,\Gamma'} = \sum_{\Gamma''} 2\mu \langle \Gamma'|v|\Gamma''\rangle F_{\Gamma,\Gamma''}$$

$$\kappa_{nj}^2 \equiv 2\mu(E-\epsilon nj) \quad , \tag{2}$$

where μ is the reduced mass, E and ϵnj are the total and atomic energy eigenstates respectively. The potential matrix $\langle\Gamma'|v|\Gamma\rangle$ is given by

$$\langle\Gamma'|v|\Gamma\rangle = \langle J'M'\ell'\lambda'j'n' \left| \frac{Z}{|R|} - \frac{1}{|R-r|} \right| nj\lambda\ell MJ\rangle \quad ,$$

Z is the nuclear charge of the ion.

Equation (2) decouples into two independent sets of four channel equations, each set having a definite parity. The total cross section for the inelastic $\lambda j \to \lambda' j'$ transitions can then be expressed as,

$$\sigma(\lambda\, j-\lambda' j') = \frac{\pi}{(2j+1)k^2_{n'j'}} \sum_{J\ell\ell'} (2J+1)\left|S^{j'\ell'\lambda'}_{j\ \ell\ \lambda}(J)\right|^2 \qquad (3)$$

where $S^{j'\ell'\lambda'}_{j\ \ell\ \lambda}(J)$ is the S-matrix of the scattering solutions to equation (2). We have calculated some cross sections for these transitions in Ar^{+17}. We have used the values $\Delta E(2p3/2\text{-}2p1/2) = 4.81eV$ for the fine structure separation, and $\Delta E(2s1/2\text{-}2p1/2) = 0.16eV$ (Wiese et al. 1966) for the Lamb shift. Some cross sections are presented in Table I.

DISCUSSION

Our results in Table I show the tendency of an enhancement in the (2s1/2-2p1/2) cross sections relative to the (2s1/2-2p3/2) cross sections in the range of energies presented. We can give a qualitative explanation for these results by resorting to a semi-classical argument. In the semi-classical picture, transitions in the ion are driven by the time dependent Coulomb field produced by the incoming proton on a given trajectory $\vec{R}(t)$. For a proton moving in a hyperbolic orbit $\vec{R}_H(t)$, the first order transition probability for the ion to go from state $|i\rangle$ to $|j\rangle$ is proportional to the integral

$$I(R_H) \equiv \left| \int_{-\infty}^{\infty} dt\, e^{i\Delta E t} \langle i | \frac{1}{|\vec{R}_H(t) - \vec{r}|} | j \rangle \right|^2$$

where ΔE is the frequency of the transition. At large impact parameter b, $I(R_H)$ is approximately equal to the straight-line integral $I(R_{SL})$, $(\vec{R}_{SL}(t) = \vec{v}t + \vec{b})$ multiplied by a screening factor $e^{-\pi|\zeta|}$ (K. Alder et al. 1956), where

$$|\zeta| = (Z-1)\mu \left| \left(\frac{1}{k_f} - \frac{1}{k_i}\right) \right| \approx \frac{(Z-1)}{v_f} \frac{|\Delta E|}{2E}$$

$$\text{i.e. } I(R_H) \approx e^{-\pi|\zeta|} I(R_{SL}) \ .$$

If the transitions are dominated by contributions coming from larger impact parameters then they are also very sensitive to the value of the ζ parameter. In our example the ζ parameter for 2s1/2-2p1/2 transition has a maximum value of .275 at 136eV, whereas for the 2s1/2-2p3/2 transition ζ has the range of values of 8.12 at 136eV to .14 at 2.04keV. The screening factor $e^{-\pi|\zeta|}$ is much smaller for the 2s1/2-2p3/2 transition than the corresponding factor for the 2s1/2-2p1/2 transitions the latter cross section is therefore larger than the former over the given energy range. Extension of our calculations over a wider energy range and for ions of different charges is now in progress.

REFERENCES

Alder, K., Bohr, A., Huus, T., Mottelson, B., and Winther, A. 1956, Rev. of Modern Physics, 28, 432.

Beigman, I.L., Burreva, L.A. and Skobelev, I.Yu. 1979, Astron. Zh. 56, 1281(Sov. Astron. 23, 725).

Boiko, V.A., Faenov, A.Ya., Pikuz, S.A. and Safronova, U.I. 1977, Mon. Not. R. Astron. Soc. 181, 107.

Grineva, Yu.I., Karev, V.I., Korneev, V.V., Krutov, V.V., Mandelstam, S.L., Vainstein, L.A., Sasilyev, B.N., and Zhitnik, I.A. 1973, Solar Phys. 29, 441.

Källne, E., Källne, J., and Rice, J.E. 1982, Phys. Rev. Lett. 49, 330.

Ljepojevic, N.N., Hutcheon, R.J., and McWhirter, R.W.P. 1984, J. Phys. B. 17, 3057.

Vinogradov, A.V., Skobelev, I.Yu. and Yukov, E.A. 1977, Fiz. Plazmy. 3, 686.

Wiese, W.L., Smith, M.W., and Glenon, B.M. 1966, Atomic Transition Probabilities Vol. 1 NSRDS-NBS4 (US Gov. Printing Office).

Table I. Proton-Impact excitation cross sections (cm^2) for the n=2 sublevels in Ar^{+17}

ENERGY	$\sigma(2s1/2\rightarrow 2p1/2)$	$\sigma(2s1/2\rightarrow 2p3/2)$	$\sigma(2p1/2\rightarrow 2p3/2)$
136eV	1.3×10^{-15}	2.8×10^{-20}	$< 10^{-20}$
271eV	1.0×10^{-15}	1.8×10^{-19}	1.5×10^{-19}
544eV	6.4×10^{-16}	1.3×10^{-17}	1.2×10^{-17}
980eV	4.0×10^{-16}	5.2×10^{-17}	2.6×10^{-17}
1.52keV	2.6×10^{-16}	8.3×10^{-17}	2.8×10^{-17}
2.04keV	2.0×10^{-16}	9.8×10^{-17}	2.4×10^{-17}

*This work was supported in part by the United States Department of Energy, Division of Chemical Sciences.

CHARGE STATE DISTRIBUTION MEASUREMENT IN AN ECR-DISCHARGE BY VUV-SPECTROSCOPY

E.H. Marlinghaus and K. Wiesemann
Institut für Experimentalphysik AG II
Ruhr-Universität Bochum
D-4630 Bochum, FRG

The charge state distribution of multiply charged Ar ions in an electron cyclotron resonance (ECR) heated microwave discharge (Bernhardi et al. 1976) was measured by means of VUV-spectroscopy in the wavelength region $\lambda \leq 100$ nm (Marlinghaus 1984). Ion densities were computed from absolute line intensities in a modified corona model. Assuming electron impact excitation of groundstate ions to play the major role and neglecting all other processes leading to excitation, the ion density n_z is given by

$$n_z = \phi_{jo} / (n_e \langle \sigma_z^j v_e \rangle \cdot \varepsilon(\lambda) \cdot \Delta\Omega / 4\pi) . \qquad (1)$$

In order to obtain ion densities from equ. (1) six quantities have to be measured or calculated absolutely:

1) the electron impact excitation cross section σ_z^j of the transition $j \rightarrow o$ of ion in charge state z,
2) the efficiency ε of the VUV-spectrometer as a function of the wavelength λ,
3) the solid angle $\Delta\Omega$,
4) the volume emission coefficient ϕ_{jo} which is proportional to the count rate integrated over the width of a line,
5) the electron distribution function $f(v_e)$,
6) the electron density n_e.

The excitation cross sections were calculated in a semi empirical Gaunt factor approximation given by Regemorter (1962). The absolute spectrometer efficiency was obtained using the branching ratio method. Calibration in the visible wavelength region was done with a tungsten strip lamp. Using an entrance slit of 10 µm width the geometrical acceptance angle was used in the calculations. Spectra were recorded with a channeltron detector using photon counting techniques. Ar charge states upto Ar VII have been measured. Due to the lack of atomic data (oscillator strength) charge states upto Ar VI were evaluated. The experimental setup is shown schematically in fig. 1.

The electron distribution f(v) parallel to the magnetic field was measured with an electrostatic energy analyser (similar to that described by Puri 1974) in the mirror throat of the discharge. Assuming f(v) to be isotropic, f(v) was evaluated from the second derivative of the probe characteristic. As found earlier by x-ray spectroscopy in the energy region 3 keV $\leq E \leq$ 22 keV (Ziemann 1983) and in the region 10 keV $\leq E \leq$ 350 keV (Bernhardi and Wiesemann 1982)

the electron energy distribution function f(E) below 2 keV followed a power law $f(E) \sim E^{-s}$, the spectral index s depending on the discharge conditions (pressure, microwave power) and varying from 1 to 4.

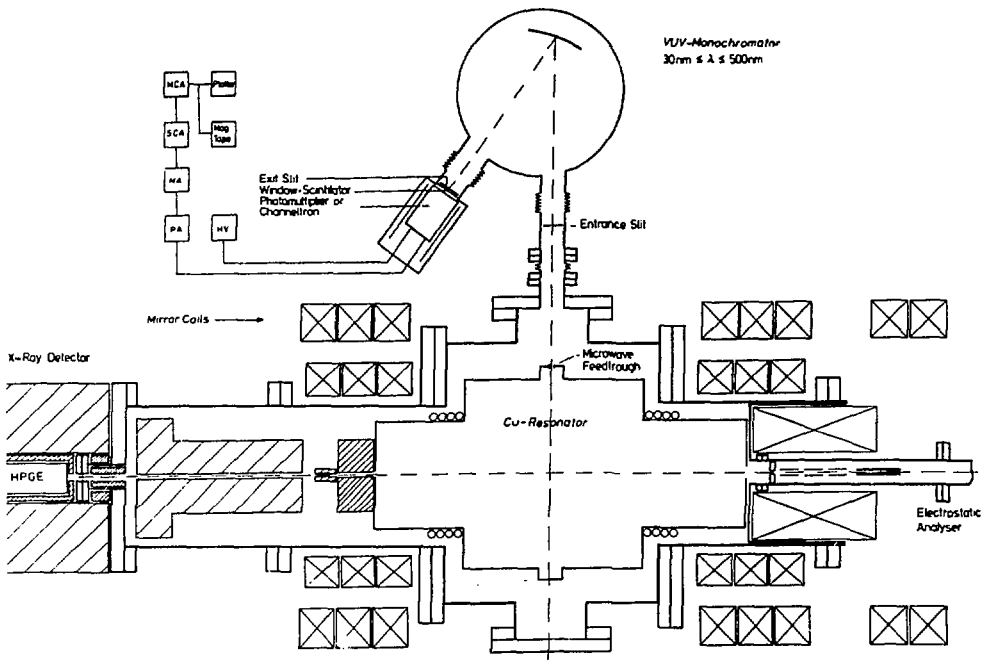

Fig. 1 Experimental setup of the ECR-experiment
Abbreviations are PA, MA = pre-,main amplifier, SCA, MCA = single-multichannel analyser, HV = high voltage power supply

Using Regemorter's cross sections and the measured distribution functions, excitation rate coefficients were calculated by numerical integration (Marlinghaus 1984). Electron density n_e was deduced from the condition of quasineutrality of the plasma

$$n_e = \sum_z z\, n_z . \qquad (2)$$

A typical measured charge state distribution is shown in fig. 2. The highest density is that of the Ar^{2+} ion. Assuming a homogenous stationary plasma it follows from particle balance calculations, that the plasma is fully ionised (Hesse 1983). Processes which are included in these calculations are

i) single, multiple and step-ionisation of atoms and ions by electron impact,
ii) charge exchange collisions between Ar atoms and ions and
iii) diffusion of ions to the wall.

The solution of the balance equation was fitted to measured

ion densities by varying two fit parameters $n_o/n_e\sqrt{kT_i}$ and $n_e\tau$ (n_o = density of the neutrals, kT_i = ion temperature, $\tau = \tau_z$ = the ion's mean diffusion time to the wall). The first parameter gives a measure for the influence of charge exchange collisions, the second parameter describes the role of step-ionisation via the plasma life time τ. Results are plotted in fig. 2.

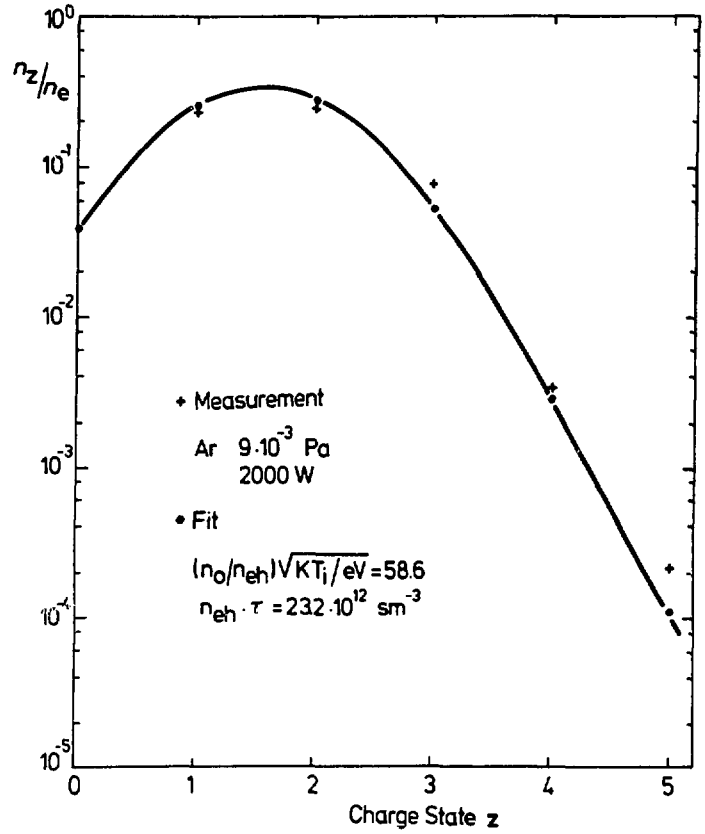

Fig. 2 Typical measured (crosses) and calculated (dots) charge state distribution. For simplicity absolutely measured ion densities are normalized to electron density. The fit yields for the neutrals $n_o/n_e = 0.04$.

Electron density is determined from (2) as $n_e = 1.1\cdot10^{17}m^{-3}$. Assuming $n_o/n_e = 0.04$ as given by the fit, one would be forced to assume unreasonably high ion temperatures. Spectroscopic measurements of the neutral density n_o yield $n_o = 1.3\cdot10^{18}m^{-3}$, pressure measurement yields $1.6\cdot10^{18}m^{-3}$. From these values one obtains $(n_o/n_e)_{exp}\sim15$ in spite of $(n_o/n_e) = 0.04$ from the fit. From this figure an ion temperature of $kT_i \sim 15$ eV is deduced which is reasonable. The solution of this contradiction is obtained by considering the time behaviour of the plasma.

Time resolved measurement show, that about 10 ms after ignition of the plasma the concentration of wall material (Cu) increases strongly while the Ar ion densities go sharply down. So we believe, that a short living fully ionised plasma is driven by an instability to the wall, sputtering wall material. Since the plasma Ar ions are neutralized at the wall, there will be a cold plasma wall boundary containing essentially neutral Ar and neutral Cu atoms. When ions from the hot plasma drift through this cold boundary layer, charge exchange reactions may become important as shown earlier (Marlinghaus et al. 1983).

The uncertainty of the ion densities is determined by the uncertainties of the quantities listed below equ. (1) and is estimated by ± 45 % relative and a factor of 2.5-3 absolute. The main contributions come from the spectrometer efficiency (± 30 % relative, factor 2 absolute) and the excitation rate coefficients. Regemorter estimates the absolute uncertainty of his excitation cross sections by a factor of 2 in the threshold region. Because of the flat form of the measured electron distribution functions (power law), the low energy contribution to the rate coefficients is small. For the same reason the influence of putting the effective Gaunt factor for ions $\bar{g}$ = 0.25 or 0.3 instead of 0.2 as discussed by Regemorter is small (± 3 %, + 13 % resp.). We estimate the uncertainty of rate coefficients ± 30 %, but the uncertainty of the oscillator strength used in the calculation (± 25...± 50 %) has to be added. It would be highly desirable that f-values for more lines were known with higher accuracy.

REFERENCES

Bernhardi, K. et al. 1976, Plasma Physics, 18, 77
Bernhardi, K. Wiesemann, K. 1982, Plasma Physics, 24, 867
Hesse, J. 1983, Thesis, Bochum
Marlinghaus, E.H., Huber, B.A., Wiesemann, K. 1983, Ann. Israel Phys. Soc., 6, 94
Marlinghaus, E.H. 1984, Thesis, Bochum
Marlinghaus, E.H. 1984, SFB-Report 84-05-120, Bochum
Puri, S. 1984, Plasma Physics, 16, 517
Regemorter, H. van 1962, Astrophys. J., 136, 3, 906
Ziemann, K. 1983; Diplomarbeit, Bochum

CRITICAL COMPILATIONS OF ATOMIC ENERGY LEVELS*

J. Sugar, W.C. Martin, J. Reader, A. Musgrove, and C. Corliss**
National Bureau of standards
Washington, DC 20234

We have been publishing new compilations of energy levels for single elements in all stages of ionization as each is completed. Those now in print in the Journal of Physical and Chemical Reference Data are helium (1973), sodium (1981), magnesium (1980), aluminum (1979), silicon (1983), potassium (1979), calcium (1979), scandium (1980), titanium (1979), vanadium (1978), chromium (1977), manganese (1977), iron (1982), cobalt (1981) and nickel (1981). A volume containing atomic energy levels of all rare earth elements was issued in 1978. We have now updated our compilations for the iron period (K through Ni, 235 spectra), which will be published in a single volume.

We also publish bibliographies of references dealing with atomic energy level and wavelength data. The last bibliography appeared in 1980 and covered the period July 1975 through June 1979. Our next supplement will extend through Dec. 1983. Work continues on the table of wavelengths for atoms in the first five ionization stages, published as NSRDS-NBS 68, with updated tables given annually in the Handbook of Chemistry and Physics.

Our bibliographic files are kept up-to-date with the current literature, and we serve as an information center on atomic energy level and wavelength data. Our published compilations are kept in a computer data base, and selected portions may be made available on magnetic tape or hard copy.

*Partially supported by Division of Magnetic Fusion Energy, Department of Energy, and by Astronomy/Relativity Branch, National Aeronautics and Space Administration

**Present address: Forest Hills Laboratory, 2955 Albermarle St., NW, Washington, DC 20008

CRITICAL COMPILATIONS OF ATOMIC TRANSITION PROBABILITIES*

G. A. Martin, J. R. Fuhr, and W. L. Wiese
Center for Radiation Research
National Bureau of Standards
Gaithersburg, Maryland 20899

INTRODUCTION

The NBS Data Center on Atomic Transition Probabilities is nearing completion of a critical compilation of atomic transition probability data on allowed and forbidden transitions in the elements scandium through nickel in all stages of ionization. This compilation constitutes a revision of a series of smaller NBS compilations published in recent years in the Journal of Physical and Chemical Reference Data. Upon completion of this project, work on updating of an even earlier compilation covering the elements hydrogen through neon will be initiated.

The world literature on atomic transition probabilities is collected and catalogued on an ongoing basis by the Data Center. A master reference list is maintained, and annotated bibliographies are issued as the number of new articles in the literature and the resources of the Center permit. A computerized bibliographic database system is being developed to enhance the capability for handling bibliographical information in the NBS data centers on transition probabilities, line shapes and shifts, and energy levels. Development of a computerized database of critically evaluated numerical data on atomic spectroscopic quantities is planned for the future.

Exchange of information between the Center staff and both producers and users of transition-probability data is encouraged. User services include responding to requests for data and new references (those not yet included in a published bibliography), reception of visitors to the Center for use of the files, and consultation on technical matters. Receipt of research results from professionals in the field in advance of publication is welcomed.

LIST OF PUBLICATIONS

1. W. L. Wiese, M. W. Smith, and B. M. Glennon
"Atomic Transition Probabilities (H through Ne--A Critical Data Compilation)," Nat. Stand. Ref. Data Ser., Nat. Bur. Stand. (U.S.) 4, Vol. I (U.S. Government Printing Office, Washington, D.C., 1966).

2. W. L. Wiese, M. W. Smith, and B. M. Miles
"Atomic Transition Probabilities (Na through Ca--A Critical Data Compilation)," Nat. Stand. Ref. Data Ser., Nat. Bur. Stand. (U.S.) 22, Vol. II (U.S. Government Printing Office, Washington, D.C., (1969).**

3. B. M. Miles and W. L. Wiese
"Critically Evaluated Transition Probabilities for Ba I and II," Nat. Bur. Stand. (U.S.) Tech. Note 474 (U.S. Government Printing Office, Washington, D.C., 1969); At. Data 1, 1-17 (1969).

4. M. W. Smith and W. L. Wiese
"Graphical Presentations of Systematic Trends of Atomic Oscillator Strengths Along Isoelectronic Sequences and New Oscillator Strengths Derived by Interpolation," Astrophys. J. Suppl. Ser. 23, #196, 103-192 (1971).

5. J. R. Fuhr, W. L. Wiese, and L. J. Roszman
"Bibliography on Atomic Line Shapes and Shifts (1889 through March 1972)," Nat. Bur. Stand. (U.S.) Spec. Publ. 366 (U.S. Government Printing Office, Washington, D.C., 1972).

6. M. W. Smith, G. A. Martin, and W. L. Wiese
"Systematic Trends and Atomic Oscillator Strengths," Nucl. Instrum. Methods 110, 219-226 (1973).

7. M. W. Smith and W. L. Wiese
"Atomic Transition Probabilities for Forbidden Lines of the Iron Group Elements (A Critical Data Compilation for Selected Lines)," J. Phys. Chem. Ref. Data 2, 85-120 (1973).

8. J. R. Fuhr, L. J. Roszman, and W. L. Wiese
"Bibliography on Atomic Line Shapes and Shifts (April 1972 through June 1973)," Nat. Bur. Stand. (U.S.) Spec. Publ. 366, Suppl. 1 (U.S. Government Printing Office, Washington, D.C., 1974).

9. W. L. Wiese and J. R. Fuhr
"Atomic Transition Probabilities for Scandium and Titanium (A Critical Data Compilation of Allowed Lines)," J. Phys. Chem. Ref. Data 4, 263-352 (1975).

10. J. R. Fuhr, G. A. Martin, and B. J. Specht
"Bibliography on Atomic Line Shapes and Shifts (July 1973 through May 1975)," Nat. Bur. Stand. (U.S.) Spec. Publ. 366, Suppl. 2 (U.S. Government Printing Office, Washington, D.C., 1975).

11. N. Konjevic and W. L. Wiese
"Experimental Stark Widths and Shifts for Non-Hydrogenic Spectral Lines of Ionized Atoms (A Critical Review and Tabulation of Selected Data)," J. Phys. Chem. Ref. Data 5, 259-308 (1976).

12. N. Konjevic and J. R. Roberts
"A Critical Review of the Stark Widths and Shifts of Spectral Lines from Non-Hydrogenic Atoms," J. Phys. Chem. Ref. Data 5, 209-257 (1976).

13. G. A. Martin and W. L. Wiese
"Tables of Critically Evaluated Oscillator Strengths for the Lithium Isoelectronic Sequence," J. Phys. Chem. Ref. Data 5, 537-570 (1976).

14. W. L. Wiese and S. M. Younger
"Atomic Oscillator Strengths in Fusion Plasma Research," Beam-Foil Spectroscopy, Vol. 2, pp. 951-960 (Plenum Publishing Corp., New York, N.Y., 1976).

15. G. A. Martin and W. L. Wiese
"Atomic Oscillator Strength Distributions in Spectral Series of the Lithium Isoelectronic Sequence," Phys. Rev. A 13, 699-714 (1976).

16. J. R. Fuhr, B. J. Miller, and G. A. Martin
"Bibliography on Atomic Transition Probabilities (1914 through October 1977)," Nat. Bur. Stand. (U.S.) Spec. Publ. 505 (U.S. Government Printing Office, Washington, D.C., Apr. 1978).

17. S. M. Younger, J. R. Fuhr, G. A. Martin, and W. L. Wiese
"Atomic Transition Probbilities for Vanadium, Chromium, and Manganese (A Critical Data Compilation of Allowed Lines)," J. Phys. Chem. Ref. Data 7, 495-630 (1978).

18. J. R. Fuhr, B. J. Miller, and G. A. Martin
"Bibliography on Atomic Line Shapes and Shifts (June 1975 through June 1978)," Nat. Bur. Stand. (U.S.) Spec. Publ. 366, Suppl. 3 (U.S. Government Printing Office, Washington, D.C., 1978).

19. B. J. Miller, J. R. Fuhr, and G. A. Martin
"Bibliography on Atomic Transition Probabilities (November 1977 through March 1980," Nat. Bur. Stand. (U.S.), Spec. Publ. 505, Suppl. 1 (U.S. Government Printing Office, Washington, D.C., Aug. 1980).

20. W. L. Wiese and G. A. Martin
"Wavelengths and Transition Probabilities for Atoms and Atomic Ions," Nat. Stand. Ref. Data Ser., Nat. Bur. Stand. (U.S.) 68, Part II. "Transition Probabilities" (U.S. Government Printing Office, Washington, D.C., 1980).

21. J. R. Fuhr, G. A. Martin, W. L. Wiese, and S. M. Younger
"Atomic Transition Probabilities for Iron, Cobalt, and Nickel (A Critical Data Compilation of Allowed Lines)," J. Phys. Chem. Ref. Data 10, 305-565 (1981).

22. W. L. Wiese and G. A. Martin
"Atomic Transition Probabilities," CRC Handbook of Chemistry and Physics, 63rd Edition, E334-E369 (CRC Press, Inc., Boca Raton, FL, 1982).

WORK IN PROGRESS

1. G. A. Martin, J. R. Fuhr, and W. L. Wiese
"Atomic Transition Probabilities (Sc through Ni--A critical Data Compilation)," J. Phys. Chem. Ref. Data, Suppl. (in preparation).

2. N. Konjevic, M. S. Dimitrijevic, and W. L. Wiese,
"Experimental Stark Widths and Shifts for Spectral Lines of Positive Ions (A Critical Review and Tabulation of Selected Data for the Period 1976 to 1982)", J. Phys. Chem. Ref. Data 13 (1984). [in press]

3. N. Konjevic, M. S. Dimitrijevic, and W. L. Wiese, "Experimental Stark Widths and Shifts for Spectral Lines of Neutral Atoms (A Critical Review of Selected Data for the Period 1976 to 1982)", J. Phys. Chem. Ref. Data 13 (1984). [in press]

SERVICES

Data, references, and technical information are supplied by the Center staff. Researchers who are interested in utilizing the services of the Center are invited to contact Georgia A. Martin, Jeffrey R. Fuhr, or Wolfgang L. Wiese either by mail or telephone [(301) 921-2071; FTS: 921-2071)].

*Supported in Part by the Astrophysics Division of the National Aeronautics and Space Administration.

** Volume II of the NBS critical data compilation of atomic transition probabilities [W. L. Wiese, M. W. Smith, and B. M. Miles, Atomic Transition Probabilities--Sodium through Calcium, Nat. Stand. Ref. Data Ser., Nat. Bur. Stand. (U.S.) 22 (Oct. 1969)] is out of print. However, it can be purchased in hardcover form (photostatic copy) or microfiche from the National Technical Information Service (NTIS), order #AD 696 884. For information on current price and method of payment, contact NTIS directly: Telephone (703) 487-4650, National Technical Information Service, U.S. Department of Commerce, 5285 Port Royal Road, Springfield, VA 22161

XUV AND SOFT X-RAY RADIATION FROM LASER PRODUCED PLASMAS AS LABORATORY SPECTROSCOPIC SOURCES*

P. Gohil, M.L. Ginter and T.J. McIlrath
University of Maryland, IPST
College Park, MD 20742

H. Kapoor, D. Ma and M.C. Peckerar
Naval Research Laboratory
Washington, DC 20375-5000

Laser produced plasmas have been shown to be excellent sources for applications in the XUV and soft X-ray spectral region. We are using a 550 mj, 25 ns (FWHM) ND:YAG laser operating at a repetition rate of 10 Hz to produce plasmas above rotatable solid targets. The focal spot of the laser beam with a 31 cm lens was measured to be 170μm (approximately twice the diffraction limit), using a diode array having a 17μm resolution. Broadband output in the soft X-ray region was studied using a windowless PIN photodiode with an Al_2O_3 surface covered with a polyethylene filter with transmission between 44 Å and 120 Å. Results are presented for the source's soft X-ray intensity for several elements as a function of laser energy, focus and driving wavelength, as are preliminary results using the source for high resolution spectroscopy and for soft X-ray lithography.

*Work supported by Air Force grant AFOSR F49620-83-C-0130. P. Gohil acknowledges support from SERC (UK).

REFERENCES

Carroll, P.K., Kennedy, E.T., and O'Sullivan, G., 1980, App. Opt., 19, 1454.

Nagel, D.J., Brown, C.M., Peckerar, M.C., Ginter, M.L., Robinson, J., McIlrath, T.J., and Carroll, P.K., May 1984, App. Opt., 23, 1428.

Theoretical Calculation of X-ray Emission from Laser-Produced Plasmas*

D. Duston, R.W. Clark, and J. Davis
Naval Research Laboratory
Washington, D.C.

The interaction of an intense short-wavelength laser beam with a solid foil target is a topic which has been studied vigorously for many years. Many inherent problems still exist, however, in our understanding of observed experimental data. In particular, the problem of transport through the target material of the deposited laser energy continues to be the focus of many investigations. Although most of the work has been dominated by particle transport phenomena, it was shown in a previous paper[1] that radiation processes and photon transport often play a major role in the redistribution of the deposited energy in laser driven plasmas. In this presentation, we continue our investigation of the role of atomic physics and radiative emission in laser-produced plasmas by studying the effects of these physical processes as a function of varying initial conditions for both aluminum and carbon foil targets.

The main computational tool employed in this study was a 1-D radiation/hydrodynamics model in which the fluid equations conserving mass, momentum, and energy are solved self-consistently with the ionization dynamics and radiation transport to yield accurate information regarding the interaction between photons and plasma particles.

The ionization model is based on collisional-radiative equilibrium (CRE) in which the population densities of ground and excited states are calculated by considering the most important particle and photon collisional processes populating them and solving for a time-independent solution of the set of atomic rate equations. A detailed atomic level structure for aluminum is used which includes all 14 ground states, 84 excited levels, 97 free-bound continuum edges, and 144 averaged emission lines (more than 3000 $n\ell$-$n'\ell'$ transitions have been included).

The carbon model has not been as thoroughly documented as the aluminum one but includes all 7 ground states, 50 excited states, 56 free-bound continuum edges, and 107 averaged emission lines. The level structure for carbon is as complete as for aluminum but, of course, it has fewer ions and consequently fewer excited states and lines. The collisional processes treated in the model include electron impact excitation and deexcitation, electron impact ionization and recombination, radiative recombination, dielectronic recombination, and spontaneous radiative decay. The radiation transport algorithm is based on a combination of probabilistic and frequency-by-frequency ray trace techniques and takes account of photoionization, inverse bremsstrahlung (of non-laser photons), photoexcitation and stimulated emission processes. Of extreme importance in stopping the soft x-rays in the dense foil regions is inner-shell opacity due to photoionization of inner-orbit electrons. This is treated along with the valence-electron

photoionization scheme in a unique way that allows the absorption edges to shift as the dense region heats up and ionizes. The opacity calculation is solved iteratively at each time step with the ionization calculation. Thus, the radiative transfer scheme treats opacity in the plasma self-consistently with the ionization dynamics and hydrodynamics.

In this study, six seperate calculations were performed; in each, one parameter (laser irradiance, laser wavelength, target material, laser pulse width, or target thickness) was varied from the "standard calculation" in which the initial conditions were assumed to be 10^{13} watts/cm^2, 0.35 μm laser light, 3.0 nsec pulse width (fwhm), and an 8.0 μm-thick aluminum foil target.

Several important conclusions were reached based on the results of these calculations. First, it was verified that the radiation emitted from the plasma is a major energy loss mechanism, accounting for 27-38% of the deposited laser energy for the aluminum targets over the parameter range studied. In addition, the radiation conversion efficiency for the carbon target calculation was 28%, putting to rest the previous belief held throughout the community that radiation was negligible when studying thin carbon targets.

Second, it was found that the radiation spectrum obtained from the rearside of the foil was strongly dependent on initial conditions. In particular, low-energy ($h\nu < 100$eV) bremsstrahlung photons are emitted directly from the backside of the target, and their spectral distribution and intensity directly reflects the plasma temperature of this region. Thus, as the foil thickness, material, and laser irradiance are changed, the rearside spectrum responds drastically.

Finally, interesting effects on the plasma profiles were found by neglecting the radiation loss term in the energy equation and turning off the photon transport. Comparisions of the calculations with and without radiation showed clear and rather significant differences in the plasma density and temperature profiles. The region containing the laser critical surface is the point of greatest emission; thus, the cooling effect of the radiation here markedly reduces the local temperatures. The resulting effect on the local density is to reduce the gradient substantially in the ablation region, increasing the ablation surface-to-critical surface seperation. Of course, this parameter is a very important one in the calculation of thermal conduction, lateral thermal smoothing, and fluid instability growth. This casts doubt on the results of a calculation which employs only approximate ionization-radiation models or, worse, neglects the impact of radiation on the plasma totally.

[1] D. Duston, R. W. Clark, J. Davis, and J. P. Apruzese, Phys. Rev. A 27, 1441 (1983).

*Supported by the Office of Naval Research.

INTERPRETATION OF PSEUDOCONTINUA IN THE SPECTRA OF HIGHLY IONIZED ATOMS FROM Tm TO W IN LASER PRODUCED PLASMAS

P. Mandelbaum, M. Klapisch, A. Krasnitz
Racah Institute of Physics
Hebrew University
91904 Jerusalem, Israel

and

A. Zigler
Soreq Nuclear Center
76400 Yavne, Israel

X-ray spectra of highly ionized atoms (Tm to Pt) emitted from Laser produced plasma are characterized by the simple structure given by resonant transitions of the NiI-like ions, accompanied by the more complex pattern of satellite transitions emitted by ions in the neighbouring states of ionization. An analysis of these structures has been given recently for the satellites of the $3d^{10}$-$3d^{9}4p$[1] and of the $3p^{6}3d^{10}$ - $3p^{5}3d^{10}4s$, 4d[2] transitions of the NiI-like ions. However, most of the radiation emitted in this spectral range [4-10Å] concentrate in a wide, rather structureless satellite feature in the long wavelength side of the $3d^{10}$-$3d^{9}4f$ Ni-I like transition, on which some lines are superimposed. Line identification has been achieved successfully with the methods of [1], [2] and will be published separately. In this communication, we deal only with the pseudocontinuum.

THE PSEUDOCONTINUUM

a. Origin of the pseudocontinuum

The electronic temperature T_e in the plasma (> 1000 eV) is sufficient to populate noticeably configuration where one 3d and some external electrons of the n = 4 shell are excited simultaneously e.g. the configuration $3d^{9}4s4p4f$ in ZnI-like that will give an observable transition to $3d^{10}4s4p$. But as the ℓ and the number of the spectator electrons get higher, so do the complexity of the transition which degenerates into Unresolved Transitions Arrays (UTA) forming a large pseudocontinuum.

b. Computation of the mean wavelength and width of the UTA.

Computation of mean wavelength and width of UTA, assuming Gaussian shape can be performed in our case using simple formula [3]. In fig. 1 a comparison is made between ab-initio computation of the whole CuI-like $3d^{9}4f4p$-$3d^{10}4p$ array in Tm XLI (curve 1) and the UTA computation assuming Gaussian distribution (curve 2). As can be seen, the assumption of Gaussian distribution is wrong because the array is spin-orbit splitted into three different groups, according to the three $3d^{9}_{j}4f_{j}$ -$3d^{10}$ transitions. In this case the 4p spectator electron contributes to the width of each individual group only. Now, new formulas have been developed [4] which enable computing of mean wavelength and width of each splitted array, assuming j-j coupling. The results of these formulas are presented here for the first time. Table 1 gives the computation of the spin-orbit-splitted arrays (S.O.S.A.) of 3 transitions for four state of ionization of Tm. Curve 3 in fig. 1 shows these results for the $3d^{9}4f4p$-$3d^{10}4p$ case. Departure from pure j-j coupling cause a little shift in

the mean wavelength of the splitted array although the width is well reproduced. To take account of the off diagonal matrix element, the mean wavelength for all the computed transition for the different ionization state has been shifted by the same amount measured in fig. 1.

c. Width of the all pseudocontinuum

The width of the pseudocontinuum is directly connected to the number of state of ionization that emits in this part of the spectrum. Indeed, for each ionization state, it has been shown [4] that the mean wavelength of each S.O.S.A. is independent of the nature of the satellite electrons in a central field approximation and thus the different transitions, in the same state of ionization are blended. Moreover, it can be seen from table 2 that only for the four state of ionization CuI, ZnI, GaI and GeI do the 3d-4f transition correspond to an energy smaller than the ionization potential. The overall width of the pseudocontinuum is thus limited by the contribution of these four states of ionization.

d. Intensity

Assuming LTE the intensity ratio of the S.O.S.A. would approximately be in the proportion 10:2.5:0.01 for the $[\frac{3}{2}, \frac{5}{2}]$, $[\frac{5}{2}, \frac{7}{2}]$ and $[\frac{5}{2}, \frac{5}{2}]$ S.O.S.A. However, the laser produced plasma is optically thick for some transitions and we use here a simple model for estimating the effect of absorption [5]. Each transition probability is multiplied by a function

$$T(\tau) = \frac{1}{\tau\sqrt{\pi}} \int_{-\infty}^{+\infty} (1-e^{-\tau e^{-y^2}}) \, dy,$$

where τ is the optical thickness of the plasma for the center of the line. For large τ ($\tau \simeq 200$ for the strongest transition in our case)

$$T(\tau) \propto \frac{1}{gf}$$

and the resulting intensity is nearly independent of gf. For this reason the theoretical intensities in fig. 2 are just taken as free parameters, whereas the width and the positions of the S.O.S.A. are calculated ab-initio.

CONCLUSION:

New formulas were used for spin-orbit splitted arrays (S.O.S.A.) and applied to laser produced spectra of Tm. There is good agreement with experiment for the position and width of transition arrays, allowing doubtless identification of the pseudocontinuum.

REFERENCES

[1] Mandelbaum P., Klapisch M., Bar-Shalom A., Schwob J.L. and Zigler A., 1983, Phys. Scripta, 27, 39.

[2] Mandelbaum, P., Klapisch, M., Bar-Shalom, A., Schwob, J.L. and Zigler, A., 1983, Phys. Letter, 99A, 84.

[3] Bauche-Arnoult, C., Bauche, J., and Klapisch, M., 1982, Phys. Rev. A. 25, 2641.

[4] Bauche-Arnoult, C., Bauche, J., and Klapisch, M., 1984, submitted to Phys. Rev. A.

[5] Schwob, J.L., 1969, rapport CEA-R-3379, 17.

Table I. S.O.S.A. calculations for 3d-4f transitions in Tm XLI - Tm XXXVIII (Results in Å)

I.S.	Transition	(3/2-5/2) $\bar{\lambda}$	(3/2-5/2) $\Delta\lambda$	(5/2-7/2) $\bar{\lambda}$	(5/2-7/2) $\Delta\lambda$	(5/2-5/2) $\bar{\lambda}$	(5/2-5/2) $\Delta\lambda$
Cu I	$3d^9 4s4f - 3d^{10} 4s$	6.969	0.007	7.117	0.008	7.231	0.019
	$3d^9 4p4f - 3d^{10} 4p$		0.020		0.017		0.036
	$3d^9 4d4f - 3d^{10} 4d$		0.035		0.045		0.073
Zn I	$3d^9 4s4p4f - 3d^{10} 4s4p$	7.017	0.021	7.166	0.021	7.280	0.041
	$3d^9 4s4d4f - 3d^{10} 4s4d$		0.036		0.046		0.076
	$3d^9 4p^2 4f - 3d^{10} 4p^2$		0.026		0.025		0.045
Ga I	$3d^9 4s^2 4p4f - 3d^{10} 4s^2 4p$	7.065	0.020	7.217	0.020	7.329	0.036
	$3d^9 4s^2 4d4f - 3d^{10} 4s^2 4d$		0.036		0.045		0.074
	$3d^9 4s4p^2 4f - 3d^{10} 4s4p^2$		0.027		0.027		0.050
Ge I	$3d^9 4s^2 4p^2 4f - 3d^{10} 4s^2 4p^2$	7.114	0.026	7.272	0.026	7.379	0.053
	$3d^9 4s^2 4p4d4f - 3d^{10} 4s^2 4p4d$		0.041		0.050		0.083
	$3d^9 4s4p^3 4f - 3d^{10} 4s4p^3$		0.028		0.028		0.053

Table 2. Ionization potential vs. 3d-4f mean energy (a.u.)

I.S.	Ionization pot.	3d-4f mean energy
CuI	71.469	63.779
ZnI	69.446	63.317
GaI	64.715	62.888
GeI	62.672	62.484
AsI	58.471	62.060

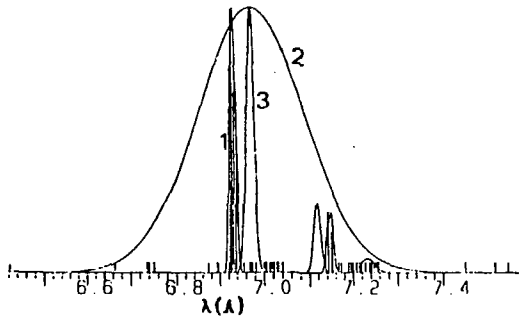

Fig.1. $3d^9 4f4p - 3d^{10} 4p$ transition in TmXLI
1. ab-initio relativistic full calculation
2. U.T.A. calculation assuming gaussian shape
3. S.O.S.A. calculation

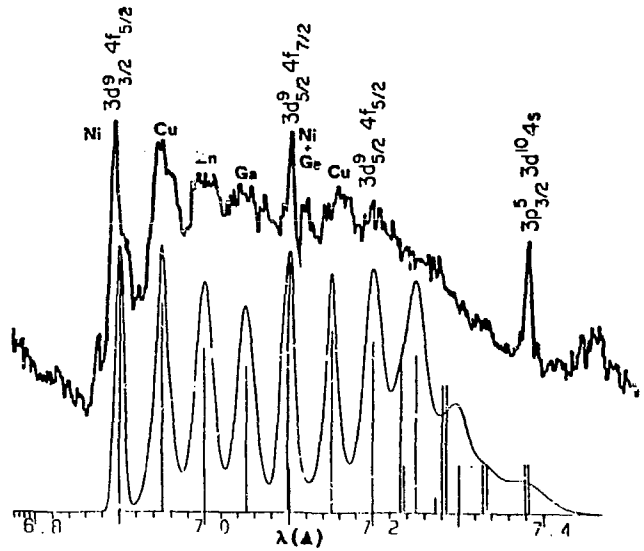

Fig.2. 3d-4f spectrum of Tm

X-RAY MEASUREMENTS FROM THE TANDEM MIRROR EXPERIMENT-UPGRADE (TMX-U)*

E.H. Silver, J.F. Clauser, and B.H. Failor
Lawrence Livermore National Laboratory
University of California
Livermore, CA 94550

We report the results of X-ray emission measurements made at various plasma locations in the Tandem Mirror Experiment-Upgrade (TMX-U). By manipulating the electron and ion density profiles within the magnetic mirror end cells, a local minimum in the axial electrostatic potential creates a barrier that thermally isolates central cell electrons from those in the end cells. This thermal barrier makes it possible to heat end cell electrons to a temperature (~1.6 keV) that is significantly higher than the central cell value (30 to 200 eV), thereby increasing the ion confining potential. Formation of this potential peak is attributable, in part, to mirror-trapped hot ions (8 keV) that are injected as beams of neutral particles. The resulting ion density profile exhibits two symmetric peaks at the locations of the ion turning points and a depression where the magnetic field is a minimum. Electron cyclotron resonance heating (ECRH) is applied at the density minimum and produces a population of hot, mirror-trapped electrons (20 to 200 keV). It reduces an already depressed electrostatic potential to establish the thermal barrier. In addition, ECRH applied at the outer density peak raises the ion confining potential and enhances central cell ion confinement by increasing the end cell electron temperature. X-ray measurements are made with solid state and scintillation detectors at the ECRH locations. Medium resolution spectra are obtained over a broad energy band and have proven to be an important tool for determining the efficiency of thermal barrier formation. We present our initial findings from these non-Maxwellian plasmas.

*Work performed under the auspices of the U.S. Department of Energy by the Lawrence Livermore National Laboratory under contract number W-7405-ENG-48.

ELECTRON CAPTURE INTO EXCITED STATES FOR $Al^{8+} + H_2$ COLLISIONS AT 3 keV/amu

M. Mayo, D. Hitz, M. Druetta, S. Dousson,
J.P. Desclaux, and S. Bliman
AGRIPPA GIS, CEA/CNRS, C.E.N.G.
85 X, 38041 Grenoble, France

The MINIMAFIOS ECR source at Grenoble has recently produced stable beams of highly charged Al.[1] We have studied electron capture into excited states for Al^{8+} ions extracted at 10 kV colliding with an H_2 molecular target under single collision conditions. Using a grazing incidence spectrometer covering the region 250 Å to 1100 Å, we have made a relative intensity measurement of the radiative decay from excited (nl) states of Al^{7+} following the charge exchange collision. The Al^{7+} spectra show known transitions from the $1s^2 2s 2p^3$ excited state. We discuss the presence of the $1s^2 2s 2p^2 (^4P)$ metastable state in the incidence Al^{8+} beam. The spectra also show many transitions which up to now are unidentified, in particular transitions for the wavelength region between 300 and 400Å and that between 600 and 700Å. To identify the transitions, we compare our spectrum with preliminary theoretical wavelengths calculated using the multiconfiguration Dirac-Fock method including transitions from n = 3, 4 and 5. These preliminary results reveal transitions from n = 5 to 4 for the observed spectra in the 600Å region and transitions from n = 4 to 3 for the observed spectra in the 300Å region.

REFERENCE

[1] Chetioui, A., Delaunay, M., Dousson, S., Geller, R., Jacquot, B., Hitz, D., Vernhet, D., to be published, Nuclear Instruments and Methods.

POPULATION OF EXCITED STATES OF AL^{10+} IN A PLASMA BY A TIME-DEPENDENT MODEL

H. Guennou and A. Sureau
Laboratoire de Spectroscopie Atomique et Ionique
Université Paris-Sud and C.N.R.S.
Orsay, France

The present model is the time-dependent version of a previous model (Sureau et al. 1983) in which the population distribution was assumed in steady state. A finite set of levels is partitioned in four subsets : the Z-ion ground-level and, contingently, the first near-degenerated levels (subset 1) ; all the successive excited Z-ion levels up to n=5 (subset 2) ; a finite number of higher Rydberg levels (because of the limitation of the series in the plasmas) which are assumed in LTE with the Z+1-ion ground-level (subset 3, called the thermal band) ; and the Z+1 ion ground-level (subset 4).

The physical processes explicitly considered are the radiative cascades and the transitions between the Z-ion bound levels induced by electron-ion collisions. The radiative-transition probabilities are given by ab-initio calculations using a modified Hartree-Fock method including the spin-orbit interaction (Sureau et al., 1984). The collision rates are derived by the Van Regemorter formula multiplied by an adjustable parameter F_c.

The ionization and recombination balance is implicitly ensured in fixing the populations of the levels of subsets 1 and 3 above with regard to the Z+1-ion ground-level population : LTE for subset 3, LTE multiplied by a parameter δ for subset 1. The situations where subsets 1 and 4 are not in LTE ratio can then be accounted for in taking $\delta \neq 1$.

The specifications of the model are summarized on the next page.

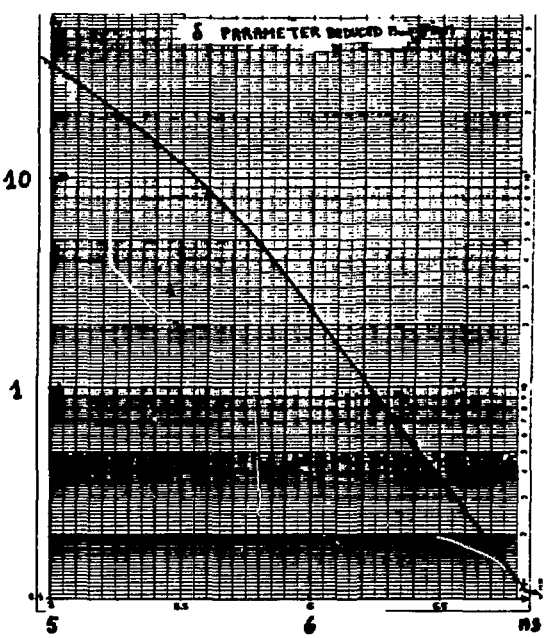

FIG.1 : δ versus time according to simulation 2 (see after)

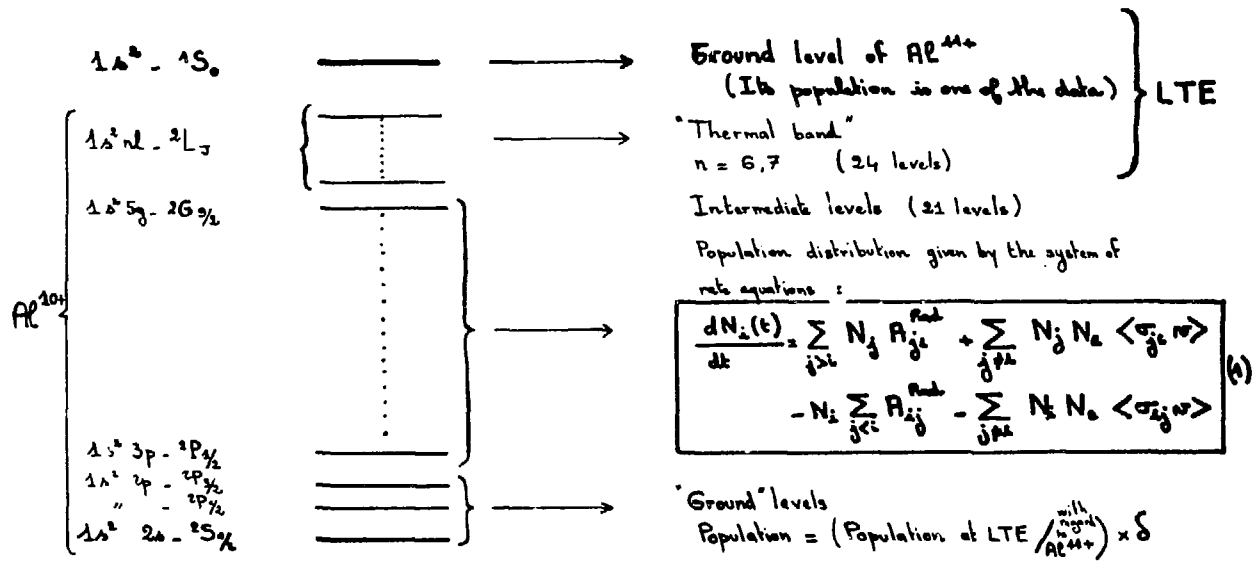

Solutions of (1) by (*) : $Y(t+h) = Y(t) + \Omega(h) * (\mathcal{B} Y(t) - C)$ $\quad h$ = step of time

Where $\Omega(h)$ is obtained by a recurrence relation:

$$\Omega\left(\frac{h}{2^{l-k}}\right) = \Omega\left(\frac{h}{2^{l-k+1}}\right) * \left[2E + \mathcal{B}\,\Omega\left(\frac{h}{2^{l-k+1}}\right)\right]$$

From:

$$\Omega\left(\frac{h}{2^l}\right) = \sum_{i=1}^{s} \frac{1}{i!} \mathcal{B}^{i-1} \left(\frac{h}{2^l}\right)^i$$

s, l = parameters chosen in order to obtain a sufficient precision.

(*) N. BAKHVALOV - Méthodes numériques - Editions Mir

The time evolution of the plasma parameters (electron density Ne and temperature Te, relative abundances of Al^{11+} and Al^{10+} ions, from which the parameter δ is deduced) being taken from a hydrodynamic simulation code for laser-produced plasmas (code FILM by Gauthier et al. 1983), the time evolution of the population of individual states has been obtained for some realistic cases, showing the occurrence of some population inversions during the recombination of the plasma. One exemple of this is given below :

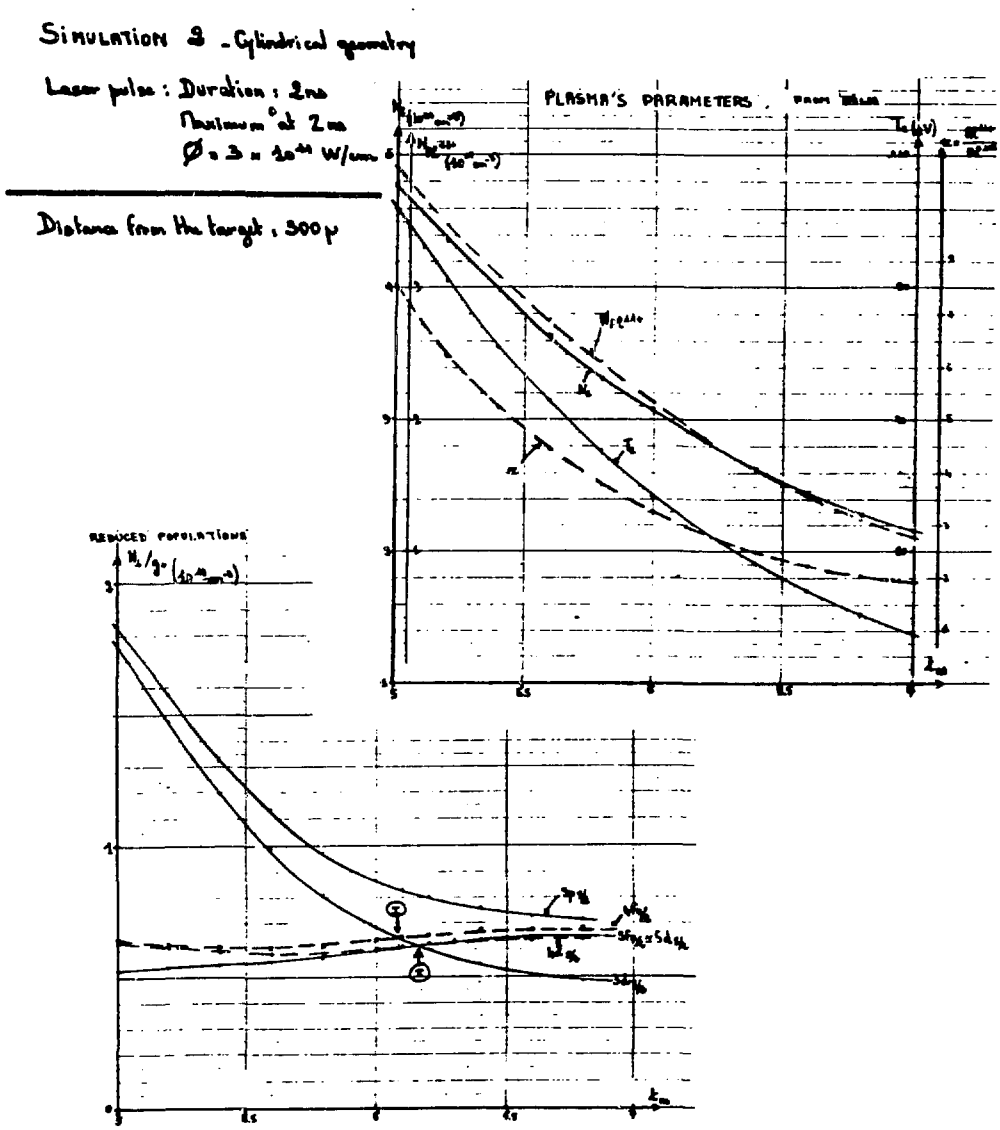

The corresponding δ values are given in figure 1.

REFERENCES

Sureau A., Guennou H., Jaeglé P., 1983 Communication at the 4th Topical Conference on Atomic Processes in High Temperature Plasmas, Princeton (N.J.) April 1983

Sureau A., Guennou H. and Cornille M., 1984 J. Phys. B : At. Mol. Phys., 17, 541

Gauthier J.C., Geindre J.P., Grandjouan N., Virmont J., 1983 J. Phys. D, 16, 321

TRANSITIONS OF THE TYPE 2s-2p IN HIGHLY-IONIZED Cu THROUGH Rb

W.E. Behring and L. Cohen (Lab. for Solar Phys. and Astrophys., Goddard)
J.F. Seely and U. Feldman (E.O. Hulburt Center for Space Research, NRL)
Samuel Goldsmith (Lab. for Plasma and Fusion Energy Studies, U. of MD)
M. Richardson (Lab. for Laser Energetics, Univ. of Rochester)

INTRODUCTION

We report here the observation of spectral lines in the F I, O I, N I, and C I isoelectronic sequences of Cu, Zn, Ga, Ge, As, Se, Br, and Rb. The plasma was produced by the spherical irradiation of solid targets using six frequency-tripled beams from the OMEGA laser system at the University of Rochester. The wavelengths were recorded using a 3 meter grazing incidence spectrograph, and the wavelengths were determined relative to several previously observed lines in the F I, O I, and Na I sequences. There is good overall consistency with the wavelengths recommended by Edlen (1983) for the F I and O I sequences and with the wavelengths measured by Kononov (1979) for the Na I sequence. Most of the observed transitions in the N I and C I sequences represent new identifications, and a complete set of energies for the $2s\,2p^4$ configuration of the N-like ions Cu XXIII, Zn XXIV, Ga XXV, and Ge XXVI is presented.

EXPERIMENT

The targets were spherically irradiated with an approximately cubic array of six beams from the OMEGA laser system. For each laser shot, the energy incident on target was between 200 J and 300 J with a pulse duration of 600 psec to 700 psec. Each laser beam was focused by an f/3.7 lens to a point a distance of 4 target radii beyond the center of the target. The average intensity of 351 nm light at the target surface was in the range 1×10^{14} to 2.5×10^{14} W/cm^2. The overall absorption of laser energy by the target was 88 to 92%. At the irradiation intensities used, the absorption process for the 351 nm radiation was almost entirely inverse bremsstrahlung with a very small fraction ($< 10^{-4}$) of the absorbed energy going to superthermal electrons.

In the case of zinc, the targets were solid fragments of pure zinc and were roughly spherical in shape with an average diameters of 450 μm. The copper, gallium, and germanium targets were coated glass microballoons. The average diameter of the microballoons was 350 μm, and the thickness of the glass shell was 1 μm. The thickness of the copper, gallium, and germanium coatings was 3 μm to 10 μm, and this was sufficiently thick so that burn-through to the glass microballoon did not occur. Spectral lines from the glass microballoon material are not present in any of the data.

The spectral data were accumulated over six shots for each of the four target materials. The spectra were recorded by a 3 meter grazing incidence (88°) spectrograph that has been described in detail by Behring et al. (1973). The spectrograph was fitted with a 600 or 1200 line/mm gold-coated Bausch and Lomb replica grating, and spectral lines were observed in the range 30 Å to 260 Å.

The wavelengths of the spectral lines from the N-like ions Cu XXIII, Zn XXIV, Ga XXV, and Ge XXVI are listed in Table I. These transitions were identified using recently calculated wavelengths (Cheng et al. 1979) and by extrapolating from the wavelengths of lower-Z ions (Z=22,24,26,27,28) measured by Lawson et al. (1981).

Listed in Table II are the energy levels that are derived from the wavelengths given in Table I. In most cases, the total number of observed transitions was insufficient to determine all the levels of the lower configuration $2s^2\ 2p^3$. In such cases, we have adopted the values recommended by Edlén (1982 and 1983) and have designated the relative uncertainties by +x, +y, etc. The accuracy of the presently measured energy levels is estimated to be 250 cm^{-1}.

A more detailed description of this work will be published in the Journal of the Optical Society of America B.

REFERENCES

W.E. Behring, R.J. Ugiansky, and U. Feldman 1973, Appl. Opt. 12, 528.

W.E. Behring, Leonard Cohen, G.A. Doschek, and U. Feldman 1976, J. Opt. Soc. Am. 66, 376.

K.T. Cheng, Y.-K. Kim, and J.P. Desclaux 1979, Atomic Data Nucl. Data Tables 24, 111.

Bengt Edlén 1982, Physica Scripta 26, 71.

Bengt Edlén 1983, Physica Scripta 28, 51.

E. Ya. Kononov, V.I. Kovalev, A.N. Ryabtsev, and S.S. Churilov, 1977 Sov. J. Quantum Electron. 7, 111.

E. Ya. Kononov, A.N. Ryabtsev, and S.S. Churilov 1979, Physica Scripta 19, 328.

K.D. Lawson, N.J. Peacock, and M.F. Stamp 1981, J. Phys. B 14, 1929.

Table I. Classification of lines isoelectronic with N I. (Å)

Transition	Cu XXIII	Zn XXIV	Ga XXV	Ge XXVI
$2s^2 2p^3 - 2s\,2p^4$				
$^4S_{3/2} - {}^2P_{3/2}$	[67.30]	63.330	[59.56]	[55.94]
$^2D_{3/2} - {}^2P_{3/2}$	[76.07]	71.901	68.011	[64.33]
$^2D_{3/2} - {}^2S_{1/2}$	79.636 bl	75.285	71.210 bl	67.425
$^2D_{5/2} - {}^2P_{3/2}$	79.636 bl,B	75.499 A	71.549	67.829
$^2P_{3/2} - {}^2P_{1/2}$	83.335 B	78.986 A	74.880	70.987
$^2P_{1/2} - {}^2P_{3/2}$	[86.37]	81.863	77.545	[73.45]
$^2P_{1/2} - {}^2S_{1/2}$	91.028	86.266	81.783	77.515 bl
$^2D_{3/2} - {}^2D_{3/2}$	92.695 B	87.700 B	[83.07]	78.701
$^2D_{5/2} - {}^2D_{5/2}$	94.847 B	89.490 A,B	84.403	79.641
$^4S_{3/2} - {}^4P_{1/2}$	96.457	90.080	84.102	[74.49]
$^4S_{3/2} - {}^4P_{3/2}$	98.892	92.225 bl	85.927	80.084
$^4S_{3/2} - {}^4P_{5/2}$	[111.05]	104.556	98.341 bl	92.637 bl
$2s\,2p^4 - 2p^5$				
$^2D_{3/2} - {}^2P_{3/2}$	[93.63]	89.040	84.724	80.719
$^2D_{5/2} - {}^2P_{3/2}$	96.762 bl	92.632	88.756	85.190
$^2P_{1/2} - {}^2P_{1/2}$	[118.11]	112.428 bl		

A. Transitions previously identified by Behring, Cohen, Doschek, and Feldman (1976).
B. Transitions previously identified by Kononov, Kovalev, Ryabtsev, and Churilov (1977).
bl. Blend
[ ]. Interpolated

Table II. Energy levels isoelectronic with N I.

Level		Cu XXIII	Zn XXIV	Ga XXV	Ge XXVI
$2s^2 2p^3$	$^4S_{3/2}$	0	0	0	0
	$^2D_{3/2}$	170900+x	188200	208500+x	233200+x
	$^2D_{5/2}$	230000+y	254500	281200+x	313200+y
	$^2P_{1/2}$	328100+x	357400	389700+x	426400+x
	$^2P_{3/2}$	446800+t	500100+t	560700+z	629100+t
$2s\,2p^4$	$^4P_{5/2}$		956400	1016900	1079500
	$^4P_{3/2}$	1011200	1084300	1163800	1248700
	$^4P_{1/2}$	1036700	1110000	1189000	
	$^2D_{3/2}$	1249700+x	1328500	1412400+x	1503800+x
	$^2D_{5/2}$	1284300+y	1372000	1466000+x	1568900+y
	$^2S_{1/2}$	1426700+x	1516600	1612800+x	1716600+x
	$^2P_{3/2}$	1485700+y	1579000	1678900+x	1787500+y
	$^2P_{1/2}$	1646800+t	1766200	1896200+z	2037800+t
$2p^5$	$^2P_{3/2}$	2317800+y	2451500	2592700+x	2742700+y

THE SOLAR X-RAY LINE SPECTRUM 5.5 - 12Å

D.L. McKenzie
Space Sciences Laboratory
The Aerospace Corporation
El Segundo, CA

The SOLEX X-ray spectrometers on the USAF P78-1 satellite have measured solar X-ray spectra in the 5.5-12Å range under a variety of flaring and nonflaring conditions. High sensitivity, obtained by summing data from several successive spectral scans, enabled the detection of 80 lines, 17 of which remain unidentified. The stronger lines were observed with individual scans during the course of flare development. This capability, along with the use of nonflare spectra, facilitated the identification of several lines. The lines of Fe XXII - XXIV, present in hot flare plasmas, are prominent in this wavelength range. For many of these lines, theoretical and observed line strengths will be compared. Diagnostically useful line ratios were evaluated for the helium-like species Mg XI, Al XII, and Si XIII. The density-sensitive R ratio was consistent with theoretical calculations of the low-density limiting value for Mg XI and Si XIII, the only species for which it was evaluated. In all cases the G ratio was below calculated values.

This work was supported by the Aerospace Sponsored Research program and by the U.S. Air Force Space Division under Contract F04701-83-C-0084.

SESSION 7. HIGH DENSITY LABORATORY PLASMAS

X-ray Spectroscopy of Laser-Produced Plasmas

Dup

Robert L. Kauffman

Lawrence Livermore National Laboratory
Livermore, California 94550

Laser-produced plasmas have some of the highest temperatures and densities obtainable in the laboratory. This offers the opportunity to perform spectroscopic studies in new temperature and density regimes under controlled laboratory conditions. Temperatures can range from greater than 1 keV to less than 1 eV, while densities range from less than $10^{20} e^-/cm^3$ to greater than $10^{23} e^-/cm^3$. X-ray spectroscopy has been an important tool in diagnosing these large ranges of temperature and density. Relative line intensities of resonance and satellite lines can be used to diagnose the lower densities and higher temperatures. (Galanti and Peacock 1975, Boilo et al. 1979) For the denser plasmas Stark broadening is a good density diagnostic. (Yaakobi et al. 1977) Absorption spectroscopy measuring edge shifts had recently been used to probe the low temperature, high density region. These plasmas, with their high-energy density, are transient with total time scales ranging from 100 psec to greater than 1 nsec, depending on the laser driver pulse. In order to make detailed measurements from these plasmas, sensitive, time-resolved spectrographs have been developed. (Lewis et al. 1980, Kauffman et al. 1983) These spectrographs can measure time histories of spectral lines with resolving powers of 300 or greater and with time-resolutions of 20 psec. By using such instruments, studies of the dynamics of the plasma can be made.

The laser-produced plasma can be divided into three different regions. The first is the corona region. This extends from critical density for light absorption [$10^{21} e^-/cm^3/\lambda^2(\mu m)$] to lower density. Temperatures can range from a few hundred eV to greater than one keV. In this region laser energy is deposited in the plasma. Not only is it characterized by high temperatures and low densities, but the light absorption can also create non-thermal electron distributions.

Spectroscopically the corona is the easiest part of the plasma to access. The high temperatures produce high brightnesses of highly stripped ions. Many of the x-ray diagnostics for the solar corona are directly applicable to this regime. Some of the major problems in interpreting the data are opacity, time-dependence, and spatial gradients. Because of the relatively high densities even in the corona, most resonance line intensities are many optical depths thick, unless care is taken to reduce these effects in the target. The time dependence and spatial gradients are a direct result of the finite time and localized area of laser energy deposition. This deposition creates large gradients, both into the cold dense material and laterally away from the deposition area. Also, as the plasma evolved the gradient scale lengths change.

One application of x-ray line intensities has been to measure the coronal temperature in a thin foil experiment. The purpose of the experiment is to create long-scalelength, underdense plasmas, such as may

be found in advanced ICF targets. The laser propagating in such plasmas can efficiently couple to electron-plasma waves, which produce high-energy electrons. The coupling efficiency depends on the plasma temperature and density. The underdense plasma was created by irradiating thin CH foils that expand during the heating to the desired density by the peak of the laser pulse. These foils are typically 1000 μm diameter and 2μm thick for irradiation by our Novette laser using 0.53 μm light. For spectroscopic purposes we have seeded only the inner 300 μm of the foil with 4% atomic concentration of Sulfur. The low concentration of the seed material was chosen in order not to effect the hydrodynamics of the foil and to reduce the opacity of the resonance lines. Only the center portion is seeded in order to minimize effects of lateral gradients as the heat spreads away from the initial spot.

Data from such an experiment is shown in Fig. 1. The data was taken using an x-ray streak camera coupled to an x-ray crystal spectrograph. (Kauffman et al. 1983) In the figure time increases upward and energy increases to the right. The time resolution is on the order of 20 psec and energy resolution is about 8eV. The sulfur helium-like and hydrogen-like lines are marked.

The relative intensity ratio of the Heα and Lyα lines from Fig. 1 are compared with calculations to obtain temperatures. This comparison is shown in Fig. 2. The calculations combine the output of a two-dimensional hydrodynamics code with a code that calculates the atomic levels dynamically. (R. W. Lee et al. 1984a) The atomic levels code uses the temperature and density of each cell derived from the hydrodynamics code and calculates the transient level populations of the sulfur at each time step. In this way effects on ionization balance due to step gradients are included. Results of this calculation are shown as the solid line in Fig. 2. The agreement with the data overall is good. Although early in the pulse during the times of steep gradients, it predicts too slow of ionization time. The dashed line is the prediction assuming the ion is in full steady-state with the local plasma parameters and the agreement is much better.

We have used other x-ray features to diagnose the corona. We have used Stark broadening of high n-state lines in the plasma to measure densities in Al plasmas down to $10^{20} e^-/cm^3$. (Lee et al. 1984b) We have also measured the time history free-bound continuum from Al plasmas. (Matthews et al. 1984) The shape of the continuum provided some indication of a non-thermal distribution during the laser heating and the plasma cooling rate after the laser was turned off. Both techniques require high concentrations of the spectroscopic ion and low background for accurate measurements.

The second region is the ablation/pusher region of the plasma. In this region energy is transferred from the corona to the inner fuel. This region is relatively dense and cool, but large thermal and density gradients can exist due to strong shocks propagating through it. Only recently has x-ray spectroscopy been applied to study the physics here, although it should receive more attention in the future. (Hares et al. 1984) have used absorption spectroscopy to measure edge shifts and widths to determine temperatures and densities of strong shocks inside of materials. Several groups have used inner-shell electron fluorescence to study electron conduction from the corona into the dense material region. (Young et al. 1977, Yaakobi et al. 1984)

The third region is the inner fuel or core of the implosion. This region remains relatively cool during the implosion, but once the center stagnates, the kinetic motion can be converted to thermal energy heating the fuel. By adding a high-Z seed gas to the D-T, spectroscopy can be used to measure the final compressed density, which is important for determining the quality of the implosion.

Line broadening data has been obtained by using the Omega laser at the University of Rochester to symmetrically irradiate the outer surface of an Ar-filled ball. The data have been fit using line broadening theory developed by C. Hooper and co-workers and opacity modeling by R. W. Lee. (Delameter et al. 1984) Opacity effects are important because they represent another broadening mechanism. Each line can be fit independently to a number of different electron densities, depending on the opacity. Fig. 3 shows the focus of best fit for each line versus the ion density in the hydrogen ground state, or optical depth. The intersection of all of the locii of best fit for each line uniquely determines both the electron density and the ion density for the implosion. Of special note is the importance of optically thick lines in the fitting procedure. These severely constrain the ion density and the region of interest for the fitting plot. The dotted lines in the figure indicate regions where 30% and 50% of the ions are in the hydrogen-like ground state. For more details, see the paper by Delameter et al. (1984).

In summary, x-ray spectroscopy is an important diagnostic tool for laser-produced plasmas. Experimental conditions, though, must be carefully tuned to obtain meaningful results. Of particular note, is the role of opacity and time dependence. Both must be included in any analysis of x-ray spectra from laser-produced plasmas.

References

Boiko, V. A., Pikuz, S. A., and Faenov, A. Ua., 1979 J. Phys. B, 12, 1989.

Delameter, N. D., Hooper, C. F., Joyce, R. F., Woltz, L. A., Ceglio, N. M., Kauffman, R. L., Lee, R. W., and Richardson, M. C., 1984, submitted to Phys. Rev. Lett., and J. Quant. Spec. Radiat. Transfer, to be published.

Galanti, M., and Peacock, N. J., 1975, J. Phys. B, 8, 2427.

Hares, J. D., Bradley, D. K., Ranking, H. J., and Rose, S. J., 1984,, Central Laser Facility Annual Report, Rutherford Laboratory, A3.1.

Kauffman, R. L., Brown, T., and Medecki, H., 1983, SPIE Vol. 427, 84.

Lee, R. W., Kilkenny, J. D., Kauffman, R. L., and Matthews, D. L., 1984b, J. Quant. Spectrosc. Radiat. Transfer, 31, 83.

Lee, R. W., Whitten, B. L., and Stout, R. E., II, 1984a, J. Quant. Spectrosc. Radiat. Transfer, 32, 91 (1984).

Lewis, C. L. S., Lamb, M. J., Kilkenny, J. D., Keats, S., and Key, M. H., 1980 Central Laser Facility Annual Report, Rutherford Laboratory, 61.

Matthews, D. L., Kauffman, R. L., Kilkenny, J. D., and Lee, R. W., 1984 Appl.. Phys. Lett 44 586.

Yaakobi, B. A., et al. 1984, Phys. Fluids 27, 516.

Yaakobi, B., Steel, D., Thorsos, E., Hauer, A., and Perry B., 1977, Phys. Rev. Lett., 39, 1526.
Young, F. C., Whitlock, R. R.,, Decoste, R., Ripin, B. H. Nagel, D. J. , Stamper, J. A., McMahon, J. M., and Bodner, S. E., 1977, Appl. Phys. Lett. 30, 45.

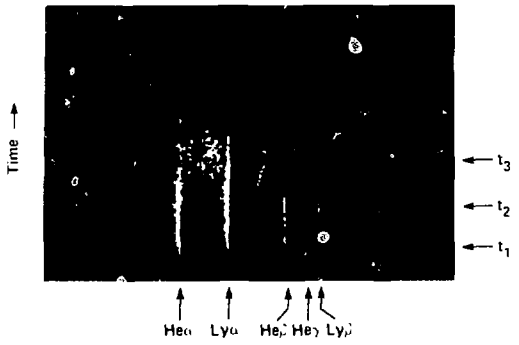

Fig. 1 Example of a time-resolved K-x-ray spectrum of Sulfur. The sulfur is a low concentration seed in CH. The relative line intensities are used to measure the time-resolved density and temperature of the foil.

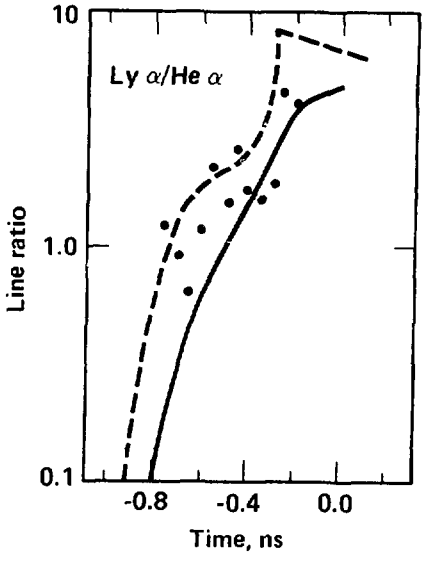

Fig. 2 Example of the time-resolved Lyα/Heα ratio of Sulfur from exploding foils. The solid and dashed curves are the predicted line ratio from a 2-d hydrodynamic code coupled with a dynamic ionization model (——) and a steady-state ionization model (---).

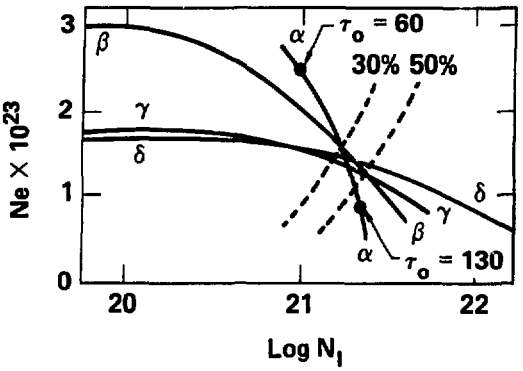

Fig. 3 Example of interpreting x-ray line broadening data to find imploded core densities. Ar-broadened Lyman series lines are fit to various electron densities, N_e, and ion densities, N_I. The intersection of the different curves determine the imploded core density. The dashed lines show the curves for when 30% and 50% of the total ion density are in the hydrogen-like ground state.

RECOMBINATION LASERS IN THE XUV SPECTRAL REGION

G.J. Pert
Department of Applied Physics, University of Hull
Hull, HU6 7RX, U.K.

INTRODUCTION

In a conventional laser operating in the near ultra-violet, optical or infra-red spectral bands the photon energies, not exceeding 10eV, are closely matched to the electronic or molecular energy levels of neutral and weakly ionised atoms. Consequently typical photon energies ($\sim$ eV), and transition lifetimes ($\sim$ ns) closely match the characteristics of fast electrical circuitry feeding a weakly ionised discharge which may be used to pump either directly or indirectly the laser medium.

In a X-ray laser operating at about 10Å, photon energies are about 1 keV, and lifetimes about 10^{-14}s (10fs). In consequence the power required to pump the laser must be expected to increase rapidly as the wavelength decreases. The gain per unit length is given by:

$$\alpha = \zeta \frac{\lambda}{\pi} \frac{A}{\Delta\nu} g_3 \left(\frac{n_3}{g_3} - \frac{n_2}{g_2}\right) \qquad (1)$$

where ζ is the line shape factor, A the spontaneous transition probability, λ the wavelength, and $\Delta\nu$ the width of the line, and (n_2,g_2) and (n_3,g_3) the population density and statistical weight of the lower and upper laser states respectively. The total power loss per unit area, p, of the medium must exceed that emitted by spontaneous decay of the laser transition.

$$p \simeq n_e \ell \cdot h\nu A > \frac{8\pi h}{\zeta c^2} \nu^4 (\alpha\ell) \frac{\Delta\nu}{\nu} = \frac{4.10^{21}}{\lambda(\text{Å})^4} (\alpha\ell) \left(\frac{\Delta\lambda}{\lambda}\right) \text{ W/cm}^2 \qquad (2)$$

where ℓ is the length of the medium. In practical devices we must expect that additional losses will increase the total power demand by as much as an order of magnitude. It must be realised that not only must this power be supplied by an external source, but it must be dissipated by the medium.

In contrast to conventional lasers only two laboratory sources are at present known which can, in principle, deliver the pump power densities $\gtrsim 10^{15}$ W/cm^2 required by an X-ray laser namely a subsidiary laser or a particle beam: we shall not discuss a third alternative, a nuclear explosion, as its suitability for non-military applications must be extremely limited. In the less restrictive XUV spectral region ($\gtrsim$ 100Å) we may add fast high voltage discharge devices such as the superfast pinch.

The problem is further complicated by the absence of simple transmitting or reflecting media at X-ray wavelengths so that the constraints cannot be relaxed by allowing the laser signal to build up in a resonant cavity, or distributed feedback system. At XUV wavelengths metals at grazing incidence must be used for mirrors in order to obtain high reflectivity, and at X-ray wavelengths crystal reflectors, but again at non-normal incidences. Under such conditions

the construction of a cavity is extremely complex. The recent development of multi-layer reflectors in this wavelength range may eventually solve this difficulty but for the present their reflectivity is low (Haelbich et al 1980; Barbee and Keith 1979). The absence of a cavity implies that the laser must operate in a weakly coherent travelling wave, or amplified spontaneous emission mode. This form of operation in which the spontaneous fluorescence is amplified by stimulated emission down a rod shaped medium requires a gain-length product ($\alpha\ell$) $\sim$ 20 (i.e. an overall amplification $e^{\alpha\ell}$ of about 100db). Such a device produces a beam whose divergence will be limited by either diffraction or geometry to approximately the larger of two values λ/d and d/ℓ, where d is the rod diameter and ℓ its length. If these are matched the divergence is minimised, and furthermore the beam will be coherent across its wavefront. Thus ideally the diameter should have the optimum value

$$d \simeq \sqrt{\lambda\ell} \qquad (3)$$

If the diameter is less than this value diffraction losses will reduce the effective gain length to a value $\ell^1 \simeq d^2/\lambda < \ell$.

Since the total power $P \simeq pd^2$ it is clear that if the total pump power is to be kept within reasonable limits (say 100TW) then $d \leq 10^{-3}\ \lambda(\mathring{A})^2$cm, and therefore $\ell \leq 10^{-6}\ \lambda(\mathring{A})^3$cm, assuming $\Delta\lambda/\lambda \simeq 10^{-4}$. Hence we may estimate that the minimum inversion density $\Delta n \simeq 6 \times 10^{21}/\lambda(\mathring{A})^4$/cc assuming the oscillator strength of the lasing transition at unity.

It is clear from the preceeding discussion that the principal limitations on constructing an X-ray laser is the high pump power required. In principle we may satisfy this condition either directly in which case the external pump must itself satisfy the power condition, or indirectly when the system is pumped to a relatively long lived reservoir state, which may be slowly filled, to be transferred into the upper laser state by some appropriate trigger. The latter approach relaxes the condition on the external pump by using the reservoir energy, but is clearly limited to short pulse action only.

RECOMBINATION LASERS

One of the most promising approaches to a laboratory XUV laser at present seems to be the recombination laser. Population inversion generated in this way is a familiar feature in many laser produced plasmas, and significant gain has been measured. The inversion is achieved during the cascade through the excited states of highly charged ions following recombination into a high lying state. Two basic approaches can be envisaged, requiring different forms of the ion term scheme. If the principal de-excitation process in the cascade is via electron collisions, the inversion forms between a pair of well separated levels within a group of closely spaced ones. In contrast with radiative decay the inversion generally forms between a pair of levels, the lower of which is well separated from its next lower state, for example, the 2p state of hydrogen. The first approach has been successfully applied by workers at Bell Labs in the visible region of the spectrum (Silfvast and Wood, 1980), whereas the latter has been used in the XUV with emphasis on hydrogen-like ions (Pert, 1976), it being relatively easy to produce a high fractional population of the parent ion by stripping the medium. In

order to achieve significantly large gain within the recombination cascade, it is necessary to first ionise the medium, and then rapidly cool it so that the dominant recombination is into high lying states rather than directly into the ground state. This, the basic problem, may be accomplished in a number of ways of which adiabatic cooling by expansion (Pert, 1976) and radiative heat loss (Suckewer and Fishman, 1980) are the most promising.

There have, within the past few years, been several reports of gain either measured directly or indirectly from expansion cooled recombination systems. Using slab targets irradiated with Nd:glass laser pulses of 10ns duration Elton and co-workers at N.R.L. (1982) have measured a gain of 2%/cm at 520Å on the hydrogen-like carbon lines CVI, P_α. Jaeglé and associates at Orsay (1981) with variable length line focussed Nd;glass laser pulses also of ns duration on aluminium targets have observed gain of the lithium-like aluminium line Al XI, 3d-5f at 105.7Å with values $\sim$ 2/cm over lengths of plasma up to 1cm. The largest gain has been measured in hydrogen-like carbon CVI, H_α at 182Å with values of $\sim$ 25/cm over 2mm length by the Hull University group (Jacoby et al, 1982).

The plasma must first be rapidly heated, and then cooled over timescales of the order of the characteristic ionisation time: for CVI ions at densities $\sim 10^{21}$ ions/cc this implies times of order 100ps. These times are characteristic of the duration of mode-locked pulses from a Nd:glass laser, and of the expansion of plasma of appropriate temperature $\sim 10^{-3}$ cm in size. In practical terms these parameters closely match those obtained by heating carbon fibres of a few microns diameter with an appropriate laser pulse, a conclusion confirmed by detailed computer modelling (Pert, 1976). In this system the inversion is achieved at sufficiently high density ($\sim 10^{19}$ ions/cc) to give an inversion density $\sim 10^{15}$/cc with gain coefficients $\sim$ 10/cm, sufficient to measure in a laboratory experiment.

CARBON FIBRE LASER SCHEME

The use of thin carbon fibre irradiated by cylindrically focussed Nd:glass laser radiation, and its harmonic as a working medium for laser action in the XUV has been investigated both experimentally and theoretically. In this system rapid cooling by adiabatic expansion of the fully stripped carbon plasma induces population inversion between the n = 3 and n = 2 levels of the hydrogenic like carbon ion CVI during the recombination cascade. In general the gain in such a system is small, limited by the optical trapping of the lower laser level n = 2. However, if the scheme is to have an application with current technology amplified spontaneous emission of travelling wave mode of operation is necessary, requiring a relatively high gain. This condition can only be achieved if the resonance line can be made optically thin at a reasonably high density.

In the carbon fibre system this handicap is mitigated by two effects. Firstly the carbon is initially fully stripped, and only relatively weakly ($\sim$ 10%) recombined at gain onset to reduce the Lyman α ground state population. Secondly the effective plasma width is kept small. This latter condition is achieved both directly by using fibres of small initial diameter, but more importantly due to the approximately linear dependence of the radial velocity, and the motional Doppler effect, which ensures that only a limited width of

the plasma is in resonance at line centre.

A direct observation of gain at 182Å has been made in the plasma formed by an expanding laser heated carbon fibre (Jacoby et al, 1982). In this experiment two spectrographs (Fig. 1) were used to simultaneously measure the spontaneous and amplified spontaneous emission from a 2mm length of heated carbon fibre. Signal amplifications of up to 30 times of the CVI H_α line along the fibres were measured and the inferred gain/length parameters are shown in Fig. 2. The strong variation with laser energy shown is in good agreement with computer modelling of the interaction. The need for extreme care in cross calibrating the spectrographs in any experiment of this type should be noted.

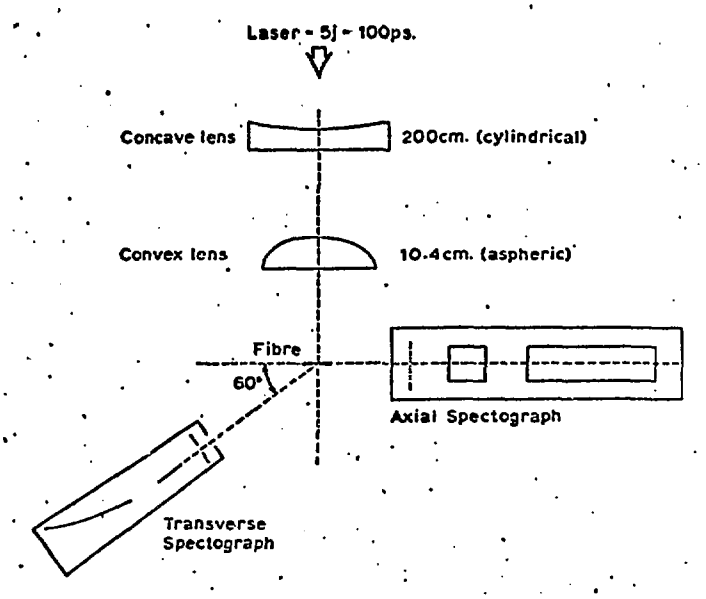

Fig. 1 Diagram of the apparatus used in the University of Hull experiments to measure gain at 182Å from laser heated carbon fibres.

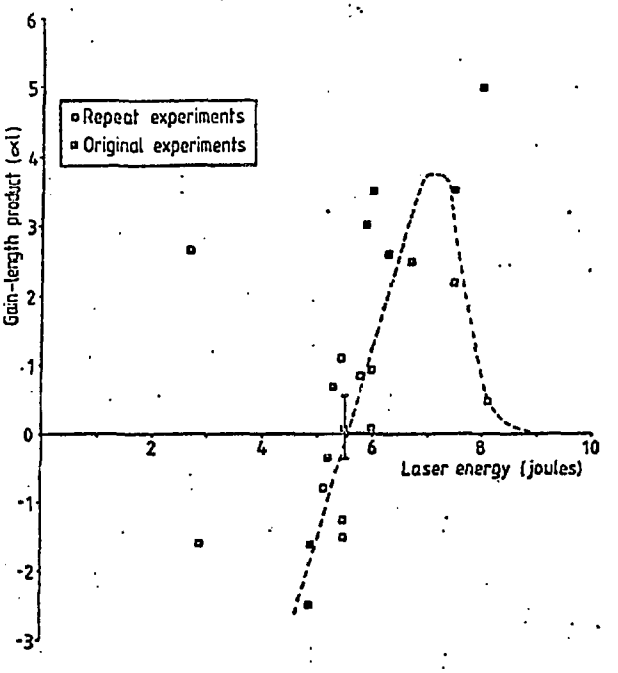

Fig. 2 Measured gain as a function of input laser energy in the low mass regime. Closed points refer to old data of Jacoby et al (1982) and open ones to repeat experiments. For comparison laser energy of 8j is approximately equivalent to absorbed density of 2½j/cm in Fig. 3.

It was found that the measured plasma parameters were only weakly dependent on the fibre diameter, provided it was not too large (≲ 6μm). This was inferred to be due to an incomplete burn of the fibre, the actual mass participating in the gain generation being strongly dependent on the absorbed laser energy. This

result has been confirmed in subsequent experiments, and the mass/energy relationship deduced for a number of pump laser configurations (Pert et al 1984) Fig. 3. Since the condition for peak gain can also be expressed in terms of an energy/mass relation, this offers the important prospect of matching the burn to the gain by the use of appropriate pump laser parameters. Since the curve overlap can be large this has two attractive features. Firstly, by operating at low energy/low mass the gain can be maximised as in the experiments of Jacoby et al (1982). Secondly, fluctuations in the absorbed energy along the line of the fibre due to shot-to-shot variation, and to imperfect lens design can be accommodated whilst still maintaining high gain by shifts along the gain-optimised mass/energy curve.

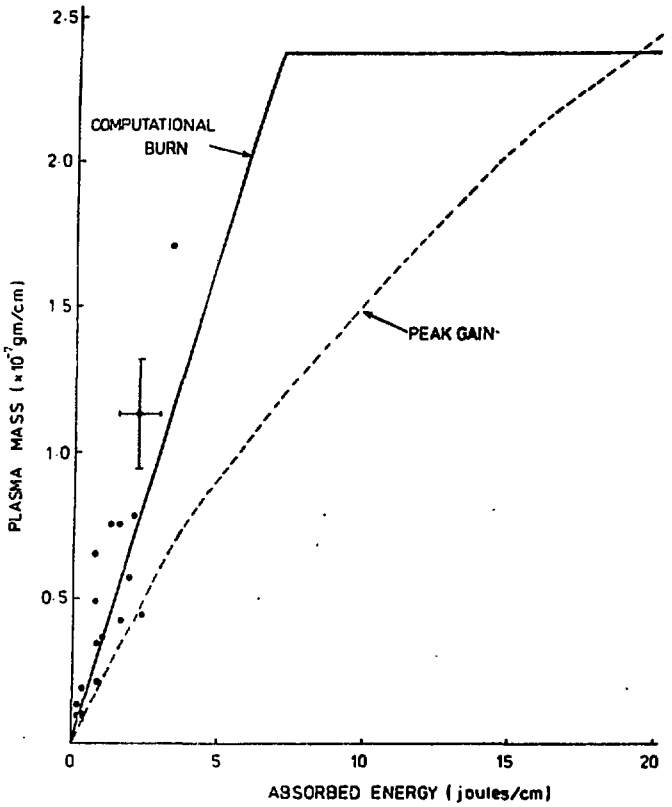

Fig. 3 Mass/energy plot for the low mass gain experiment, Fig. 2. The computational data plotted as lines and the experimental burns the points.

The importance of operation in the low mass/low energy regime and of burn/gain matching has been clearly demonstrated in high energy experiments at the C.L.F. (Pert et al, 1984) in which only relatively weak gain was observed, but which confirmed the role of incomplete heating.

Two distinct measurements of the effective mass were carried out. Simple ion probe measurements were made routinely. In addition interferograms allowed a direct observation of the density profile of the plasma which can be integrated to give a check on the ion probe results. Excellent agreement between the data validated the ion probe method. These results are compared with the computational predictions of 1 and 2 dimensional codes in fig. 4, with good overall agreement.

The interferograms clearly show the presence of the cold dense core, whose radius is much less than that of the expanding plasma. Density profiles measured from two shots with very similar effective mass and absorbed energy at different times are compared with the calculated distribution predicted by the 1 dimensional code in fig. 5.

When allowance is made for the uncertainty of the timing zero of the laser pulse, the agreement is most satisfactory.

One of the attractive features of the recombination laser in hydrogen-like ions is that the scaling along the iso-electronic sequence is relatively well-known (Pert 1976) and thus systems can be extrapolated towards X-ray wavelengths with some degree of confidence. The analysis given in Pert (1976) indicates similar behaviour can be expected for ions of charge number Z, if the temperature is scaled as Z^2, the diameter as Z^{-3}, the ion density as Z^6. The resultant gain scales as $Z^{7.5}$. Since the lasing wavelength scales as Z^{-2}, some estimates can be made of the necessary conditions for short wavelength. If this is done a laser operating with aluminium at about 39Å appears to be feasible using thin foils irradiated with pulses of about 10ps duration (Davé and Pert 1984). For shorter wavelengths the scaling is at present more speculative.

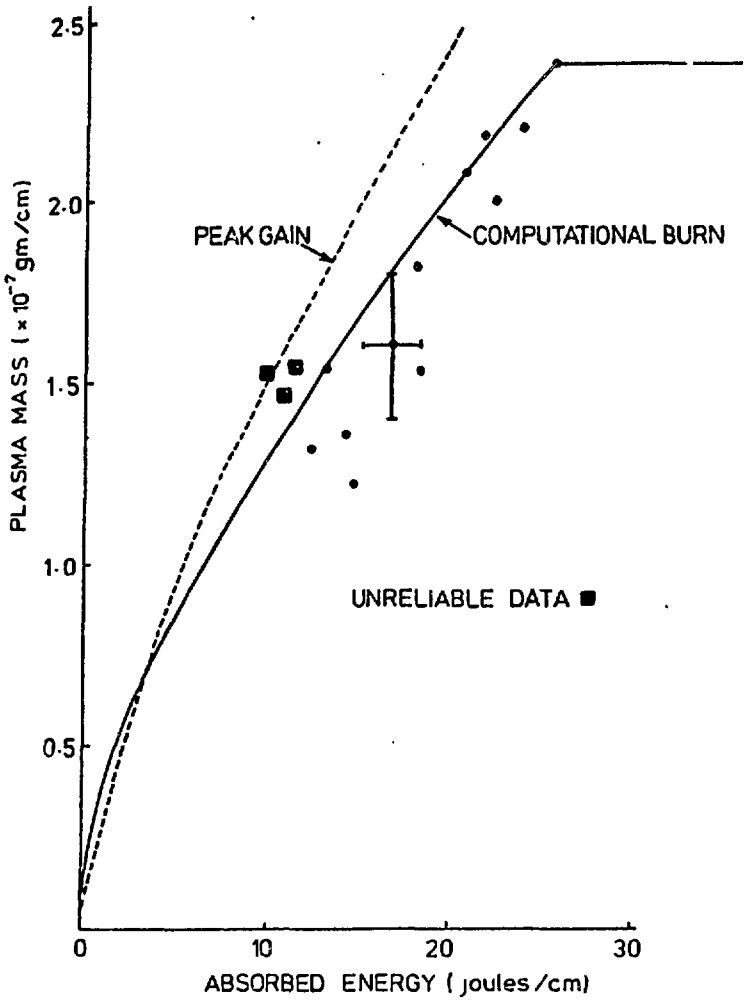

Fig. 4 Mass energy/plot for the high mass interferometry experiment; the data is presented as in fig. 3.

ACKNOWLEDGEMENTS

It is a pleasure to acknowledge the contributions made by many colleagues to this project: in particular Drs. Jacoby, Shorrock and Tallents at University of Hull, Drs. Lamb and Lewis, Mr. Corbett and Miss Mahoney at Queen's University, Belfast, and Drs. Eason, Hooker, Key and Pivizhong at the Rutherford Laboratory. The programme is supported by S.E.R.C.

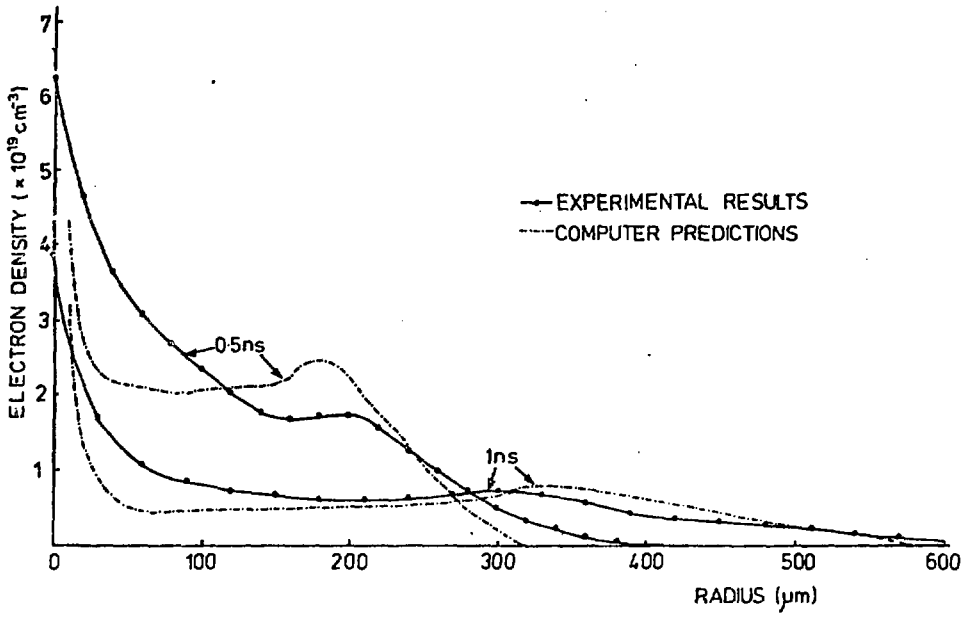

Fig. 5 Comparison of experimental and computational electron density profiles at two times during the expansion of an incompletely burnt fibre with effective mass 1.5 x 10^{-7}gm/cm and absorbed energy 13j/cm.

REFERENCES

Haelbich R.Pl, Segmuller A. and Spiller E. 1980, Appl. Phys. Lett. 34, 6.

Barbee T.W. Jr. and Keith D.L. 1979 in Lithography/Microscopy Beamshine Workshop, ed. C.R. Dannemiller. SSRL Report No. 79/02, 185.

Silfvast W.T. and Wood O.R. Jr. 1980, J. de Physique, 41, C9, 439.

Pert G.J., 1976, J. Phys. B, 9, 3301.

Suckewer S. and Fishman H. 1980, J. Appl. Phys., 51, 1922.

Elton R.C., Seely J.F. and Dixon R.H., 1982, Paper presented at 1st Topical Meeting on Laser Techniques in the Extreme Ultraviolet, Boulder, USA.

Jamelot G., Jaegle P., Carillon A., Bideau A., Moller C., Guennou H. and Sureau A., 1981, in Proc. Int. Conf. on Lasers '81, New Orleans, December 1981, ed. C.B. Collins (S.T.S. Press, McLean Va.) 178.

Jacoby D., Pert G.J., Shorrock L.D. and Tallents G.J., 1982, J. Phys. B, 15, 3557.

Pert G.J., Shorrock L.D., Tallents G.J., Corbett R., Lamb M.J., Lewis C.L.S., Mahoney E., Eason R.B., Hooker C. and Key M.H., 1984, Paper presented at IInd Topical Meeting on Laser Techniques in the Extreme Ultraviolet, Boulder, USA, and Central Laser Facility Annual Report, RAL 84.049, A4.2.

Davé A.K. and Pert G.J., J. Phys. B: in press.

3s - 3p AND 3p - 3d TRANSITIONS IN NEON-LIKE IONS OF THE IRON GROUP ELEMENTS

U. Litzén and C. Jupén
Physics Department
Lund University
Lund, Sweden

The spectra of highly ionized scandium, titanium, vanadium and chromium emitted from laser-produced plasmas have been recorded in the region 270 - 600 A. The radiation from a Quantel NG24 Nd:YAG/glass laser giving the maximum energy 4J in 3ns pulses was focused on plane metal targets. The target was placed at the Sirk's focus of a 3-m normal incidence spectrograph with the target surface parallel to the slit. The laser beam was perpendicular to the target and to the entrance axis of the spectrograph. By this arrangement the spectral lines from different ionization stages differ in length, the highest states giving the shortest lines. Well-determined lines from spark recordings of sodium-, magnesium-, aluminium-, and silicon-like ions were used for the wavelength determinations.

The identification of 3s-3p and 3p-3d lines of the neon-like ions was based on two different methods of isoelectronic comparisons with theoretical predictions. The first method uses an ab-initio calculation of energy levels through Z-expansion with relativistic corrections (Bureeva and Safronova 1979). Wavenumbers for transitions between the theoretical energy levels were derived, and the differences between the calculated wavenumbers and those observed up to and including Ar IX were extrapolated to higher Z. The second method is based on the extrapolation of empirical scaling factors for Hartree-Fock values of energy integrals. These two methods have led to the identifications in the laboratory spectra of 3s-3p and 3p-3d lines in Sc XII, Ti XIII, V XIV, and Cr XV. Further extrapolation has led to the identification of the corresponding lines of Fe XVII in the spectra of solar flares (Jupén 1984).

In Ti XIII and Fe XVII the number of identified lines was large enough for establishing the energy level structure of $2p^5$ 3s, 3p and 3d. Comparisions with levels derived from Hartree-Fock wavefunctions were made by fitting Slater and spin-orbit parameters. This further improved the possibility to interpolate and extrapolate scaling factors for ab-initio integrals and thus to predict the wavelengths of the 3s-3p and 3p-3d lines in all neon-like ions of the iron-group elements. Accurate extrapolations to heavier elements would require relativistic calculations.

A full description of the work presented here will appear in Physica Scripta (Jupén and Litzén 1984). The investigation of the neon-like sequence is now being continued with an isoelectronic study of hydrogenic levels ($l > 2$), which will lead to improved values for the ionization potentials for these ions. Beam-foil spectra recorded at the Bochum 4MV Dynamitron tandem accelerator laboratory and the Lund University 3MV Pelletron accelerator will be used together with the spectra from laser-produced plasmas in that work (Jupén et al 1984).

REFERENCES

Bureeva, L.A. and Safronova, U.I. 1979, Physica Scripta, 20, 81

Jupén, C. 1984, Month. Not. Royal Astr. Soc., 208, 1P

Jupén, C. and Litzén, U. 1984, Physica Scripta (in press)

Jupén, C. Litzén, U., and Träbert, E., work in progress.

DIRECT COMPARISON OF ELECTRON DENSITY MEASUREMENTS IN LASER-CREATED PLASMAS USING STARK BROADENING AND SATELLITE LINE INTENSITIES

Ph. Alaterre, P. Audebert, J.P. Geindre, P. Monier,
C. Popovics and J.C. Gauthier
Greco Interaction laser matière, Ecole Polytechnique,
91128 Palaiseau (France)

Spectral line profiles, broadened mostly by Stark effects from electric fields produced by charge particles, and diélectronic satellite line intensities have recently been used for determining electron densities in the dense region of laser-created plasmas [1-3]. We present here a direct comparison of electron density measurements in the conduction region of laser created plasmas on a plane target using these two techniques.

Experiments were carried at the GRECO laser facility, using the Nd phosphate glass laser at its second harmonic (0.53 μm) and 600 ps pulse length. The laser was focused on a 160 μm focal spot in which was centered a 25 or 50 μm diameter aluminum dot implanted on a carbon substrate. Laser intensities were in the range 1×10^{14}-3×10^{14} W/cm^2. The $1s4p$-$1s^2$ He-like transition, the 4p-1s H-like transition and the Ly α satellites were recorded on the same spectrum with a PET flat crystal spectrograph. Spot spectroscopy provided quasi-homogeneity and low reabsorption along the line of sight which was tilted 7° out the target surface. 3 μm resolution along the laser axis was obtained with an imaging knife-edge placed 1 mm apart from the target [4].

Electron densities were deduced comparing the He-like and H-like resonance Stark broadened lines to theoretical profiles calculated for H-like lines [5]. Lines of n = 4 quantum number are the most suited for the measurement as they merge out the continuum and are not much reabsorbed. Instrumental and Doppler broadening were taken into account. The electron density and an optical depth around 1.5 were introduced as parameters to obtain the best fit of the experimental data. Figure 1 shows the precision of the measurement on a He-like profile. The assymetry of the profile due to blended forbidden lines decreases slightly the accuracy of the density measurement.

Satellite line intensities were calculated in a collisional radiative model including photon pumping effects [6-7]. The complete experimental satellite spectra were compared to the theoretical ones. A Voigt profile broadened by an instrumental profile of 4 mA width reproduces better the line shapes. The gaussian width includes 2 mA Doppler broadening. The Lorentzian width is introduced as a parameter and appears to be compatible with recent Stark broadening theory [8] (2 mÅ at $n_e = 10^{20}$ cm^{-3}). Figure 2 shows an experimental spectra measured with 10 μm spatial resolution for 22 J of laser energy

incident on a 50 μm diameter and the fit of the theory obtained for a density of 1.0 x 10^{20} cm^{-3}.

Typical electron density measurements obtained for several shots conditions (different laser energy and aluminum dot diameter) are shown on figure 3. Stark broadening of the n = 4 resonance lines provides the whole electron density profile while the satellite lines give a single value of the electron density at the satellite peak intensity. The error bar on these preliminary result is rather large. One of the reasons for it is that the measured density is close to the region where opacity effects become important. Indeed, taking into account radiative transfer across the plasma length cuts down the region of fast dependence of the line intensity ratio versus electron density as can be seen on figure 4.

Figure 3 shows that the satellite lines diagnostic gives electron densities compatible but systematically higher by about 50 % than the Stark widths diagnostic. This discrepancy can be due to integration effects since satellite lines are emitted at a position close to H-like and He-like resonance lines [7] but are emitted only briefly near the maximum of the laser pulse [9].

REFERENCES

[1] Kilkenny J.D., Lee R.W., Key M.H. and Lunney J.G., Phys. Rev. A, 22, 2746 (1980).

[2] Lee R.W., Kilkenny J.D., Kaufman R.L., and Matthews D.L., J. Quant. Spectrosc. Radiat. Transfer, 31, 83 (1984).

[3] Audebert P., Geindre J.P., Gauthier J.C. and Popovics C., Phys. Rev. A, 30, 768 (1984).

[4] Alaterre P., Popovics C., Geindre J.P. and Gauthier J.C., Opt. Commun., 49, 140 (1984).

[5] Kepple P.C. and Griem H.R., NRL Memorandum, Report n° 3634 (1978).

[6] Duston D. and Davis J., Phys. Rev. A, 21, 932 (1980).

[7] Audebert P., Geindre J.P., Monier P., Popovics C. and Gauthier J.C., à paraître.

[8] Banon J., Koenig M. and Nguyen H., Proceed. of the 7th International Conference on Spectral Line Shapes, Aussois France, (1984).

[9] Key M.H., Lewis C.L.S., Lunney J.G., Moore A., Ward J.M., and Thareja R.K., Phys. Rev. Lett., 44, 1669 (1980).

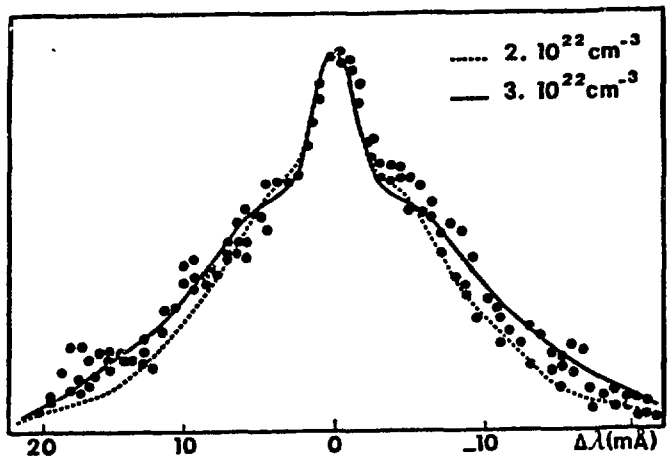

Figure 1 : Profile of the 1s4p-1s^2 Al^{11+} line. Theoretical profiles are the full and dotted lines (ion dynamics is included). Experimental points are obtained for an incident intensity of 3.10^{14} W/cm^2.

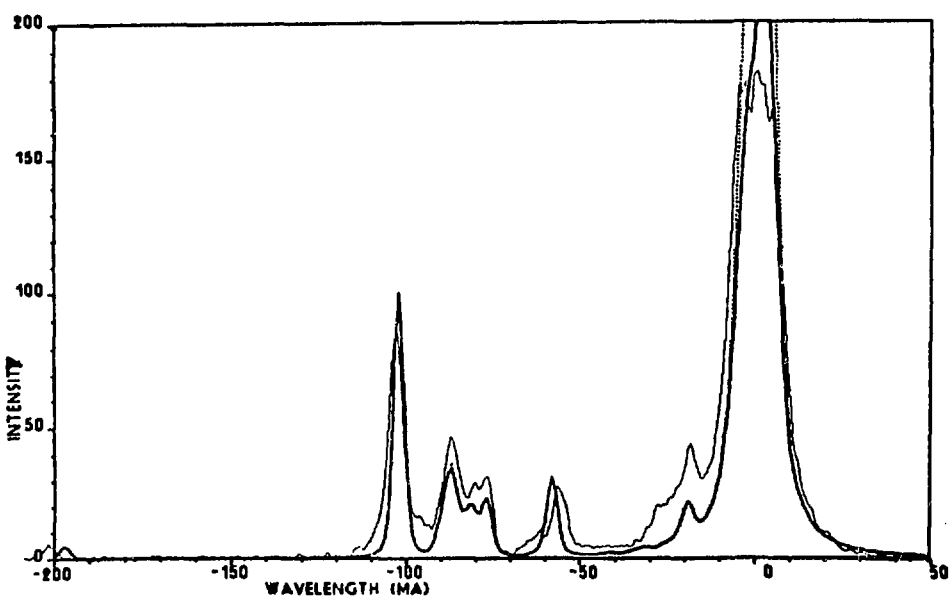

Figure 2 : Dielectronic satellites of the Lyα line. The experimental spectrum (noisy curve) is fitted with theoretical ones obtained for the following conditions : $n_e = 10^{23}cm^{-3}$, T_e = 400 eV, optical thickness of the plasma = 25 µm, the ratio of the populations of hydrogenic and helium-like ions is half of the collisional-radiative equilibrium value.

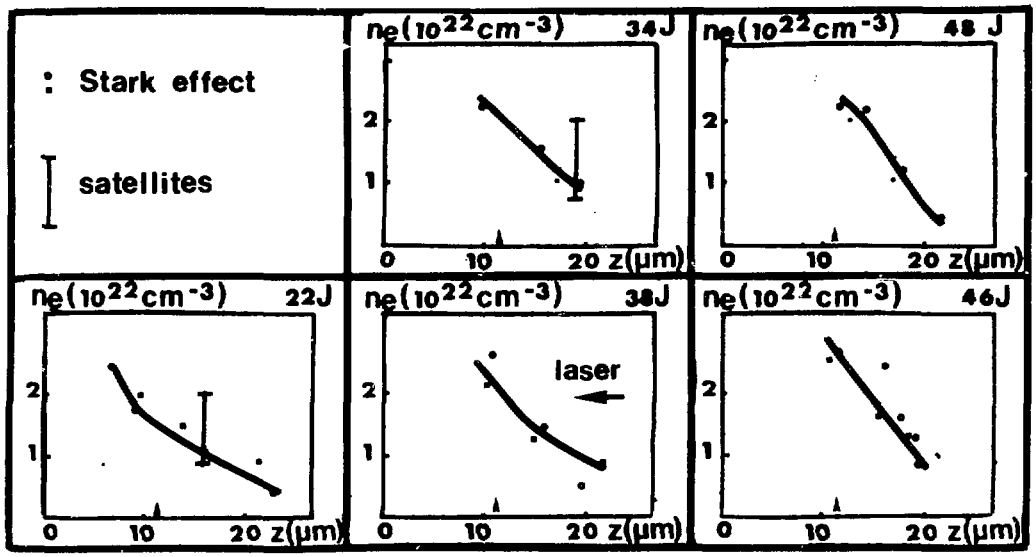

Figure 3 : Electronic density along the laser axis for several laser shots (22 to 48 Joules). The upper profiles obtained on a 50 μm diameter aluminum microdot and the lower on a 25 μm diameter microdot give similar results. The arrow indicates the maximum of emission of the Al^{11+} 1s4p-1s^2 line. Circles are measured on this Al^{11+} line, and square from the Al^{12+} 4p-1s line.

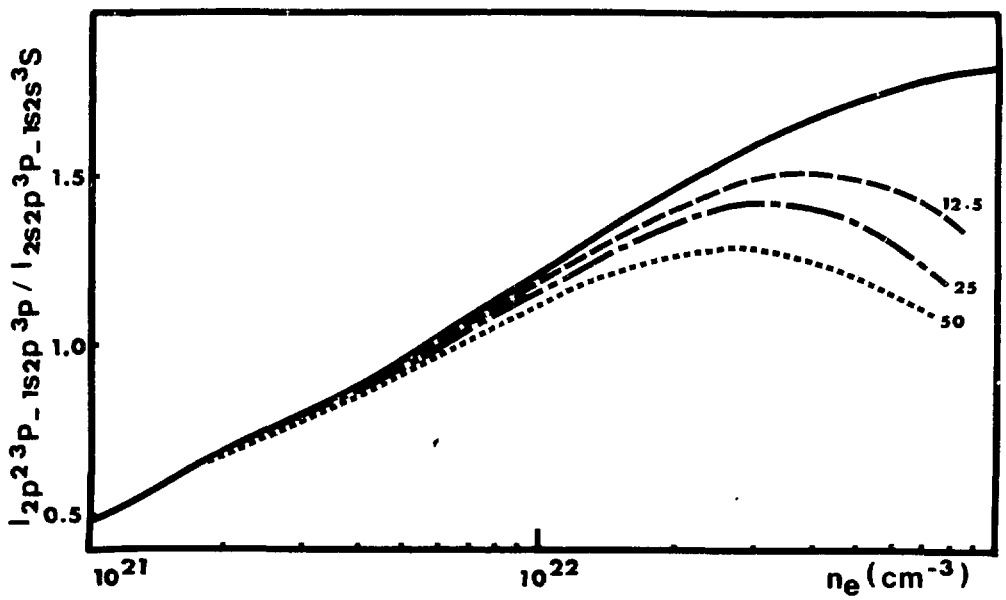

Figure 4 : Effects of reabsorption on the intensity ratio of Ly α satellite lines. Ratio of the $2p^2\ ^3P$-$1s2p\ ^3P$ to $2s2p\ ^3P$-$1s2p\ ^3S$ line is plotted versus electronic density. Electronic temperature has been fixed at 400 eV. Full line : no reabsorption - Dotted lines : 12.5 μm, 25 μm and 50 μm optical thickness of the plasma.

HIGH RESOLUTION LITHIUM LIKE SATELLITES TO THE $1s^2\ {}^1S_0 - 1s\ 3p\ {}^1P_1$ LINE IN LASER-PRODUCED DENSE PLASMAS

P. Audebert, J.P. Geindre, J.C. Gauthier
Ph. Alaterre and C. Popovics
Greco ILM, Ecole Polytechnique
F 91128 Palaiseau Cedex, France

M. Cornille and J. Dubau
Observatoire de Paris, Daphe, F 92190 Meudon, France

The dielectronic satellite lines from the $1s2l_a\ 3l_b$ and $1s3l_a\ 3l_b$ double-excited configurations of lithium-like ions have been studied experimentally and theoretically under dense-plasma conditions. Good agreement between theory and measurements performed in laser-target interactions at 0.53 m wavelength, 10^{14} W/cm^2 laser irradiance show that collisional equilibrium conditions are reached between n - 3 singly and double excited levels at electron densities greater than 10^{22} cm^{-3} in Al and Si.

OPACITY BROADENING AS A DENSITY DIAGNOSTIC FOR SPOT SPECTROSCOPY

J. P. Apruzese
Naval Research Laboratory, Plasma Physics Division
Plasma Radiation Branch, Washington, D. C. 20375

Recently, a novel technique known as spot spectroscopy has been developed[1-4] for use in diagnosis of laser-produced plasmas. This method involves the implantation of tracer microdots (circular or rectangular) of material in laser targets whose composition and size (typically about 100 μm) are known. Aluminum has been a popular choice since its K-shell lines are readily produced; however, any element appropriate to the experiment may be chosen. A major advantage of this technique is that the plasma produced from each microdot is generally homogeneous in the direction parallel to the plane of the original target. Since the dots can be distinguished spectroscopically, the diagnosis of each spot is not subject to the ambiguities created by the presence of gradients. Gradients do exist in each blowoff tracer perpendicular to the target plane; however, it is possible to resolve spatially the cylindrical blowoff created by each dot with appropriate orientation of the spectrograph slit.[2]

It is our purpose to demonstrate and quantify an additional important benefit of this technique. The radius of the spot blowoff has been found to be equal to that of the original target implant, with little lateral spreading. Therefore, if the line center optical depth τ_o of a particular spectral line can be determined from the line profile, the density N of the ionic species emitting the line is unambiguously determined from $N = \tau_o/\sigma_o r$, where σ_o and r are the line center cross section and spot radius, respectively. The total ion density N_I is obtainable from calculations of the fractional abundance of the active species based on line ratios or other temperature diagnostics. Therefore, spectroscopic resolution of line profiles may serve as an important density diagnostic in conjunction with the spot spectroscopy technique.

A multistage, multistate model of ionized aluminum, analogous to the Ar model of Ref. 5, has been used to calculate the full-width-half-maximum (FWHM) of the helium-like resonance line $1s^2$-$1s2p\,^1P$ as a function of spot size, temperature, and density. As is described in Ref. 5 the line profiles are calculated with detailed multifrequency solutions of the radiative transfer equation, which are self-consistent with the steady-state atomic rate equations. The particular line chosen is most suitable for opacity-based density diagnosis for several reasons. First, it is the strongest and therefore most easily measured K-shell line. Second, it has the largest opacity of any line for a wide range of temperatures where K-shell ionization stages dominate. Third, the complicating effects of fine structure[5], which exist for the Lyman series, are absent. Finally, the Stark width of this line is negligible for the low-to-moderate densities considered here. Detailed Stark profile calculations[6] show that the Stark width of $1s^2$-$1s2p\,^1P$ is at most 10% of the Doppler width for the temperatures and densities considered here, for $10 \leq Z \leq 18$. Therefore, our assumed Voigt profile describes the line opacity accurately. Of course, the higher lines of the helium-like resonance series have much larger Stark widths, which may themselves be employed[3,4] for corroborative density diagnosis.

These calculations have been performed for a cylindrical geometry, which is appropriate for the blowoff created by circular tracer dots. The length of the cylinder is assumed to be much greater than the diameter. Two tracer diameters, 65 μm and 220 μm have been considered, each at three assumed ion temperatures (T_I, where $T_e = T_I$) of 300, 450, and 750 eV. Assumed ion densities (N_I) ranged from 10^{18} to 4 x 10^{20} cm^{-3}.

Some typical calculated profiles for Aℓ XII $1s^2$–$1s2p\,^1P$ appear below. The absolute intensity at the surface of the blowoff cylinder is plotted vs. displacement from line center in mÅ for 65 μm diameter spot cylinders. As the ion density increases the line broadens and develops the expected self-reversal as the higher optical depth forces the photons to the thinner line wings to escape the plasma.

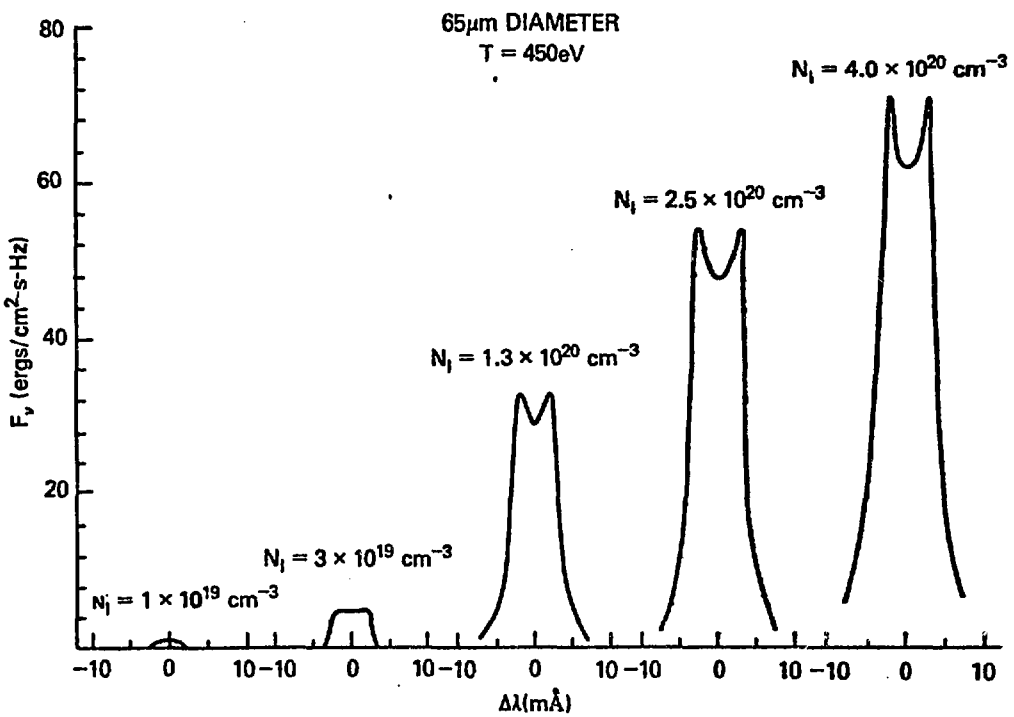

The principal numerical result, directly applicable to experimental measurements, is the evaluation of line width (FWHM) as a function of plasma size, temperature, and density. This appears in the two figures below for aluminum plasma cylinders of diameter 65 μm and 220 μm, respectively. These calculations are strictly accurate only for aluminum. Note, however, that the densities, temperatures, and widths are scaled in these figures to provide for similar approximate diagnoses for elements of different atomic number. It is recommended that these scalings not be employed outside the range $10 \leq Z \leq 18$. A derivation of these Z-independent variables is given elsewhere[7].

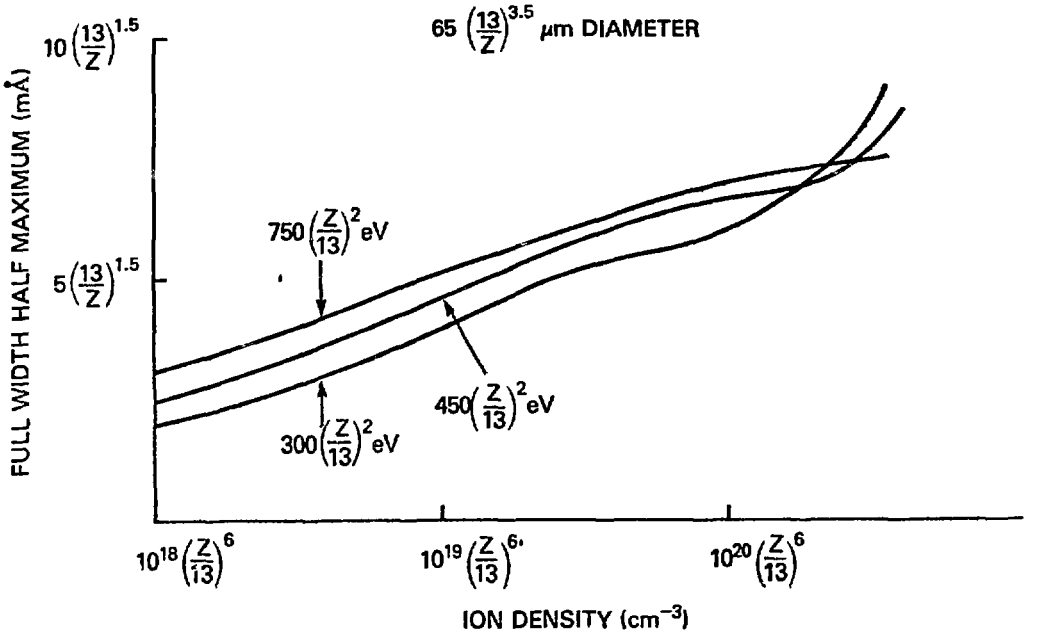
65 $\left(\frac{13}{Z}\right)^{3.5}$ μm DIAMETER
$10\left(\frac{13}{Z}\right)^{1.5}$
$5\left(\frac{13}{Z}\right)^{1.5}$
FULL WIDTH HALF MAXIMUM (mÅ)
$750\left(\frac{Z}{13}\right)^2$eV
$450\left(\frac{Z}{13}\right)^2$eV
$300\left(\frac{Z}{13}\right)^2$eV
$10^{18}\left(\frac{Z}{13}\right)^6$
$10^{19}\left(\frac{Z}{13}\right)^6$
$10^{20}\left(\frac{Z}{13}\right)^6$
ION DENSITY (cm^{-3})

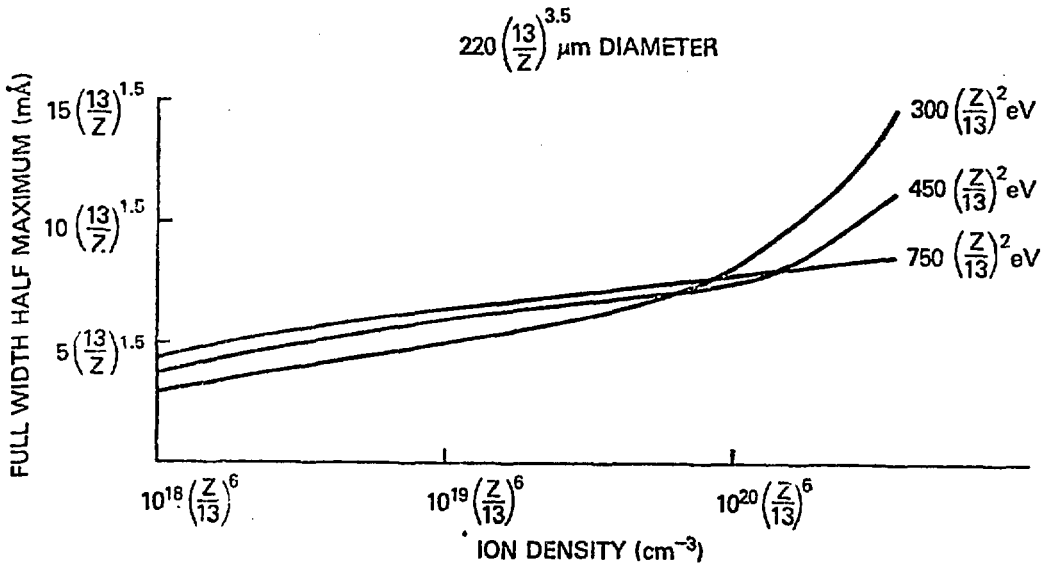
$220\left(\frac{13}{Z}\right)^{3.5}$ μm DIAMETER
$15\left(\frac{13}{Z}\right)^{1.5}$
$10\left(\frac{13}{Z}\right)^{1.5}$
$5\left(\frac{13}{Z}\right)^{1.5}$
FULL WIDTH HALF MAXIMUM (mÅ)
$300\left(\frac{Z}{13}\right)^2$eV
$450\left(\frac{Z}{13}\right)^2$eV
$750\left(\frac{Z}{13}\right)^2$eV
$10^{18}\left(\frac{Z}{13}\right)^6$
$10^{19}\left(\frac{Z}{13}\right)^6$
$10^{20}\left(\frac{Z}{13}\right)^6$
ION DENSITY (cm^{-3})

In applying the curves above to tracer dot sizes and temperatures other than those given, the following procedure using linear interpolation is recommended. First, determine the density which reproduces the observed width for both the 65 μm and 220 μm cases. Next, interpolate to find the density for the actual size of the experimental tracer plasma. Extrapolation to sizes as low as 50 μm or as large as 300 μm is reasonable. Needless to say, the "observed" width referred to above is the "bare" line width, i.e., all source and instrumental broadening should be deconvolved from the raw measured profile.

ACKNOWLEDGMENTS

The author has benefitted from valuable discussions with P. Burkhalter. This work was supported by the U. S. Department of Energy.

REFERENCES

1. Herbst, M. J., Burkhalter, P. G., Grun, J. Whitlock, R. R., and Fink, M., Rev. Sci, Instrum. 53, 1418 (1982).
2. Burkhalter, P. G., et al., Phys. Fluids 26, 3650 (1983).
3. Gauthier, J. C., et al., J. Phys. D 16, 1929 (1983).
4. Alaterre, P., Popovics, C., Geindre, J. P., and Gauthier, J. C., Opt. Commun. 49, 140 (1984).
5. Apruzese, J. P., Davis, J., Duston, D. and Clark, R. W. Phys. Rev. A 29, 246 (1984).
6. Kepple, P. C. and Rogerson, J. E., Naval Research Laboratory Memorandum Report No. 4216 (1980).
7. Apruzese, J. P., J.Q.S.R.T., in press.

ABSORPTION SPECTRA OF LIGHT IONS IN THE EXTREME ULTRAVIOLET

E. Jannitti
Istituto Gas Ionizzati, C.N.R., Padova
P. Nicolosi, F. Pinzhong, G. Tondello
Istituto di Elettrotecnica ed Elettronica, Università di Padova, Italy

We have used the method of two laser produced plasmas (Jannitti et al. 1984a) to measure the absorption spectra of the ions Be^{++} (Jannitti et al. 1984b), Be^{+} (Jannitti et al. 1984c) and B^{+} in the grazing incidence and normal incidence region. Both discrete and continua transitions have been measured and values of the photoionization cross sections are derived.

The experimental set up referring to the normal incidence investigation is shown in Fig. 1. A laser beam of 10 J of energy and 15 ns (FWHM) duration is split in two parts and generates two plasmas: one on target T of high atomic number (Cu) used as a background continuum emitting source and a second on target A for producing the absorbing species to be studied. For the latter a sphero-cylindrical lens is used producing a focal spot 100 μm wide and up to 10 mm long. The continuum radiation produced on a target tilted 45° both with respect to the laser beam and to the axis of observation was collected by a toroidal mirror whose radii of curvature, $R = 640$ mm in the plane of incidence and $\rho = 530$ mm in the plane perpendicular to the former are such to compensate the astigmatism of the 2 m radius grating.

On the focal surface of the spectrograph a movable trolley carries a plate, coated with $\tilde{\sim}$ 1 mg/cm^2 of scintillator (TPB). The latter is imaged outside the vacuum with two high speed objectives (N.A. = 0.75) on an intensified photodiode array (512 elements) connected to an optical multichannel analyzer (OMA). In between the objectives a filter selects only the radiation emitted by the scintillator. The output of the OMA is sent to a PDP 11 computer for further data processing. A sequence for acquiring the absorption coefficient $k(\lambda)$ is:

1) acquisition of $I_o(\lambda)$, the spectrum of the background source;
2) acquisition in the same condition of the stray light $I_s(\lambda)$ by moving the stigmatic spectrum out of position;
3) acquisition of $I(\lambda)$, the absorption spectrum with both plasmas;
4) acquisition of the emission spectrum $I_e(\lambda)$ by producing the absorbing plasma alone. Then $k(\lambda) = \ln \left\{ I_o(\lambda) - I_s(\lambda) \right\} / \left\{ I(\lambda) - I_s(\lambda) - I_e(\lambda) \right\}$; from 10 to 30 complete sequences were acquired for any spectral position $\cong$100 Å wide.

Several of such portions were later cumulated together and joined.

Fig. 2 shows the absorption spectrum of B^{+} in the region 450-1380 Å, recorded at 1.5 mm distance from the target. All of the main transitions in the normal spectrum and several of the displaced one are present with several newly observed lines (Ölme, 1970). Clearly visible are the jumps

corresponding to the photoionization of a $p(2p \rightarrow \varepsilon d)$ and $s(2s \rightarrow \varepsilon p)$ electron. The region below 450 Å has not been measured because of the lack of reflectivity of the present system (toroidal mirror and grating). Only a minor contribution is present in the spectrum of Fig. 2 from the ion B^{++} and none from neutral boron indicating the selectivity of the present technique.

The region around the $2p \rightarrow \varepsilon d$ limit is shown enlarged in Fig. 3. Here the experimental data are indicated with dashes and refer to a distance from the target of 1 mm. It comprises also few 2p-ns lines. The true absorption coefficient of the series 2p-nd has been derived with the method explained by Jannitti et al. (1984b,c). Briefly a syntetic spectrum, consisting of a series of Voigt profiles simulating the true absorption spectrum, shown with dotted lines in Fig. 3, is convoluted with the instrumental function yielding a model absorption spectrum (solid line in Fig. 3) that is compared with the experimental one. The instrumental function has been carefully determined recording the absorption from a narrow line. A best-fit process is carried on with free parameters the normalized Voigt profiles $\phi_i(\lambda)$ that mainly affect the width of the lines and the line density: $\int n(^3P)d\ell$ where $n(^3P)$ is the density in the $2s2p\ ^3P^\circ$ state and the integral is taken along the plasma length ℓ, that determines the peak value of the absorption coefficient $k(\lambda_o)$ at the centre of the line profile λ_o. The fit obtained is quite good despite the fact that there is nearly a factor of two distortion in the measured absorption coefficient on the 2p-5d and 2p-6d lines due to the instrumental function. The relative values of the oscillator strengths both for discrete and continuous transition can now be determined. Unfortunately no measurements of absolute f values exist for high n numbers 2p-nd lines. We have used the calculations by Markiewicz et al. (1981). The 2p-5d line is not well suited because of a merging with a strong B^{++} line, similarly the 2p-6d line is merged and perturbed by the $2s2p\ ^3P^\circ$-$2p3p\ ^3D$ line. Using the 7d and 8d lines we get: $\int n(^3P)d\ell = (8.2 \pm 0.5) \times 10^{16}\ cm^{-2}$ and $\sigma(2p \rightarrow \varepsilon d) = (4.2 \pm 0.4) \times 10^{-18}\ cm^2$.

Merging lines can be resolved moving further out from the target. At 1.5 mm the density of the plasma is lower and the lines are resolved. However the broadening of the lines is now comparable with the instrumental one and the convolution process becomes less precise. Fig. 4 shows the true absorption coefficient (solid line) for the same region as in Fig. 3 with the various components present (dotted lines as marked).

We conclude that the present technique is well suited for the measurement of relative f-values both for discrete and continuous transitions in ions.

ACKNOWLEDGMENTS

F. Pinzhong on leave from the Institute of Optics and Fine Mechanics Shanghai, People Republic of China was supported by the International Centre

for Theoretical Physics (Trieste, Italy).

REFERENCES

Jannitti, E., Nicolosi, P. and Tondello, G. Physica, 124C, 139, 1984a.

Jannitti, E., Nicolosi, P. and Tondello, G. Opt. Commun., 50, 225, 1984b.

Jannitti, E., Mazzoni, M., Nicolosi, P., Tondello, G. and Yongchang, W., submitted to J.O.S.A. part B, 1984c.

Markiewicz, E., McEachran, R.P. and Cohen, M. Phys. Scripta, 23, 828, 1981.

Ölme, A. Phys. Scripta, 1, 256, 1970.

Fig. 1

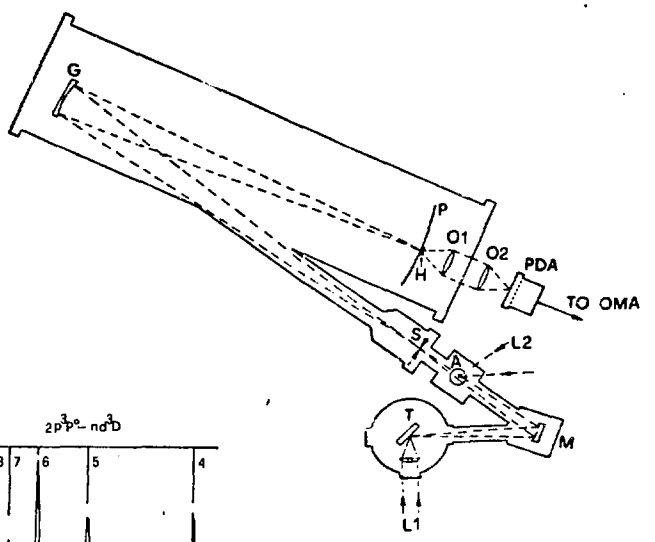

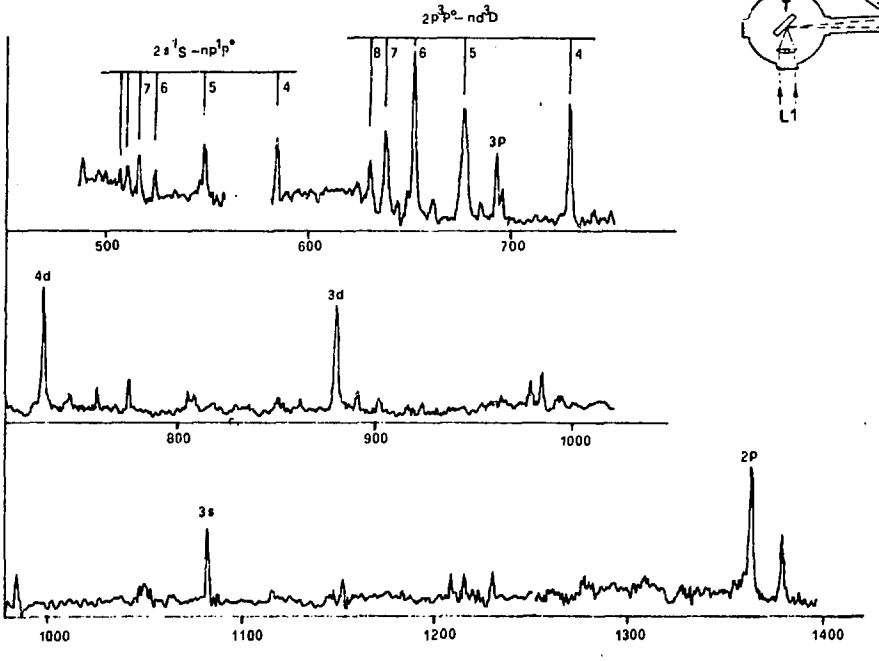

Fig. 2

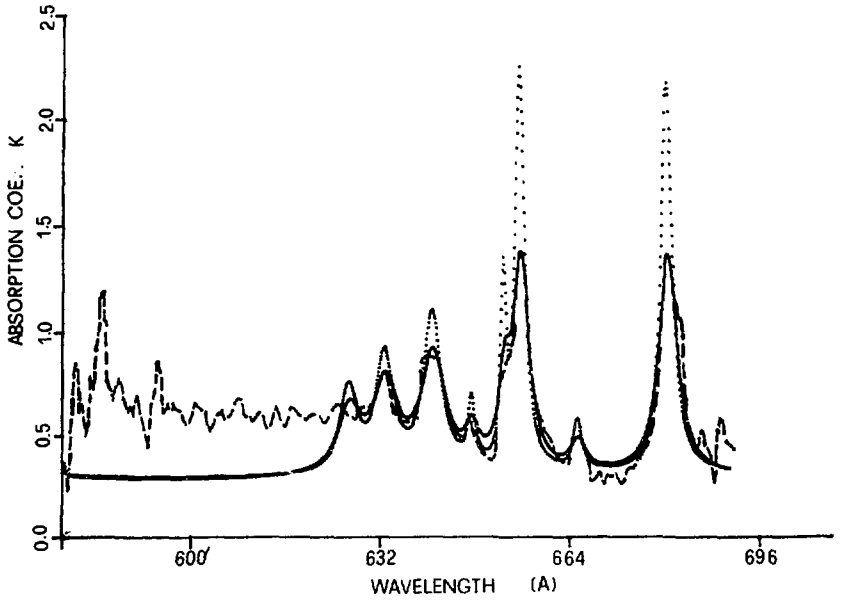
ABSORPTION COE.. K
0.0
0.5
1.0
1.5
2.0
2.5
600
632
664
696
WAVELENGTH (A)

Fig. 3

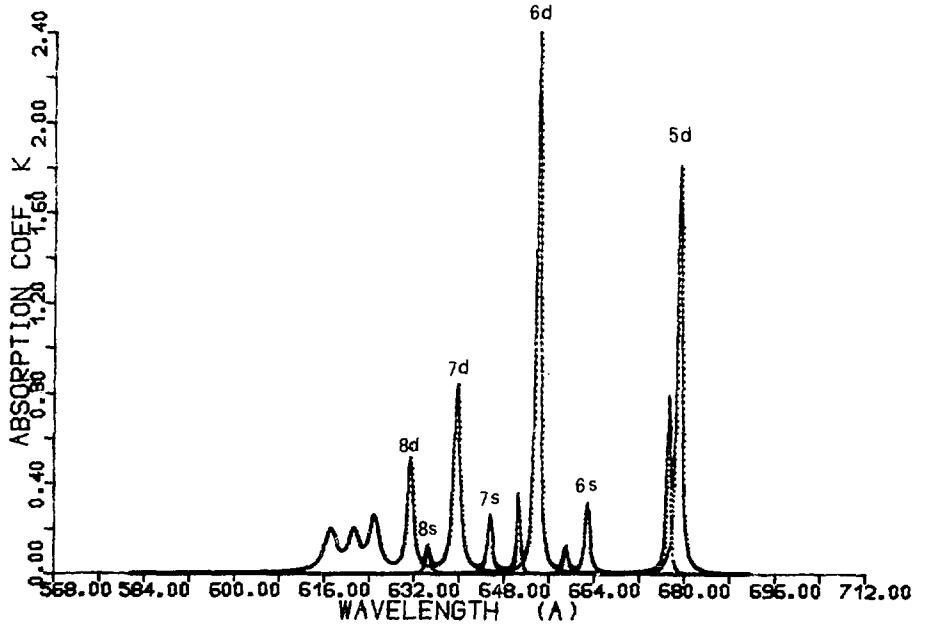
ABSORPTION COEF. K
0.00
0.40
2.00
2.40
6d
5d
7d
8d
8s
7s
6s
568.00 584.00 600.00 616.00 632.00 648.00 664.00 680.00 696.00 712.00
WAVELENGTH (A)

Fig. 4

X-RAY SPECTROSCOPY TO DETERMINE LINE COINCIDENCES BETWEEN K- AND L-SHELL TRANSITIONS

P.G. Burkhalter, D. Newman*, J.V. Gilfrich and D.B. Brown
Naval Research Laboratory
Washington, DC 20375

P.D. Rockett and G. Charatis
KMS Fusion, Inc.
Ann Arbor, MI 48106

C. Hailey and D.L. Matthews
Lawrence Livermore National Laboratory
Livermore, CA 94550

B. MacGowan
Imperial College
London, England

Accurate wavelengths for highly-ionized L-shell spectra were measured in the 10-16Å region. The purpose being to determine lines in coincidence with L-shell transitions from the elements oxygen, fluorine, and neon. L-shell transitions have been proposed for resonant photopumping of K-shell electrons in these elements to generate lasing between upper levels in the 40-150 eV region.[1] The current effort improves on and expands the earlier spectroscopic work performed at KMS Fusion, Inc., where possible line coincidences were identified for photoionizing in the 1-3 and 1-4 levels in fluorine.[2] New experimental techniques have led to a wavelength accuracy now believed to be $\pm$ 2 mÅ for cases in which adequate calibration lines are available. Exact spectral line matches were found for Mn with the F H_β line at 12.643Å and for both Mn and Cr with the F He_β line at 14.458Å. The Mn line at 12.643Å has been identified, using ab initio atomic structure calculations, as the $^1D_2 - {}^1F_3$ transition in Be-like Mn XXII. The Mn line emissivity was determined to be 30 MW into 2π steradians for a conversion efficiency of 0.04%. Photopumping with Mn coated gas-filled targets is presently being tried in gain measurement experiments at LLNL.[3]

X-ray spectra were collected under controlled illumination and target conditions in order to examine a number of potential L-shell lines. These lines represented cases where near agreement between L-shell transitions and the 1-3 transitions in He- or H-like O, F and Ne had been previously reported. The KMSF CHROMA laser was used to generate a plasma source of soft x-ray emission. The glass laser was operated in the frequency-doubled mode ($0.527\,\mu$m) for enhanced light absorption at an irradiance of $1.5 \cdot 10^{14}$ W/cm^2.

Several new techniques were used in this experiment to improve the wavelength accuracy. These included (1) the use of a cylindrically-focused lens and end-on viewing of the plasma source, (2) the use of short-laser pulses of 120 psec duration to reduce the extent of x-ray

(*Sachs/Freeman Associates, Inc., Bowie, MD 20715)

emission due to plasma expansion, (3) the targets were viewed at 90° to the laser beam to minimize the Doppler shifts, (4) the use of high-sensitivity x-ray film and active-element intensified spectrographs, and (5) in a few shots, a split target was used to confirm the line coincidences in single laser shots.

Two high-resolution spectrographs viewed the target in the same plane, both at 90° to the laser beam. This arrangement allowed viewing the plasma end-on, resulting in an effective source size of about 100 μm. Another intensified spectrograph viewed from behind the target. Its diffraction crystal was set to record spectral data at wavelengths corresponding to the 1-2 transitions in the ionized gases.

Spectral data were collected directly onto film in the passive spectrograph. the film selected was Kodak direct exposure film S0445 (DEF). This film has a good sensitivity and a low background fog level. The DEF film is about 3 times more sensitive than Kodak No Screen film.[4] Spectral data were recorded in either one or two shots per element with the passive spectrograph, and with intensified spectrographs incorporating microchannel plates.[5]

The data were recorded as spectral pairs on the spectrograms. Target elements for calibration purposes were carefully selected for each of the spectral regions investigated. Fig. 1 shows a typical spectrogram collected with a beryl diffracting crystal directly onto film. The 2p-3d F-like Fe XVIII transitions were used for calibration of the Mn lines. Fig. 2 shows spectrograms collected with one of the intensified spectrographs near 12.6Å. Line calibration for the Mn spectra was provided by Fe, Ca, and Cr lines in this spectral region. These juxapositioned spectral pairs were read on a Grant comparator densitometer which was set up to read both strips alternately with a Decker system. In a few shots, confirmation of the line coincidences was observed in spectrograms from split targets. These targets were formed by coating half the plastic substrate with the candidate element and the other half with CaF_2. By using spatial imaging, the upper spectra in Fig. 2 were collected in a single laser shot.

The results of the wavelength measurements are listed in the Table for the various spectral regions. Exact line coincidences were found in the first two cases with fluorine 1-3 transitions. The wavelengths for the nearest lines are listed for other metal L-spectra that match K-lines in neon and oxygen (in two cases within 4 mÅ). Lines were absent in Mn spectra that coincided with 1-2 transitions in fluorine. These would have spoiled the lasing scheme by filling the lower level.

References

1. P.L. Hagelstein, Plasma Physics 25, 1345 (1983), and "Physics of Short Wavelength Laser Design," UCRL-53100 (1981).
2. P.G. Burkhalter, G. Charatis, and P.D. Rockett, J. Appl. Phys. 54, 6138 (1983).
3. D.L. Matthews, et al. (current experiments on Novette).
4. P.D. Rockett, et al. (to be published).
5. C. Hailey, et al. Second Topical Meeting on Laser Techniques in the Extreme Ultraviolet, Mar. 5-7, 1984, Boulder, CO.

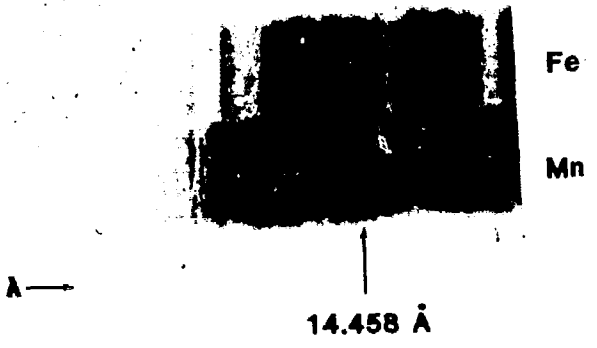

Figure 1. Spectral lines for Fe and Mn collected with passive spectrograph.

L-SERIES X-RAY WAVELENGTH MEASUREMENTS

LINE TO BE PUMPED		PUMP WAVELENGTH	TARGET PAIRS	MEASURED WAVELENGTH	ELEMENT
FLUORINE	He_β	14.458Å	Mn,Cr/Fe Mn,Cr/CaF_2 Mn/Cr	14.458 ± 2 mÅ	Mn/Cr
	H_β	12.643	Mn/Fe,Cr Mn,Cr,Fe/CaF_2	12.643 ± 2	Mn
NEON	He_β	11.547	Ni/Fe Ni/Mn	11.551 ± 3 11.556	Fe Ni
	H_β	10.239	Zn/Co Zn/V	10.242^5 ± 3 10.244	Zn Co
OXYGEN	H_β	16.006	V/Fe V/FORMVAR	15.998 ± 3 16.003	V Fe

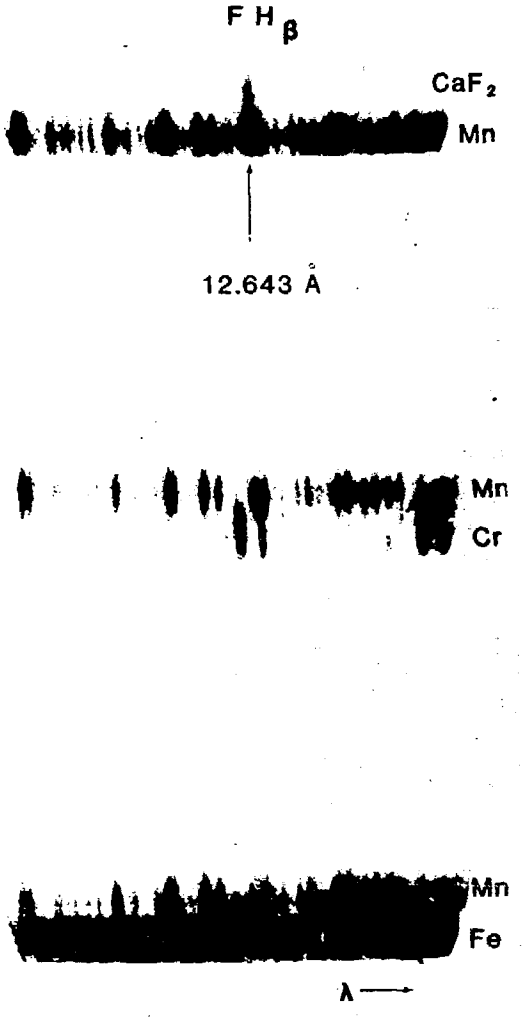

Figure 2. Spectrograms from an intensified detector system. Upper set shows line coincidence for F and Mn lines at 12.643 Å.

SPECTRAL LINE INTENSITIES FOR $\Delta n = 0$ (L-SHELL) TRANSITIONS OF N, O, AND F-LIKE IONS

Y. T. Lee and K. Reed
University of California, Lawrence Livermore National Laboratory
Livermore, California 94550

Many laboratories are actively investigating radiation spectra emitted from high temperature/high density plasmas produced using gas-puff Z-pinch machines and high power lasers. Spectral-line intensities from these plasmas can be useful temperature and density diagnostics. In a well-diagnosed plasma, information on the emission spectrum can also be used to test the accuracy of theoretical rate coefficients.

Recently time-resolved spectra[1] from an oxygen-like argon plasma produced in a gas-puff z-pinch were measured in the wavelength range 150-200 Å. Over this wavelength range the spectrum contains mostly the $\Delta n = 0$ (L-shell) transitions in ArX-ArXIV and some weak transitions for $n = 3$ to $n = 4$ of ArVI-ArVIII. The measured spectra show the predominance of O-like Ar L-shell transitions.

We have developed a model to calculate spectral-line intensities for all the $\Delta n = 0$ (L-shell) transitions in ArXII to ArX as a function of electron temperature and density. Applying these results, we have obtained: (1) spectral-line intensity ratios which can be used to estimate electron temperature and density, (2) synthetic emission spectra to fit experimental measurements.

Our calculation assumes that the plasma has small temperature and density gradients and also neglects the effects of radiation transport. Rather than simulating all the complexity of the plasma, we have developed a simple model which treats only the atomic physics completely. In situations where gradients or radiation transport are important, our model is still very useful to give an upper-bound on experimental data.

Our calculation consists of two steps. First, we apply an ionization balance code[2] to calculate the population of the $n = 2$ states of N, O, and F-like ions as a function of electron temperature and density. This code lumps the energy levels with the same principle quantum number together to form a single level. The code includes ionization not only from the ground state but also from the excited states. The effect of excited state ionization is to increase the charge-state abundance at lower temperatures. Based on our ionization balance calculation and the predominance of O-like Ar transitions after pinch time, we estimate an electron temperature of 90 eV in these experiments.[1]

The second step is to employ results from the ionization balance calculation to normalize the relative populations given by the detailed atomic spectroscopy code. In the spectroscopy code the relative population for the excited states of an ion is determined by the balance between electron collisional excitation and dexcitation and radiative decay. We assume the effects of ionization and radiative recombination on the excited state populations are negligible since the electron collisional excitation rates are larger than both the ionization and radiative recombination rate by a large factor (approximately 10^2).

The energy levels and oscillator strengths[3] employed in the calculation were computed using the code SUPERSTRUCTURE.[4] Available measurements[5] of the energy levels were also used. The electron collision strengths[3] for all the $\Delta n = 0$ (L-shell) transitions were computed in a distorted-wave approximation using programs developed by Eissner, Seaton,[6] and Saraph.[7] The calculation employs configuration interaction wavefunctions which are generated using single particle orbitals for modified Thomas-Fermi potentials.

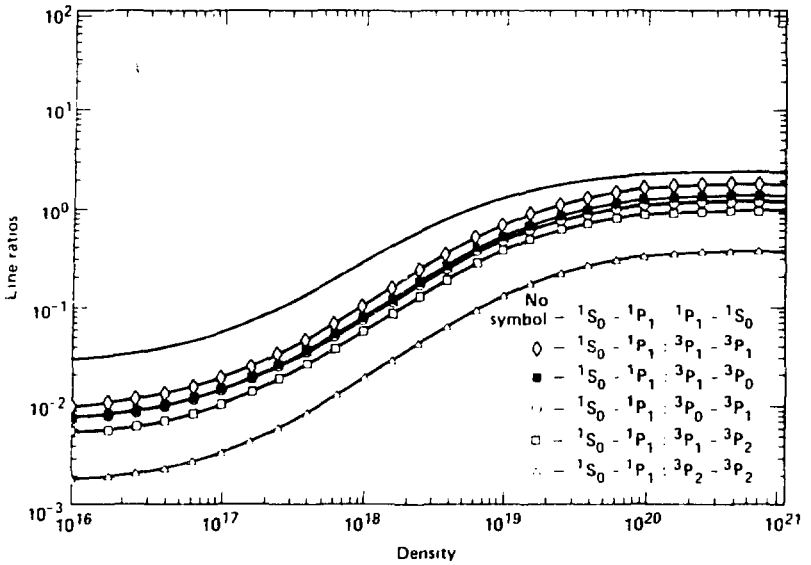

FIG. 1 Density sensitive spectral-line intensity ratios for O-like Ar.

In Fig. 1 we present density sensitive line ratios for $\Delta n = 0$ transitions of O-like Ar. These ratios involve the $^1S_0 - {}^1P_1$ transition from the doubly-excited state to a singly-excited and six transitions from singly-excited states to states in the ground state configuration. These ratios strongly depend on the electron density at 10^{17} cm^{-3} $\leq n_e \leq$ 10^{19} cm^{-3} and approach the LTE limits at $n_e \geq 10^{20}$ cm^{-3}. Since these line intensity ratios all contain a transition which ends up in a state in the ground configuration, their values are significantly affected by the opacity of the plasmas.

In Fig. 2 we give a line-intensity ratio which can be used to estimate the electron temperature of the plasma if its electron density is known. This ratio involves two transitions from a doubly-excited state to a singly-excited state. Since both transitions end up in the excited state, the probability for absorption of the emitted photon is very small. Therefore, this line-intensity ratio should be a good temperature diagnostic once the electron density is determined.

Also plotted in Fig. 2 is a data point for the line-intensity ratio obtained from a recent measurement.[1] Based on the line-intensity ratio for $\Delta n = 0$ transition of O-like Ar (Fig. 1), the electron density of the plasma core was estimated to be 10^{19}cm^{-3}. Using this result for the density, Fig. 2 gives an electron temperature of 90 eV.

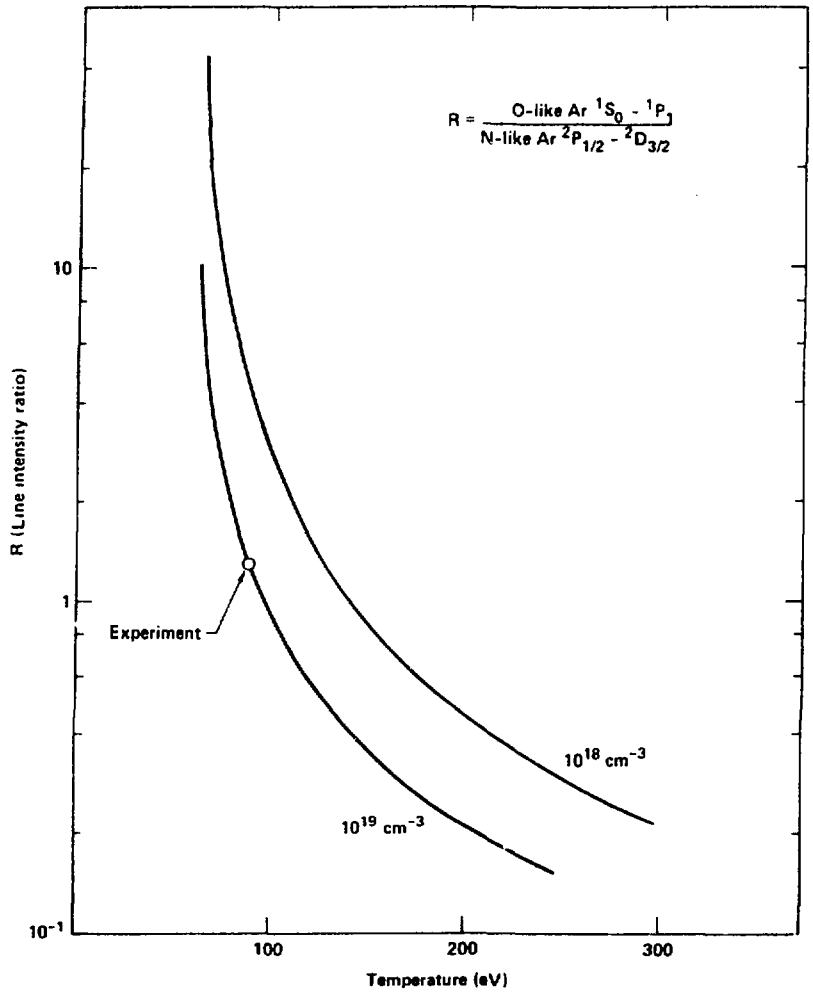

FIG. 2 Temperature sensitive spectral-line intensity ratios. Both transitions start from a doubly-excited state to a singly-excited state.

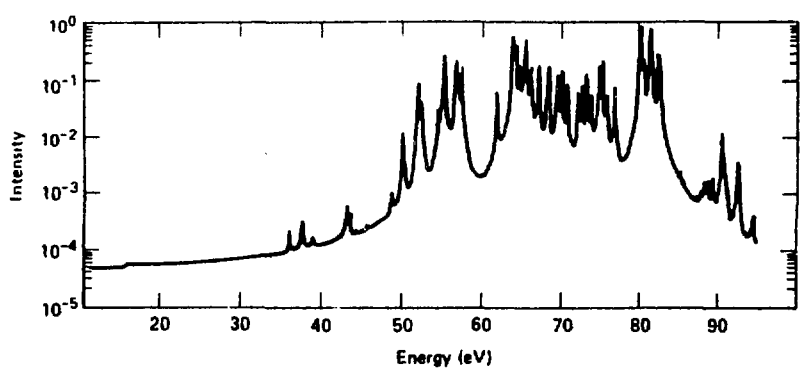

FIG. 3 A synthetic spectrum for the following plasma conditions: (1) electron density = 10^{19} cm^{-3}, (2) ion density = 10^{18} cm^{-3}, (3) temperature = 90 eV, (4) line-width = 0.1 eV, and (5) plasma size = 0.01 cm.

In Fig. 3 we present a typical synthetic spectrum produced using the code SPECTRA[8] for the excited state populations from our calculation.

In summary, we have developed a simple model to calculate spectral-line intensities emitted from a plasma as a function of electron density and temperature. Line-intensity ratios which are useful diagnostics for electron temperature and density are obtained. We have produced synthetic spectra which can be used to fit experimental data to determine plasma temperature and density.

This work was performed under the auspices of the U. S. Department of Energy by the Lawrence Livermore National Laboratory under contract No. W-7405-ENG-48.

REFERENCES

1. R. E. Marrs, D .D. Dietrich, R. J. Fortner, M. A. Levine, D. F. Price, R. E. Stewart, and B. K. F. Young, Ap. Phys. Lett. 42, 946, 1983.

2 Y. T. Lee, "Ionization Balance in Non-Equilibrium Plasmas," LLNL H-Division Quarterly Report, UCID-18574-83-3, 1983.

3. Some of the energy levels, oscillator strengths, and collisional strengths used in the calculation were provided to us by U. Feldman.

4. W. Eissner, M. Jones, and H. Nussbaumer, Comp. Phys. Commun. 8, 270, 1974.

5. B. C. Fawcett, Atomic Data and Nuclear Data Tables 16, 135, 1975.

6. W. Eissner and M. J. Seaton, J. Phys. B 5, 2187, 1972.

7. H. E. Saraph, Com. Phys. Comm. 1, 232, 1970.

8. R. W. Lee, B. L. Whitten, and R. E. Strout II, JQSRT 32, 91, 1984.

DIELECTRONIC RECOMBINATION OF HIGHLY STRIPPED ARGON IONS: THEORETICAL CALCULATIONS AND DIRECT OBSERVATIONS IN AN EBIS SOURCE

M. Loulergue and J. Dubau
Observatoire de Paris Meudon

J.P. Briand and P. Charles
Université P. et M. Curie and Institut Curie, Paris

H. Laurent
Institut de Physique Nucléaire, Orsay

The dielectronic recombination is one of the most important atomic processes in highly ionised plasmas. It corresponds to the simultaneous capture of a free electron and excitation of an ion, i.e.

$$X^{+m+1} + e^- \rightarrow (X^{+m})^{**} \text{ (doubly excited)} \rightarrow (X^{+m})^* + h\nu.$$

It is a collisionally resonant process which occurs only at the energy of the corresponding autoionisation electron. We present here a preliminary theoretical analysis of the results of an experiment using a novel technique in which it is possible to observe the interaction of a given ion with an electron at a given energy and so to measure the differential dielectronic cross section corresponding to each resonant level of this ion.

This technique uses an electron-beam ion EBIS source (Briand et al, 1984) in which a very intense and very narrow electron beam is used to ionise a neutral gas that has been injected into the system. After being prepared the ions are trapped for a very long time (up to 10 s) inside the source. The electron-beam energy is then scanned incrementally in order to study the various dielectronic resonances of the ions by the observation of x rays which are emitted through a small hole drilled into the cathode. Each measurement at energy E of the electron beam corresponds a narrow electron-energy distribution G(E) of 16 eV. The x rays are detected after the plasma has reached a stationary equilibrium following each increment of the electron-beam energy. The relative abundance of the ions is given by the ionisation balance equation

$$Ne\ N(X^{+m})\ S = Ne\ N(X^{+m+1})\ (\alpha_r + \alpha_d) \qquad (1)$$

where $N(X^{+m})$ and $N(X^{+m+1})$ are the density of the ion ground states. S and α_r were calculated respectively using the Lotz ionisation cross sections (Lotz, 1967) and the hydrogenic photoionisation formulae given by Burgess (1969). Both cross sections were integrated over the energy distribution G(E). In this work, α_d, the dielectronic recombination coefficients were calculated using the usual nomenclature: SUPERSTRUCTURE AUTOLSJ (Bely-Dubau et al, 1982). In this preliminary work, the charge exchange was neglected in formula (1).

We then calculated the x-ray yield below 3 keV -i.e. the 1s-2p excitation threshold, where only dielectronic recombination can occur as a resonant process- and above 3 keV where only direct excitation behaves as a continuous process.

In both cases, the intensity I is given by:

$$I = Ne\, N(X^{+m}) < \sigma v > \qquad (2)$$

where $< \sigma v >$ is the excitation rate and the G(E) distribution was used.

For the dielectronic contribution we used the same calculations as the ones used for α_d and for the direct excitation contribution we used the calculations of Sampson et al (1978, 1979), for He-like and Li-like systems, and for Be-like and B-like systems we estimated them the former ones.

The theoretical results using an electron-beam resolution of 16 eV are given in Fig.1 and can be compared to the experimental results shown in Fig.2.

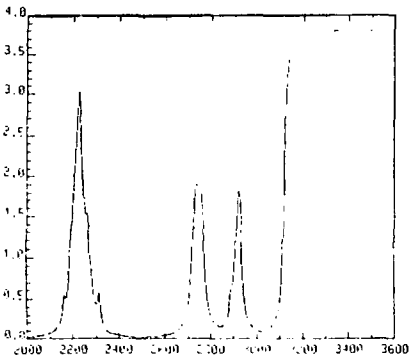

Fig. 1. Argon synthetic spectrum.

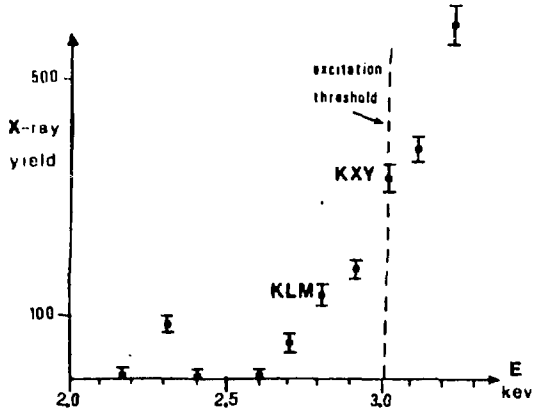

Fig. 2. Experimental x-ray yield (absolute counting rate). The horizontal error bar represents the uncertainty in the absolute energy of of the electrons.

The most proeminent experimental feature is at 2.3 keV, which corresponds to the dielectronic recombination of Ar^{14+}, whereas from the theoretical model used in Fig.1. the most proeminent feature corresponds to the dielectronic recombination on Ar^{15+} at 2.25 keV. This shift between the two features could be explained by too high abundance value of He-like ion compared to Li-, Be-, B-like abundances. Furthermore the excitation increase above 3 keV is steeper in the experimental results than in the theoretical model. We intend to introduce in the calculations, dielectronic recombination for larger quantum number which will fill the gap around 2.8 keV-3 keV. This will increase the x-ray field

and the theoretical results will be closer to the experimental ones in this energy range. This kind of theoretical analysis, whose feasibility has been tested in this work, will be used for ion source diagnostics as well as a test for the atomic data.

References

. Bely-Dubau F., Dubau., Faucher P., and Gabriel A.H., Mon. Nat. R. Astr. Soc. 198 239 (1982).
. Briand J.P., Charles P., Arianer J., Laurent H., Goldstein C., Dubau J., Loulergue M., and Bely-Dubau F., Phys. Rev. Lett. 52 617 (1984).
. Burgess A., Astrophys. J., 157 1008 (1969).
. Lotz W., Astrophys. J., Suppl. 14 207 (1967).
. Sampson D.H., Clark R.E.H., and Parke A.D., J. Phys. B: Atom. Molec. Phys. 12 3257 (1979).

A HIGH-RESOLUTION VUV SPECTROMETER WITH ELECTRONIC PARALLEL SPECTRAL DETECTION

C.L. Cromer, J.M. Bridges,
T.B. Lucatorto and J.R. Roberts
National Bureau of Standards
Washington, DC 20234

We demonstrate a new high resolution grazing incidence spectrometer system for spectroscopic applications in the range 50 to 400 Å. The instrument is comprised of a laser-plasma VUV continuum source, a 1.5 m grazing incidence spectrometer, and a 1024-channel VUV optical multichannel analyzer (VUV-OMA). The VUV-OMA is of new design, featuring a special resolution-enhanced channel electron multiplier array in an overall configuration chosen to optimize the spatial resolution of the detector while maintaining single-photoelectron sensitivity. The instrument has the capability of bringing the advantages of linear response and parallel spectral detection to general VUV photoabsorption studies of atoms, ions, molecules, and thin solid samples, as well as studies involving laboratory plasmas. The instrument has the additional special capability of performing time resolved absorption spectroscopy of transient species. The characteristics of the source and detector, along with various applications of the instrument to atomic physics will be discussed.

PAPERS NOT PRESENTED AT THE MEETING

A number of principal transitions of ions isoelectronic with copper 1 have been reported in several papers (1,7,8). We have observed all those transitions, and in addition we report here (Table-II) the following new transitions: 4s-6p; 4p-6p, 6d, 7d; 4d-6p, 7f; 5s-6p; and 5p-6s, 6d of Ag XIX and Cd XX which have not been observed so far. We have also observed $3d^{10}4s$-$3d^{9}4s4p$ and $3d^{10}4s$-$3d^{9}4p^{2}$ transitions in the region 29 - 33 A^{o}.

The 3d-4p, 5p and 3d-4f,5f transitions of Ag XX were reported by Schweitzer et al (9) while Wyart et al (10) reported $3d^{9}$-$3d^{8}$ 4p transitions of Ag XXI. We have identified the principal transitions of the ions Ag XVII - Ag XXI and Cd XVIII - Cd XXII involving energy levels with n=4,5,6,7 where n is the principal quantum number. A comprehensive listing of these transitions will appear in a separate publication (11).

One of us (MAK) would like to thank the Australian National University for a visiting fellowship position. The support of UPM research office is also acknowledged.

REFERENCES

(1) Reader,J., Acquista,N., and Cooper,D., 1983, J. Opt. Soc. Am. 73,1765.

(2) Khan,M.A., 1982 , J. Opt. Soc. Am, 72, 268.

(3) Desclaux,J.P., 1975, Comp. Phys. Commun., 9, 31.

(4) Rashid,K., 1980, Physica Scripta, 22, 114.

(5) Cheng,K.T. and Kim,Y.K. 1978, Atomic Data & Nucl. Data Tables 22, 547.

(6) Rashid,K., 1978, Atomic Data & Nucl.Data Tables, 21, 77.

(7) Khan,M.A., and Rashid,K. 1975, Opt. Commun. 15, 396 .

(8) Klapisch,M. et al, 1981, Phys. Lett. 84A, 177.

(9) Schweitzer,N. et al, 1981, J.Opt. Soc. Am. 71, 219.

(10) Wyart,J.F. et al, 1982, Physica Scripta 26, 141.

(11) Khan,M.A., Al-Juwair,H.A. and Tallents,G.J. 1984 to be published.

Table - I

Sample Comparison of our Calculated/Measured Wavelengths with thosepreviously Calcualted/Measured

Ion	Transition	Calculated Wavelength(A^o)		Observed Wavelength (A^o)	
		Present	Previous	Present	Previous
AgXIX	$4s\ ^2S_{1/2} - 5p\ ^2P_{3/2}$	52.46	52.98 (a)	52.37	52.37 (b)
	$4s\ ^2S_{1/2} - 5p\ ^2P_{3/2}$	53.15	53.85 (a)	53.14	53.16 (b)
Cd XX	$4d\ ^2D_{3/2} - 5f\ ^2F_{5/2}$	61.73	61.97 (c)	61.75	61.73 (b)
	$4d\ ^2D_{5/2} - 5f\ ^2F_{7/2}$	62.13	62.46 (c)	62.25	62.23 (b)
	$4s\ ^2S_{1/2} - 5p\ ^2P_{3/2}$	48.43	48.46 (c)	48.35	48.35 (b)
	$4s\ ^2S_{1/2} - 5p\ ^2P_{1/2}$	49.12	49.23 (c)	49.12	49.12 (b)

(a) Reference (6)

(b) Reference (1)

(c) Reference (5)

Table II

Classifications of Spectral Lines in the XUV Spectra of Ag XIX and CdXX

Transition	J-J	Ag XIX		Cd XX	
		λ_{obs} (A^o)	$\lambda_{calc.}$ (A^o)	λ_{obs} (A^o)	$\lambda_{calc.}$ (A^o)
$3d^{10}\ 4s(^2S)-3d^{10}6p(^2P)$	$\frac{1}{2}-\frac{3}{2}$	37.85	37.82	—	34.84
4s — 6p	$\frac{1}{2}-\frac{1}{2}$	38.1	38.01	—	35.02
$3d^{10}4p(^2P)-3d^{10}7d(^2D)$	$\frac{1}{2}-\frac{3}{2}$	35.32	35.50	32.58	32.56
$3d^{10}4p(^2P)-3d^{10}6d(^2D)$	$\frac{1}{2}-\frac{3}{2}$	40.83	40.76	37.62	37.45
$3d^{10}4p(^2P)-3d^{10}6s(^2S)$	$\frac{1}{2}-\frac{1}{2}$	44.69	44.64	40.98	40.91
$3d^{10}4d(^2D)-3d^{10}7f(^2F)$	$\frac{5}{2}-\frac{7}{2}$, $\frac{5}{2}-\frac{5}{2}$	43.17	43.28	39.52	39.48
4d — 7f	$\frac{3}{2}-\frac{5}{2}$	42.88	43.12	39.30	39.33
$3d^{10}4d(^2D)-3d^{10}6p(^2P)$	$\frac{3}{2}-\frac{3}{2}$	56.57	56.98	51.59	51.79
$3d^{10}5s(^2S)-3d^{10}6p(^2P)$	$\frac{1}{2}-\frac{3}{2}$	111.15	110.59	102.29	101.60
5s — 6p	$\frac{1}{2}-\frac{1}{2}$	112.7	112.19	103.66	103.18
$3d^{10}5p(^2P)-3d^{10}6s(^2S)$	$\frac{3}{2}-\frac{1}{2}$	154.12	154.12	141.05	140.84
5p — 6s	$\frac{1}{2}-\frac{1}{2}$	148.46	148.41	135.59	135.33
$3d^{10}5p(^2P)-3d^{10}6d(^2D)$	$\frac{3}{2}-\frac{5}{2}$	115.80	115.76	106.75	106.46
5p — 6d	$\frac{3}{2}-\frac{3}{2}$	116.20	116.10	107.17	106.81

NEW METHODS IN DEVELOPMENT OF X-RAY OPTICS FOR PLASMA DIAGNOSTICS OF LASER - PRODUCED PLASMA

R. Hudec and B. Valníček
Astronomical Institute
Czechoslovak Academy of Sciences
Ondřejov, Czechoslovakia

A new technology was developed for manufacturing of precise and low-cost X-ray grazing incidence microscopic optics.

CZECHOSLOVAK X-RAY MIRROR PROGRAM

Imaging experiments represent one of the main directions in the Czechoslovak X-ray astronomy program. The Space Research Department of the Astronomical Institute of the Czechoslovak Academy of Sciences in Ondřejov has been active in the development of X-ray mirrors since 1970. We have participated in 7 space X-ray imaging experiments. 6 experiments were flown onboard the Vertical 8, 9 and 11 rockets in the years 1979, 1981 and 1983 (Hudec et al. 1984a), one experiment was flown onboard the Soviet orbital station Salyut 7 in the year 1982 (Valníček et al. 1983 and Hudec et al. 1984b). The experiments represent both small solar X-ray imaging telescopes and big stellar X-ray telescope.

In the first stage (1970-1980) the grazing incidence mirrors of the Wolter 1 type were made using a technique where massive nickel replicas (wall thickness between 5 and 12 mm) were deposited onto a highly polished glass matrix, which was then removed. Although highly precise, the use of thick galvanoplastic technology was connected with the danger of damage of polished glass mandrels during the removing process due to stresses occuring during the electroplating.

After a number of tests a new technology is used since 1981 based on thin (0.1 to 0.5 mm) metallic replicas reinforced by specially filled thermoreactive plastics. This technology allows the replicas to be absolutely without stresses and thus to manufacture more copies from only one optically polished mandrel.

Since 1970, about 25 X-ray mirrors having diameters between 20 and 240 mm were made.

SOME PROBLEMS RELATED TO THE MICROSCOPIC X-RAY OPTICS

Previous experiments using X-ray imaging to investigate

laser-produced plasma has employed pinhole cameras having poor spatial resolution (not better than 5 arcmin) and small sensitivity due to small collecting area.

The use of grazing incidence imaging X-ray mirrors represents much better possibility to get diagnostic images of laser-produced plasmas. For laboratory experiments, the most advantageous system seems to be ellipsoid-hyperboloid mirror because of finite distance of the source (Chase and Silk 1975). In recent years, there have been efforts at several laboratories aimed to the development of such X-ray microscopic optical systems (Silk 1980). Although the optics are small, the effort required to produce them was not. Usually the manufacture was performed by using conventional grinding, polishing and lapping of small inner surfaces of revolution having diameters of order of 1 cm. This is difficult and expensive - and all this results in the high cost of X-ray microscopic systems in order of US $ 100 000 (Silk 1980).

The high cost thus does not allow:

(i) the wide use of X-ray microscopic systems.

(ii) the use of cameras working with several mirrors and paths with different spectral filters simultaneously.

For these reasons, we have searched for possibility to produce small X-ray mirrors at low costs without remarkable loss of quality.

POSSIBLE SOLUTION: REPLICA MIRRORS

Our new thin-galvanoplastic and epoxy technology allows up to date to produce 5 to 10 perfect copies from only one optically polished glass mandrel. Considering that the manufacture of the master is the most costly and most laborious operation, the cost of such replicas is very low, representing only 10 to 20% of the cost of mirrors produced by classical technology. Moreover, the production usually proceeds very quickly. Although typically several months are necessary to produce one glass master, thereafter the production of each replica does not exceed several days.

Although developed for big astronomical X-ray mirrors, we have proposed to use this technology also in the field of small X-ray optics for investigation of laser-produced plasmas. Our tests show that we are able to produce numerous and low-cost mirrors this way with diameters as small as 5 mm and all this without problems(we are polishing and lapping <u>outer</u> surface).

The advantages of our mirrors are:

(i) the wide use of X-ray optics.

(ii) the possibility of production of numerous X-ray mirrors.

(iii) the possibility to built (large) arrays of identical optical systems (LAMAR in X-ray astronomy), multiple cameras with several optical paths and several spectral filters to allow more precise diagnostics (in the plasma physics).

and all this at reasonable costs.

Our X-ray microscopic program is summarized in Table 1.

TABLE 1 Czechoslovak microscopic X-ray optics program

Type +)	PP	EH
Magnificance	1x	5x
Object distance (mm)	300	150
Image distance (mm)	300	750
Grazing angle (^{o})	1	1
Working range (nm)	≥ 6	≥ 6
Diameter at midplane (mm)	20	17
Lenght of each surface (mm)	~ 25	~ 20
Outside diameter (mm)	28	25
Material of reflecting surface	Ni	Ni
Number of systems already produced	4	0
Number of systems to be produced in near future	4	12

+) PP = Paraboloid-Paraboloid, EH = Ellipsoid-Hyperboloid

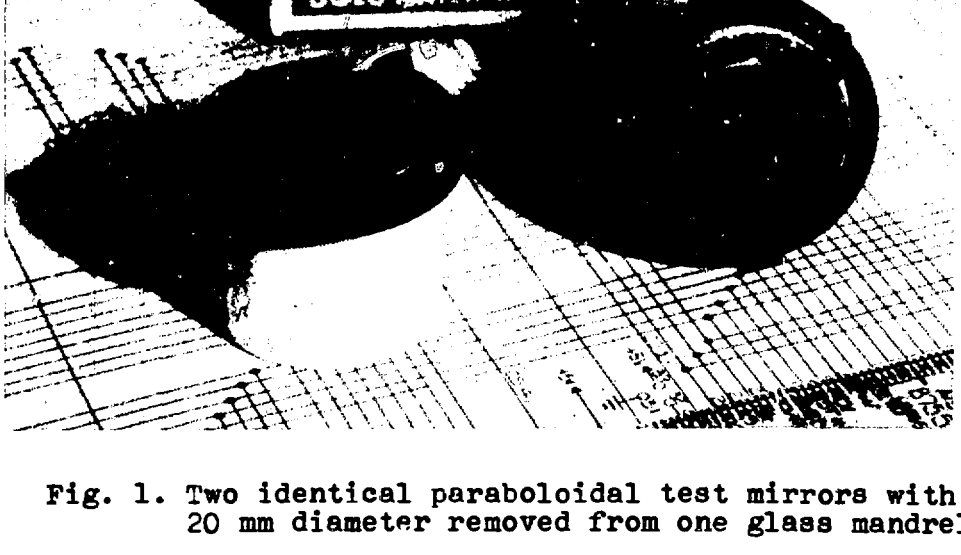

Fig. 1. Two identical paraboloidal test mirrors with 20 mm diameter removed from one glass mandrel.

First preliminary results of different tests show that the mirrors produced this way exhibit good properties and that the replica technology is well suited for applications. The replicas render a highly accurate copy of the polished glass surface as well as of the shape of the master and a

XUV SPECTRA OF Ag XVII - Ag XXI AND Cd XVIII - Cd XXII FROM LASER PRODUCED PLASMAS

M.A. Khan, H.A. Al-Juwair
Department of Physics
University of Petroleum & Minerals
Dhahran, Saudi Arabia

G.J. Tallents
Department of Engineering Physics
Research School of Physical Sciences
The Australian National University
Canberra, Australia

The spectra of highly ionized Ag and Cd in the region 20-200 A^{o} excited in laser produced plasmas were recorded and analyzed. The spectral lines identified correspond to Ag XVII - Ag XXI and Cd XVIII - Cd XXII involving transitions of the type $3d^{k}$ nl - $3d^{k}$ nl' and $3d^{k}$ - $3d^{k-1}$ nl" where k = 9,10; n = 4,5,6; l = s,p,d,f; l' = s,p,d,f,g, and l" = p,f.

The experimental work was carried out at the Australian National University Research School of Physical Sciences. The Nd=glass laser system delivered pulsed powers of the order of $10^{15}W/cm^{2}$ onto flat metalic targets placed in a vacuum. The target could be positioned accurately in the focal plane of the input lens. The spectra were recorded photographically on Kodak SC5 plates with a 2-m grazing incidence spectrograph (Hilger & Watts E-580) employing a 600 lines/mm grating at 88.157^{o} incidence. A maximum of three laser pulses gave the desired plate exposure while a single shot exposure from a pure carbon target plasma provided the reference points for wavelength calibration. The well-known Lyman spectra of CVI and CV appeared strong and could be clearly identified upto their 5th order. The wavelengths of some strong lines of Ag XIX and Cd XX previously measured (1) were used as secondary wavelength standards and a best fit was then made with the wavelengths computed from the dispersion equation of the grating. The accuracy of the measured wavelengths was within $0.02A^{o}$ and better than $0.005A^{o}$ at points closer to the reference lines.

The line classifications are based on simple extrapolations along isoelectronic sequences as well as on comparisions with the calculated transition energies (2) computed from electron orbital binding energies for different configurations by a multiconfigurational relativistic Dirac-Fock computer code developed originally by Desclaux (3). A point nucleus was assumed for the calculations. The effect of the finite size of the nucleus has been investigated to be neglegibly small (4). In Table-I we compare some of our computed and measured wavelengths with previously published data (1,5,6).

surface finish considerably superior to that of directly polished metal can be achieved.

Fig. 2. Two identical hyperboloidal parts of the 130 mm inner mirror of the Salyut 7 mirror assembly removed from only one glass mandrel.

REFERENCES

Chase, R.C., Silk, J.K. 1975, Appl. Optics, 14, 2096.

Hudec, R., Valníček, B., Pražák, V., and Šolc, I. 1981, Bull. Astron. Inst. Czechoslovakia, 32, 182.

Hudec, R., Valníček, B., Sylwester, J., and Kordylewski, Z. 1984a, Bull. Astron. Inst. Czechoslovakia, in press.

Hudec, R., and Valníček, B. 1984b, Adv. Space Res., 3, No. 11-12, 545.

Silk, J.K. 1980, Annals of the New York Academy of Sciences, 342, 116.

Valníček, B., Hudec, R., Šolc, I., Landa, V., Svátek, L., Mareček, R., Urban, J., Vainstein, L.A., Mitropolskij, M.M., Plotkin, M.E., Slemzin, V.A., Suchodrev, N.K., and Sumbatov, V.G. 1983, Preprint Fizicheskij Institut Akademii Nauk SSSR, No. 46.

PROGRAM

Monday August 27

8:30 AM Welcome - Dr. H. Gursky, Superintendent, Space Science Division
Naval Research Laboratory, USA
Comments - Dr. G.A. Doschek, Naval Research Laboratory, USA

SESSION 1. SOLAR ASTROPHYSICS Chairperson: Dr. R.W.P. McWhirter
Rutherford Appleton Laboratory, UK

9:00 AM Invited Paper

I.1 The Soft X-ray and EUV Spectra of Solar Flares
K. Nishi
Tokyo Astronomical Observatory, Japan

9:30 AM Contributed Papers

O.1 Soft X-ray Spectroscopy from the X-ray Polychromator on the Newly Repaired Solar Maximum Mission
K.T. Strong
Lockheed Palo Alto Research Laboratory, USA
J.R. Lemen
Mullard Space Science Laboratory, UK
K.J.H. Phillips
Rutherford Appleton Laboratory, UK

O.2 Measurement of the Increase in Altitude of the Soft X-ray Emission Regions of Solar Flares
J.F. Seely and U. Feldman
Naval Research Laboratory, USA

O.3 Derivation of the Ionization Balance for Fe XXIV/Fe XXV Using Solar X-ray Data
E. Antonucci and M.A. Dodero
Universita di Torino, Italy
A.H. Gabriel
Rutherford Appleton Laboratory, UK
K. Tanaka
Tokyo Astronomical Observatory, Japan

O.4 Observational Evidence for Coronal Magnetic Reconnection During the Two-Ribbon Flare of 21 May 1980
R.A. Kopp
Los Alamos National Laboratory, USA
G. Poletto
Osservatorio Astrofisico di Arcetri, Italy

MEETING SCHEDULE AND PROGRAM

0.5 Variation of the Observed Coronal Calcium Abundance for Various X-ray Flare Plasmas
J. Sylwester
Space Research Center, Polish Academy of Sciences, Poland
J.R. Lemen
Mullard Space Science Laboratory, UK
R. Mewe
Laboratory for Space Research, The Netherlands

10:30 AM COFFEE

11:00 AM Invited Paper

I.2 HRTS Ultraviolet Solar Spectroscopy
K.P. Dere
Naval Research Laboratory, USA

11:30 AM Contributed Papers

0.6 Interpretation of Electric Fields in Coronal Magnetic Loops
P. Foukal
Atmospheric and Environmental Research, Inc., USA
D. Landman
University of Hawaii, USA

0.7 The Solar Wind Generation Experiment for the Spartan 2 Mission
J.L. Kohl, H. Weiser, and G.L. Withbroe
Harvard-Smithsonian Center for Astrophysics, USA
R.H. Munro
High Altitude Observatory, USA

0.8 HRTS Observations of Spicular Emission at Transition Region Temperatures Above the Solar Limb
J.W. Cook, G.E. Brueckner, J.-D.F. Bartoe, and D.G. Socker
Naval Research Laboratory, USA

12:10 PM LUNCH

SESSION 2. LOW DENSITY LABORATORY PLASMAS Chairperson: Professor W.R.S. Garton
Imperial College, UK

2:00 PM Invited Papers

I.3 X-ray Satellite Lines of Highly Ionized Atoms
J. Dubau
Observatoire de Paris, France

I.4 The Relevancy of Magnetically Confined Plasmas - Tokamak and Mirror - for Atomic Spectroscopy and Astrophysical Plasma Diagnostics
M. Finkenthal
The Hebrew University of Jerusalem, Israel

3:00 PM COFFEE

3:30 PM Contributed Papers

0.9 Intensities in Complex Spectra of Highly Ionized Atoms
M. Klapisch, A. Bar-Shalom, and A. Cohen
Hebrew University of Jerusalem, Israel

0.10 Supra-Thermal Electron Tail Effects on X-ray Line Emission in a Tokamak Plasma
R. Bartiromo, F. Bombarda, and R. Giannella
Associazione EURATOM-ENEA sulla Fusione, CRE Frascati, Italy

0.11 Recombination Process from a Metastable State
T. Kato, K. Masai, and K. Sato
Nagoya University, Japan

0.12 New Calculations of Inner-Shell X-ray Lines in Ti, Cr, and Ni as Density Diagnostics
J.R. Lemen
Mullard Space Science Laboratory, UK
K.J.H. Phillips
Rutherford Appleton Laboratory, UK
G.A. Doschek
Naval Research Laboratory, USA
R.D. Cowan
Los Alamos National Laboratory, USA

5:30 PM RECEPTION

Tuesday August 28

SESSION 3. NON-SOLAR ASTROPHYSICS Chairperson: Dr. H. Gursky
Naval Research Laboratory, USA

9:00 AM Invited Papers

I.5 Spectroscopy of Cool Stars from IUE
C. Jordan
Oxford University, UK

I.6 Soft X-ray Spectroscopy with EXOSAT
R. Mewe
The Astronomical Institute at Utrecht, The Netherlands

I.7 UV Spectra of Nebulae and Novae
M.J. Seaton
University College London, UK

10:30 AM COFFEE

11:00 AM Contributed Papers

O.13 Broad-band Spectroscopy of Late-Type Stars with EXOSAT
M. Landini, B.C. Monsignori-Fossi, and R. Pallavicini
Arcetri Astrophysical Observatory, Italy

O.14 The Proposed Columbus Mission: High and Low Resolution Spectroscopy in the 100-2000 Å Spectral Region
J.L. Linsky, for the Columbus Science Working Group
Joint Institute for Laboratory Astrophysics, USA
University of Colorado, USA
National Bureau of Standards, USA

O.15 X-ray Spectroscopic Measurements of Non-Equilibrium Ionization in Supernova Remnants
T. Markert, C.R. Canizares, T. Pfafman, and P. Vedder
Massachusetts Institute of Technology, USA
P.F. Winkler
Middlebury College, USA
A. Pradhan
Joint Institute for Laboratory Astrophysics, USA

O.16 Objective Grating Soft X-ray Spectra of Compact Binary X-ray Sources
S.M. Kahn and S.D. Vrtilek
Columbia University, USA

O.17 High Resolution EUV/Soft X-ray Spectrometers Using Variable Groove Spacings
M. Lampton, M. Hettrick, and S. Bowyer
University of California, Berkeley, USA

O.18 The Statistical Equilibrium of H and He and the H/He Ratio in WR Stars
A.B. Underhill and A.K. Bhatia
NASA/Goddard Space Flight Center, USA

12:00 PM LUNCH

SESSION 4. THEORETICAL SPECTROSCOPY Chairperson: Dr. A. Temkin
NASA/Goddard Space Flight Center, USA

2:00 PM Invited Paper

I.8 Distorted Wave Calculations: Application to Astrophysical and Tokamak Plasmas
A.K. Bhatia
NASA/Goddard Space Flight Center, USA

2:30 PM Contributed Papers

O.19 Effect of Two Types of Non-Maxwellian Electron Distributions on Temperature Spectroscopic Diagnostics
M. Lamoureux, C. Moller, and P. Jaegle
University of Paris-Sud, France

O.20 Radiative Corrections to the Intensities of Dielectronic Satellite Lines Emitted from Helium- and Lithium-Like Argon
V.L. Jacobs and J.E. Rogerson
Naval Research Laboratory, USA

O.21 A Comparison of Various NLTE Codes in Computing the Charge-State Populations of an Argon Plasma
S.R. Stone and J.C. Weisheit
Lawrence Livermore National Laboratory, USA

O.22 Collision Strengths and Line Strengths for Transitions from the $1s^2\ ^3$ Levels to the $1s2\ ^3$ " Levels in Li-Like Ions
D.H. Sampson, S.J. Goett and G.V. Petrou
Pennsylvania State University, USA
R.E.H. Clark
Los Alamos National Laboratory, USA

O.23 New Results of the Unresolved Transition Arrays Method
M. Klapisch, A. Krasnitz, and P. Mandelbaum
The Hebrew University of Jerusalem, Israel
C. Bauche-Arnoult and J. Bauche
Lab. Aime Cotton, France

3:30 PM COFFEE

SESSION 5. EXPERIMENTAL ATOMIC PHYSICS

Chairperson: J.L. Schwob
The Hebrew University of Jerusalem, Israel

4:00 PM Invited Paper

I.9 Recent Laboratory Studies of Dielectronic Recombination
G.H. Dunn
Joint Institute for Laboratory Astrophysics, USA

4:30 PM CONTRIBUTED PAPERS

O.24 VUV High-Resolution Absorption Spectra Obtained with Synchrotron Light, and Interpretations
M.A. Baig, J.P. Connerade, W.R.S. Garton, J. Hormes, C. Mayhew, G. Noldeke, and K. Sommer
Physikalisches Institut, Germany
Imperial College, UK

O.25 Absolute Wavelength Determination in the Soft X-ray Wavelength Range with Double Reflections in Single Crystals
B.S. Fraenkel
The Hebrew University of Jerusalem, Israel

O.26 High-Resolution Photoabsorption Spectrum of Cs+ ($5p^6\ ^1S_0 - 5p^5ns,nd$) Between 504 Å and 600 Å Using a Laser Ionized Cs Vapor Column
T.J. McIlrath
University of Maryland, USA
V. Kaufman, J. Sugar, W.T. Hill, III, and D. Cooper
National Bureau of Standards, USA

O.27 The Measurement of Branching Ratios of Spontaneous Radiative Transition Probabilities for Be-Like Ions N IV and O V
J. Lang, R.A. Hardcastle, and P.H. Spurrett
Rutherford Appleton Laboratory, UK

O.28 Observation of Ionization of Laser Excited Atoms by Synchrotron Radiation
J.M. Bizau, F. Wuilleumier, P. Gerard, and P. Dhez
University of Paris-Sud, France
B. Carre and G. Spiess
Service des Atoms et des Surfaces, C.E.N. Saclay, France
D.L. Ederer
National Bureau of Standards, USA
J.L. Picque, J.L. Legouet, and J.C. Keller
Laboratoire Aime Cotton, C.N.R.S., France
P. Koch
State University of New York, Stony Brook, USA

O.29 Study of Electronic Capture in the N^5-He, H_2 Collision by UV Spectroscopy
P.H. Cotte and M. Druetta
Universite Lyon I, France

6:00 PM COCKTAIL HOUR

7:00 PM BANQUET

After-dinner topic and speaker: "On the Threshold of Space"
Dr. David H. DeVorkin
Curator, Space Science and
Exploration Department
National Air and Space Museum

Wednesday August 29

SESSION 6. POSTER PAPERS - 8:30 AM - 6:00 PM

P.1 The Solar X-ray Line Spectrum 5.5-12 Å
D.L. McKenzie
The Aerospace Corporation, USA

P.2 Solar Coronal Fe XVII X-ray Line Ratios
H.R. Rugge and D.L. McKenzie
The Aerospace Corporation, USA

P.3 Atomic Calculations for the Highly Ionized Iron Ions Produced in Solar Flares
H.E. Mason
University of Cambridge, UK
A.K. Bhatia
NASA/Goddard Space Flight Center, USA

P.4 High Spectral Resolution Observations of Coronal X-ray Emission from the RS CVn Binary Sigma Corona Borealis
G.R. Riegler
Jet Propulsion Laboratory, USA
P.C. Agrawal
Tata Institute of Fundamental Research, India
T.H. Markert
Massachusetts Institute of Technology, USA

P.5 Spectroscopic Diagnostics of the UV Emitting Plasmas in Solar Flares Observed from SMM
C.-C. Cheng
Naval Research Laboratory, USA
E. Tandberg-Hanssen
NASA/Marshall Space Flight Center, USA

P.6 Precision Measurement of Wavelengths in Solar Flare X-ray Spectra
U. Feldman, J.F. Seely, and S. Daniels
Naval Research Laboratory, USA

P.7 Analysis of Intensity Ratio for Mg XII Ly α Components from Intercosmos 7 Observations
J. Sylwester, B. Sylwester
Space Research Center, Polish Academy of Sciences, Poland
J. Jakimiec, M. Tomczak
Wroclaw University, Poland
S.L. Mandelstam, I.A. Zhitnik, V.V. Korneev
P.N. Lebedev Physical Institute, USSR

P.8 Effect of a non-Maxwellian Electron Distribution on the Linear Polarization of Chromospheric Lines During Solar Flares
J.C. Henoux, G. Chambe, D. Herist-Chi, R. Shine, B. Woodgate, and J. Beckers
Observatoire de Paris, France
NASA/Goddard Space Flight Center, USA
University of Arizona, USA

P.9 The Solar and Heliospheric Observatory
G. Noci
Padua University, Italy
Observatory of Arcetri, Italy

P.10 Atomic Data in Astrophysics
N.G. Bochkarev
Sternberg State Astronomical Institute, USSR

P.11 A New Type Spectrometer for Plasma Diagnosis
T. Oshio
Hiroshima Institute of Technology, Japan
E. Ishiguro and R. Iwanaga
Osaka City University, Japan

P.12 Measurement of the A-Value of the $3s^2\ {}^1S_o - 3s3p\ {}^3P_1{}^o$ Intersystem Transition in Al II at 2670 Å: A Progress Report
B. Carol Johnson and H.S. Kwong
Harvard-Smithsonian Center for Astrophysics, USA

P.13 Photodissociation of Neutral Free Radicals of Astrophysical Interest
L.D. Gardner, M.M. Craff, and J.L. Kohl
Harvard-Smithsonian Center for Astrophysics, USA

P.14 Time-Resolved Spectra in the 5-330 Å Region Emitted from Tokamak Plasmas
J.L. Schwob, A. Wouters, and S. Suckewer
Princeton University, USA
M. Finkenthal
The Hebrew University of Jerusalem, Israel

P.15 Relative Intensities of Lines in F I - B I - Like Ti, Cr, Fe, Ni, and Ge: A Comparison of Theory and Experiment
B. Stratton and H.W. Moos
Johns Hopkins University, USA
U. Feldman and J.F. Seely
Naval Research Laboratory, USA
S. Suckewer
Princeton University, USA
M. Finkenthal
The Hebrew University of Jerusalem, Israel

P.16 Measurements of Absolute Collisional Cross Sections at Harvard-Smithsonian Center for Astrophysics
J.L. Kohl, L.K. Deutsch, L.D. Gardner, G.P. Lafyatis, and A. Young
Harvard-Smithsonian Center for Astrophysics, USA

P.17 Atomic Potentials in Very Dense Aluminum Plasmas
R. Cauble and U. Gupta
Berkeley Research Associates, USA
J. Davis
Naval Research Laboratory, USA

P.18 Comparative Study of Electron Bremsstrahlung in Various High T-ρ Potentials
M. Lamoureux
Universite of Paris-Sud
R. Cauble
Berkeley Research Associates, USA
L. Kim
University of Pittsburgh, USA
F. Perrot
CEA Limeil, France
R. Pratt
University of Pittsburgh, USA

P.19 Inverse Scattering Theory for Inelastic Collisions
Cao xuan Chuan
Institute of Physics, Algeria

P.20 The Effect of Resonances on the Excitation Rates for the Ions of the He-Like Isoelectronic Sequence
P. Faucher and F. Bely-Dubau
Observatoire de Nice, France
J. Dubau
Observatoire de Meudon, France

P.21 Proton-Induced Fine-Structure Transitions
B. Zygelman and A. Dalgarno
Harvard-Smithsonian Center for Astrophysics, USA

P.22 Charge State Distribution Measurement in an ECR-Discharge by VUV Spectroscopy
E.H. Marlinghaus and K. Wiesemann
Ruhr-Universitat, Germany

P.23 Critical Compilations of Atomic Energy Levels
J. Sugar, W.C. Martin, J. Reader, A. Musgrove, and C. Corliss
National Bureau of Standards, USA

P.24 Critical Compilations of Atomic Transition Probabilities
G.A. Martin, J.R. Fuhr, and W.L. Wiese
National Bureau of Standards, USA

P.25 XUV and Soft X-ray Radiation from Laser-Produced Plasmas as Laboratory Spectroscopic Sources
P. Gohil, M.L. Ginter, and T.J. McIlrath
University of Maryland, USA
H. Kapoor, D. Ma, and M.C. Peckerar
Naval Research Laboratory, USA

P.26 Theoretical Calculation of X-ray Emission from Laser-Produced Plasmas
D. Duston, R.W. Clark, and J. Davis
Naval Research Laboratory, USA

P.27 Interpretation of Pseudocontinua in the Spectra of Highly Ionized Atoms from Tm to W in Laser-Produced Plasmas
P. Mandelbaum, M. Klapisch, and A. Krasnitz
The Hebrew University of Jerusalem, Israel

P.28 X-ray Measurements from the Tandem Mirror Experiment-Upgrade (TMX-U)
E.H. Silver, J.F. Clauser, and B.H. Failor
Lawrence Livermore National Laboratory, USA

P.29 Electron Capture into Excited States for $Al^{8+} + H_2$ Collisions at 3 keV/amu
M. Mayo, D. Hitz, M. Druetta, S. Dousson, J.P. Desclaux, and S. Bliman
Agrippa GIS, CEA/CNRS, C.E.N.G., France

P.30 Population of Excited States of Al^{+10} in a Plasma by a Time-Dependent Model
H. Guennou, and A. Sureau
Universite Paris-Sud and C.N.R.S., France

P.31 Transitions of the Type 2s-2p in Highly-Ionized Copper to Rubidium
W.E. Behring and Leonard Cohen
NASA/Goddard Space Flight Center, USA
J.F. Seely and U. Feldman
Naval Research Laboratory, USA
Samuel Goldsmith
University of Maryland, USA
M. Richardson
University of Rochester, USA

SESSION 7. HIGH DENSITY LABORATORY PLASMAS — Chairperson: Dr. W.H. Parkinson
Harvard-Smithsonian Center for Astrophysics, USA

2:00 PM Invited Talks

I.10 Diagnostics of Laser-Produced Plasmas
D. Matthews
Lawrence Livermore National Laboratory, USA

I.11 Recombination Lasers in the XUV Spectral Region
G. Pert
University of Hull, UK

3:00 PM Contributed Papers

O.30 3s-3p and 3p-3d Transitions in Neon-Like Ions of the Iron-Group Elements
U. Litzen and C. Jupen
Lund University, Sweden

0.31 Direct Comparison of Electron Density Measurements in Laser-Created Plasmas Using Stark Broadening and Satellite Line Intensities
Ph. Alaterre, P. Audebert, J.P. Geindre, C. Popovics, and J.C. Gauthier
Ecole Polytechnique, France

0.32 High Resolution Lithium-like Satellites to the $1s^2\ ^1S_0$ - $1s3p\ ^1P_1$ Line in Laser-Produced Dense Plasmas
P. Audebert, J.P. Geindre, J.C. Gauthier, Ph. Alaterre, and C. Popovics
GRECO ILM, Ecole Polytechnique, France
M. Cornille and J. Dubau
Observatoire de Paris, France

0.33 Opacity Broadening as a Density Diagnostic for Spot Spectroscopy
J.P. Apruzese
Naval Research Laboratory, USA

0.34 Absorption Spectra of Light Ions in the Extreme Ultraviolet
E. Jannitti
Instituto Gas Ionizzati del CNR, Padova, Italy
P. Nicolosi and G. Tondello
Universita di Padova, Italy

0.35 X-ray Spectroscopy to Determine Line Coincidences Between K- and L- X-ray Transitions
P.G. Burkhalter, D. Newman, J.V. Gilfrich, and D.B. Brown
Naval Research Laboratory, USA
P.D. Rockett and G. Charatis
KMS Fusion, Inc., USA
C. Hailey and D. Matthews
Lawrence Livermore National Laboratory, USA
B. MacGowan
Imperial College, UK

0.36 XUV Spectra of Ag XVII-Ag XXI and Cd XVIII-Cd XXII from Laser-Produced Plasmas
M.A. Khan and H.A. Al-Juwair
University of Petroleum and Minerals, Saudi Arabia
G.J. Tallents
The Australian National University, Australia

0.37 Calculation of Ar XI Spectral Line Intensities from High Density/High Temperature Plasmas
Y.T. Lee and K.J. Reed
Lawrence Livermore National Laboratory, USA

0.38 Dielectronic Recombination of Highly Stripped Argon Ions: Theoretical Calculations and Direct Observations in EBIS Source
M. Loulergue and J. Dubau
Observatoire de Paris-Meudon, France
J.P. Briand and P. Charles
Institut Curie, Universite P. et M. Curie, France

0.39 A High-Resolution VUV Spectrometer with Electronic Parallel Spectral Detection
C.L. Cromer, J.M. Bridges, T.B. Lucatorto, and J.R. Roberts
National Bureau of Standards, USA

5:00 PM DISCUSSION OF NEXT CONFERENCE

6:00 PM END OF MEETING

LIST OF PARTICIPANTS

Loren Acton
Ester Antonucci
John Apruzese
Anand Bhatia
William E. Behring
Milan Blaha
Richard Bleach
S. L. Bliman
N. Bochkarev
Francesca Bombarda
Alain Bourdier
Jean Pierre Briand
Phillip Burkhalter
Robert Cauble
George Charatis
Chung-Chieh Cheng
Cao Xuan Chuan
Ara Chutjian
Charles Clark
Robert E.H. Clark
Leonard Cohen
Francoise Combet-Farnoux
John Cook
M. Cornille
David Crandall
Christopher Cromer
R. Cruddace
K.P. Dere
D.H. DeVorkin
Michel Druetta
G.A. Doschek
Jacques Dubau
Gordon Dunn
Dwight Duston
D.L. Ederer
Gabriel Epstein
Robert Farland
Paul Faucher
Uri Feldman
Michael Finkenthal
Peter Foukal
Benjamin S. Fraenkel
Joel Frehaut
L.D. Gardner
W.R.S. Garton
Jean Claude Gauthier
Ruggero Giannella
Marshall Ginter
P. Gohil
Margaret Graff
Hans Griem
Uday Gupta
Herbert Gursky
M.C. Huber
E. Jannitti
V.L. Jacobs
Kenneth Jensen
B. Carol Johnson
Carole Jordan
Steven M. Kahn
Takako Kato
Robert Kauffman
Victor Kauffman
Richard Kelley
Long Huan Kim
Marcel Klapisch
Joachim Koeppen
John L. Kohl
Roger A. Kopp
Robert W. Kreplin
Joseph A. Kunc
Jean Paul Laget
Denis Lambert
Michelle Lamoureux
Michael Lampton

James Lang
T.N. Lee
Yim T. Lee
James R. Lemen
Jeffrey L. Linsky
Ulf Litzén
Michelle Loulergue
Pinchas Mandelbaum
Phillip W. Mange
Stephen P. Maran
Thomas H. Markert
E.H. Marlinghaus
Georgia A. Martin
William C.Martin
Indrek Martinson
John T. Mariska
Thomas McIlrath
Remy Marmoret
Yutaka Matsui
Helen E. Mason
Kuniaki Masai
David L. McKenzie
Edgar McLean
R.W.P. McWhirter
Rolf Mewe
F.G. Meijer
William Molander
Warren Moos

Arlene Musgrove
Werner Neupert
K. Nishi
Giancarolo Noci
William Ott
Roberto Pallavicini
W.H. Parkinson
G.J. Pert
Andrei N. Petelin
Fan Pinzhong
Giannina Poletto
Claude Popovics
John C. Raymond
Joseph Reader
Kennedy Reed
Guenter R. Riegler
Michel Rostaing
Diane Roussel-Dupre
Hugh Rugge
Edmond M. Reeves
Julia Saba
Douglas H. Sampson
Edward Saloman
Jean Louis Schwob
M.J. Seaton
John F. Seely
Peter B. Seidl
Eric Silver

Charlotte Sitterly
Barham W. Smith
Peter L. Smith
Robert E. Stencel
Robert Stern
Samuel R. Stone, III
Brent Stratton
Keith Strong
S. Suckewer
Jack Sugar
Alain Sureau
Janusz Sylwester
Bruce Tarter
Michel Tavernier
Aaron Temkin
Roger Thomas
Giuseppe Tondello
David L. Tubbs
Anne B. Underhill
Saeqa Dil Vrtilek
Rosemary Walling
Robert P. Weaver
Kenneth G. Widing
Bernard Wilde
Alan Wouters
Bernard Zygelman